### FINAL REPORT

for

# DESIGN AND DEVELOPMENT OF A BRUSHLESS, DIRECT-DRIVE SOLAR ARRAY REORIENTATION SYSTEM

(APRIL 1972)

Contract No. NAS 5-10459

Prepared by

Westinghouse Electric Corporation Aerospace Electrical Division Lima, Ohio

for

Goddard Space Flight Center Greenbelt, Maryland

### FINAL REPORT

for

### DESIGN AND DEVELOPMENT OF A BRUSHLESS, DIRECT-DRIVE SOLAR ARRAY REORIENTATION **SYSTEM**

(April 1972)

Contract No. NAS 5-10459

Prepared by

Westinghouse Electric Corporation Aerospace Electrical Division Lima, Ohio

Prepared by:

R. D. Jessee, Engineer Solid-State Systems Development

Approved by:

F. C. Stump, Project Manager

Solid State System Development

for

Goddard Space Flight Center Greenbelt, Maryland

# Page intentionally left blank

Page intentionally left blank

#### **ABSTRACT**

This report covers the design and development of the laboratory model required by Contract NAS 5-10459, Phase II. In addition, design and development reports of the system components are included. The report is essentially a compilation of reports covering the system and its various parts. To enhance completeness, the final report of Phase I covering circuit development of the controller is also included as part of this report.

The purpose of Phase I, reported in section II, was to develop a controller for a brushless, direct-drive, single-axis solar array reorientation system for earth-pointed, passively-stabilized spacecraft. A control system was designed and breadboard circuits were built and tested for performance. The results obtained meet the intent of the contract.

The controller is designed to take over automatic control of the array on command after the spacecraft is stabilized in orbit. The controller will orient the solar array to the sun vector and automatically track to maintain proper orientation. So long as the orbit is circular, orientation toward the sun is maintained even though the spacecraft goes into the shadow of the earth. Particular attention was given in the design to limit reaction between the array and the spacecraft.

The control system is capable of reorienting a simulated solar array having an inertia of 5 to 10 slug feet square from any position, smoothly within a three-minute period. Acceleration from rest to a speed-controlled return to proper orientation occurs with a minimum of speed oscillation. Acceleration is limited by the design of the controller to minimize reaction between the array and the spacecraft. Upon approaching proper orientation, anticipatory circuits in the controller act to prevent undesirable reactions caused by overshoot or hunting and thus cause a smooth transfer from the reorientation mode to the normal tracking mode.

Operating in the sunlit normal tracking mode, the controller tracks the sun vector at almost a constant error of 0.7 degree. There is no perceptible oscillation and the variation in tracking errors is about 0.1 degree. Transition of the system into the dark period has little effect on the average tracking error (a maximum of 1/2 degree). Total variation of the tracking error during the dark period tracking

was observed to be 1.2 degree, while the maximum deviation from the sun vector was less than 2 degrees.

In developing the circuits of the controller, it was necessary to compensate for irregularities in the magnetic sensor signals incorporated in the drive motor. It was recommended that in further development of the system, the magnetic sensor outputs be corrected to provide a reliable interface between the motor and the controller. Also, several other problem areas were left unresolved at the close of contract NAS 5-10263 covering the brushless dc torque motor. The motor was transferred to Phase II of the present contract, NAS 5-10459, for resolution of these problems. Necessary modifications were made to correct the problems in the motor design and the changes and test results are reported in section III.

A rotary transformer for the reorientation system was developed on previous NASA - Goddard contracts with Matrix and Neotec. The resulting rotary transformer was tested by Westinghouse and found suitable as a design base for further development to complete the laboratory model. This further development required the re-design of the rotary transformer to include five signal transformers for use in control of the system and mechanical re-design of the power section to reduce the diameter of the large bearing and provide integrity of the entire unit.

The design, reported in section IV, includes a power transformer and five signal transformers built into a single package. The unit was assembled into the laboratory model to simulate transmission of power from a solar array across an air gap to loads on a spacecraft.

Section V covers the completion of the laboratory model required by contract NAS 5-10459, Phase II. Primarily a physical description is given for the redesigned control unit, the inverter, and the laboratory model as a whole. An assembly procedure is included. Performance tests conducted on the laboratory model show it to meet the intent of the specification of the contract.

# CONTENTS

Section		Page
	Abstract	iii
I	Solar Array Reorientation System - General Description	1
II .	Controller Circuit Design Discussion	5 6
	Operating Modes	6 6 7 7 7
	Reorientation System Operation  Solar Sensor Signal  Speed Control Method  Large-Error Reorientation  Dark Period Speed Control	8 10 16 29 36
	Tests  Performance Testing  Functional Tests	50 50 58
	Glossary of Logic Signal Symbols	65
III	D-C Torque Motor Modifications Discussion	67 67
	Problem Areas and Corrective Action Magnetic Sensor Pulse-Width Variation Torque Variation Due to Irregu- larities in Switching Angle	67 67 68 70
	Test	74
IV	Rotary Transformer Design Discussion	89 89
	Function	89 90 92 93

# CONTENTS - continued

Section		Page
V	Solar Array Reorientation System - Laboratory Model	99
	Solar Sensor Amplifier	100 100 100 106
	Printed Circuit Board No. 3 Printed Circuit Board No. 4 Printed Circuit Board No. 5	106 106 112
	Printed Circuit Board Layouts Solar Sensor Amplifier Assembly External Command Unit	112 125 125
	Interconnection of Control Compo- nents	129
	Inverter  Description of Laboratory Model  and Assembly Procedure	132 138
	Mechanical Assembly Electrical Connection	138 150
	Tests Operation Limitations	150 153
VI	Conclusions and Recommendations	155
	Functional Operation	155 156 157
VII	References	<b>159</b>
	Appendices	161
	<pre>I - Rotary Transformer Magnet</pre>	1-1
	<pre>II - Rotary Transformer; Temperature</pre>	II-l
	<pre>III - Detailed Manufacturing</pre>	III-1
	<pre>IV - Advanced Brushless D-C Torque</pre>	IV-1

# LIST OF ILLUSTRATIONS

Figure	Title	Page
	SECTION I	
1	Block Diagram of Brushless Direct-Drive Solar Array Control System	2
2	Complete Laboratory Model and Suspension System	4
	SECTION II	
1	Functional Block Diagram	<b>7,9</b>
2	Solar Sensor System Arrangement	11
3	Solar Sensor Signals	12
4	Solar Sensor Signal Processing Circuit	14
5	Voltage-to-Pulse-Width Converter	15
6	Magnetic Sensor Output Signals (Rectified Envelopes)	17
7	Derivation of Waveforms Used in Speed Control Method	18
8	Superimposed Magnetic Sensor Signals Showing Slopes Required for Forward and Reverse Motion Used in Speed Control	19
9	Illustration of Error Signal Development for Forward Rotation of Motor	20
10	Connection of Six Channels for Drive Logic and Magnetic Sensor Reference	22
11	Drive Logic and Magnetic Sensor Reference - One Channel	23
12	Magnetic Sensor Signal Processing Circuit	24
13	Speed Reference Ramp Generator	25

Figure	Title	Page
	SECTION II - continued	
14	Speed Control Amplifier Circuit	26
15	Voltage-to-Frequency Pulse Generator	28
16	Acceleration and Speed Control Circuit	30
17	Logic Circuits for Mode Selection and Transition	32
18	Block Diagram for Simplified Conceptual Dark-Period Speed Control	38
19	Block Diagram of Dark-Period Speed Control	40
20	Logic Diagram for Single Stage of Counter, Memory and Comparator for Dark-Period Speed Control	43
21	Interstage Connections for Counters, etc	44
22	Dark-Period Control Logic Circuit	45
23	Direction Logic Circuit	48
24	Mechanical Test Setup	52
25	Typical Start-Up Characteristics. Displacement Angle and Speed vs. Time. Start-Up From Rest at 30° Error (5 Slug-ft <sup>2</sup> Array)	54
26	Typical Start-Up Characteristics. Displacement Angle and Speed vs. Time. Start-Up From Rest at 30° Error. (10 Slug-ft <sup>2</sup> Array)	54
27	Array Error and Speed vs. Time During Final 30° of Reorientation From Large Forward Error (5 Slug-ft <sup>2</sup> Array)	55
28	Array Error and Speed vs. Time During Final 30° of Reorientation From Large Forward Error (10 Slug-ft <sup>2</sup> Array)	55
29	Array Error and Speed vs. Time During Final 30 <sup>0</sup> of Reorientation From Large Reverse Error (5 Slug-ft <sup>2</sup> Array)	56

Figure	<u>Title</u>	Page
	SECTION II - continued	
30	Array Error and Speed vs. Time During Final 30° of Reorientation From Large Reverse Error (10 Slug-ft <sup>2</sup> Array)	56
31	Solar Sensor Amplifier Output Characteristics	59
32	Rectified Output From Magnetic Sensors	61
33	Modified Output From Magnetic Sensors	61
34	Solar Array Reorientation System Control Diagram	62
	SECTION III	
1	Maximum Sensor Output Versus Motor Rotation	69
2	Motor Torque Variation Versus Switching Points	72
3	Brushless Motor Commutator Control Logic	73
4	Derivation of Commutator Control Signals	75
5	Controller-Commutator Circuit Schematic- Revised	77
6	Magnetic Sensor Characteristics-Test Curves	79
7	No Load Speed Control Characteristics	80
8	Torque Versus Rotor Position	83
9	Speed-Torque Curves	84
10	Speed-Torque Curves	85
11	No Load Speed Control Characteristics	87
	SECTION IV	
1	Test Circuit	91
2	Rotary Transformer Assembly	95

Figure	Title	Page
	SECTION V	
1	Solar Sensor Amplifier	101
2	Solar Sensor Signal Processing Circuit	. 102
3	Acceleration and Speed Control Circuit	103
4	Speed Reference Ramp Generator	104
5	Speed Control Amplifier Circuit	105
6	Logic Circuits for Mode Selection and Mode Transition	107
7	Magnetic Sensor Signal Processing Circuit	108
8	Drive Logic and Magnetic Sensor Reference - One Channel	109
9	Connection of Six Channels for Drive Logic and Magnetic Sensor Reference	110
10	Dark-Period Control Logic Circuit	111
11	Counter Y, Memory Y, Comparator Y Showing Interconnections	113
12	Counter Z, Memory Z, and Comparator Z, Showing Interconnections	114
13	Multiple Voltage Regulated Power Supply	115
14	Control Unit With Cover Removed	116
15	Printed Wiring Layout For Printed Circuit Board No. 1	117
16	Component Layout For Printed Circuit Board No. 1	118
17	Printed Wiring Layout for Printed Circuit Board No. 2	119
18	Component Layout For Printed Circuit Board No. 2	120

Section	<u>Title</u>	Page
	SECTION V - continued	
19	Printed Wiring Layout For Printed Circuit Board No. 3	121
20	Component Layout For Printed Circuit Board No. 3	122
21	Printed Wiring Layout For Printed Circuit Board No. 4	123
22	Component Layout For Printed Circuit Board No. 4	124
23	Solar Sensor Amplifier	126
24	Printed Circuit and Component Layout For Solar Sensor Amplifier	127
25	Circuit of External Command Unit	128
26	Components of Reorientation Control	130
27	Schematic Diagram 500-Watt, 10 kHz Inverter.	133
28	500-Watt, 10-kHz Inverter With Rotary Transformer	134
29	Internal View of 500-Watt, 10-kHz Inverter.	135
30	Efficiency and Regulation Versus Output Power 500-Watt, 10-kHz Inverter	136
31	Completely Assembled Laboratory Model	139
32	Tripod Base and Light Projector	141
33	Motor/Rotary Transformer Subassembly	143
34	Assembling the Motor/Rotor Transformer Subassembly to the Rotating Mounting Fixture	144
35	Solar Array Suspended Above Drive Assembly	146
36	Connections	147

Figure	<u>Title</u>	Page
	SECTION V - continued	
37	Connections	148
38	Complete Laboratory Model and Suspension System	149
39	Laboratory Model Connection Diagram	151

## LIST OF TABLES

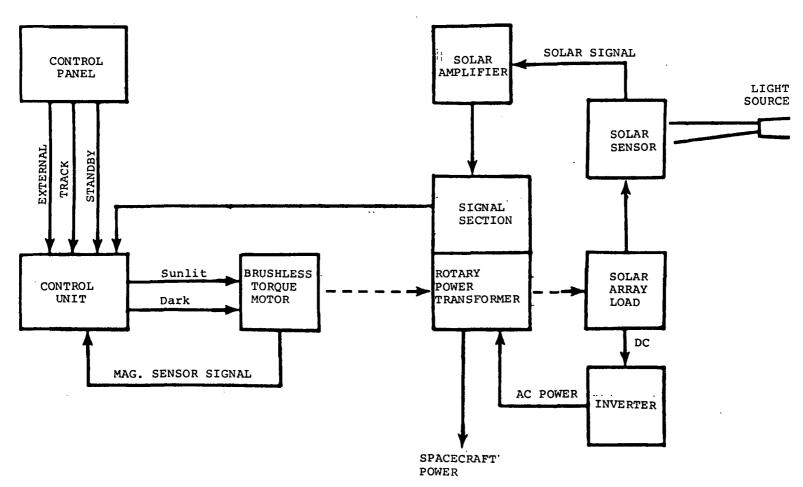
Number		Page
	SECTION V	
I	Wiring Table	131
II	Inverter Parts List	137
III	Laboratory Model Wiring Chart	152

#### SECTION I

#### SOLAR ARRAY REORIENTATION SYSTEM - GENERAL DESCRIPTION

Consider an earth-pointing satellite in earth orbit such that the satellite has an axis of rotation always perpendicular to the orbit plane, and the orbit is sun synchronous. If a solar array is mounted on this axis the array can be continuously pointed toward the sun simply by rotation about the axis. Maximum power is obtained, of course, when the solar array directly faces the sun. Maximum life and reliability is achieved if the array orientation is provided by a system that is mechanized WITHOUT the use of any gears, brush and commutator assemblies, slip-rings, sealed chambers (through which mechanical power must be transmitted), rapid-rotation components, etc. Such a brushless, direct-drive solar array control system was designed and developed, and a laboratory model was constructed to test and demonstrate its operation.

A block diagram of the laboratory model brushless, directdrive system is given in figure 1. In operation d-c power is supplied to an inverter which is mounted on the solar array shaft. The a-c output from the inverter drives a rotary transformer which transmits power and signals from the solar array to the The control torque required to rotate the solar array shaft is obtained using a brushless d-c torque motor. The torque motor is controlled in a closed-loop mode corresponding to sunlit operation, and it is controlled open-loop corresponding to dark period control. The motor receives all commands from the control unit, and the control unit responses to appropriate signals from the solar sensor and amplifier (via the rotary transformer), the magnetic sensor, and the control panel. The control panel permits simulation of solar array operation for various orbital conditions. External (or manual) control allows power to be removed from the motor drive circuits and permits movement of the array in either When the "Track" command is given, the motor accelerates slowly up to a pre-determined speed and rotates the array toward proper orientation. As the desired position is approached, the motor slows down to prevent overshooting the target and subsequent perturbations. Once proper orientation is attained the mode of control is changed so that the motor is under direct control of a solar position sensor and the array continues to automatically track the sun. During the dark period of the orbit the sun reference is lost. If no provision were made to maintain motor rotation, reorientation would be required upon leaving the shadow. A feature is incorporated in the controls to maintain orientation of the array toward the sun even in the earth's shadow, so that minimum disturbance is encountered upon



State of the state

Figure 1. - Block Diagram of Brushless Direct-Drive Solar Array Control System

re-entering the sunlight. This is done by collecting the necessary rate information during the sunlit portion of the orbit for use during the dark period.

The laboratory model incorporates some previously developed components. The purpose of Phase II was to develop a working laboratory model of the system. To this end work was done in five different areas: (1) Modification of the electronic commutation circuit of the brushless motor to improve performance, (2) Design and build a 500 watt rotary power transformer with 5 integrated signal sections, (3) Packaging of the system controller, (4) Design and build an inverter (5) Assembly and test of all components into a laboratory model.

The laboratory model construction is shown in figure 2. In the model a light projector pointed at the solar sensors simulates the sun. The solar array is mechanically simulated by the large cylinder which is suspended along with the rotating parts of the motor and the rotary transformer. These parts are balanced with a 45-pound counterweight to simulate a zero-gravity condition. This assembly is free to rotate. The motor and rotary transformer housings are mechanically connected together. The motor housing is mechanically connected through gearing to a pair of small motors mounted to the tripod base. Rotation in either direction of this pair of motors turns the brushless motor housing and thus simulates orbital rotation of the satellite.

# Page Intentionally Left Blank

#### SECTION II

#### CONTROLLER CIRCUIT DESIGN

Work performed in Phase I was the design and building of breadboard circuits of a controller and system testing to prove feasibility.

The solar array reorientation system is intended primarily for use on earth-pointing, passively-stabilized spacecraft such as gravity-gradient stabilized satellites. reorientation system is to be a brushless direct-drive system without gears or slip rings, capable of operating in a singleaxis mode. The system is to consist of a solar array to convert solar energy to electric energy, a rotary transformerinverter assembly for transmitting electric power to the satellite by brushless means, a brushless dc motor incorporating rate and position sensing for direct drive of the array, and a control system to maintain orientation of the array relative to the sun. The rotary transformer-inverter, brushless dc torque motor, and magnetic rotor-position-and-rate sensor have been developed on earlier NSAS in-house and contractual programs. To complete the reorientation system, the controller is required. Work on the present phase of the contract included controller circuit design, building of breadboard circuits and system performance testing using a simulated array, but excluding the rotating transformer.

The function of the controller is to control operation of the brushless motor to maintain the solar array in a sun-oriented position at all times. When the satellite is in sunlight, the tracking error may be determined directly from photovoltaic sensors and used to control movement of the motor. Control of other modes of operation which are required are not as straightforward. Orientation during the dark portion of an orbit and reorientation from a large misalignment require limiting of the motor speed.

The magnetic sensor is designed with an offset-tooth configuration so that there is always one voltage available which changes linearly with motor rotation, as described in reference l. Comparison of this sensor signal with a controlled input voltage can, therefore, be used as an error detector on a continuous angular basis. The idea of using the linearly changing signal from the offset-tooth sensor to achieve continuous angular position and rate control was first presented by L. J. Veillette of GSFC. This principle is employed in the reorientation control system described in this report in preference to a "run and coast" scheme initially considered.

Circuit diagrams showing functional blocks are referred to throughout the discussion section of the report. A composite of the functional circuits is provided in figure 34 showing all circuits and values used in the design of the controller other than the dark period control shown in figure 22.

#### DISCUSSION

#### OPERATING MODES

There are four distinct modes of operation required of the solar array reorientation system. Two of these modes may occur during each orbit: (1) normal tracking during the sunlit period and (2) programmed tracking during the dark portion of the orbit. When a large error exists, a speed-limited reorientation mode is required to restore the sunlit array to its proper position. The fourth mode required, which takes precedence over all other modes, is the external command mode which, on command, allows the array to be moved to any desired position at a controlled rate or to be stopped.

## Normal Tracking Mode

The normal tracking mode of operation takes place during the sunlit portion of the orbit when the signal from the solar sensor is less than a predetermined value. In this mode the drive motor responds to two signals derived from the solar sensor: (1) a speed-torque signal and (2) a direction signal. The speed-torque signal varies in magnitude with the magnitude of the alignment error, having a null at the zero-error point. The direction of the alignment error determines the direction signal which responds to polarity of the difference in signal magnitude of two adjacent solar sensors.

## Dark Period Operation

When the spacecraft moves into the shadow of the earth, the control signal from the solar sensors disappears and a shadown signal, SH, appears. The position reference for normal tracking during the dark period, a substitute signal must be provided to the motor. It is necessary that a reference signal be received from the spacecraft. This reference is used to determine the motor speed. The control acts to maintain the average motor speed at the same rate as was present during the normal tracking mode.

## Large Error Reorientation

If the position of the array is off target by a large amount, as may be the case after launch, it is desirable to orient the array in a relatively short period of time. This would require a speed much greater than that during normal tracking. As the array approaches proper orientation, however, it is desirable that the speed decrease to a value approaching the normal tracking speed to reduce overshoot and minimize undesirable reaction between the array and the spacecraft. Speed control is, therefore, employed in the control or reorientation from large errors.

#### External Control

External control may be gained at any time regardless of the operating mode in command. Three external commands are applicable in this mode, external forward EXF, external reverse EXTR, and standby. An additional signal required is a speed signal, which is a pulse train, a direct substitute for the dark period control signal. The motor speed will respond to the pulse frequency, thus the speed may be controlled to any value desired. Thus, speed control is accomplished exactly as in the dark period control mode.

## Mode Selection (Motor Drive Direction Logic

The direction of the motor rotation can be controlled only by introduction of one of two signals, FWD or REV. In the normal tracking mode, forward or reverse signals to the motor are merely a function of the direction of the error signal. A positive error signal, for example, always applies a torque which tends to drive the motor in a forward direction.

In all other modes of operation, however, the motor speed is controlled and the direction of rotation is preprogrammed. The speed control circuit supplies a signal which tells whether the motor lags behind the commanded position or leads it. Thus, the speed control can supply direction information relative to the commanded direction. When the commanded direction is forward, for example, a lag condition from the speed control provides a forward (acceleration) signal to the motor, while a lead condition provides a reverse (braking) signal to the motor. The opposite is true for a reverse-commanded direction.

In the logic diagram, shown at the bottom of figure 17, the command direction signals, EXF, STF or SF, are used in conjunction with the LAG signal to produce the output signal, FWD. In the external command mode, either EXF and LAG or the absence of

both produce an output, FWD. This same relation is provided between STF and LAG and between SF and LAG, so that either pair of signals, when not inhibited by other conditions, can produce a FWD output signal. The signals STF and LAG are inhibited under all operating conditions except for the dark-period mode, i.e., there is no external command EX and a shadow signal SH exists. Likewise, the signals SF and LAG are inhibited for all conditions other than the large-error reorientation mode, where a speed limit signal SL exists, but there is no external command EX, and no shadow signal, SH.

The normal tracking mode is indicated by the signal N which exists unless any of three conditions are present: (1) shadow, SH, (2) external command, EX, or (3) speed limit, SL. In this mode the signal SF determines the motor direction.

It will be noted in figure 17 that a STANDBY command overrides all motor direction commands by causing both FWD and REV to turn off.

#### REORIENTATION SYSTEM OPERATION

Two basic operational control methods are used in the reorientation system. The first, and by far the simplest, is a
position control wherein the solar sensors look at the sun and
give signals, depending upon the magnitude and direction of the
misalignment of the solar array. The system response to such
a signal is that the motor runs in the direction that will reduce the magnitude of the signal to zero. Rotation of the spacecraft which tends to increase misalignment also tends to increase the restoring signal, which causes the motor to run at
whatever speed is necessary to maintain a minimal error. This
method is used in the sunlit normal tracking mode.

The second method, used in all other operating modes, is one of speed control. Speed is controlled through use of magnetic sensors incorporated in the motor. Output voltages from the magnetic sensors vary as a function of motor position. Thus, motor position data, in combination with a function of time, are used as speed data for the control of motor speed.

A functional block diagram, figure 1, shows the main functions of the control and the primary signal flow routes. In the normal tracking mode, only the blocks in the upper portion of the figure are active. The signal is received from the solar sensors, amplified and fed to the motor control. Also, the dark-period control collects speed data from the magnetic sensor processing circuit to be used later.

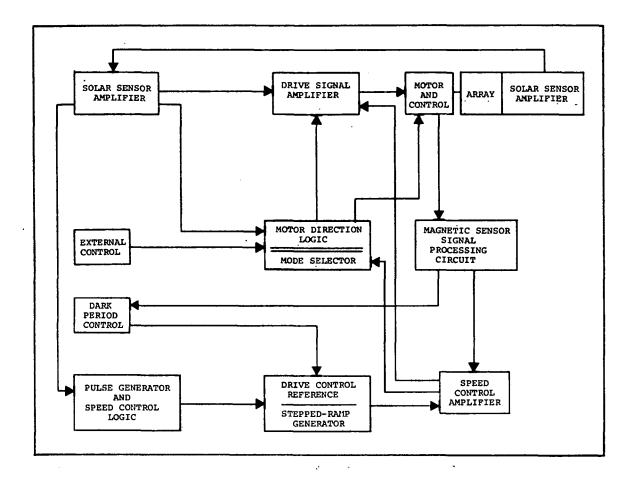


Figure 1. - Functional Block Diagram

The dark-period control takes over upon leaving sunlight and supplies the signal to the stepped-ramp generator as shown in figure 1. The speed control amplifier compares the stepped ramp to the magnetic sensor signal and supplies the motor drive signals through the motor direction logic and the drive signal amplifier.

During reorientation from a large error, the signal from the solar sensor amplifier is supplied to the pulse generator and speed control logic which in turn supplies the signal for the stepped-ramp generator, figure 1. Signals are processed in the same manner as in the dark period.

Also shown in figure 1, the external control supplies signals directly to the motor direction logic which controls the motor in response to the external control signals.

## Solar Sensor Signal

Development. - Signals for tracking and reorientation are developed by the solar sensors. These signals indicate the position of the solar array relative to the sun. Figure 2 shows the arrangement of the solar sensors. Four similar sensors are mounted at 90 degree intervals on the axis of the motor shaft. sensor system incorporates a shadow fin extending along the zeroerror vector for the purpose of increasing the sensitivity of the tracking error signal. When the solar array is perfectly aligned, sensors No. 1 and No. 4 are both in view of the sun, at an angle of incidence of 45 degrees, figure 2(A). Both sensors have the same signal strength so that sensing their difference gives a null, indicating zero error. As the array is misaligned, the shadow fin casts a shadow on one of the sensors, reducing its signal strength to zero during a small rotation as illustrated in figure 2(B). The difference in signal strength thus increases rapidly providing a strong error signal. The sensitivity of the error signal depends on the length of the shadow fin relative to the diameter of the sensor. Sensors No. 2 and No. 3 are shaded during normal tracking, but provide an output when the error is greater than 45 degrees.

Each pair of solar sensors is connected in parallel. Sensors No. 1 and No. 2 provide a signal for counterclockwise errors, while sensors No. 3 and No. 4 provide the clockwise error signal. The output signals derived from the solar sensors are depicted in figure 3 for counterclockwise errors. The outputs for sensors No. 1 and No. 2 are shown in their relative positions. The outputs of sensors No. 4 and No. 3 (not shown) are symmetrical about zero on the error angle coordinate. The parallel connection of the solar sensors provides a composite signal equal to the sum of the individual signals. Two composite signal equal to the sum of the individual signals. Two composite signals are thus processed by preamplifiers to give outputs  $E_{\rm CC}$  and  $E_{\rm CW}$ . A difference amplifier provides the signal  $(E_{\rm CC}-E_{\rm CW})$ , shown in figure 3(B). The magnitude of this signal is used to control the array position in the normal tracking mode, where the error is less than 2 degrees.

The signal used to control the motor speed during large error reorientation is shown in figure 3(C). The signal covers almost the entire error range, increasing from zero near the maximum error point (180°) to maximum strength at 90 degree error, and falling to zero near the zero-error point, where the normal tracking mode automatically takes control. As the error is reduced toward zero, the motor will slow down because the control signal is reduced toward zero.

Signal processing circuits. - The five signal processing circuits are described below.

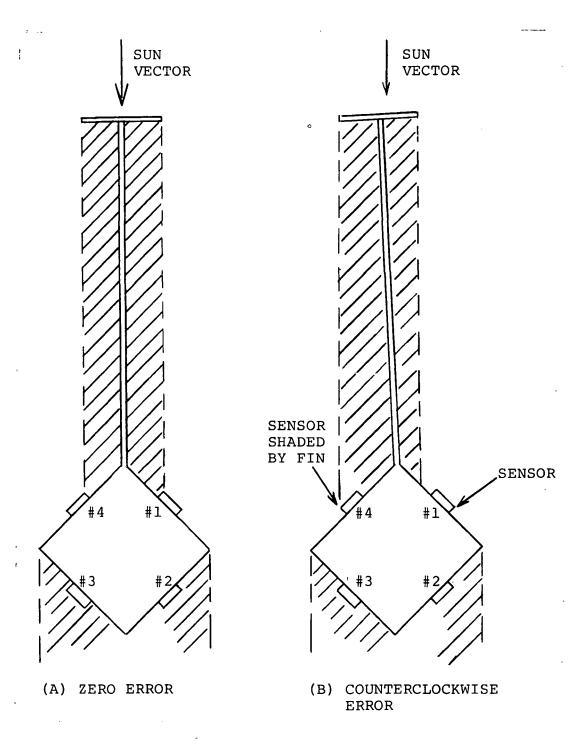


Figure 2. - Solar Sensor System Arrangement

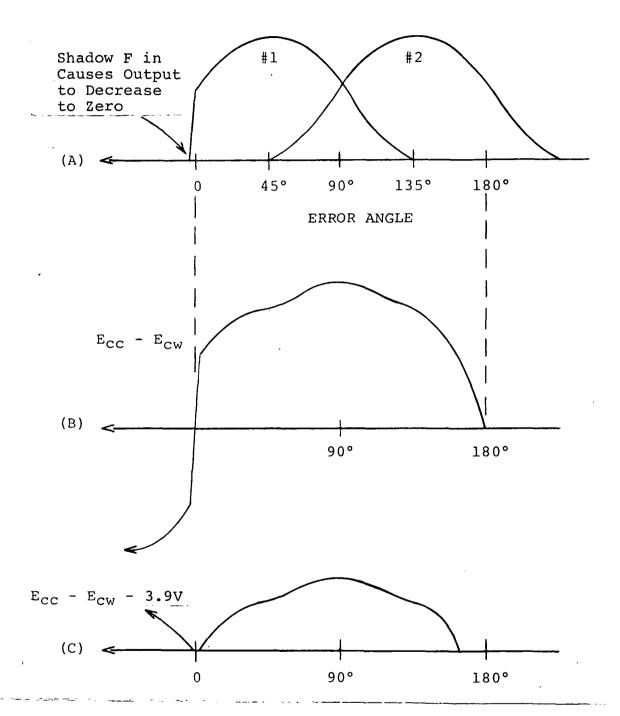


Figure 3. - Solar Sensor Signals

Solar sensor preamplifier: Solar sensors No. 1 and No. 2 are connected in parallel and sense a counterclockwise position error of the array. The sensor output is fed directly to the input terminals of an operational amplifier, as shown in figure 4(A). The operational amplifier, through its feedback resistor, acts to adjust its output voltage so that its differential input voltage is near zero. The sensor thus operates into a short circuit which gives a linear response with variation in light intensity. The output voltage level relative to input current is determined by the value of resistors connected to the amplifier inputs. The value chosen results in an amplification of approximately 32 millivolts per microampere. Thus, an error signal of 100 microamperes from the sensor provides a voltage,  $E_{\rm CC}$ , of 3.2 volts. The preaplifier for solar sensors No. 3 and No. 4 uses the same circuit, The preamfigure 4(B), and the same calibration, but senses clockwise errors. The sensors are connected so that both  $E_{CC}$  and  $E_{CW}$ , are used to provide sensing for 1) the logic signal SH, 2) the normal tracking mode speed signal, and, 3) the direction-sensing comparator, SF.

Difference amplifier  $(E_{CC}-E_{CW})$ , figure 4(C): The preamplifier outputs  $E_{CC}$  and  $E_{CW}$  are supplied to an operational amplifier connected as a difference amplifier. With this connection, the output voltage is equal to the ratio of the feedback resistance to the input resistance times the difference in input voltages, approximately 1.34  $(E_{CC}-E_{CW})$ . Variations in the magnitudes of  $E_{CC}$  and  $E_{CW}$  cause the output to vary both positively and negatively, depending on which of  $E_{CC}$  or  $E_{CW}$  is greater.

Error signal rectification  $|E_{CC}-E_{CW}|$ : The motor speed control operates from a positive signal only, as does the voltage-to-pulse converter stage which supplies the motor speed signal. The signal voltage,  $(E_{CC}-E_{CW})$ , must therefore be rectified. This is accomplished by an operational amplifier circuit. Connected through a resistor and diode network as shown in figure 4(D), the operational amplifier acts as a voltage follower when the input voltage is positive, and as an inverting amplifier when the input is negative. The resulting output voltage is always positive, approximately the absolute value of the input. Because of the forward voltage drop in the diodes, a dead zone occurs in the output when the input is less than 0.3 volt, which is desirable.

Signal transfer switch, figure 4(E): The motor speed control signal must be applied by alternate routes depending on the system operating mode. The signal  $|E_{CC}-E_{CW}|$ , is transferred to the motor control ( $V_O$ ) through a resistor and an isolating diode when its control transistor is off, indicating the normal tracking mode.

Voltage-to-pulse-converter, figure 5: The motor speed control signal is converted to pulses in the circuit of figure 5.

15

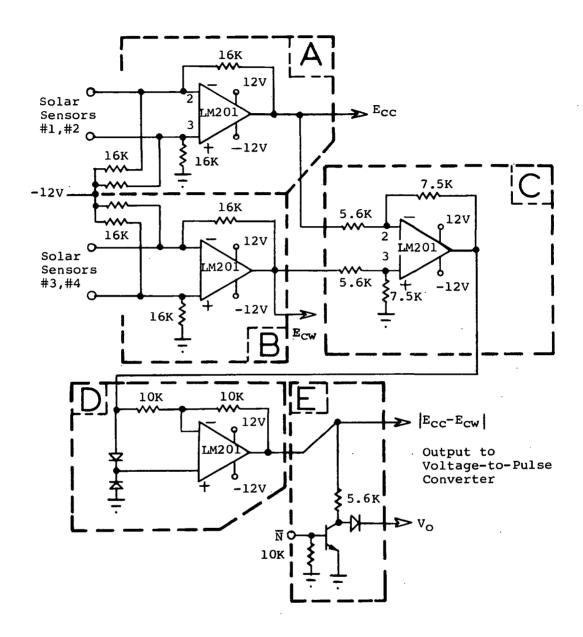
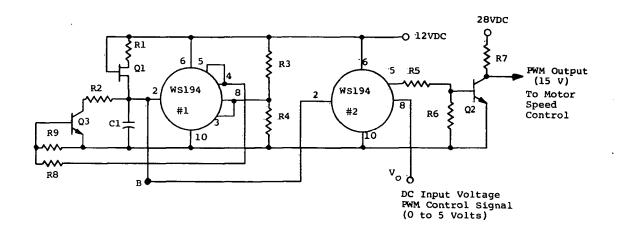


Figure 4. - Solar Sensor Signal Processing Circuit



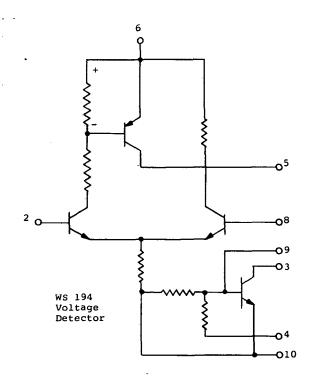


Figure 5. - Voltage-to-Pulse-Width Converter

The pulse rate is fixed by a ramp generator while the pulse width is determined by the voltage level of the input signal,  $V_0$ . A ramp voltage is generated by charging capacitor Cl from a constant current source consisting of Rl and Ql, a field effect transistor. The WS 194, No. 1 compares the capacitor voltage to the fixed reference voltage at pin 8. Whenever the capacitor voltage exceeds that of the reference, the capacitor is discharged through R2 and transistor Q3. Note that during capacitor discharge, the voltage applied to pin 8 is reduced to approximately 0.3 volt.

The WS 194, No. 2 compares the input signal at pin 8 to the generated ramp voltage (from B) at pin 2. So long as B, the ramp voltage, is less than the signal level, transistor Q2 is turned off and an output signal is available to the motor from the 28-volt source through R7. When the ramp voltage gets larger than the dc reference, Q2 is turned on and short circuits the output signal. The output signal therefore, has a pulse width which varies in proporation to the dc level.

## Speed Control Method

Description. - A magnetic sensor, which supplies signals to the motor commutation control, is provided as an integral part of the motor. Variation in sensor output voltages repeats each 45 degrees of rotation of the motor. The sensor outputs are variable-amplitude ac square-wave voltages, which are rectified and filtered for use in motor speed control. The variable amplitude envelopes of the six magnetic sensor signals are phase displaced 7.5 degrees in position. The positive half of the envelopes, as shown in figure 6, are used for speed control. The sensor voltages may be used as produced, (and discussed in quarterly reports), but a much more useful wave form is obtained by summing three adjacent sensor voltages. This produces a waveform symmetrical about its half-amplitude as shown in figure 7.

If the middle half of one side of these sensor signals are sampled in a sequence ABC while the motor is turned at a constant speed, a saw-tooth voltage waveform which rises linearly is obtained. Sampling the opposite sides gives a falling saw-tooth waveform. These waveforms are illustrated in figure 8 by the bold portion of the curves. By selecting the proper sensor signal then, a motor-position signal of constant volts-per-degree rotation is obtained. Such a signal may be compared to a time-varying, saw-tooth wave to derive a useful error signal for controlling motor speed.

<sup>&</sup>lt;sup>1</sup>See references 1 and 2 of Bibliography.

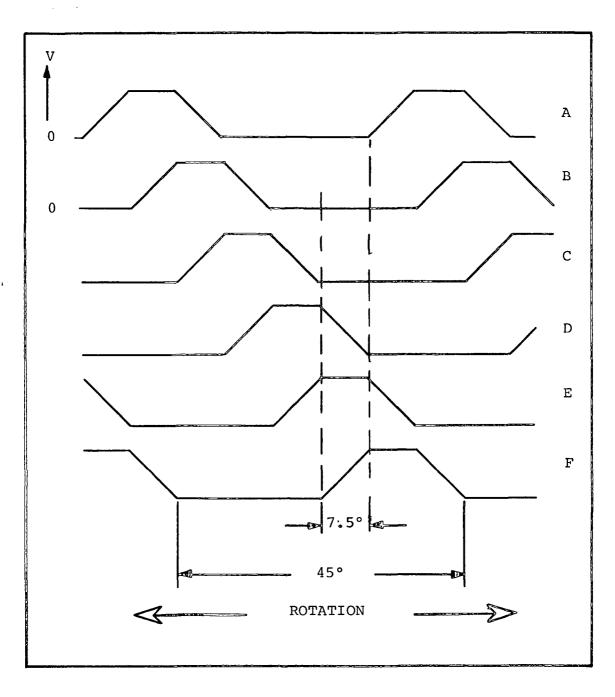


Figure 6. - Magnetic Sensor Output Signals (Rectified Envelopes)

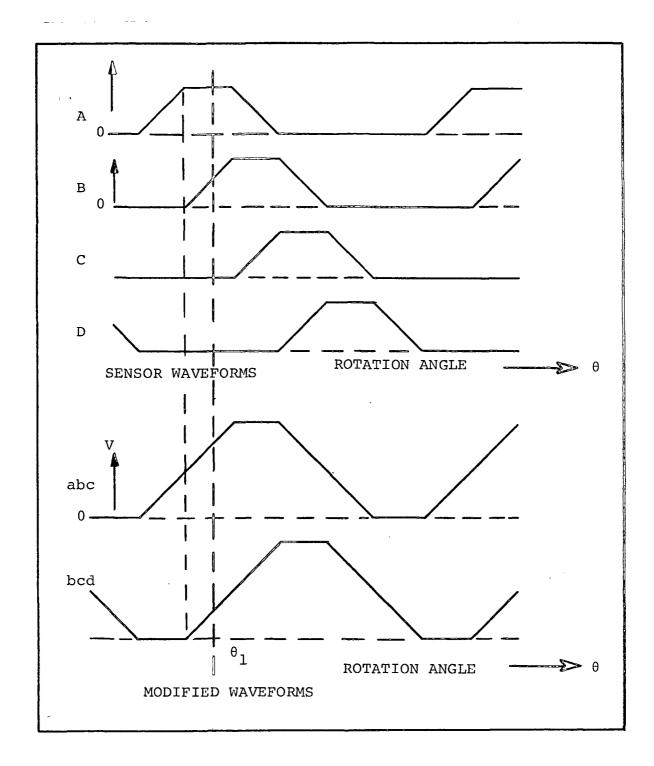


Figure 7. - Derivation of Waveforms Used in Speed Control Method

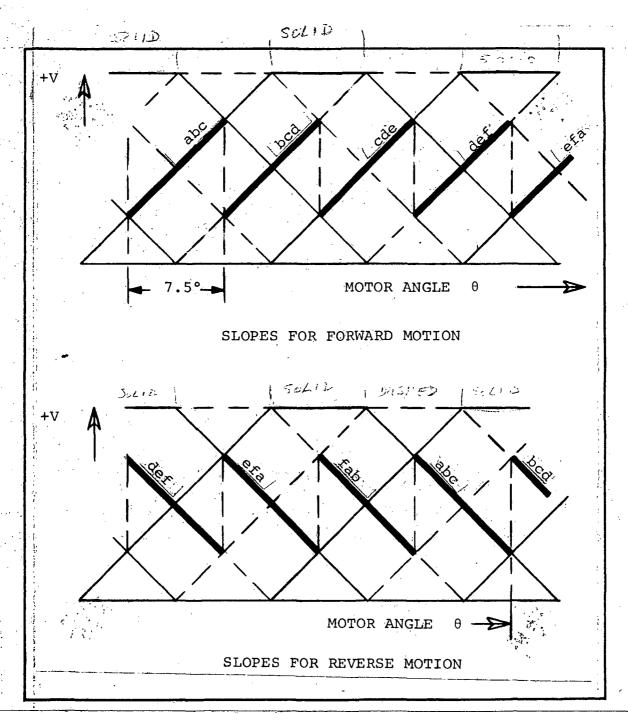


Figure 8. - Superimposed Magnetic Sensor Signals Showing Slopes
Required for Forward and Reverse
Motion Used in Speed Control

Consider the case where the motor is running at a constant speed. The sensor signals from the motor can be visualized as two time-varying, saw-tooth voltages, phase displaced by one-half a period, if we consider only the rising portion of the signals. These are shown as dashed lines in figure 9. A reference saw-tooth voltage, slightly higher in frequency and half

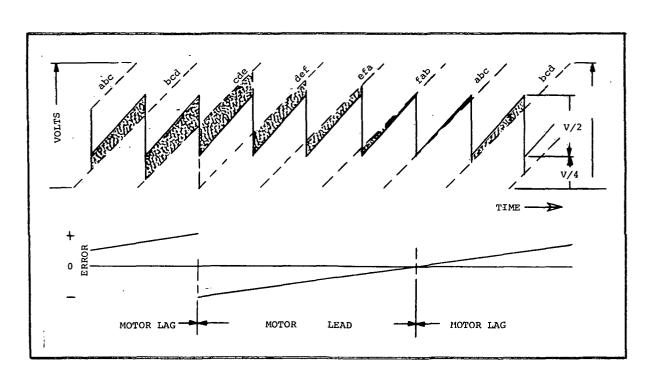


Figure 9. - Illustration of Error Signal Development for Forward Rotation of Motor

the magnitude of the sensor voltage swing is superimposed on the figure. The shaded area between the saw-tooth reference and the sensor signal represents the error voltage that would be generated by monitoring the difference between the two signals. The error is also plotted separately. The left side of figure 9 shows a positive error signal which indicates that the motor lags the reference ramp (saw-tooth wave). As time passes, a discontinuity occurs in the error signal which means that the error has exceeded the control limit. At this point the error becomes negative, indicating that the motor leads the reference ramp. As time goes on, the higher frequency reference

ramp catches up with the sensor signals, reducing the error signal to zero. Once more the motor lags the reference ramp, producing a positive error signal. If the error signal were applied to the motor drive system, it would cause the motor to speed up when the error were positive so as to reduce the error signal. If, conversely, the error signal were negative, the motor would slow down, likewise reducing the error signal.

To produce the error signal for use as a speed-controlled drive signal, the following rules apply to its fabrication:

- (1) Only one composite magnetic sensor signal may be on at one time.
- (2) The sensor signal is selected at the beginning of each period of the reference ramp.
- (3) The sensor signal must increase if the motor turns in the commanded direction.
- (4) The magnitude of the sensor signal, when selected, must be less than approximately half its maximum.
- (5) The sensor signal must stay on until a new selection is made at the beginning of a new ramp period.
- (6) The reference ramp voltage must have a peak-to-peak magnitude equal to the difference between two adjacent rising sensor signals (half the maximum sensor signal) and centered between maximum and minimum sensor voltages.

Magnetic sensor signal selection circuit for speed control. - The magnetic sensor signal, which is selected for use at any time, appears at a point referred to on the circuit diagrams of this report as BUS. The logic circuit for developing the signal, BUS, is shown in figures 10 and 11. The circuit consists of six identical interconnected channels, one for each magnetic sensor signal. One channel is shown in figure 11. The output from a resistor-summing junction which sums three adjacent sensor voltages is fed to BUS through an isolating diode when the control transistor is controlled by a NAND gate flip-flop.

To analyze operation of the sensor selection logic, refer to figure 7 and assume the motor position is  $\theta_1$ . The comparator signals A', B', C', etc. (see figure 12) are in the high state when A is greater than D, B is greater than E, and C is greater than F, etc. Assume a forward command (FW=1, FW'=1) when the reference ramp starts and produces signals T and T', both of which are pulses, T being of much longer duration. The signal T' trips all six flip-flops to assure that only one

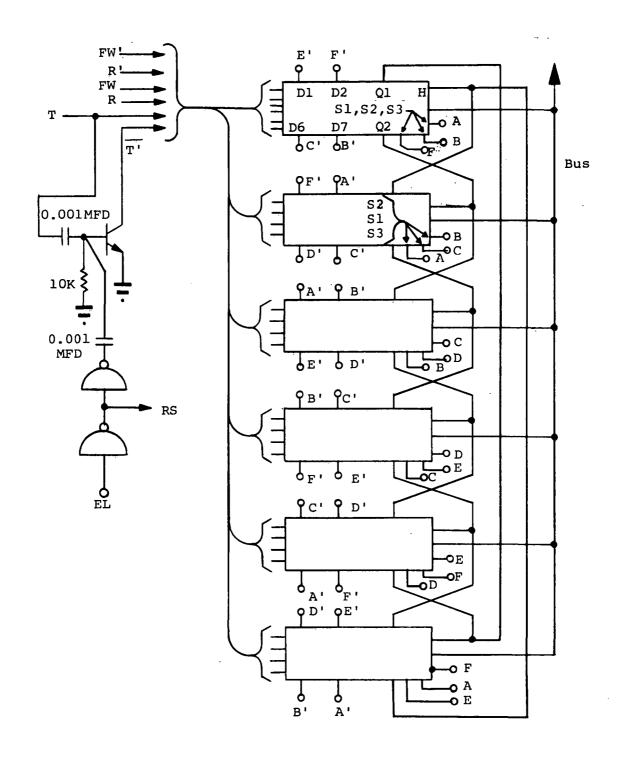


Figure 10. - Connection of Six Channels for Drive Logic and Magnetic Sensor Reference

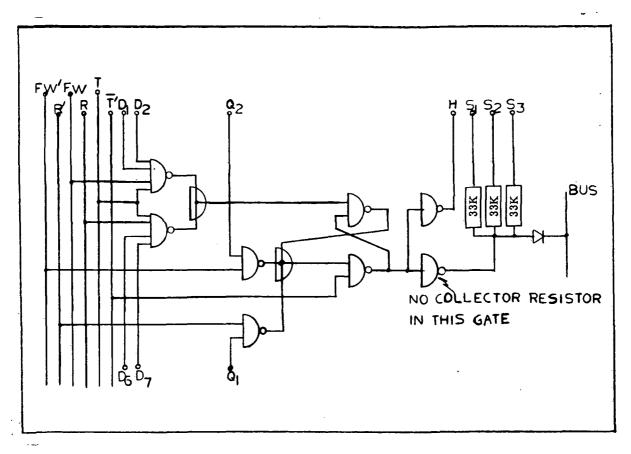


Figure 11. - Drive Logic and Magnetic Sensor Reference One Channel

channel can be connected to BUS at one time. Logic signals A', B', and F' are high (F not shown in figure). In figure 10, the second and third channels receive signals at terminals  $D_1$  and  $D_2$ . (Terminals  $D_6$  and  $D_7$  need not be considered because R=0.) Both the second and third channels are turned on as soon as T' disappears, and a signal appears at terminal H of both channels. Signals appear at terminal  $Q_2$  of the second channel and at  $Q_1$  of the third channel. Since FW'=1, the signal at  $Q_2$  immediately trips out the second channel and leaves the third channel to supply the signal to BUS. Thus the signal bcd is selected in agreement with the rules set down.

Reference ramp. - The extremely low speeds at which the motor must operate requires a very low frequency reference ramp for speed control. The speed range demands ramp frequencies of about 12 ramps per minute to as low as two ramps per hour. It is, therefore, logical to use a digital approach, fabricating a stepped ramp rather than a continuous one. To do this, a pulse counter operates into a resistor network such that each input

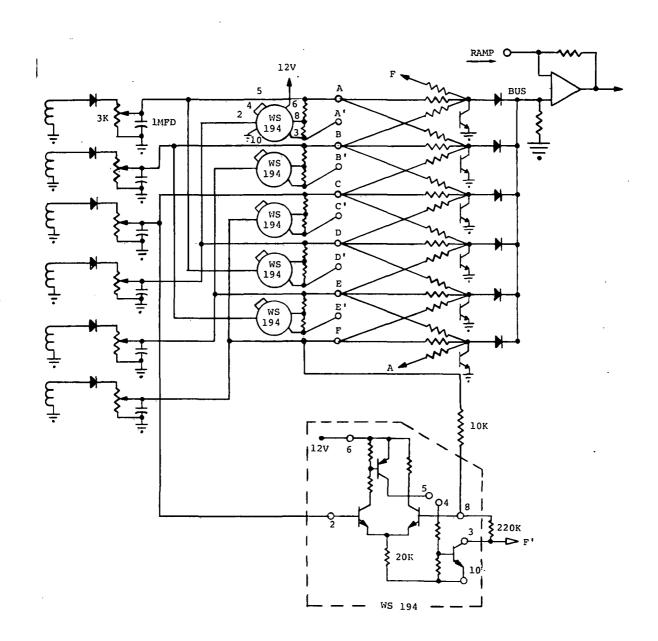


Figure 12. - Magnetic Sensor Signal Processing Circuit

pulse raises the voltage at the output terminal of the resistor network by one step. The average rate of rise of the ramp and thus its frequency is, therefore, controlled by the input pulse frequency. The counter selected for the system produces a 16-step ramp. Each step drives the motor slightly less than 0.5 degree. More steps could be used if finer motor control is desired.

The circuit for the ramp generator is shown in figure 13. The circuit consists of four binary counters (WM 213G) connected

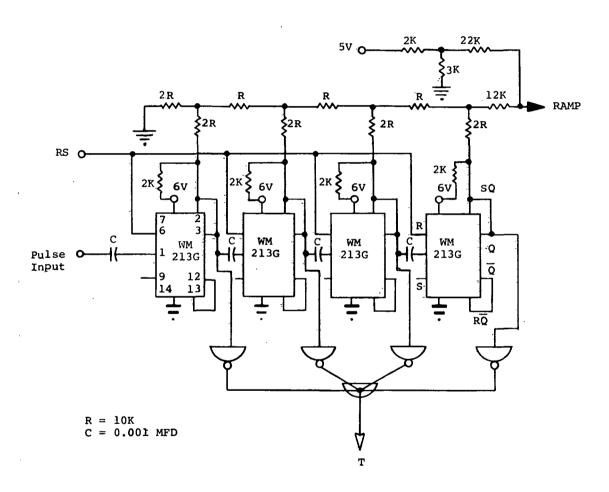


Figure 13. - Speed Reference Ramp Generator

serially and operating into a resistor network. Each counter changes state when the input signal goes from high to low, but is not affected by a rising signal. The first stage receives the unit pulse and changes state with the fall of each pulse.

The second stage receives a signal from the first stage, and changes state each time the first stage output goes low. larly, the third and fourth stages change state when the output of the previous stage goes low. Thus, the first stage counts units, the second counts two's, the third four's, and the fourth The resistor network is designed so that each stage, eight's. when on, contributes twice the voltage at the ramp output as does the previous stage. Input to the network from the counters is either approximately six volts or zero. The network presents a constant resistance as viewed from the output terminal. resistance represents an input resistance of the operational amplifier in the following stage, figure 14. The output of the counter is connected to a summing junction so that the output The output of the signal, RAMP, is the sum of the counter output and a fixed refer-The fixed reference is used to center the reference ramp between maximum and minimum voltage of the magnetic sensor output as shown in figure 9.

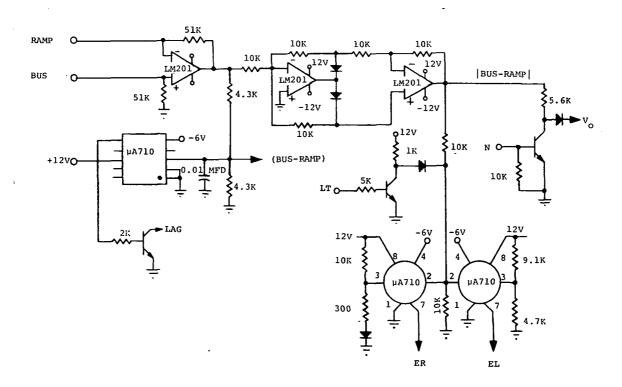


Figure 14. - Speed Control Amplifier Circuit

A logic circuit is included in figure 13, the output (T) of which signals the beginning of a new ramp. This signal is used to trigger the drive logic of figure 10.

Speed control - output stage (figure 14). - To make use of the two derived signals, BUS and RAMP, it is necessary to derive the difference between the two. This is done by means of an operational amplifier connected as a difference amplifier. The output signal is rectified and transmitted to the motor speed control.

A comparator ( $\mu A$  710) is used to detect the polarity of the difference amplifier. A positive output indicates that the reference ramp signal (RAMP) is greater than the magnetic sensor reference (BUS) and thus the motor lags its command signal. The motor is, therefore, driven in the commanded direction because of the presence of the comparator signal (LAG). Should the motor be driven too fast, the difference amplifier output would become negative and the comparator signal (LAG) would go to zero, causing the motor to get a reverse command and slow down.

The fact that the reference ramp is generated by means of discrete pulses makes the speed control, in reality, a position control when operating at orbital rotational speeds. At these very low speeds, each pulse provides a signal causing the motor to turn just enough to reduce the signal below its threshold. The motor comes to a stop at a stable position where it remains until another pulse (seconds or minutes later) causes an error signal to be developed to drive the motor through another increment.

Operation in the upper end of the speed range, as during reorientation of the array, is somewhat different. In this case, the inertia of the array and the speed are great enough to cause the array to coast through the zero-torque areas with little change in speed. Once steady-state speed is reached, the system rotates rather smoothly.

Speed control pulse generation. - Inasmuch as motor operating speed is controlled by incremental rotational response of the motor to a stepped-ramp signal, it is necessary to convert the speed-control signal to a pulse train. The frequency of the pulse train determines the motor speed. A pulse generator having a pulse frequency proportional to its input signal level is, therefore, required. Figure 15 shows the circuit of the pulse generator, which consists of an operational amplifier connected as an integrator, and a unijunction transistor (UJT) used as a pulse

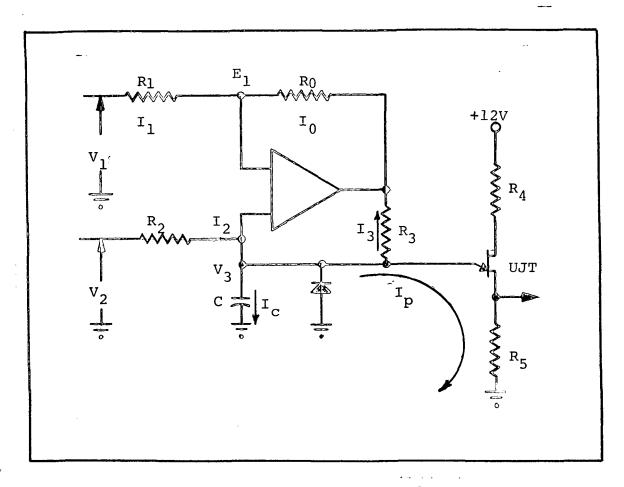


Figure 15. - Voltage-to-Frequency Pulse Generator

trigger. If the pulse current, Ip, is neglected in figure 15 the equation for capacitor voltage may be developed as

$$v_3 = \frac{1}{R_2C} \int_0^t (v_2 - v_1) dt$$

where

$$R_1/R_2 = R_0/R_3.$$

The capacitor voltage,  $V_3$ , rises until it reaches the voltage determined by the intrinsic standoff ratio of the UJT. At this point the UJT turns on, applying the capacitor voltage across R5, the output point. The capacitor discharge current,  $I_p$ , flows through  $R_5$  until the UJT emitter voltage falls to the valley point where the UJT turns off. The integrator circuit then

starts a new charge cycle. Thus, the output pulse frequency is determined by the charge time constant,  $R_2C$ , and the UJT characteristic, and varies with the input signal voltage. A diode connected across the capacitor serves to prevent saturation of the operational amplifier when the input signal is negative.

An important feature which is used in the control circuit should be noted. The input circuit to the operational amplifier may be replaced by its Thevenin equivalent, utilizing any number of voltage sources desired. By so doing, summing junctions are formed so that input signals may be added together. The pulse generator as used in the reorientation system is shown in figure 16. Several system functions are performed by varying input voltage and capacitance as will be seen in later discussions.

## Large-Error Reorientation

When the position of the array is off target by a large amount, as may be the case after launch, it is desirable to orient the array in a relatively short period of time. This requires a speed much greater than that during normal tracking. As the array approaches proper orientation, however, it is desirable that the speed decrease to a value approaching the normal tracking speed to reduce overshoot and minimize undesirable reaction between the array and the spacecraft. Speed control is, therefore, employed in the control of reorientation from large errors.

Acceleration from rest. - When the array starts from rest at some arbitrary position the difference in the two control signals, BUS and RAMP, may be at any value within their range, unless special provisions are made to prevent it. A large difference in these signals at the beginning of reorientation produces a relatively high rate of acceleration of the array and subsequent oscillation in array speed. On the other hand, if the initial signal difference is small, the acceleration is low and speed builds up smoothly. It is, therefore, desirable to start the reorientation cycle with as small a difference signal, |BUS-RAMP|, as possible.

With normal speed control logic, the magnetic sensor voltage selected in the fabrication of the signal, BUS, has a magnitude between zero and half the maximum value. The signal, RAMP, may have any value between one-fourth and three-fourths of the maximum sensor voltage. The chances are 50 percent then, that BUS will be below the minimum value of RAMP, and thus it may not be possible to obtain the small error signal desired by varying RAMP.

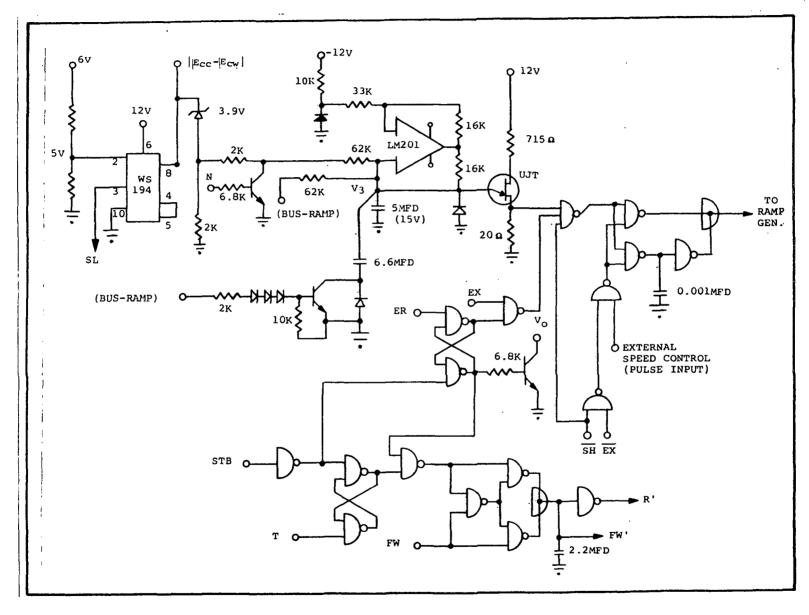


Figure 16. - Acceleration and Speed Control Circuit

To assure that a minimum difference in BUS and RAMP can be obtained, a special control is included which selects the magnetic sensor next in reverse normal sequence. After the selection has been made the special control is disabled. The signal, BUS, then will be at a level between the maximum sensor voltage and one-half maximum. When the reorientation cycle is started, the counter is reset and made to count. This causes RAMP to start at its minimum value and increase by steps until it reaches If the level of BUS is greater than the maxithe level of BUS. mum level of RAMP, the counter counts through a full cycle and The reset causes the normal selection of a magnetic sensor voltage, reducing BUS to a level within the range of RAMP. As the counter continues, RAMP again increases from its minimum level to the level of BUS. Once this level is reached, the speed control signal is applied to the motor, starting acceleration.

Reorientation starts from standby: It is assumed that the control system will be in the standby condition when the space-craft is launched. In addition, external commands, forward, reverse, and track should be preceded by the standby command. This assures that the reorientation operation starts from the standby condition, which sets up control for proper acceleration of the array.

The primary function of the standby command is to remove power from the motor. This is accomplished by removing both FWD and REV signals from the motor control terminals (see figure 17). The result is to stop the oscillator in the motor commutation control, which in turn de-energizes the magnetic sensors. Consequently, the signal, BUS, (figure 10) goes to zero, and since RAMP is always substantially greater than zero, the signal, |BUS-RAMP|, (figure 14) goes to its maximum value, causing the two comparators to turn on, producing signals ER and EL. The error-limit signal, EL, resets the ramp generator counter so that RAMP goes to its minimum value. At the same time a signal T' is produced which resets the magnetic sensor logic (figure 10).

The signal ER is produced when |BUS-RAMP| is slightly greater than the normal level during reorientation. The purpose of ER is to prevent acceleration of the array until the controls have reduced |BUS-RAMP| to an acceptable value for starting reorientation.

Starting circuit (see figure 16): The logic circuit for performing the special control function of starting the reorientation cycle is shown in figure 16. When the system is in STAND-BY, logic signals STB, T, ER, and EX are high. Two significant results are obtained in this condition: (1) the transistor is turned on making the motor drive signal,  $V_{\rm O}=0$ , and (2) the direction signal is reversed, FW' =  $\overline{\rm FW}$ . The system remains at

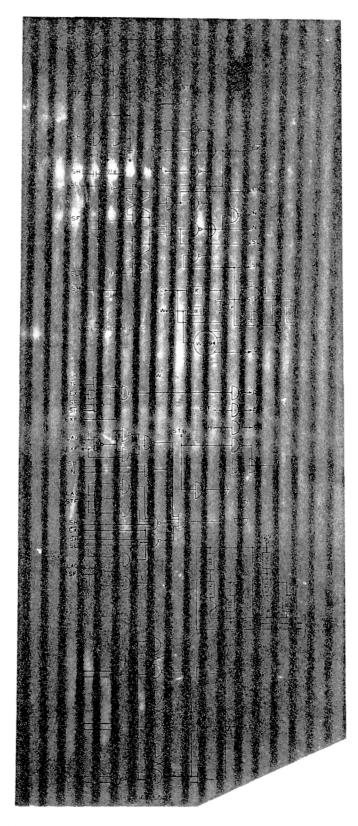


Figure 17. - Logic Circuits for Mode Selection and Transition

rest so long as this condition exists. The counter is not counting because the magnetic sensors are not energized in STANDBY, causing the signal (BUS-RAMP) to be at maximum negative voltage. Consequently, the pulse generator has no output to the counter.

The reorientation cycle is actuated by transferring the external command from STANDBY to TRACK. Logic signals STB and EX go low. The magnetic sensor voltages rise to normal. The drive logic makes the selection of the magnetic sensor voltage. Since the signals FW' and R' are at this point opposite the normal direction signals FW and R, the selection sequence is reversed (see figures 10 and 11 for logic), assuring that BUS is greater than RAMP. The signal (BUS-RAMP) thus becomes positive and the pulse generator resumes operation causing the counter to increase RAMP, unless the spacecraft is in the shadow. At the first count, T goes low, releasing the latch causing FW' to change state so This returns the magnetic sensor selection logic that FW' = FW. to normal. Note that the motor drive signal  $V_{\rm O}$  is still short circuited by the transistor and remains in that state until ER The counter continues until RAMP becomes nearly equal to BUS, at which time the error signal |BUS-RAMP| is low enough to cause ER to go low, and release the latch holding the transistor on. When the transistor turns off,  $V_{\rm O}$  assumes the value of BUS-RAMP, to which the motor now responds.

Speed-controlled reorientation. - Speed-controlled reorientation is described below.

Speed determined by pulse rate: The speed at which the solar array moves toward proper orientation depends on the rate at which pulses reach the counter. The pulse rate of the pulse generator is primarily a function of the solar sensor signal strength. When the solar sensor signal is first applied, the motor speed is zero. Obviously, the motor cannot respond instantaneously, so immediately falls behind its command. The further behind the motor gets, the larger the error signal becomes and the higher the acceleration force. If the motor accelerates the array too rapidly, speed will get higher than the control signal demands. The control then will cause deceleration of the system. Successive acceleration and deceleration will continue until damped out by motor friction which is relatively small.

To minimize the speed oscillation, a feedback signal is employed. The feedback signal is the error between the motor position and the commanded position, BUS-RAMP. The effect of the feedback is to slow down the pulse rate whenever the motor lags behind the position demanded by the speed control and to raise the pulse rate when the motor leads the command. This allows the motor to catch up with the position reference while the pulse rate is low. As the motor catches up, the error signal,

BUS-RAMP, gets smaller and allows the pulse rate to increase. If the motor speeds up more than necessary, the feedback-error signal reverses polarity and increases the pulse rate above normal, thus the motor is allowed to coast down to normal speed without appreciable braking. When the motor is running at the commanded speed, the feedback is negligible and the normal pulse rate drives the motor at normal speed.

Once up to normal speed, the motor runs at a speed proportional to its control signal, such as shown in figure 3(C). As the orientation error approaches zero, the motor speed gradually reduces to zero, following the speed signal.

Speed control circuit: Refer to figure 16 which shows the pulse generator circuit. The solar sensor signal,  $|E_{CC}-E_{CW}|$ , is fed into the non-inverting (+) input of the operational amplifier (LM201) through a 3.9-volt Zener diode. Use of the Zener diode modifies the solar sensor signal figure 3(B) into the speed control signal figure 3(C) so that the speed signal decreases gradually as the proper orientation angle is approached.

The feedback signal, BUS-RAMP, is also applied to the non-inverting input. The resultant signal input is, therefore, the sum of the two signals ( $|E_{CC}-E_{CW}|-3.9$ ) + (BUS-RAMP), and the equivalent input resistance to the operational amplifier is the parallel combination of the individual resistances.

In addition to the capacitor (5 MFD) permanently connected to the operational amplifier, a second capacitor (6.6 MFD) is connected through a transistor when the magnitude of the error |BUS-RAMP| is large. This slows down the charge rate (and thus the pulse rate) during acceleration of the array asisting the feedback and giving the motor more time to catch up with its drive signal.

In figure 16, also note that the inverting (-) input of the operational amplifier is negatively biased by a diode drop. During the final approach to zero-orientation error, the speed control signal, figure 3(C), goes to zero. The function of the negative bias voltage is to cause the pulse generator to continue operation slowly to assure movement of the array to zero reorientation error.

Transfer to normal tracking mode. - The following describes the transfer to the normal tracking mode.

Making a smooth transfer: When the system operates in the sunlit normal tracking mode, the motor drive signal is derived directly from the solar sensor output. The sensor is designed to give a high rate of change in signal strength about the null, figure 3(B).

Suppose the system were being reoriented and the array were approaching zero error. The speed control signal would be also approaching zero. Now suppose that at some small error (one or two degrees) the control were transferred to the normal tracking mode. A large signal,  $E_{\rm CC}-E_{\rm CW}$ , would be applied to the motor control, causing the motor to accelerate. As the array moves to the zero-error position, the error signal would go to zero, but the speed of the array would be substantial and the array would go on past the zero-error point. A restoring signal would then be applied, bringing the motor to a stop and accelerating it in the reverse direction. Thus, an oscillation would be set up. While such an oscillation would be within the normal tracking bank and die out after a few cycles, it is undesirable and can be avoided.

The means for preventing the problem is simply to prevent the initial acceleration upon transfer of the normal tracking mode. By making the system stay in its speed-controlled mode until the array has moved past the zero-error position, the initial force applied upon transfer will be a decelerating force. In addition, the transfer can be controlled to take place when the magnitude of the signal,  $E_{\rm CC}-E_{\rm CW}$ , is low. Thus, reorientation ends in a smooth transition to the normal tracking mode.

The transfer circuit: The logic for the transition is shown in figure 17. Control signals are derived from two conditions: (1) direction and (2) magnitude of the orientation angle. When signal, SF, is high the array is misoriented in a counterclockwise direction ( $E_{CC} > E_{CW}$ ) and forward movement is demanded. When SL (figure 16) is high, the array is misoriented by an appreciable angle as indicated by the magnitude of the solar sensor signal, thus speed-limited control is commanded.

The normal tracking mode is in operation when the signal, N, is high, otherwise the speed control is in effect. From the logic diagram, figure 17, N will be low if there is an external command, EX, or if the system is in the earth's shadow, SH, or if signal SLD is high. During reorientation, there is neither a shadow nor an external command signal, so SLD determines the state of N.

The signal, SLD, is developed any time speed-limited control is indicated by SLl which is high when either SL or STANDBY is high. The signals SLl and SF operate into two flip-flops producing the output, SLD, any time SLl is high, regardless of the state of SF. The flip-flops remain latched-up after SLl goes low, until SF changes state and causes SLD to go low, which in turn produces the signal N.

The result is that the system operates in a speed-controlled manner until the orientation error has been reduced to zero. Since the array is brought to proper orientation of a controlled speed, overshoot and oscillation are negligible.

# Dark Period Speed Control

When the spacecraft moves into the shadow of the earth, the control signal from the solar sensors disappears and a shadow signal, SH, appears. The position reference for normal tracking is thus lost. A substitute signal must therefore be provided to the motor to maintain tracking during the dark period. The method available for control in the dark period is the speed-controlled method of operation described previously in the paragraph entitled "Speed Control Method".

It is assumed that the spacecraft orbit is circular. Thus, a sun-oriented array mounted on an earth-oriented spacecraft turns at a constant average speed. The problem of dark-period control is essentially one of supplying a series of pulses at the proper rate to drive the motor at the same average speed as that in sunlight. Allied problems involve the transient conditions encountered when entering and exiting the shadow.

Speed-control pulse requirements. - Recall from the discussion on the speed control method section "Reorientation System Operation", "Speed Control Method", paragraph "Description", several facts concerning the magnetic sensor signals, and the signal, RAMP.

- (1) The sensor signal repeats each 45 degrees of motor rotation.
- (2) There are six sensor signals each of which are sampled in sequence during 7.5-degree increments of motor rotation.
  - (3) The signal, RAMP, varies in amplitude in 16 increments.

The speed control causes the motor to move 7.5 degrees for each cycle of the signal, RAMP, which requires 16 pulses. Thus, during a complete cycle of one magnetic sensor signal, 96 pulses are required. The problem of speed control during the dark period is to produce pulses at the rate of 96 pulses in the time required for 45 degrees of rotation.

Assume that a pulse source of constant frequency is available to be used as a timing reference. Suppose that while the space-craft orbits in sunlight in the normal tracking mode, the number of pulses produced by the reference source during 45 degrees of

rotation is counted. Call this number n. Now, suppose the system is operated by the speed-controlled method at the same average speed. Since 96 pulses are required to drive the motor 45 degrees, there are n/96 reference-source pulses developed for each speed-control pulse. The digital control employed in the speed-controlled method makes it possible, therefore, to make use of a pulse-counting system to maintain accurate position control of the array during the dark period. Knowing the number of source pulses per control pulse, one can design a counter to give a control pulse each time the proper number of source pulses is counted.

A hypothetical case. - A simplified block diagram of a dark-period control is shown in figure 18. During a selected 45-degree interval of rotation in sunlight, the reference pulse, P, is transmitted to counter No. 1 which counts 96 pulses, resets, and repeats the count. Counter No. 2 counts the number of times counter No. 1 counts a complete cycle of 96 pulses. If n pulses, P, are developed during the 45 degree rotation, then counter No. 2 will contain the number n/96 at the end of the 45-degree rotation. This number represents the average interval between output-control pulses in terms of source pulses. The number n/96 in counter No. 2 is stored in a memory as a reference during dark-period control.

Entering the shadow allows the source pulse, P, to be transmitted to counter No. 3. The number in counter No. 3 is compared to that in the memory (n/96). When the two numbers become equal, the comparator puts out a pulse to the speed control and resets counter No. 3 to zero. The counting continues, each time counting n/96 source pulses. Thus, the time interval between output pulses is determined by the number (n/96) stored in the memory, and is of the proper timing to drive the motor at the same rate as in sunlight.

One of the main considerations in the design of the counting system for dark-period control is the required accuracy. In the system of figure 18, it will be noted that the number left in counter No. 1 at the end of the 45-degree counting period is disregarded in determining the output pulse interval. The number stored in memory is thus an integer which may have an error of one. For example, assume that the number of source pulses, P, during the 45-degree counting period were 1055. Counter No. 1 would count through ten times, and have a count of (1055-960) = 95 at the end of the period. The number 10 would be stored in the memory, while the fraction 95/96 is dropped. The error is, therefore, almost 10 percent.

To achieve a tracking accuracy of two degrees requires that the dark-period control hold the average speed to within approximately 0.5 percent. This means that the minimum number required

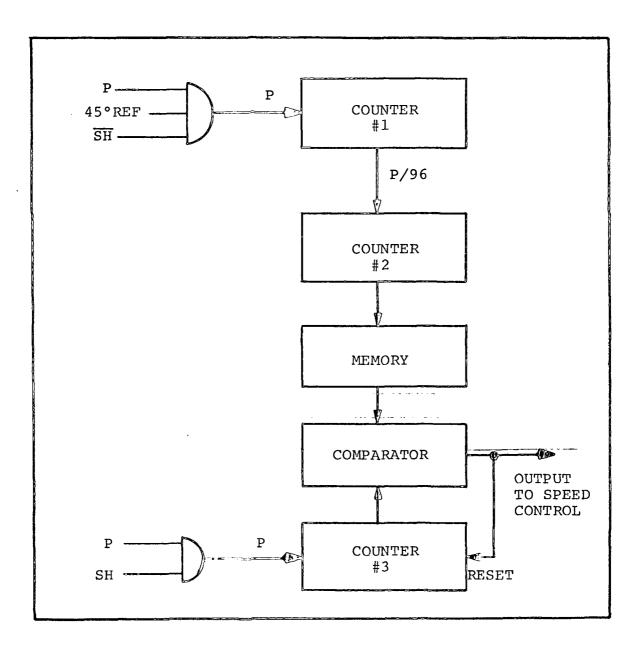


Figure 18. - Block Diagram for Simplified Conceptual Dark-Period Speed Control

in memory be 200. This requires an eight-stage binary counter and memory, with a capacity of 256.

The number of source pulses per 45 degrees rotation is a function of source frequency and of the orbital altitude. For example, suppose a source-pulse frequency is chosen to generate the reference number 200 at the minimum 90-minute orbit. Suppose further it is desired to use the same pulse frequency at a 24-hour orbit. The pulse-counting time is increased by a factor of 16. This requires an additional four stages in counter No. 2 and memory as well as in counter No. 3.

It is recognized that the functions of counter No. 2 and counter No. 3 may be combined since these counters are used at different times. In a practical circuit, a further reduction in counter stages can be made by making use of the most significant stages of counter No. 1, to develop a fractional remainder which can be added to the integer number generated by counter No. 2.

A practical control scheme. - The counting system designed for the dark-period control uses the integer and remainder concept, and thereby requires a lower frequency pulse rate than otherwise necessary. A block diagram of the system used is shown in figure 19. The diagram is shown in two parts for simplicity. Figure 19(A) shows only those functions necessary during the sunlit portion of the orbit. Although the logic functions are not shown, at the beginning of each 45-degree rotation period, the contents of counters Y and Z are transferred to the memory and all counters are reset to zero. The source pulses, P, are counted until the end of the 45-degree period. At the beginning of each new 45-degree period, the memory is updated by the contents of counters Y and Z. The total count of counter Z is the integer number n/96. The final count in counter Y represents the numerator of the fractional portion to be added to the integral number n/96. In this design, counter Y consists of four binary stages and contains the remainder fraction to the nearest 1/16 at the end of each counting period.

Figure 19(B) shows the connections of the counters after the spacecraft has gone into the shadow. The counters are initially reset to zero and source pulses are transmitted simultaneously to both counters Y and Z. Counting continues until the number in counter Z equals that in memory Y, at which point comparator Y senses the equality, and gives a "stop" signal to a flip-flop. The flip-flop output inhibits further pulses, P, reaching counter Y which holds its last count until a "start" signal is received by the flip-flop. Counter Z continues to count until its number becomes equal to that of memory Z, at which point comparator Z senses the equality and gives an output pulse. The output pulse

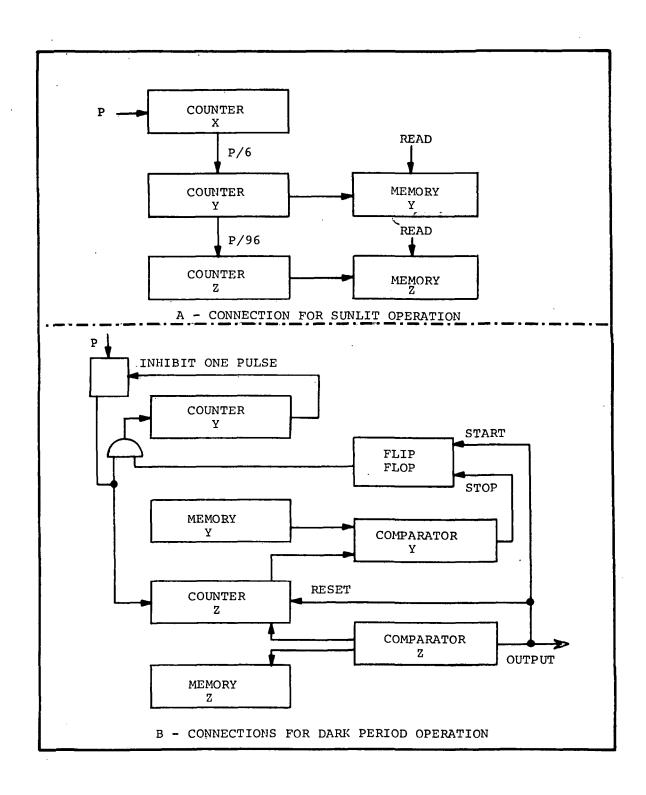


Figure 19. - Block Diagram of Dark-Period Speed Control

is sent to the motor control causing approximately 0.47 degree rotation. In addition, the output pulse resets counter Z to zero and sets the flip-flop to "start". Counter Y resumes counting with the next pulse, P, while counter Z continues from zero. Counting continues as in the previous cycle until counter Y reaches its full count (15) and resets to zero. On the reset pulse, an inhibit signal is applied at the pulse, P, input point. The next pulse P merely removes the inhibit condition but does not get through to the counters. With the inhibit command removed, subsequent pulses, P, are transmitted normally until counter Y once again completes its full count.

The result of operating the counters in this manner is perhaps best explained by numerical example. Assume that the average number of source pulses per output pulse were 18-34/96, for example. The total number of source pulses counted during the 45-degree counting period would be  $96 \times 18-34/96 = 1762$ . The number would be distributed among counters X, Y, and Z as follows at the end of the period.

- (1) Counter Z = 18
- (2) Counter Y = 30/96 = 5/16
- (3) Counter X = 4/96

The contents of counters Y and Z are stored in memories Y and Z, while counter X is disregarded. The counters are set to zero and counting begins. On each of the first three passes (or counting cycles of counter Z), counter Y counts five pulses and stops while counter Z counts 18 pulses and gives an output pulse. On the fourth pass, counter Y receives its 16th pulse and resets, preventing the next pulse from reaching either counters. Thus, 19 pulses are required to drive counter Z to its reset point on the fourth pass. Note, however, that counter Y counts five pulses as usual. Similar action continues through 16 passes. The result is that five times during each 16 passes, one extra pulse is required to complete the count of counter Z. A running score on the counters is tabulated below for 16 passes.

PASS	NUMBER IN COUNTER Y	INHIBIT PULSE	SOURCE PULSES PER OUTPUT PULSE					
1	5	0	18					
2	10	0	18					
3	15	0	18					
4	4	1	19					
5	9	0	18					
6	14	0	18					
7	3	1	19					

PASS	NUMBER IN COUNTER Y	INHIBIT PULSE	SOURCE PULSES PER OUTPUT PULSE	]
8	8	0	18	
9	13	0	18	
10	2	1	19	
11	7	0	18	
12	12	0	18	
13	1	1	19	
14	6	0	18	
15	11	0	18	
16	0	1	19	

As seen in the table, the average number of pulses per output pulse is 18-5/16 for 16 passes. Also note that the extra pulses are distributed as evenly as possible, which gives minimum variation in the average speed.

The minimum number of source pulses per output pulse which can be reliably used with this counting method is equal to the storage capacity of memory Y, which is 16 in this design. The maximum error that can be developed in the average output-pulse interval is therefore 1/16 part in 16, or 0.39 percent.

The logic circuit. - Logic circuit diagrams for the dark-period control are shown in figures 20, 21, and 22. The basic control elements are the pulse counter (WC213D) and the NAND gate. A single counting stage is shown in figure 20. The output, Q, changes state each time the input pulse at C goes to the zero state. The output, Q, goes to the zero state at any time the reset, R, goes to the zero state. The counter output may be transferred to the memory flip-flop only when so commanded by the signal GO which is normally in the zero state. The comparator output is in the high state only when the signal at X is the same as the output of the memory.

The counters, memories, and comparators Y and Z are made up of single stages, interconnected as shown in figure 21. The counters are serially connected as binary counters. The comparators are completed by connection of the single-stage comparators to NAND gates. Thus, a comparator output is possible only when all stages of the comparator are in the high state.

The logic circuit for the complete dark-period control is shown in figure 22. It shows, in addition to the basic counting functions shown in figure 19, the control functions necessary for operation in the proper mode. When operating in sunlight, the signal  $\overline{SH}$  is high and  $\overline{SH}$  is low. The signal P, a function of the input pulse, is transmitted only to counter X, which gives one

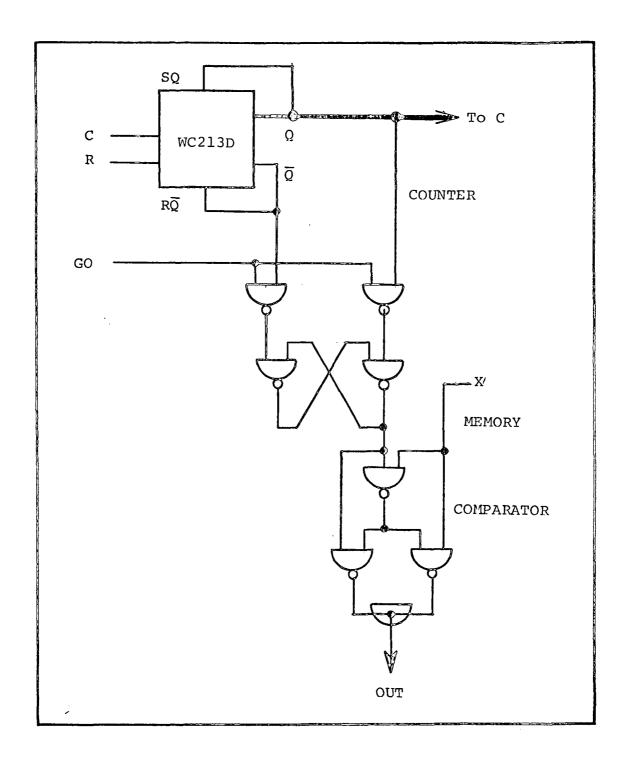


Figure 20. - Logic Diagram for Single Stage of Counter,
Memory and Comparator for
Dark-Period Speed Control

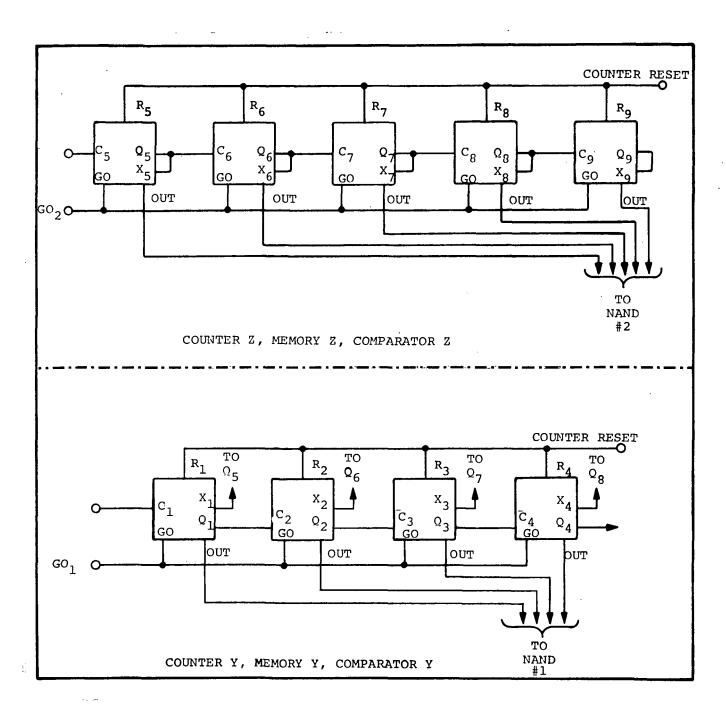


Figure 21. - Interstage Connections for Counters, Etc.

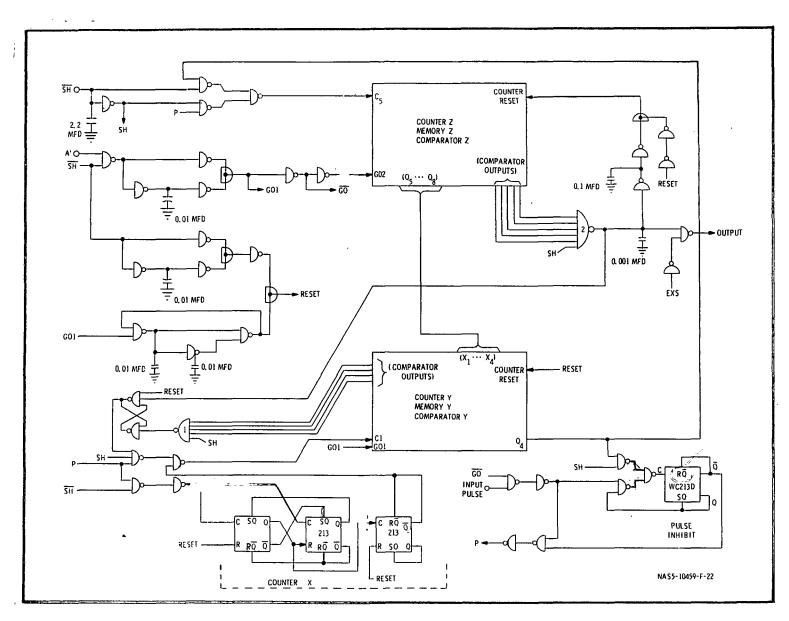


Figure 22. - Dark-Period Control Logic Circuit

Output pulse for each six input pulses. This output is transmitted through a NAND gate to counter Y which requires 16 pulses at Cl to produce one output pulse. The output of counter Y is transmitted through two NAND gates to counter Z. The capacity of counter Z must be great enough to hold 1/96 of the maximum number of pulses generated during 45-degree rotation of the motor. Five stages are used in counter Z which is the minimum number required in this design.

During operation in sunlight, the only function of the controls is to develop a speed reference. The signal A' is high when magnetic sensor A has an output greater than that of sensor D. Thus, A' controls the counting interval to 45 degrees of rotation of the motor. In figure 22, it may be seen that A' operates into a pulse-forming circuit.

A pulse is formed at GOl when A' goes to the high state. (When A' goes low there is no effect on GOl.) The signals GOl and GO2 cause the contents of counters Y and Z to be transferred to the memories. The pulse GOl also operates into a second pulse-forming circuit, the output of which is a counter-reset signal. The signal, RESET, which is normally high is delayed in going low until the signal GOl has gone low. This assures that the numbers in the counters at the end of a 45-degree interval are transferred to the memories before the counters are reset to zero. Once reset, the counters begin counting a new set of data during the next 45-degree interval. In this way, the speed reference is periodically updated during sunlit operation.

Going into the shadow causes the signal  $\overline{SH}$  to go low and SH high. This causes the pulse, P, to be rerouted from counter X directly to counters Y and Z. Thus, counters Y and Z count in parallel and counter X no longer counts. Also, the signal  $\overline{SH}$  is applied to a pulse-forming circuit, which provides a negative going pulse at RESET, so that counting begins from zero. In addition, enable signals, SH, are provided for the comparators and for the pulse inhibit circuit.

Starting at zero, both counters Y and Z count until the number in memory Y is reached. Comparator Y senses this condition and NAND gate No. 1 latches a flip-flop which then inhibits P being transmitted to counter Y. Counter Z continues to count until the number in counter Z matches that in memory Z, at which point comparator Z gives an output via NAND gate No. 2. Besides providing an output for motor operation, counter Z is reset to zero and the flip-flop inhibiting pulses to counter Y is reset, so that counter Y resumes counting. This cycle of operation is repeated until counter Y reaches its full count and the output at Q4 falls to zero. This causes the signal at C on the pulse-inhibit counter to fall to zero, changing the state of the output, Q, from low to high, and  $\overline{Q}$  from high to low. The next input

46. --

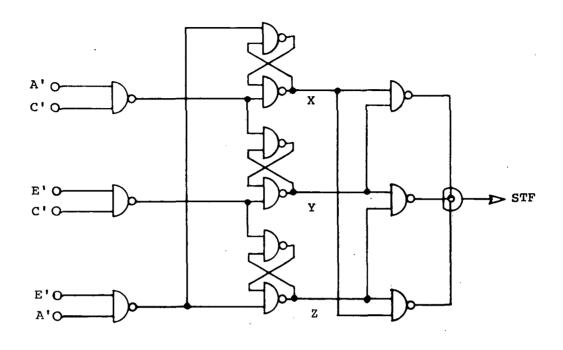
pulse cannot get through the NAND gate to P because it is inhibited by the zero state of  $\overline{\mathbb{Q}}$ . The high state of  $\mathbb{Q}$ , however, allows the input pulse to reach C on the pulse-inhibit counter. When the input pulse returns to zero, the counter once again changes its output state, and subsequent pulses are routed directly to P without effect on pulse-inhibit counter. One input pulse has thus been rejected and the interval between output control pulses increased by one count.

The return of the satellite to sunlight merely reconnects the counters serially and inhibits output pulses. No attempt is made to preserve the reference numbers in memory, as they are regenerated within the next 90 degrees of rotation.

Entering the shadow. - While the reorientation system is operating in the sunlit normal tracking mode, the speed control, of course, is not in operation, and thus the magnitude of (BUS-RAMP) makes no difference. Once in the shadow, however, the system responds to the signal (BUS-RAMP). It is necessary, then that the controlling signal (BUS-RAMP) be near zero at the time it assumes control, else a tracking error will be immediately introduced.

The magnetic sensor signals continually change during rotation of the motor causing the signal, BUS, to likewise change. To maintain a low error signal (BUS-RAMP), it is necessary to cause a change in the signal RAMP corresponding to the change in BUS during the normal tracking mode. Such a change is accomplished in the control system through the feedback signal used to smooth speed transients during reorientation from large errors. Referring to figure 16, it will be seen that the feedback signal (BUS-RAMP) is the only signal applied to the non-inverting input of the integrating operational amplifier. (In the normal tracking mode the signal, N, operates a transistor, short circuiting the other signal.) When (BUS-RAMP) is positive, its voltage is integrated by the operational amplifier circuit, eventually triggering the unijunction transistor (UJT) which gives a pulse to the ramp generator and raises the signal RAMP. This, in turn, reduces the signal (BUS-RAMP). As motor rotation continues, the signal, BUS, continues to increase, again increasing the feedback signal (BUS-RAMP). Once again the integrating circuit responds as before. In this manner, pulses are supplied to the ramp generator at just the proper rate to cause the signal, RAMP, to follow the signal, BUS. Thus, when the shadow is encountered, the control signal (BUS-RAMP) is near minimum.

It should be noted at this point that the motor-direction control during dark-period operation is determined by the signal, STF, which depends on the direction history. The logic circuit shown in figure 23 requires a rotation of 7.5 to 15 degrees after



IN	<b>199</b>		Ε'				Α¹			A		<b>₹</b>		E'		<b>EX</b> 2		E'		10
OUT		Δ'	<b>⊗</b>		<u>c'</u>	,	35%		Ε'	3		Cr		3.75		A'		30	U	
x	-	0	0	0	0_	1	1	0_	0	0	1	1	1	1	0	0_	0	0	0	0
Y	ı	0	0	1	1_	0	0	0	0	-0	0	0	1	1	1	1	1	1	1	1
z	ı	1_	1	0	0	0	0	1	1	1	1	1	0	0	1	1	1	1	0	0
STF	ı	1_	1	1	1_	1	1	1	1	1	0	0	0	0	0	0	0	0	1	1
			_	RE	٧ .			_				F	WD	_	-			ļ ;	REV	-

Figure 23. - Direction Logic Circuit

a reversal to change the state of the output signal, STF (see truth table). This means that the system must operate in the normal tracking mode for 15 degrees to assure proper direction control and minimum error signal (BUS-RAMP) upon entering the shadow.

Leaving the shadow. - After the orientation system has operated in the shadow for some time, it is expected that a small error would have accumulated within the normal tolerance. Should the motor drive control be arbitrarily switched to the normal tracking mode, a large restoring signal would be applied to the motor. The reaction would be a tendency to overshoot the zero

error point and oscillate. This is exactly the same problem as discussed in section "Reorientation System Operation", "Large Error Reorientation", paragraph "Transfer to Normal Tracking Mode", concerning the final approach to reorientation from a large error. Since we are dealing with the same problem, we also use the same solution. When the signal, SH, goes low the controls are made to momentarily simulate a large error and a standby condition.

Recall that when the controls are set in the STANDBY command, the magnetic sensors are not energized and that this results in a low signal, BUS. As may be seen in figure 14, the signal, | BUS-RAMP|, is therefore high, and comparators produce signals ER and EL. In addition, STANDBY produces the signals SL1 and STB (see figure 17). Recall also in figure 17 that SL1 causes the controls to be removed from the normal tracking mode (by producing  $\overline{\text{N}})$  until the solar sensor signal SF changes state. When STANDBY is removed, the speed control takes over and moves the array slowly into proper orientation where the normal tracking mode takes over, as discussed in section "Reorientation System Operation", "Large-Error Reorientation", paragraph "Transfer to Normal Tracking Mode".

Simulation of the standby condition upon leaving the shadow may be seen in the upper portion of figure 17 where SH is applied to a pulse-forming circuit, the output of which is normally zero. When SH goes low, the pulse causes LT to go low and STB to go high. In figure 14 the low state of LT turns off a transistor which applies a voltage simulating a high signal, |BUS-RAMP|, at the inputs of two comparators which produce signals, ER and EL. To complete simulation of STANDBY, the signal, SH, is also used to simulate SLl in the center portion of figure 17 where SH is applied through capacitors directly to two flip-flops. When SH goes low, the input to the two flip-flops goes low momentarily, assuring a high output at  $\overline{N}$ .

If, during the dark period, the array were driven a bit too slowly so that the solar sensor signal, SF, comes on in agreement with the stored direction signal, STF, the simulation of standby is omitted. In figure 17  $\overline{SF}$  and STF are applied to a NAND gate comparator which inhibits the pulse when SH goes to zero if SF=STF. The system is thus kept in speed-controlled operation until it catches up and reduces the tracking error to zero. If the simulated standby condition were allowed, the motor would be stopped until RAMP is counted through one cycle. This would increase the tracking error because of this waiting period.

#### **TESTS**

### Performance Testing

Testing of the solar array reorientation system was limited to performance testing of the control system in its various modes of operation. During the course of testing, several modifications were made in the breadboard circuits to improve performance. Particular attention was given to smooth operation to minimize unnecessary accelerations, and to providing a reasonably realistic test setup.

Test setup. - The laboratory test setup was designed to simulate the operating conditions of its intended application. The motor was mounted on a rotatable fixture to simulate the rotation of the spacecraft. The mounting fixture, and thus the motor frame, may be rotated in either direction, driven by an electric motor at speed simulating orbital rotation. The speed is approximately 0.01 rpm, simulating the minimum orbital altitude. It was found that a single drive motor (a small-geared timing motor) allowed a great deal of backlash in the system. A second drive motor was coupled to the rotatable fixture through a gear ratio slightly different from the original. The difference in normal output speeds of the two drive motors took up the backlash so that virtually none was left in the system.

The solar array was simulated by a cylinder having an inertia of approximately five and ten slug feet square. The weight of the cylinder was supported by suspension by a cord from an overhead support. The motor was mounted with its shaft in a vertical position and connected to the simulated array through a sliding coupling so that the motor bearings support only the weight of the rotor assembly.

The solar sensor assembly was mounted on the simulated array such that a view of the light source is available through a vertical angle of 30 degrees or more. The light source used for performance tests was a photographic projector located about four feet from the sensors. A sketch showing the arrangement of the test setup is shown in figure 24. A photograph of the controller breadboard is also included in the figure.

Normal tracking mode. - Tests conducted in the normal tracking mode were primarily observations of steady-state conditions.

The system was set initially so that the output signals of the two pairs of solar sensors were equal when the light source was

turned on. The drive motors were run in a clockwise direction simulating orbital rotation. The drive motors were later reversed. The maximum deviation during this test was ±0.7 degree from the zero-error vector.

Operation was observed during continuous operation in each direction. Movement of the simulated array was so slight that it was very difficult to see. Total variation in position relative to the light source during operation in a single direction was less than 0.1 degree.

Reorientation mode. - Reorientation of the array ordinarily starts from any arbitrary position when the external command is changed from standby to track. Reorientation tests were made using simulated-array inertia of both 5 and 10 slug feet square.

Typical startup characteristics are shown in figures 25 and 26. These tests were made, starting from a 30-degree error, by plotting the angular displacement from the starting point versus time. The speed curves were calculated from the displacementangle data and plotted on the same time scale. Comparison of the two figures shows that the higher inertia array has a slightly higher peak speed and settles down quicker. The speed and displacement are approximately the same for both arrays after nine seconds.

Figures 27, 28, 29, and 30 show typical characteristics of the end of reorientation. In making these tests, reorientation was started at an error of 40 degrees or more and position data versus time were taken starting at the 30-degree error point. Data were taken for both the 5 and the 10 slug feet square arrays approaching from each direction. Here too, the speed curves were calculated from displacement versus time data. It will be noted in all four figures that the array comes to a stop before reaching the zero error point. The reason for this is the slow speed control designed into the circuit to prevent overshoot when reorientation begins at a 4 to 8 degrees error. It will also be noted that the approach from a reverse (ccw) error takes more time than does the approach from a forward (cw) error. The reason for this is the difference in solar sensor characteristics, as there was no attempt made to match them.

A test was made to determine the reorientation time, starting from the maximum error of 180 degrees. Moving in the forward direction, the restoring time was 2-3/4 minutes, while moving in the reverse direction it took 2-1/4 minutes. The time difference was due to the mismatch in solar sensors. In our test setup, the reorientation speed will normally slow down as the projector lamp ages. Therefore, a test made with an old lamp will show a longer reorientation time. The effect on other modes of operation however, is negligible.

Pages 52 + 53

Photomits

Fig 24 - 2 page.

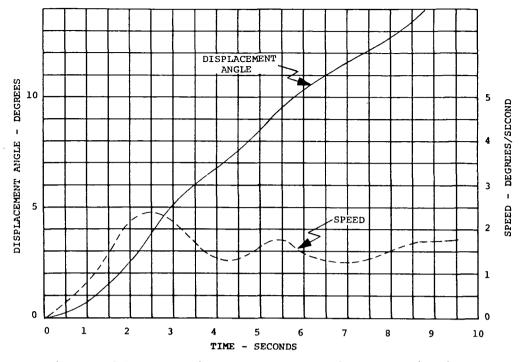


Figure 25. - Typical Start-Up Characteristics.

Displacement Angle and Speed Vs. Time.

Start-Up From Rest at 30° Error.

[5 Slug-ft<sup>2</sup> Array]

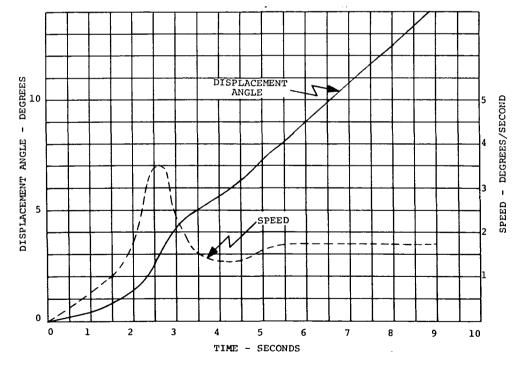


Figure 26. - Typical Start-Up Characteristics.

Displacement Angle and Speed Vs. Time.

Start-Up From Rest at 30° Error.

[10 Slug-ft² Array]

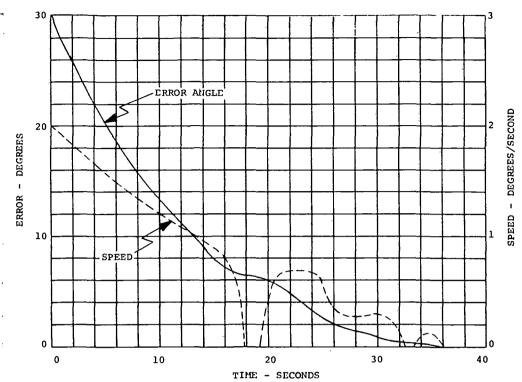


Figure 27. - Array Error and Speed Vs. Time During Final 30° of Reorientation From Large Forward Error [5 Slug-ft<sup>2</sup> Array]

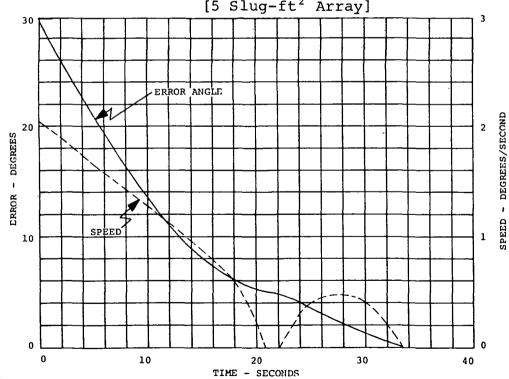


Figure 28. - Array Error and Speed Vs. Time During Final 30° of Reorientation From Large Forward Error [10 Slug-ft<sup>2</sup> Array]

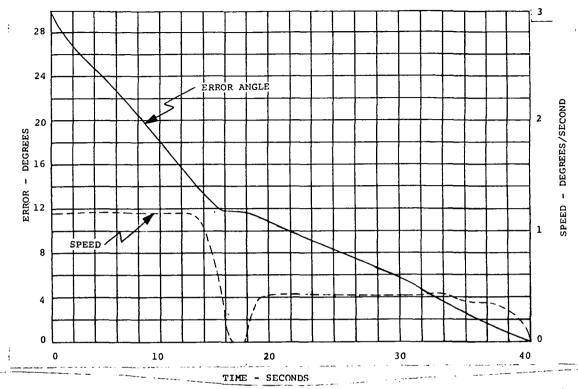


Figure 29. - Array Error and Speed Vs. Time During Final 30° of Reorientation From Large Reverse Error [5 Slug-ft<sup>2</sup> Array]

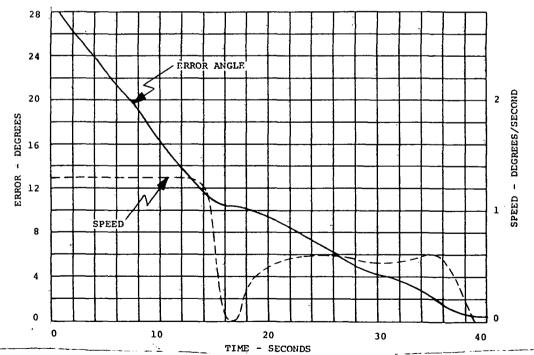


Figure 30. - Array Error and Speed Vs. Time During Final 30° of Reorientation From Large Reverse Error [10 Slug-ft<sup>2</sup> Array]

Dark-period mode. - To test the dark-period tracking control, the reference-pulse source was set at approximately three pulses per second and the system was allowed to track the light source normally during a 45-degree calibration period. The signal A' was monitored to determine the start and finish of the period. (A' goes high at the beginning of each period.) After a full 45degree calibration period was completed, the light was turned off. The position of the array was observed for the next 70 minutes. During this period, the total variation was approximately 1.2 degrees. The error at the beginning of the dark period was 0.7 The maximum error during the period was 1.7 degrees. The accumulated error at the end of the 70-minute period was negligible. During the period, the motor rotated approximately 250 degrees. With each control pulse, the array was moved counter to the rotation of the motor stator, an average of 0.47 degree. The observed variation in increments of movement was approximately one-third to one degree. There are several factors which contribute to this variation: (1) variation in motor "ripple torque" when not energized, (2) non-linearities in the magnetic sensors, non-linearities in the signal, RAMP, (4) mismatch in the magnitudes of RAMP and BUS signals, and (5) possible variation in the reference-pulse frequency.

External control. - External controls incorporated into the system are (1) Track, the normal command for automatic control, (2) Standby, which removes control signals from the motor allowing an idle condition, (3) Forward, which allows forward movement of array on command, (4) Reverse, which allows reverse movement of array on command, and (5) Speed control, a pulse source which determines the average slew rate during manual control.

Tests show that all external control functions operate properly. The standby command overrides all other control functions. When an external pulse is applied, the array is moved an average of 0.47 degree in the commanded direction (Forward or Reverse).

Tests show that best results are obtained if a standby command precedes any other external command. This assures proper initializing of control signals before the specific command takes control. It is recommended that the external control be designed to automatically give a standby command any time the command is changed.

As the system is presently designed, the external speed control is simply a series of pulses. This is satisfactory so long as the pulse rate is low (in the order of one pulse per second or lower). Higher rates may be used if acceleration is considered, i.e. if the pulse rate is increased from zero at a controlled rate so that the array may accelerate and keep up with the external pulses.

An alternative to the external speed control would involve a design change to incorporate the automatic speed control on external command. The acceleration characteristic would then be controlled by the feedback circuit in the same way as in automatic reorientation from a large error. The external speed control signal would be a voltage of adjustable level rather than a pulse train.

#### Functional Tests

Functional tests were made on all circuit functions to determine their operational ability. Most of the circuit functions are logic functions and must operate according to the design intent. Once it was determined that logic circuits were functioning properly, no further functional tests were made.

A few circuits, however, required some adjustment and deserve further comment. These circuits have to operate at particular voltage levels and form interfaces with other circuits external to the controller.

Solar sensor output. - The circuit was designed to operate from a maximum solar sensor output current of 60 to 80 micro-amperes. This level was chosen to be compatible with the light source available. This current range was confirmed by test.

Figure 31 shows the response of the amplifiers of figure 4, used to process the solar sensor signals. The curves show the response to a signal applied from sensors No. 3 and No. 4, operating in parallel while the signal from the other pair of sensors (No. 1 and No. 2) is zero. The output of the first-stage amplifier,  $E_{\rm CW}$ , is a linear function of the solar sensor current, and has an output of 48 millivolts per microampere. (A similar amplifier is used to obtain  $E_{\rm CC}$ .) The output of the second-stage amplifier is the difference signal,  $E_{\rm CW}-E_{\rm CC}$ , amplified by a factor of two. Amplifier saturation limits the maximum output to approximately 8.5 volts.

The response to a signal from sensors No. 1 and No. 2 is the same as shown in figure 31 except that the second stage output,  $2(E_{\text{CW}}-E_{\text{CC}})$ , is negative. When both pairs of solar sensors produce an output, similar characteristics are obtained, where in figure 31 the input current is the difference of currents in the two pairs of sensors and the lower curve represents  $E_{\text{CW}}-E_{\text{CC}}$ .

If the same solar sensors were to be used in direct sunlight it would be necessary to modify the control circuit by changing the feedback resistor in the first stage amplifiers, figures 4(A) and 4(B), to give the proper output voltage to the circuit.

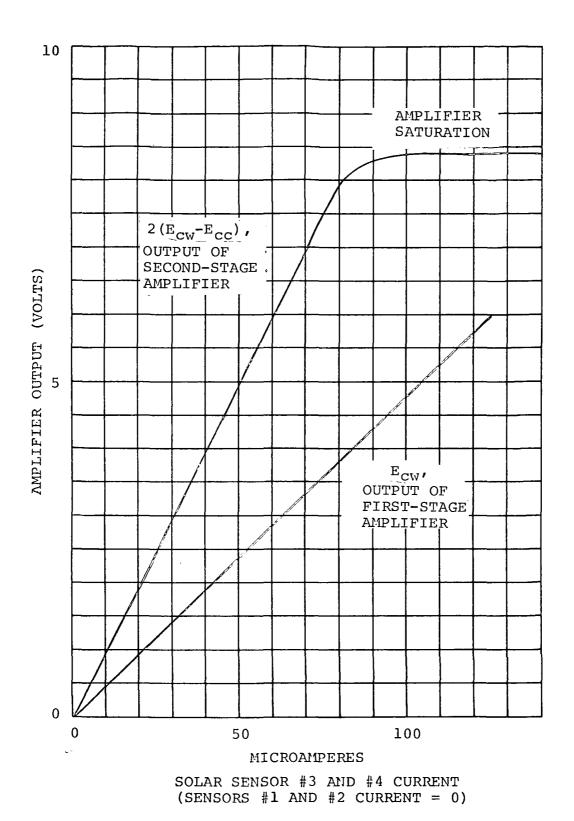


Figure 31. - Solar Sensor Amplifier Output Characteristics

Magnetic sensor output. - A test was made to determine the output characteristics of the magnetic sensor which is part of the motor assembly. Figure 32 shows a plot of the rectified output voltages from the magnetic sensor. The variation in amplitude from phase to phase was considered excessive so that adjusting potentiometers were installed in the breadboard circuit (figure 12). Adjustment was made so that the output of all the signals had approximately equal maximum values. Test results are shown in figure 33, where the maximum output voltages are approximately 8.5 volts. It will be noted also that the variation in slopes and angular position of the curves is slight.

It is important to note that if a different motor were used with the controller, the controller would require adjustment for proper operation. It is, therefore, recommended that in further development a reliable interface be provided by providing the adjustment within the motor commutator circuit.

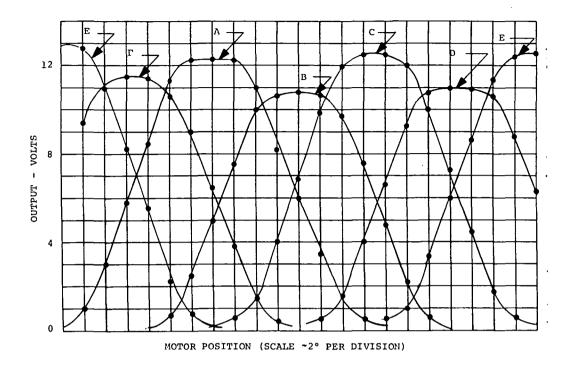


Figure 32. - Rectified Output From Magnetic Sensors

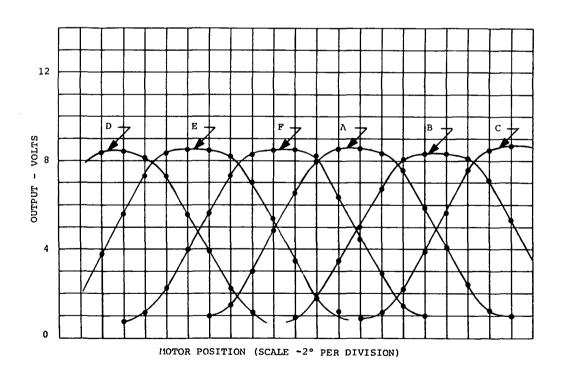


Figure 33. - Modified Output From Magnetic Sensors

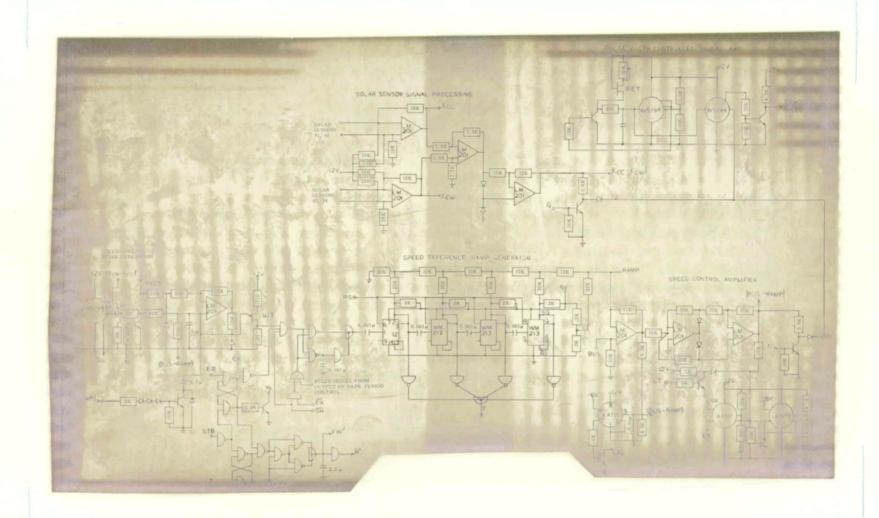


Figure 34. - Solar Array Reorientation System Control Diagram

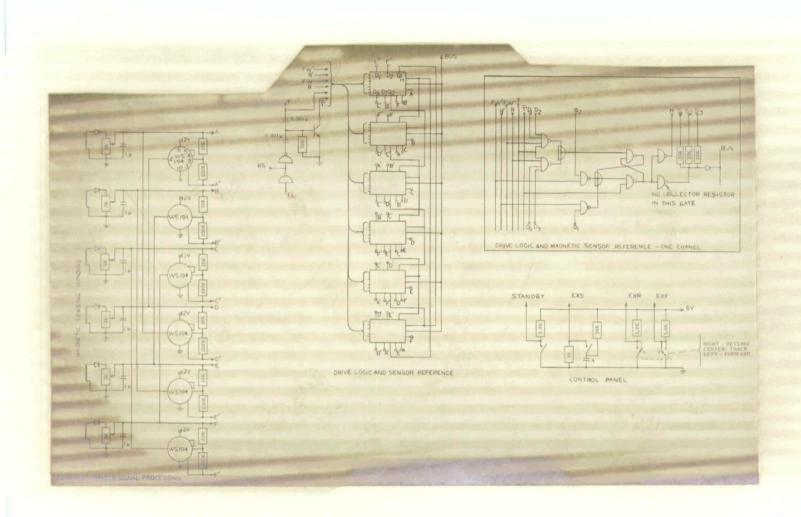


Figure 34. - Continued

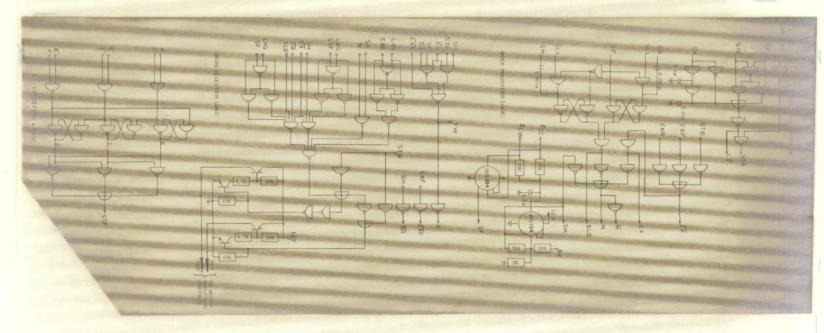


Figure 34. 1 Continued

# GLOSSARY OF LOGIC SIGNAL SYMBOLS

A',B',C', D',E',F' -- Signals corresponding to magnetic sensor output voltages. E.g. A'=1 when A>D, B'=1 when B>E, etc. -- Error limit signal. EL=1 when |BUS-RAMP| ELapproaches the maximum value (8.5 volts). -- Error signal. ER=1 when |BUS-RAMP|>2 volts. ER  $\mathbf{E}\mathbf{X}$ -- Any external command signal. EXF -- External command for forward drive. -- External command for reverse drive. EXR -- Forward command for all speed-limited modes of FW operation. FW' -- A conditional forward command. FW' = FW except at the beginning of acceleration in the reorientation mode. -- The signal to transfer information into memory, GO1, GO2 GO1 = GO2. LAG -- A signal indicating that the motor position lags its command. LT -- A signal used in the transition from dark to light operation -- used to simulate the standby condition. -- The normal tracking mode. Ν P -- The derived pulse used in dark-period control. -- <del>FW</del> R -- <del>FW</del> R¹ RS -- A direct reset signal used to set RAMP to minimum. Т -- Signal indicating that RAMP changes from maximum to minimum. T = 1 when the ramp counter is at count

of zero.

T' -- A pulse which occurs when T turns on, or when EL goes high.

SF -- A forward command from the solar sensors.

SH -- The shadow signal.

SL -- A solar sensor signal indicating a larger than normal tracking error which commands speed-limited control.

SL1 -- SL or STANDBY

SLD -- A signal indicating that SLl is on or has been on and that no change has been indicated in the direction signal SF from the solar sensors.

STB -- Standby or simulated standby.

STF -- A stored signal indicating a history of forward rotation.

#### SECTION III

# D-C TORQUE MOTOR MODIFICATIONS

A brushless dc torque motor, described in appendix IV was developed on Contract NAS 5-10263. Three motors were assembled. The first of these motors was used in the Phase I of the present contract, NAS 5-10459, for system tests. The second motor was transferred to Phase II of the present contract for modification to correct unresolved problems in the electronic controller-commutator of the motor. The third motor was assembled from left-over parts and is not expected to be as good as the second motor. Nevertheless, the controller-commutator of the third motor will be modified to conform to the findings of this study.

The problem areas as discussed in appendix IV are (1) magnetic sensor outputs are unequal and wave form irregular, (2) pulse width of the motor voltage varies as a function of rotor position, and (3) another area, not specifically pointed out as a problem, is torque variation. These problem areas were analyzed and modifications were made to correct the problems.

## DISCUSSION

#### PROBLEM AREAS AND CORRECTIVE ACTION

# Magnetic Sensor

The six output voltages of the magnetic sensor deviated from the intended design as reported in appendix IV. The difficulty is shown in figure 4l of appendix IV where the magnitude of the sensor outputs, which should be equal, are not the same. The outputs, as shown in the figure, are alternately high and low. The second motor was tested and found to follow a similar pattern.

Investigation of the reason for the alternate high-low variation in magnitude led to the magnetic sensor wiring diagram, figure 13 of appendix IV. It will be noted that the number of turns varies from 87 to 109. It was further learned that the magnetic sensor used in the first motor was tested in a fixture external to the motor and adjustments in the number of turns were made to equalize the outputs of the sensors. The results of the adjustment are shown in figure 40 of appendix IV. There

is evidence that the test fixture used was faulty, probably eccentric. Further, the magnetic sensor used in the second motor was wound having the same number of turns as the first. Hence, similar output variations existed in both motors.

Inspection of figure 13 of appendix IV reveals that the lower group of coils have an average of almost 10 percent more turns than do the upper group. Analysis of the sensor does indeed show that alternate sensor outputs would be about 10 percent different in magnitude as shown in figure 41 of appendix IV.

A second variation in magnetic sensor output was also observed. As the motor is rotated the sensor output should repeat eight times per revolution. There is, however, a variation of approximately 5 percent in the maximum value of each sensor output throughout a motor revolution. This variation is evidently caused by eccentricity of the sensor rotor, and no attempt was made to correct it.

The maximum output voltages of two sensors prior to modification are shown in figure 1 (A). Output B (from one of the coils in the lower group figure 13 of appendix IV) was consistently higher than output E (from the upper group), because of a greater number of coil turns. Figure 1 shows the variation in maximum output as a function of rotation.

The magnetic sensor was modified by removing 16 turns from each of three lower coils having the greatest number of turns. This lowered the outputs B, D, and F. Figure 1 (B) shows the variation in outputs B and E after the modification was made. While there is still variation in outputs with rotation, the difference in sensor outputs was reduced from about 16 percent to approximately 6 percent, a variation that can be tolerated.

## Pulse-Width Variation

As discussed in appendix  $\overline{IV}$ , the pulse width of the voltage applied to the motor windings by the electronic control varied with position of the rotor. The effect was to reduce the motor voltage in the region where commutation takes place. The motor torque normally is minimum at the commutation points. Thus, the reduction in pulse width accentuated the ripple torque, and made the motor run roughly at low speed.

In the original circuit (figure 17, appendix ÎV) the drive transistor (Qll or Ql4, etc.) is turned on as a result of turn-on of the Schmidt trigger WM208T, which turns on when the magnetic sensor voltage reaches a preset positive level. The turn-on of Qll, Ql4, etc. completes the circuit through the output winding

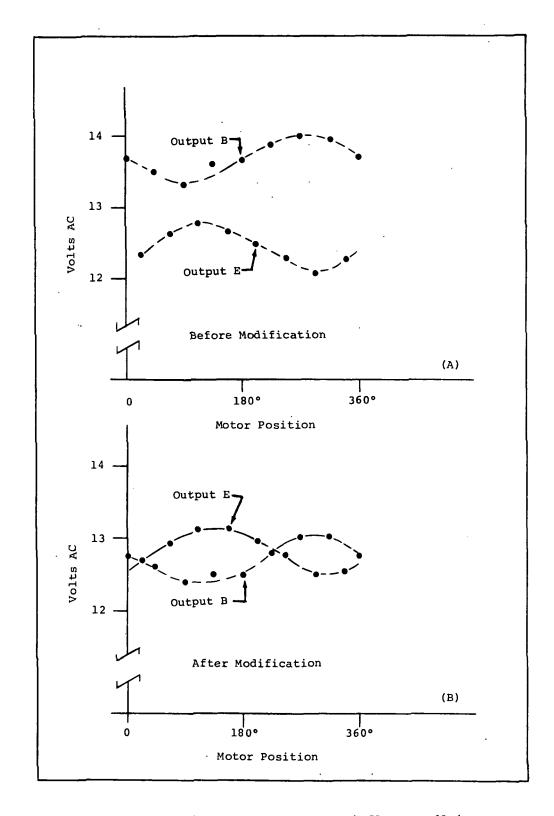


Figure 1. - Maximum Sensor Output Versus Motor Rotation

of the magnetic amplifier, ARI, which supports voltage for a time depending on the current level in the magnetic amplifier control winding. When the magnetic amplifier saturates, base drive current is supplied to the power transistor (Q12, Q15, etc.) through the drive transistor (Q11, Q14, etc.). The pulse to the motor continues until the magnetic sensor voltage goes negative, turning off the Schmidt trigger and subsequently the drive transistor. The magnetic amplifier is reset during the negative half cycle of the magnetic sensor output.

As the magnetic sensor output increases, the period of time between turn-on of the Schmidt trigger and turn-off of the drive transistor increases, while the saturation time of the magnetic amplifier remains constant, as reported in appendix. IV. The major cause of pulse-width variation was thus attributed to the non-square wave form of the sensor voltages. Attempts made to improve the magnetic sensor wave form were without much success. Another method of control was, therefore, developed to correct the pulse-width variation problem.

To eliminate the effect of the magnetic sensor wave form, it was decided to rectify the sensor output and thus turn on the Schmidt trigger for the full angular position of the rotor demanded by the logic. The pulse width is, thereby, divorced from the magnetic sensor outputs. The magnetic amplifier circuit was modified by connecting its output winding to the ac power supply transformer, through a diode. The magnetic amplifier output winding, which is energized when the transformer voltage goes positive, supports this voltage until saturation takes place, and subsequently conducts current to the drive transistor until the end of the positive half cycle. The pulse width is, therefore, determined by the supply voltage and the magnetic amplifier control current, but is not affected by magnetic sensor output. The pulse width of the applied voltage, and thus the average magnitude, is made independent of the position of the rotor.

Torque Variation Due To Irregularities in Switching Angle

Analysis of the motor and control circuit reveals three causes of incremental torque variaton, (1) normal variation due to flux distribution, (2) transient variation due to commutation, and (3) variation due to error in switching angle.

The variation in torque with angular position is a function of pole shape, winding placement and magnetic flux distribution of the rotor poles. In this motor the torque varies approximately sinusoidally for a particular winding connection (i.e. between switching points). This variation is beyond the scope

of the present contract, thus no modification was made to alter the characteristic.

The transient variation due to commutation is a normal function which occurs following each switching point. During the commutation period the currents in the motor windings must change to new values. During the current change there is a momentary decrease in torque, which is restored following commutation.

The variation in torque due to error in switching angle is a function of both the magnetic sensor and the control circuit. Effort was confined to this area in reducing torque variations.

The first consideration in providing accuracy of switching points, of course, is to align the magnetic sensors so that the crossover points between adjacent sensor outputs occur at equal torque points of adjacent motor windings. This can be done with reasonable accuracy, provided the rotor poles are magnetized uniformly and the sensor outputs are well balanced.

In the original circuit the Schmidt trigger acts as a pulse amplitude comparator (as explained in appendix IV, pp. 66-67) in conjunction with a lock-out circuit. Two magnetic sensor outputs are compared on the basis that the Schmidt trigger sensing the larger amplitude would turn on and lock out the others. this method should function well provided all Schmidt triggers have equal turn-on voltage, and good square-wave pulse signals are applied. It was found, however, that a fairly wide tolerance exists in turn-on voltage (4.2 to 6.4 volts). Unfortunately the circuit does not lend itself to convenient calibration and, as previously pointed out, the magnetic sensor does not produce quality square waves. As a result of these variatons, the switching points deviate from the sensor crossover points causing transfer from one motor winding to another at points of unequal torques. Figure 2 illustrates how errors in switching points cause discontinuities in motor torque. If the control transfers the motor winding at the magnetic sensor crossover there is a minimum of change in torque.

Because of the difficulty in sensing the magnetic sensor crossover points by the original method, it was decided to try the direct approach. A circuit was devised to detect the crossover points by sensing the difference in amplitude between magnetic sensor outputs, and providing logic to switch the proper power transistor at the crossover points. The six Schmidt triggers were replaced by three type 710 voltage comparators. Integrated circuit NAND gates are used as logic elements.

The replacement control circuit is shown in figure 3. The magnetic sensor outputs from the direction control logic transistors

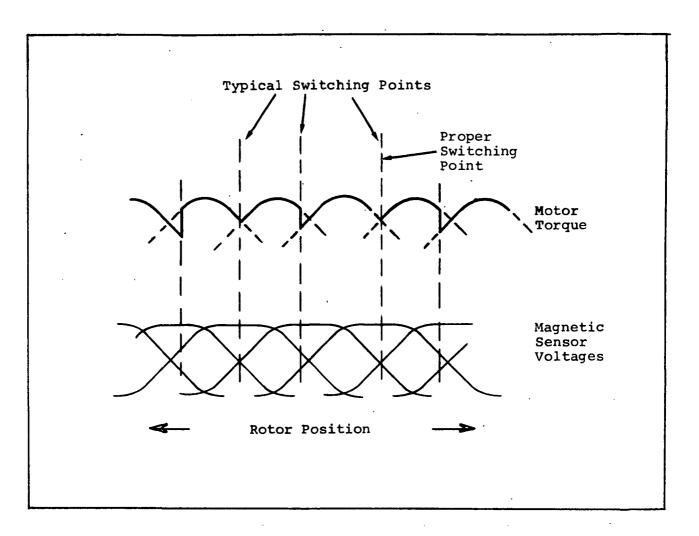


Figure 2. - Motor Torque Variation versus Switching Points

are brought in to diodes which serve as rectifiers for the sensor voltages and also as OR gates. The output from each pair of diodes is a dc voltage proportional to the greater of two adjacent magnetic sensor signals. The output from sets of diode pairs are sensed by the differential comparators, thus detecting the crossover points of two sensor outputs.

The signal X, for example, in figure 3 is a logical "one" when the signal at either K or N is greater than that at either P or J. The sensor outputs appearing at K, N, P, J etc. depend on the direction control. Reversing the direction control simply interchanges the magnetic sensor signals appearing at K and N with those at P and J.

The signals Y and Z are derived from appropriate sensor signals in the same manner as in X. The signals X, Y, and Z are used to

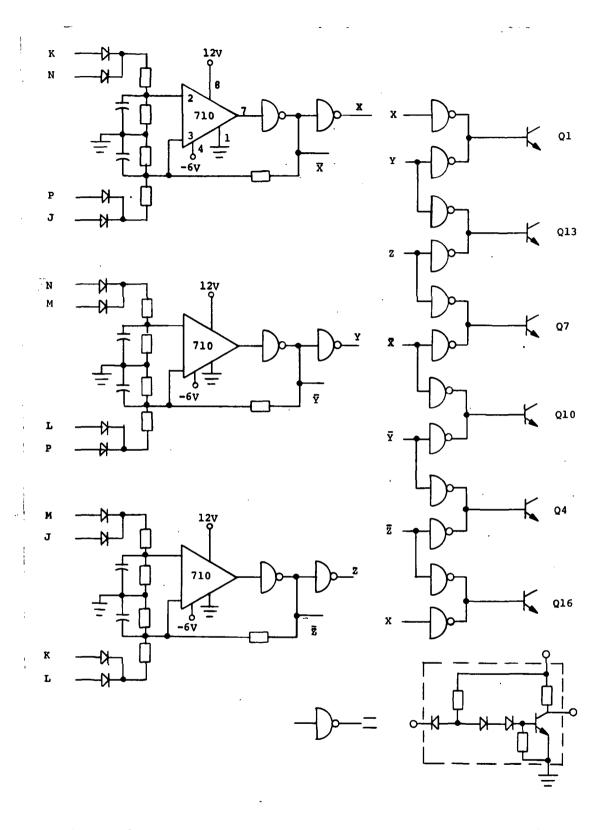


Figure 3. - Brushless Motor Commutator Control Logic

form control signals for the steering transistors Ql, Ql3, etc. A signal to turn on transistor Ql is developed when both X and Y are low (Ql = X.Y). Likewise, Ql3 = Y.Z, Q7 = Z.X, Ql0 = X.Y, etc. The output of the NAND gates to the transistors from wired AND logic. Thus two NAND gates must be in the high state to turn on the transistor, which is driven through the collector resistors of both NAND gates.

Referring once again to figure 3, note that filter capacitors are provided at the inputs of the comparators and that feedback resistors are connected from X, Y, and Z to the input of the comparators. This circuitry serves to provide a clean transfer from one state to another, eliminating dither or instability. The capacitors eliminate the effect of differences in sensor wave form, while the feedback resistors increase slightly the difference voltage applied to the comparator after the comparator has changed state.

Derivation of the commutator control signals is shown in figure 4. The sensor outputs which appear at points P, L, K etc. are shown at the top of the figure. The diode output from K or N is shown in bold lines as is the output from J or P. When K or N is greater than J or P the signal X appears. It will be noted that X is "on" for an angular rotation equal to that for which it is "off" (a square wave, relative to position). The same is true for Y and Z. One of these signals changes state at each of the sensor crossover points. By combination of these signals as shown in figure 3, the drive signals are thus derived.

A revised schematic diagram of the modified controller-commutator is shown in figure 5, which incorporates the circuit of figure 3 into the complete circuit. Connections between signal points have been omitted for clarity. These connections are indicated by symbols (signal symbol or terminal marking). Although no change was made in the direction control logic, some space economy could be made in a redesigned unit by using NAND logic for direction control.

#### Test

The tests conducted on the motor were the applicable performance tests outlined in reference 2. The initial test consisted of adjustment of the magnetic sensor assembly. Once proper alignment was accomplished the following tests were conducted.

(1) Oscillator (28-volt input)

Wave Form - The wave form was observed to be a reasonably good quality square wave.

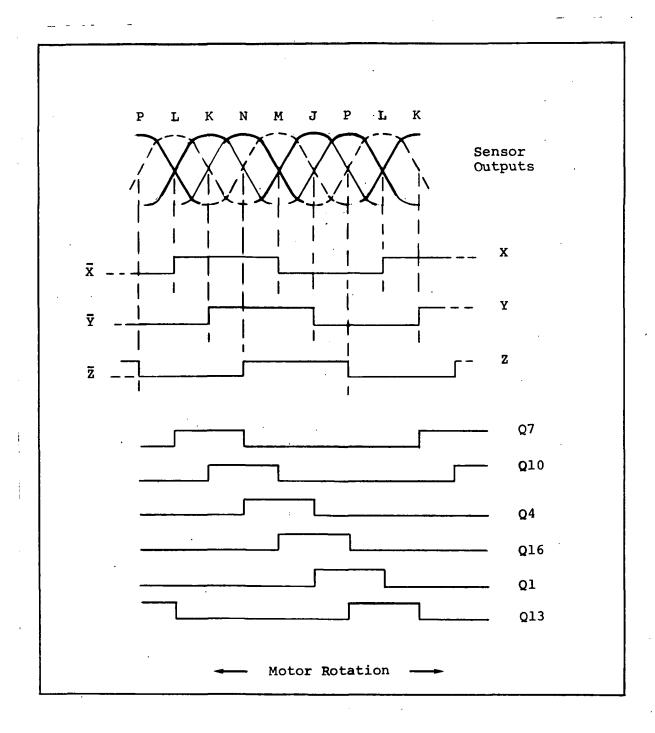


Figure 4. Derivation of Commutator Control Signals

Frequency - 10620 cps

Output Voltage (peak reading of square wave)

í. ì

Terminals	Volts
12-13	6.1
13-14	6.1
15-10	9.0
10-16	9.0
8-10	6.1
10-11	6.1

## (2) Magnetic Sensor (28-volt input)

Wave Form - The wave form is substantially the same as previously reported in appendix IV. A good deal of ringing is apparent but suppression resistors have not been used since this ringing is not troublesome.

Voltage Level - The ac output voltages were plotted for one full cycle (45 degree rotation). The results are shown in figure 6. In other rotor positions these curves will vary slightly as discussed previously.

## (3) Reversing Bridge

Operational check - performance is normal.

(4) Voltage Comparators and Switching Logic.

Operational check - Switching occurs in proper sequence at proper points.

#### (5) Speed Control (28-volt input)

A speed control voltage was applied to pin E of connector Jl and varied to determine the no-load speed characteristic. These data are plotted in figure 7. Minimum no-load speed was 15 to 20 rpm at 2 volts control voltage. Maximum speed is slightly higher than 150 rpm at 12 volts. Higher control voltage increases the speed only slightly.

#### (6) Control Losses

The input power with the motor inoperative was measured.

Supply voltage -	28 volts
Control voltage -	15 volts
Input current -	24 ma
Power dissipation -	672 milliwatts

Foldont

78.

Kint Or. Br.

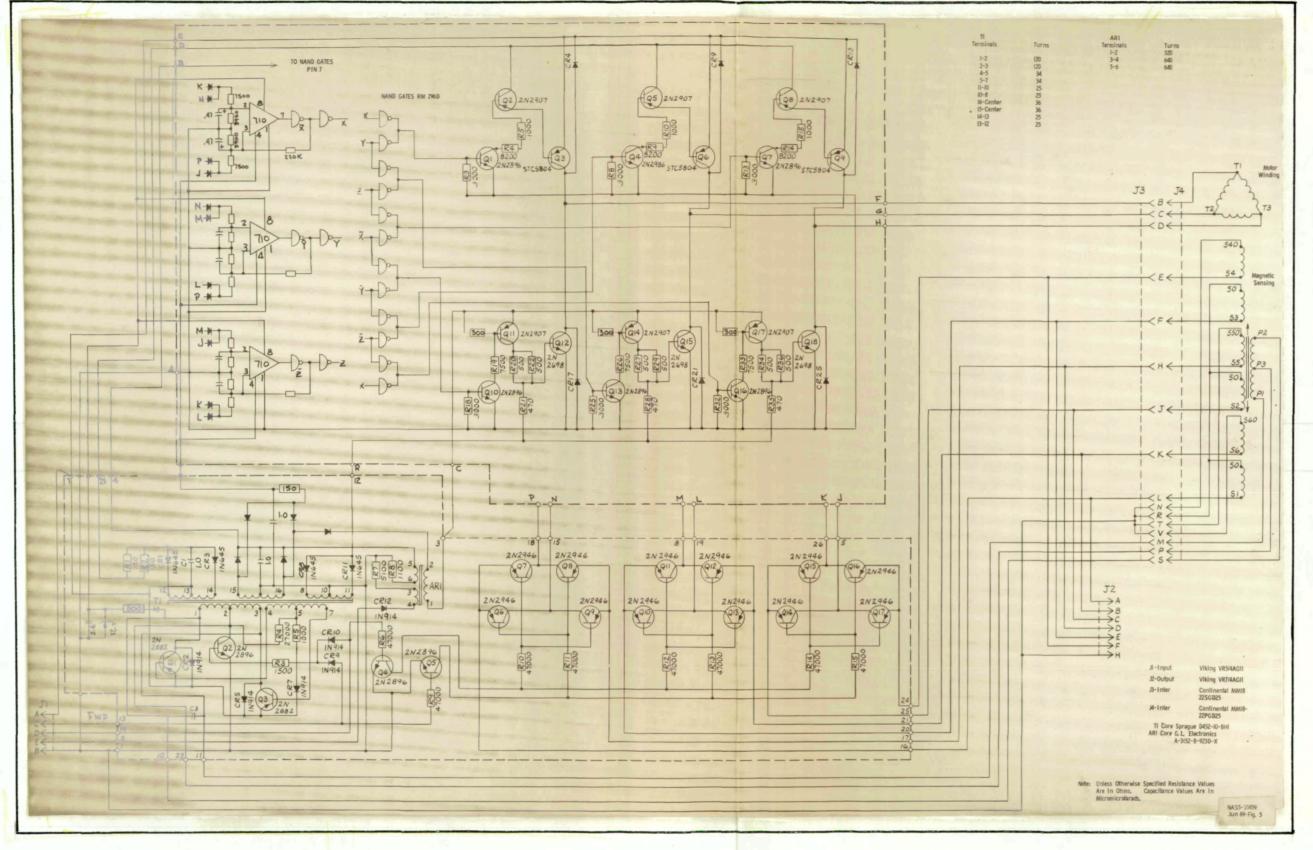
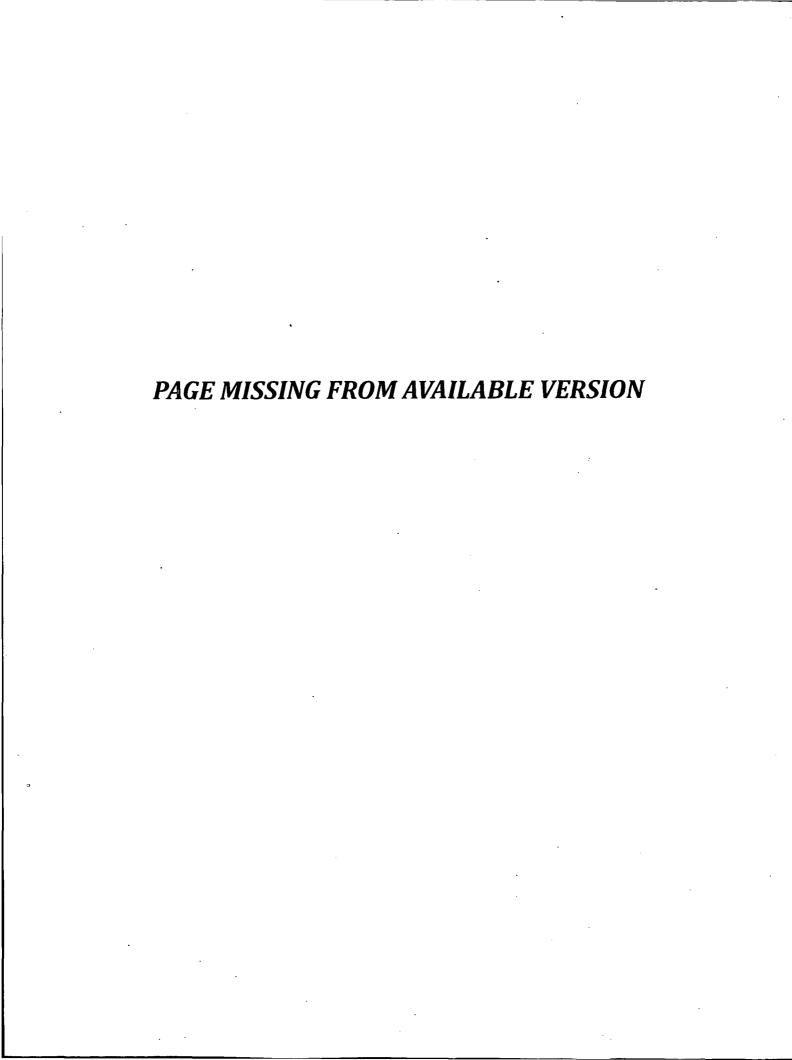


Figure 5. - Controller-Commutator Circuit Schematic - Revised



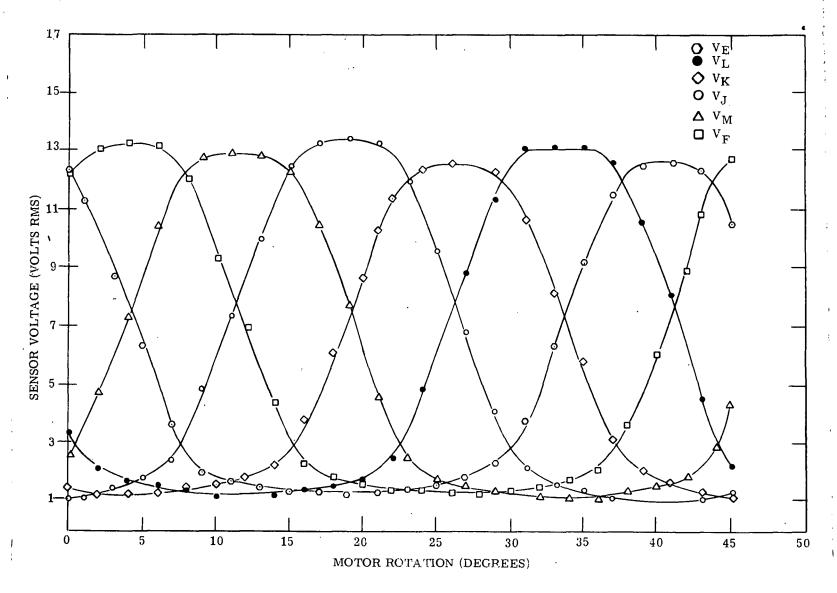


Figure 6. - Magnetic Sensor Characteristics - Test Curves

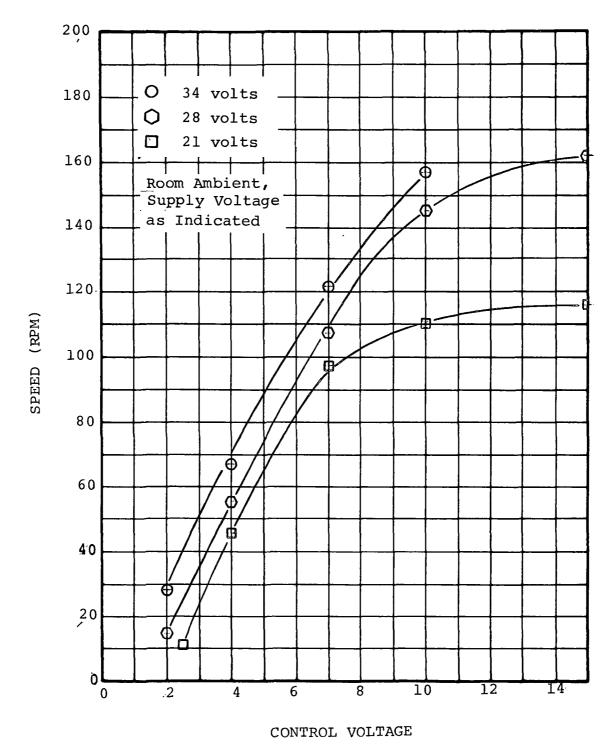


Figure 7. - No Load Speed Control Characteristics

# (7) Power Dissipation, Motor Operating

The input power was measured at maximum speed-control voltage at both no load and locked rotor.

Supply voltage - 28 volts Control voltage - 15 volts

		No Load	Locked	Rotor
-	Current	150 ma	500	ma
	Power	4.2 watts	14	watts

## (8) Operating Voltage Range

Supply voltage was varied over a range of 12.5 to 34 volts. The motor operated satisfactorily in both directions throughout the voltage range. The minimum voltage at which the motor would run was 12.5 volts.

## (9) Forward Drop In Power Transistors

The conduction voltage drops in the power transistors were measured at locked rotor as follows:

	Volts
Q3	0.2
Q6	0.15
Q9	0.15
Q12	0.4
Q15	0.7
018	0.6

These values indicate that the transistors were operating within their saturation region as designed.

# (10) Winding Resistance

Winding terminals are identified by terminals of connector J4.

Motor Winding	Ohms
B-C	15.2
C-D	15.19
B-D	15.2

## Magnetic Sensor

Primary	Ohms
M-P	0.84
S-P	0.84

## Magnetic Sensor

Secondary	Ohms
$\mathbf{E} - \mathbf{N}^{-}$	3.00
F-R	2.94
H-T	3.01
J-R	3.00
K-V	2.96
L-R	2.90

## (11) Break-Away Torque

Break-away torque, which includes both friction and cogging torque, was measured as the torque required to start the motor with power turned off. This torque was 3.37 ounce-inches, both directions.

# (12) Torque Variation with Rotor Position

Locked rotor torque data were taken on the motor at 28 volts supply voltage and 15 volts control voltage. Figure 8 shows torque as a function of rotor position for 45 degrees of rotation. This curve shows approximately 15 percent variation in torque due to ripple, which is caused by near sinusoidal flux distribution in the rotor poles.

Additional data were taken over a complete revolution, measuring the maximum and minimum torque points. The total variation in torque measured was 72 to 90 ounce-inches.

#### (13) Speed-Torque Curves

Torque-speed data were taken at various control voltages with supply voltages of 21, 28, and 34 volts, in both forward and reverse rotation. The data shown in figures 9 and 10 for forward rotation result in practically linear curves. Reverse rotation values were within 3 percent of the forward values.

#### (14) Miscellaneous Tests

Tests were made using various combinations of spring and mass loads to determine if instability existed at any point. The general procedure was to wrap a length of cord around the motor shaft to form a windlass, to load the windlass with a weight and spring, and lift the weight by running the motor at minimum speed. The motor was started by increasing the control voltage enough to life the weight. Once

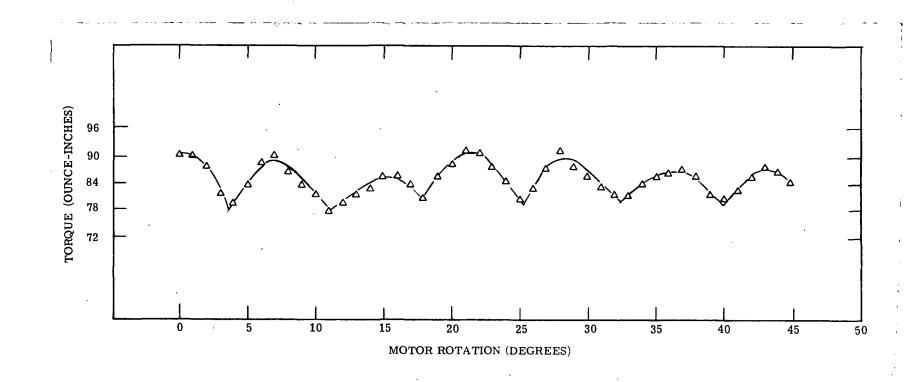


Figure 8. - Torque Versus Rotor Position

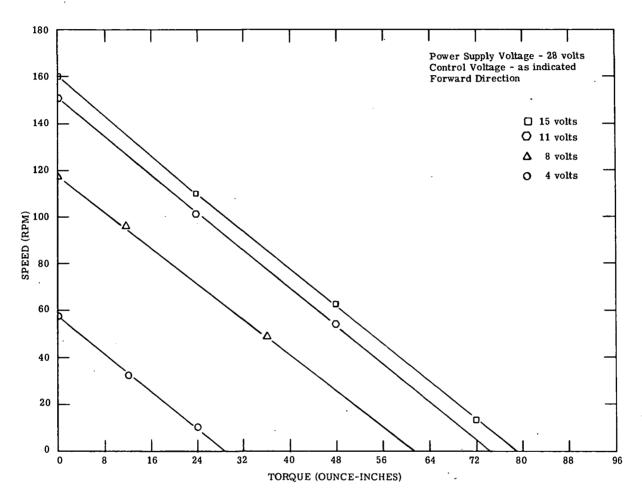


Figure 9. - Speed-Torque Curves

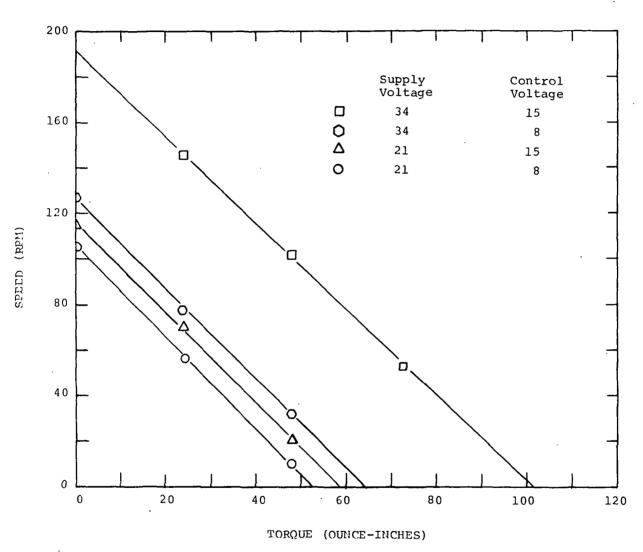


Figure 10. - Speed-Torque Curves

the weight was lifted, the motor continued to run with no sign of instability or dither. Although many combinations of spring and mass were tried, no instability was found in the motor under any condition when it was loaded with a linear continuous type load. An unstable loading condition such as holding the motor shaft by hand can result in oscillatory motion of the rotor, but this is not considered a practical load.

# (15) High and Low Temperature Tests

The motor was run at the specified temperature extremes of -10°C. Performance checks were made at both temperatures. The motor ran normally in both cases indicating that there was no malfunction in the commutator-control circuit. No-load speed was tested as a function of control voltage over a range of supply voltage 21 to 34 volts. The speed characteristics at nominal supply voltage are plotted in figure 11 for temperatures of -10°C and +70°C. Speed increases slightly with temperature for any control voltage.

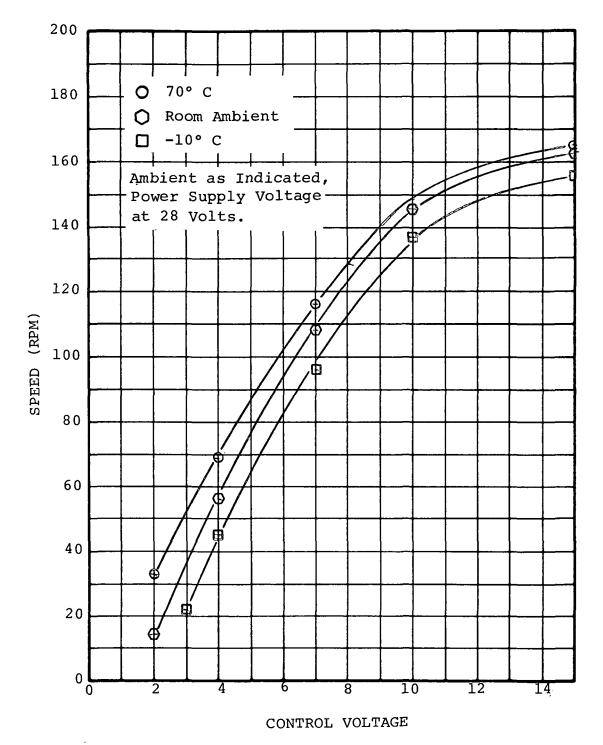


Figure 11. - No Load Speed Control Characteristics.

Pg 88

Blank,

#### SECTION IV

#### ROTARY TRANSFORMER DESIGN

A rotary transformer was built for NASA Goddard on a previous contract by Neotec Corporation as part of the development of a solar array reorientation system. This unit consisted of a single power transformer. The development of the reorientation system now requires five small transformers packaged with the power transformer to transmit control signals between the solar array assembly and the spacecraft. A new transformer assembly design was, therefore, required to complete the laboratory model.

Tests on the Neotec unit proved that it would handle the required 500-watt load with no trouble. In fact, the design is quite conservative. While it was not possible to accurately measure the efficiency of the Neotec unit, the design was verified by calculation. Computed efficiency was approximately 99 percent.

A new design was made using the approximate electrical design of the Neotec unit for the power section and a modified mechanical design incorporating five signal transformers. The power unit was designed to provide high efficiency and low exciting current.

#### DISCUSSION

#### FUNCTION

The function of the brushless, direct-drive, solar array reorientation system is to efficiently supply power collected by
the solar array to the spacecraft. The prime link between the
power developed at the array and that used in the spacecraft is,
thus, the rotary transformer. The transformer must accept power
from the array through an inverter and supply power to the spacecraft due to rotation. The only mechanical contact allowed between the primary and secondary sections of the transformer is
through the support bearings which allow freedom of rotation and
maintenance of an air gap through which magnetic energy is transferred to the transformer secondary winding.

A prime consideration in the power transfer system is good efficiency. Since the system comprises, in addition to the transformer, an inverter to obtain ac power from the solar array, and an output rectifier, the transformer losses will be only a small part of the total. While it is important to maintain high transformer efficiency, it is even more important that the transformer characteristics be such as to produce minimum losses in the inverter and

output rectifier. For example, a major part of the losses in an inverter occurs during switching. At the same instant the exciting current of the transformer is at its peak value. It is, therefore, highly desirable that the exciting current be kept low relative to the load current, even though a more efficient transformer design would require a higher excitation current. The use of a parallel inverter having only two power transistors requires good coupling between the two sections of the transformer primary winding to keep voltage spikes to a minimum. Although building of a maximum efficiency inverter is beyond the scope of the present contract, an effort is being made to build a high efficiency inverter for the laboratory model.

Control of the reorientation system requires that control signals be transmitted between the solar array and the spacecraft. A second function of the rotary transformer assembly is, therefore, to provide means for transmitting these signals. Five signal transformers are provided to fulfill this requirement. Three are used in the reorientation control and two are available for other sensing functions. The minimum physical size of the signal transformers are limited by mechanical considerations.

## TRANSFORMER DESIGN CONSIDERATIONS

Design of the power transformer was based on the previous development work done for NASA - Goddard by Matrix and the rotary transformer built by Neotec. Development work by Matrix is reported in reference 3 which includes a comprehensive report on the transformer design. The unit built by Neotec, based on the Matrix development, was tested by Westinghouse to determine the adequacy of the unit as a design base for the rotary transformer to be used in the laboratory model of the present contract.

The desired result of the tests on the Neotec-built unit was an evaluation of the power handling capability. The initial approach was to construct an inverter circuit (shown in figure 1) and attempt to measure the efficiency of the rotary power transformer at various loads. Problems were encountered in taking power measurements such that the data was unreliable. It was not practical to properly account for load power factor and other inductive effects because of the "square" wave-form produced by the inverter. It was apparent, however, that the transformer efficiency was very high.

Since the ultimate rating of a power transformer is determined by its maximum hot-spot temperature, it was decided to evaluate the power handling capacity of the rotary transformer on a temperature-rise basis. The transformer was instrumented with thermocouples and run at power levels of nominally 300 and 500

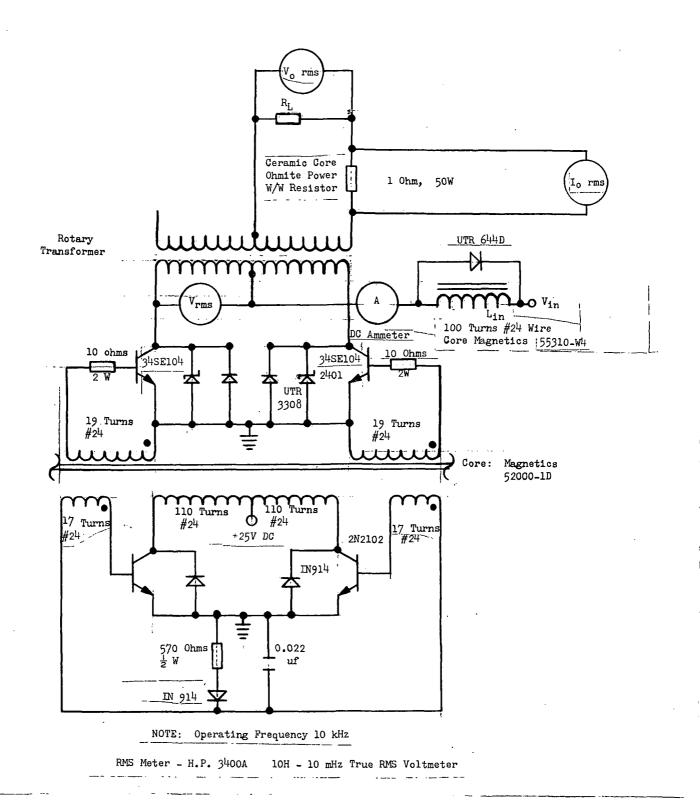


Figure 1. - Test Circuit

12 h 11

watts. Two thermocouples were located on the surface of the transformer case; one near the hollow shaft at the end of the primary winding, and the second at the end of the secondary winding.

An input square-wave voltage of approximately 100 volts, 10,000 Hertz was applied to the transformer primary through the inverter. A 300-watt resistive load was connected to the transformer secondary. After one and one-half hours, the temperature at both thermocouples had stabilized at 33°C, an 8°C rise. The test was repeated at a load of 500 watts with temperature rises at 19°C and 17°C at the thermocouples. The winding temperature rise also was measured by the resistance change method. The rise in both the primary and secondary windings was 21° to 25°C at 500 watts.

Based on the temperature rise data, it was concluded that the transformer built by Neotec is a conservative design which is more than adequate for 500-watt operation. It was, therefore, decided to use the Neotec-built unit as the basis for design of the rotary transformer assembly for the Laboratory Model.

# DESIGN SPECIFICATIONS

The parameters selected for design of the rotary power transformer are as follows:

#### Power Section

Power rating
Input voltage
Frequency
Output voltage
Efficiency (full load)
Exciting current

29 volts 99% lowest consistent with good efficiency

500 watts 80 volts 10,000 Hertz

Other characteristics derived from previous development work:

Air gap	0.004 inch
Magnetic material	Ferrite
Bearings	Space Quality
	dry lubricant
Shaft diameter	1.5 inch, same
	as motor shaft

11 11

# Signal\_Section

Number of transformers
Input voltage
Output voltage
Frequency
Coil configuration
Air gap

5 0-15 volts 0-15 volts 10,000 Hertz center-tapped 0.004 inch

### ELECTRICAL DESIGN

Design equations for the electrical design appear in appendix I. To use these equations, physical dimensions as well as input electrical parameters are selected. Power loss and efficiency are determined by calculation using the equations. The temperature rise is then calculated using the method outlined in appendix II which assumes that all heat generated escapes through the cylindrical surface. The losses and temperature rise of the Neotec rotary transformer were calculated using the equations of appendices I and II. The calculated temperature rise checked within 15 percent of the measured values which is a reasonable correlation.

Using the Neotec-built unit as a design base, several sets of calculations were made for a new design using various numbers of turns, winding density, etc. For 80-volt input, the maximum efficiency occurred with a 14-turn primary coil. However, it was observed, that if the number of turns was increased to 19, the exciting current would be cut by approximately 50 percent while the transformer loss increased by about 20 percent. By decreasing the exciting current the input inverter efficiency could be improved by reducing the switching losses by 10 to 15 percent. Therefore, it was decided to use a 19-turn winding in the interest of overall efficiency. The transformer efficiency is approximately 99 percent at full load; thus, the slight increase in winding loss due to the larger number of turns will be much more than offset by a decrease in inverter loss.

Five signal transformers are required to transfer control signals between the solar array and the spacecraft. Three transformers are needed to provide reorientation signals to the control unit. Two additional signal transformers are available for other functions.

The main problem involved with the signal transformers is a mechanical one. The minimum size of the transformers is limited by the necessity for handling the parts. The size of the magnet cores are, therefore, arbitrary; a result of a mechanical judgement decision. The coil design was chosen to be compatible with the requirements of operational amplifiers used in the solar

124!

signal transfer circuitry. Both primary and secondary coils are wound in a bifilar manner with 80 turns of number 30 enameled copper wire. (See Appendix III - Detailed Manufacturing Drawings.)

#### MECHANICAL DESIGN

A cross-sectional view of the rotary transformer is shown in figure 2. Significant mounting and envelope dimensions are included. A complete set of manufacturing drawings with dimensions of all parts is contained in appendix III. Component and subassembly part numbers which appear in these drawings are referred to in the following discussion.

As seen in figure 2, the power transformer section is located at one end of the complete rotary transformer assembly, and the signal section is located at the other end. Each section occupies about half the package volume. The general assembly drawing for the complete rotary transformer is EDSK 349968.

The complete assembly consists of two main subassemblies - the stator and the rotor. The stator is comprised of the frame assembly, EDSK 349967, and the end bell, EDSK 349962-11. The frame assembly contains the secondary coil assemblies for both the power and signal sections. Secondary leads are brought out and terminated at two connectors attached to the frame, EDSK 349958-1.

The rotor consists of the primary coil assemblies for both the power and signal sections mounted on a hollow shaft. Primary leads are brought out through the shaft inside diameter. The rotor subassembly is defined by EDSK 349966.

The frame assembly and the rotor assembly are preassembled individually; then assembled together with the bearings and the end bell to form the complete rotary transformer.

The bearings are special large bore, extra-thin section ball bearings with AISI 440C stainless steel races and teflon spring separators. Lubricant is MIL-L-6085A. It was originally planned to use the same special solid lubricated bearings suitable for space environment used in the brushless dc drive motor, part number 915F359. However, program schedule and bearing delivery problems prompted selection of these bearings which differ only in separator and lubricant from the other bearings. These bearings are designed specifically for low torque performance under

The suffix number following the dash is the item number of the particular part where more than one component/item is contained on the same drawing indicated by the basic number.

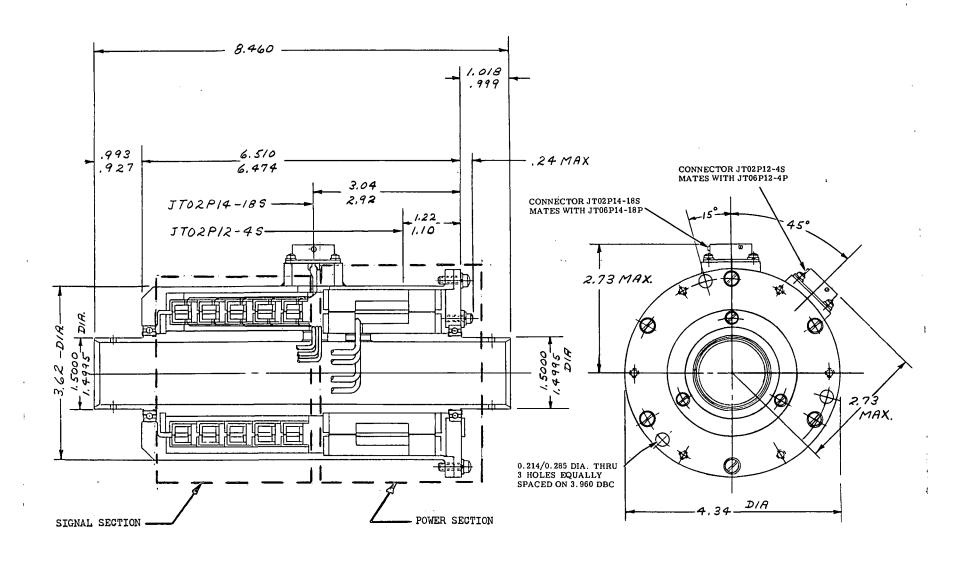


Figure 2. - Rotary Transformer Assembly

low speed and/or oscillating operating conditions; therefore, they will similate the low drag performance expected under the weightless conditions of space. For actual performance in a vacuum, these bearings must be replaced with the solid lubricated bearings. These bearings were procured from the Barden Corporation, part number A543ZA3C 0-11.

All metal structural parts are made from Inconel 600. The magnetic cores for the power and signal coil assemblies are made from a high initial and maximum permeability ferrite, Ceramagnetics, Inc., MN-60.

MN-60 is a brittle material, like most ferrites. During the design phase, it was regarded so fragile (based on consultation with the supplier) that emphasis was placed on achieving a design to minimize machining of the MN-60 parts and provide maximum mechanical integrity. This is accomplished by:

- 1. Impregnating all MN-60 parts with Scotchcast 280, a heat resistant, solventless, epoxy resin exhibiting a partially elastic characteristic after curing. This is done to inhibit chipping, flaking, or galling of the parts and to impart added cohesiveness.
- 2. Fabricating all assemblies and subassemblies by bonding the parts together and potting with Scotchcast 280. This provides a solid mass-like structure with cushioning resilience against shock provided by the Scotchcast impregnation/bonding at the part interfaces.
- 3. Providing the signal coil cores, considered particularly delicate, with Inconel 600 support members (EDSK 349957-4 for secondary coils and EDSK 349957-5 for primary coils). The signal coil subassemblies with support members (EDSK 349962-1 through -10) are then bonded to intermediate Inconel 600 support members and potted to form the signal coil assemblies EDSK 349964, secondary and EDSK 349965, primary. These are then bonded and potted to the frame, EDSK 349958 and shaft, EDSK 349957-1, respectively.

The power coil cores are bonded directly to the frame and shaft, as appropriate, without intermediate metal support members, since the power coil cores (or spools) have larger and more substantial cross-sections.

The secondary power coil is wound and bonded into the magnetic ferrite housing (or core), EDSK 349956-2. This subassembly is then assembled into the frame, the ferrite end cover is assembled to form the secondary coil spool, and the entire assembly is bonded and potted with Scotchcast 280. (See EDSK 349967.)

The primary power coil spool, EDSK 349956-3, is bonded to the shaft and the primary coil wound directly on the spool followed by potting. Both primary and secondary coils of the power transformer are wound in a bifilar fashion. Initially both coils were made of two flat copper strips separated by insulating strips of mylar. The flat strips provide good coupling between bifilar coil sections and good winding utilization. However, difficulty was experienced in achieving the necessary number of primary winding turns within the prescribed coil outside diameter. Several attempts were made to reduce the insulation thickness build-up by substituting alternate insulation systems. These attempts resulted in shorts between the primary coil conductor and the ferrite core. Finally the primary coil was rewound using round insulated wire.

The electrical design dictated a radial clearance between the power section primary and secondary core diameters of less than 0.004 inches on a side. This required very close concentricity and runout tolerances between the stator bore and rotor outside diameter. To avoid grinding of the ferrite surfaces of the stator and rotor assemblies (as discussed previously), an attempt to achieve the close tolerances was made by:

- 1. Machining individual component parts to close tolerances. (The ferrite parts supplier provided the close tolerances on these parts because of special capability and experience in performing these operations.)
- 2. Bonding, potting, and assembly fixtures machined to very close tolerances were used to hold and align the parts to the necessary close concentricity and alignment tolerances during bonding and potting.

This procedure was only partially successful. A light, clean-up, grinding operation was required on both the stator assembly bore and the rotor outside diameter to achieve satisfactory run-out (alignment) tolerances. This operation was previously required by excessive potting buildup, and very little grinding was required on ferrite surfaces.

Although the design of the rotary transformer assembly has been aimed at space quality, there was no attempt to minimize weight. In future designs weight reduction would be one of the principal objectives. The weight of the rotary transformer is approximately 16 pounds, of which 50 to 60% is in the housing. The weight of the power section is nearly the same as that of the signal section.

Page 98

Blank

#### SECTION V

#### SOLAR ARRAY REORIENTATION SYSTEM - LABORATORY MODEL

One of the objectives of Phase II was to modify the design of the breadboard version of the control unit to incorporate rotary sensing transformers. Another objective was to build a packaged unit having printed circuit boards with a reduced number of circuit components.

The control unit circuit is basically the same as that of the breadboard unit. Some minor changes were made to improve the reliability of performance. And, of course, it was necessary to separate the solare sensor amplifier circuit from the control unit because the amplifier must be located on the solar-array side of the rotary transformer. Otherwise, there have been no changes in the operational concepts of the control system. Discussion of the theory of operation is covered adequately in section II and is not repeated here. Circuit diagrams of the final packaged control unit are shown in this report and are cross-referenced to diagrams of the breadboard unit found in section II so that changes may be readily seen. Discussion of any significant changes are contained herein.

Although the specification did not require an inverter as part of the laboratory model, it was necessary to design and build one so that the rotary transformer (section IV) could be tested. A brief description of the inverter is included in this report.

The final objective of Phase II was to provide a working model of a brushless, direct-drive solar array reorientation system including the components previously developed for this project. The report contains a word and picture description of the laboratory model including an assembly procedure.

It is expected that a thorough review of section II precede the study of this document for proper understanding.

# SOLAR SENSOR AMPLIFIER

The solar sensor amplifier receives direct-current signals from the solar sensors and converts them to alternating-current voltage signals which are transmitted to the control unit through a pair of rotary sensing transformers. The circuit is shown in figure 1. Solar sensor current is sensed by operational amplifiers which give an output voltage proportional to solar sensor currents. Input power is received from the power supply of the control unit (a 28-volt, 10-kHz square wave) through a rotary sensing transformer, and used to switch the two pairs of transistors alternately. This action chops the outputs of the two operational amplifiers to provide the a-c signals proportional to the solar sensor currents. The signals are transmitted across the air gap of the rotary sensing transformers to the control unit. Input power is also rectified to supply d-c power to the operational amplifiers.

These signals are received in the control unit as shown in figure 2 where they are rectified to form signals  $E_{\rm CC}$  and  $E_{\rm CW}$  having d-c levels approximately proportional to the solar sensor currents. These signals are processed as in the breadboard circuit.

# CONTROL UNIT CIRCUIT MODIFICATIONS

Schematic diagrams of the control unit are shown in figures 2 to 12. These diagrams are substantially the same as those presented in reference 1 except for minor changes to accomplish better performance and component reduction. The control signals are indicated by the same symbols as used in section II. The numbers in parentheses refer to the pin numbers of the printed cuit board connectors.

# PRINTED CIRCUIT BOARD NO. 1

The circuits for control in the normal tracking mode and for control of speed and acceleration in the other modes are located on printed circuit board number 1. The circuit diagrams are shown in figures 2, 3, 4 and 5. The only significant change in these circuits occurs in the speed-reference ramp generator of figure 4. Here a 4-stage binary counter is used in place of four separate counters. Improved performance was obtained by use of diode-transistor logic (DTL) NAND gates without collector resistors to drive the output resistor networks. This results in a RAMP signal having nearly equal step changes in output.

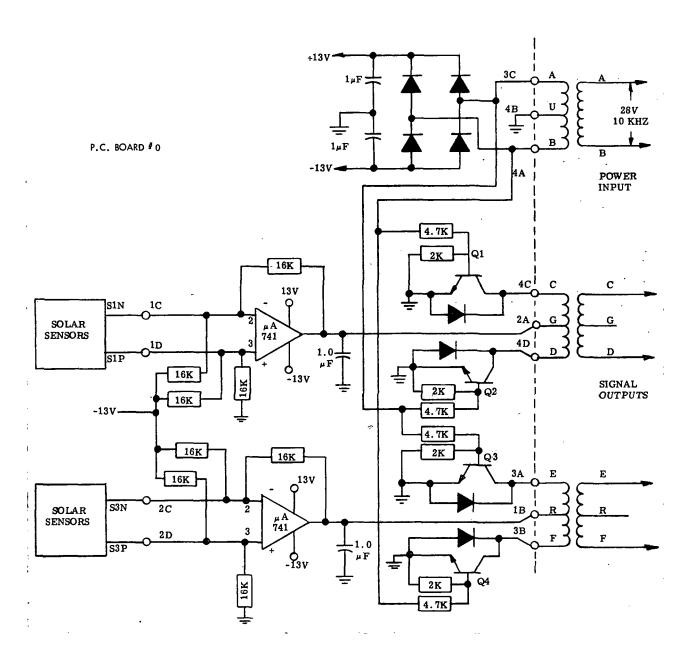


Figure 1. - Solar Sensor Amplifier (See sec. II, figure 4)

100

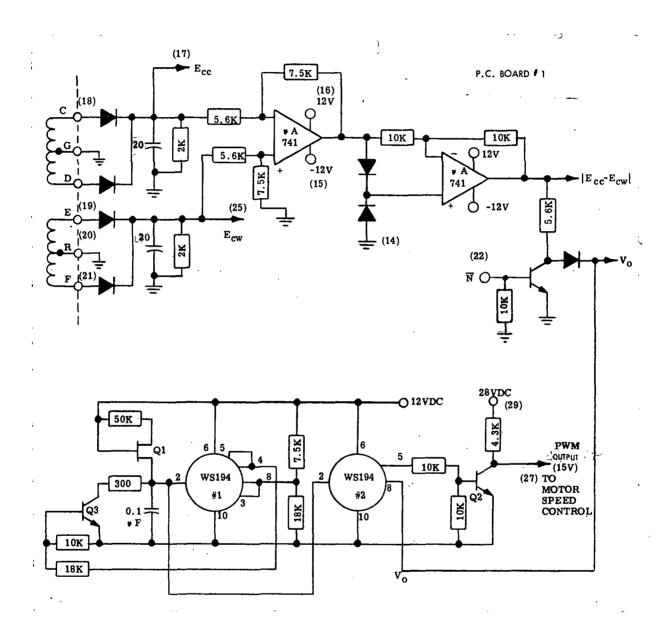


Figure 2. - Solar Sensor Signal Processing Circuit (See sec. II, figure 1)

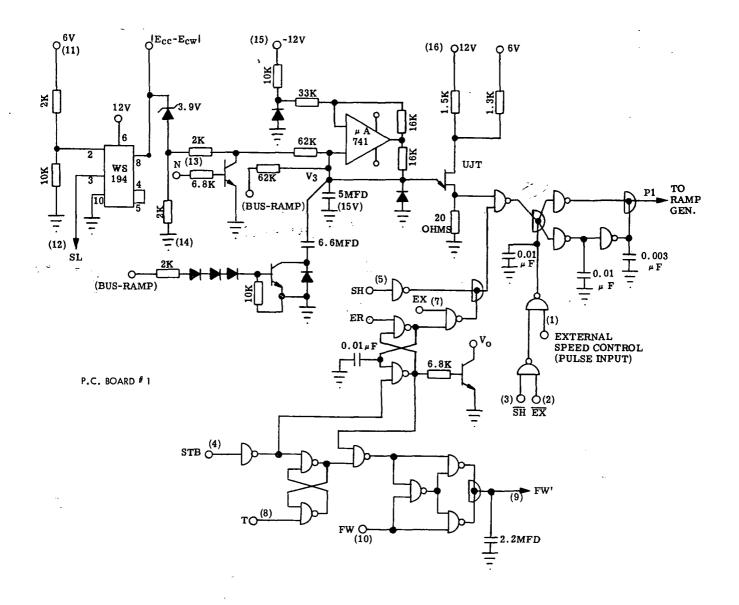


Figure 3. - Acceleration and Speed Control Circuit (See sec. II, figure 16)

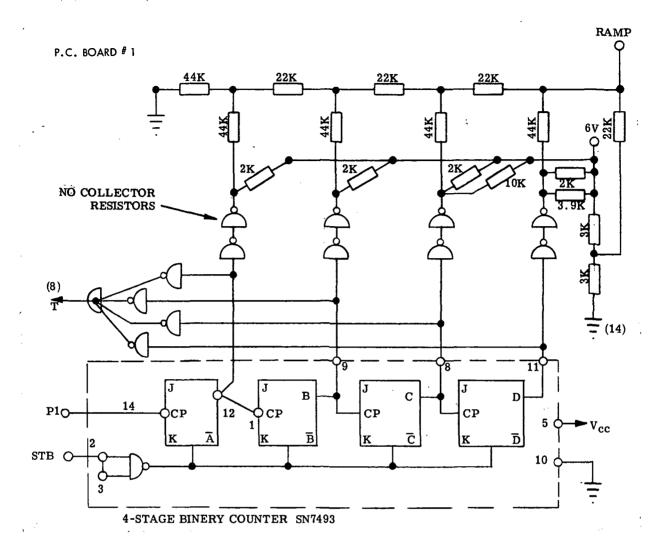


Figure 4. - Speed Reference Ramp Generator (See sec. II, figure 15)

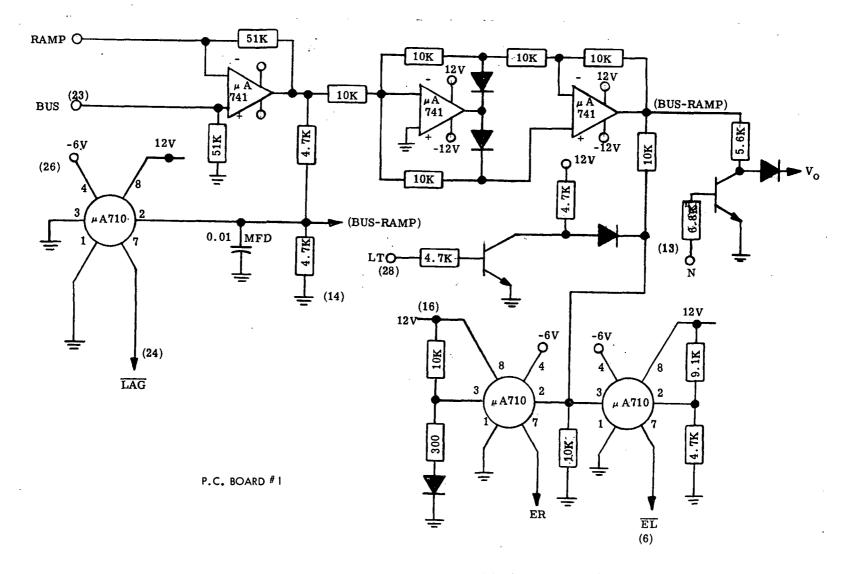


Figure 5. - Speed Control Amplifier Circuit (See sec. II, figure 14)

105

#### PRINTED CIRCUIT BOARD NO. 2

The logic circuits for mode selection and mode transition, located on printed circuit board number 2, are shown in figure 6. It was found that when the simulated solar array came under the influence of an external force to rotate it, the control circuit would lock up. The Error Limiting Circuit (EL in figure 6) was modified by combining the circuit with signal N. This change provided a pulse when the position error was exceeded. This pulse gives a STB signal when the signal, EL, is produced. The effect is the same as if the system were put in the standby mode momentarily. After the pulse has disappeared the control operates as if switched from standby to an operating mode. (See sec. II, p. 27.)

### PRINTED CIRCUIT BOARD NO. 3

The motor position reference signal used for speed control is derived by the circuits of printed circuit board number 3. These circuits which are essentially the same as those used in the breadboard unit, are shown in figures 7, 8 and 9. The amplitude of the magnetic sensors and their associated logic signals are derived as shown in figure 7. This circuit was changed to eliminate three WS194 detectors by substitution of three NAND gates to produce signals A', C' and E' which are complimentary to D', F' and B'.

The drive logic and magnetic sensor reference circuit is shown in figure 8, and the interconnection of the required six channels is shown in figure 9. No change was made in this logic. The input signal, EL, was eliminated, however, because of the change in the function of EL as indicated in the description of printed circuit board number 2.

### PRINTED CIRCUIT BOARD NO. 4

Most of the modifications made in the control unit were made on printed circuit board number 4. However, there was no change in function of the circuit nor in the method of obtaining the function. The change was made in circuit component reduction. Rather than using single stage binary counters and simple NAND logic, 4-stage counters, memories, and comparators were used. This not only reduced the component count but also expanded the capacity of the pulse counters, allowing a greater range of orbit altitude.

Printed circuit board number 4 contains only the dark period control logic of figure 10. Counter X which was made,

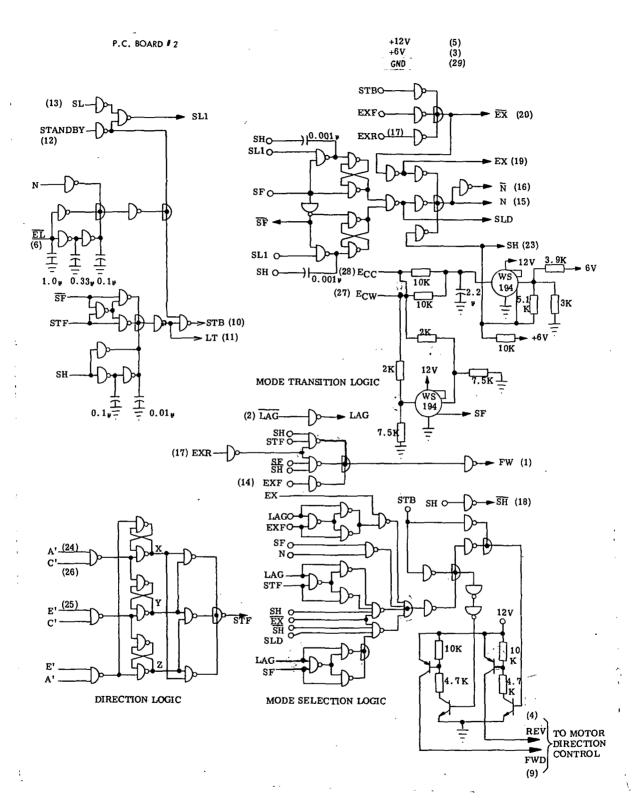


Figure 6. - Logic Circuits for Mode Selection and Mode Transition (See sec. II, figure 17)

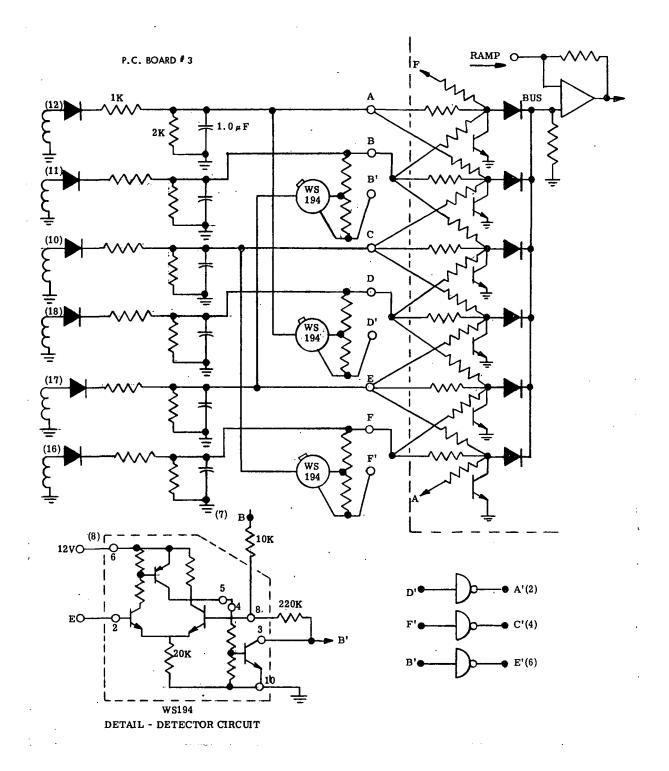


Figure 7. - Magnetic Sensor Signal Processing Circuit (See sec. II, figure 12)

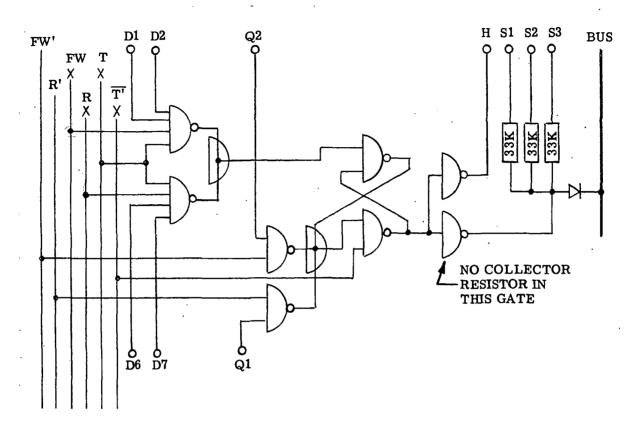


Figure 8. - Drive Logic and Magnetic Sensor Reference - One Channel (See sec. II, figure 11)

, ;

1 3

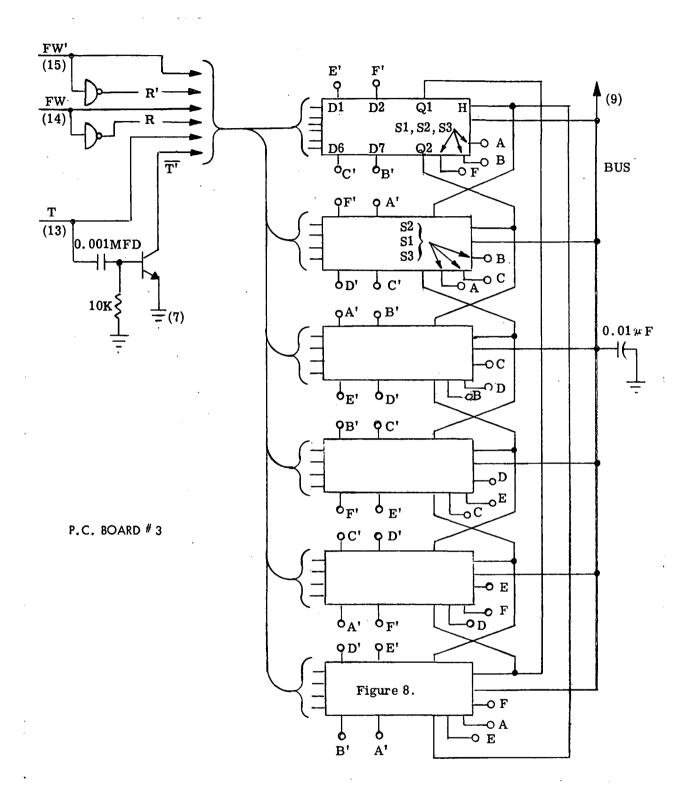


Figure 9. - Connection of Six Channels for Drive Logic and Magnetic Sensor Reference (See sec. II, figure 10)

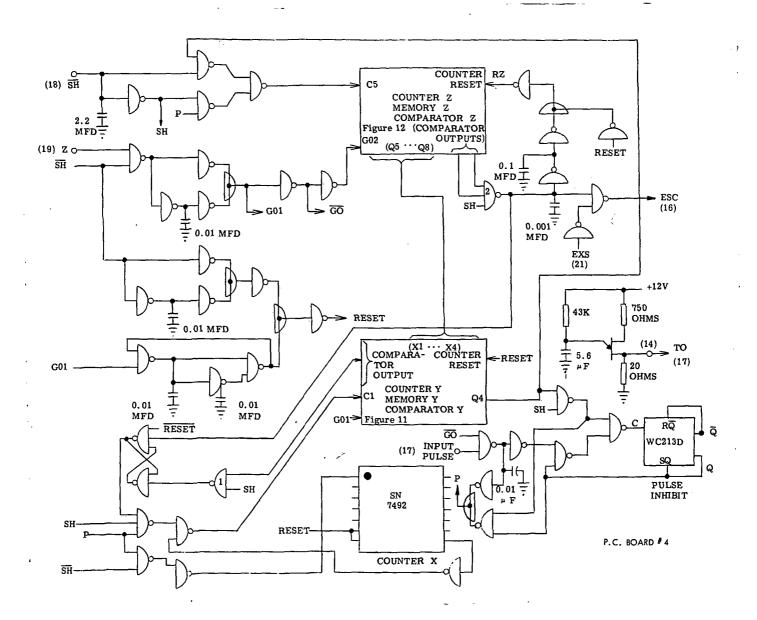


Figure 10. - Dark-Period Control Logic Circuit (See sec. II, figure 22)

from three binary counters in the breadboard gives one output pulse for every three input pulses. Counter Y, memory Y, and comparator Y are composed of 4-stage components as shown in figure 11. This eliminated nine components. Counter Z, memory Z, and comparator Z are also composed of 4-stage components as shown in figure 12. Six components are used, replacing 15 previously required. The pulse counting capacity was increased from 32 to 256 with this change. A reduction of 20 dual-in-line packages was realized on printed circuit board number 4.

For convenience, a unijunction transistor pulse generator to drive the dark period logic was installed on printed circuit board number 4. The output is brought out on pin 14. A jumper is provided on the control unit connector to connect this pulse to the normal pulse input point. If it is desired to use an external pulse source, the jumper may be removed and the source connected to pin 17.

### PRINTED CIRCUIT BOARD NO. 5

Printed circuit board number 5 contains the power supply for operating the controls. The circuit diagram is shown in figure 13. The power supply operates from an input voltage of 22 to 35 volts d-c and provides regulated output voltages of +12, -12, +6 and -6 volts required by the controls. In addition, 28 volt, 10 kHz is provided to power the solar sensor amplifier through the rotary transformer. Short circuit protection is provided for all d-c outputs.

## PRINTED CIRCUIT BOARD LAYOUTS

Circuits for the control unit are laid out on 4-3/4- by 7-inch printed circuit boards having printed wiring on both sides of the boards. The printed wiring is connected to 29-pin connectors. Mating connectors installed in the control unit box are wired for printed circuit board interconnections and external wiring is brought out through an external connector. Assembly of the control unit is shown in figure 14.

The printed circuit boards are shown in figures 15 to 22. Both sides of each board are shown. Components are drawn in and identified. Resistors are identified only by their ohmic values since power dissipation is low enough that 1/8-watt resistors serve throughout. Capacitors are identified by the capacitance value. Transistors of all types used are identified by their registered type numbers. All diodes used are 1N194 or

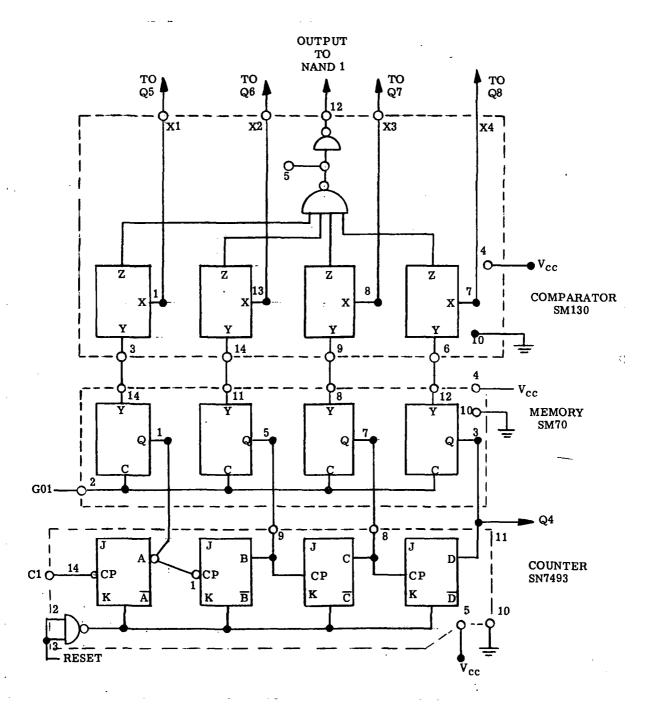


Figure 11. - Counter Y, Memory Y, Comparator Y
Showing Interconnections
(See sec. II, figures 20 and 21)

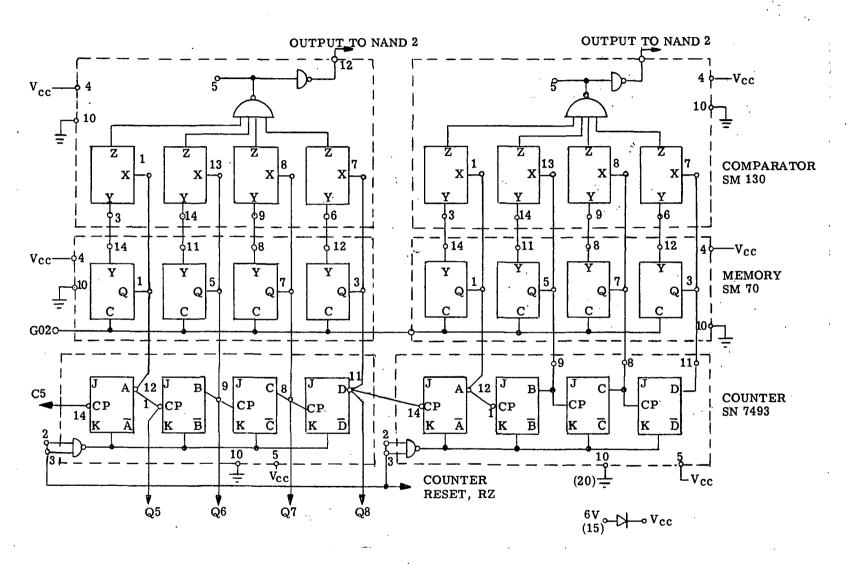


Figure 12. - Counter Z, Memory Z, and Comparator Z, Showing Interconnections (See sec. II, figures 20 and 21)

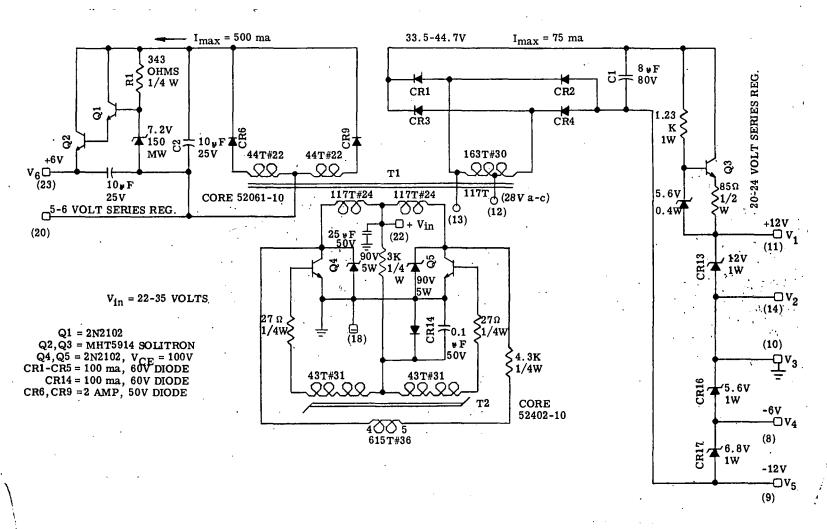
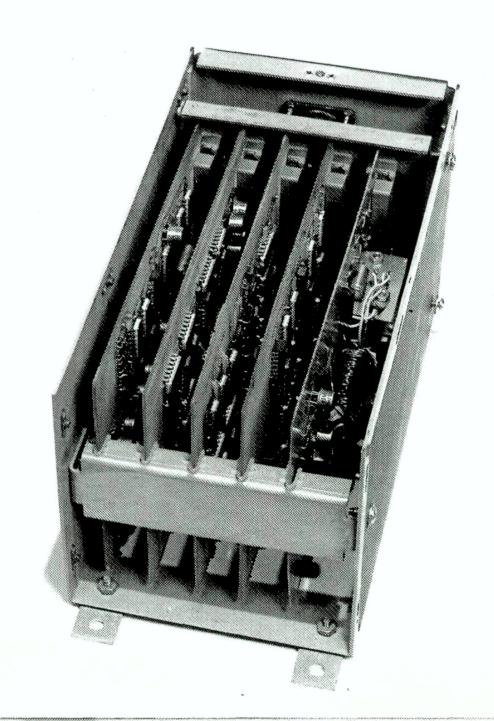


Figure 13. - Multiple Voltage Regulated Power Supply



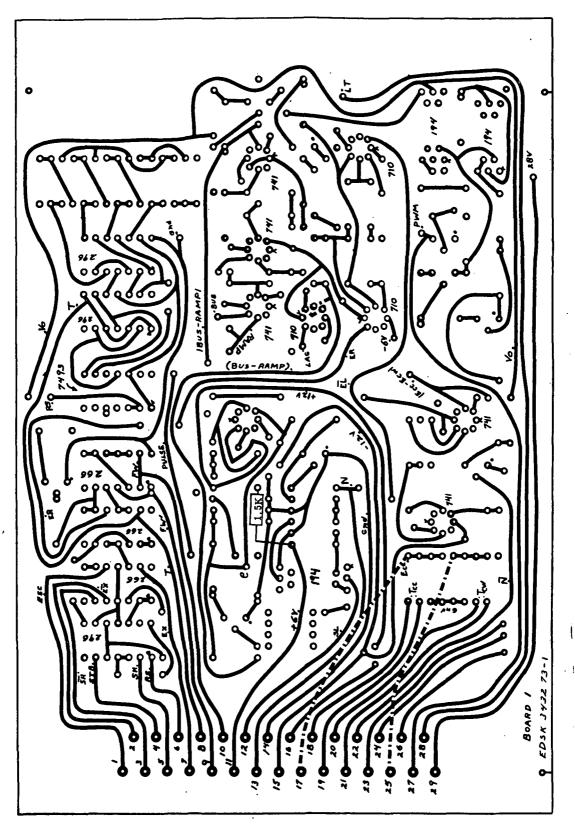


Figure 15. - Printed Wiring Layout For Printed Circuit Board No. 1

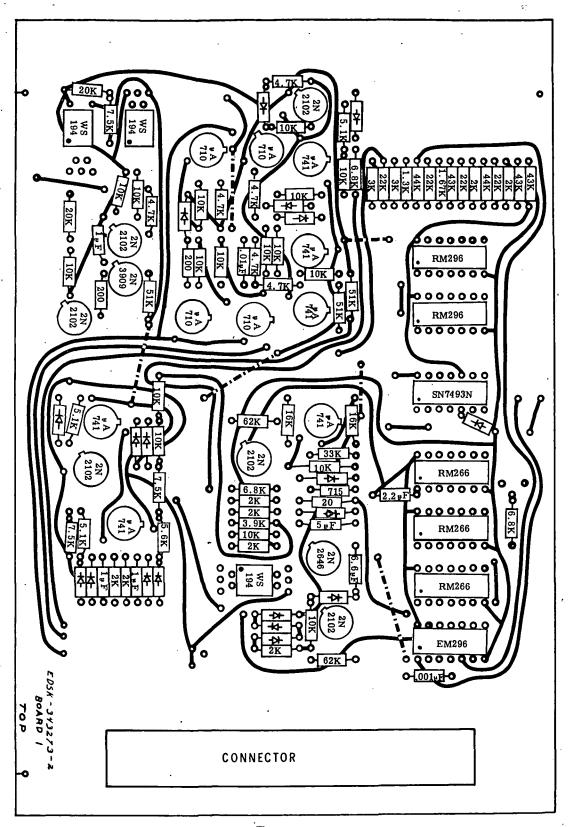


Figure 16. - Component Layout For Printed Circuit Board No. 1

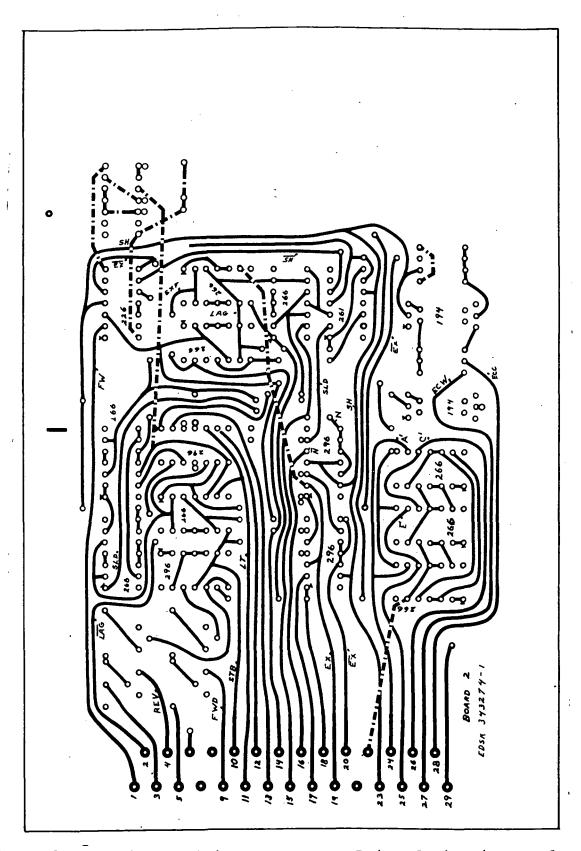


Figure 17. - Printed Wiring Layout For Printed Circuit Board No. 2

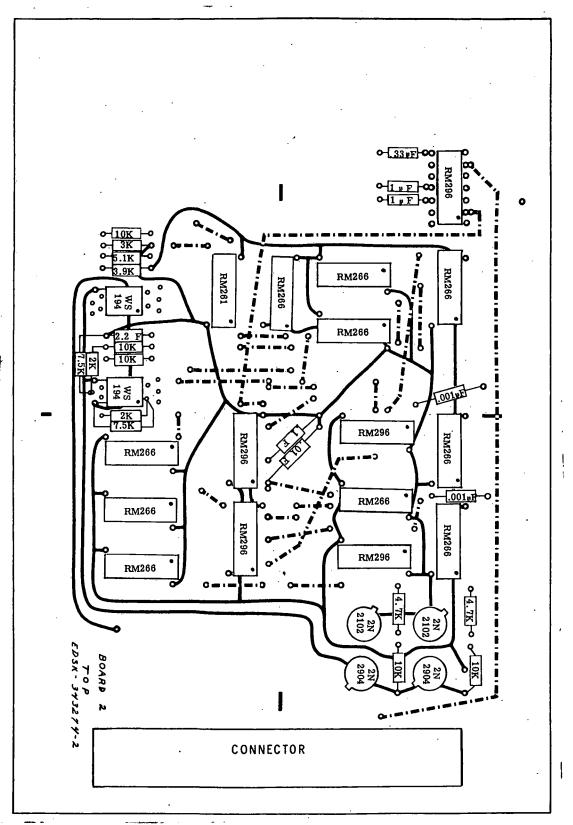


Figure 18. - Component Layout For Printed Circuit Board No. 2

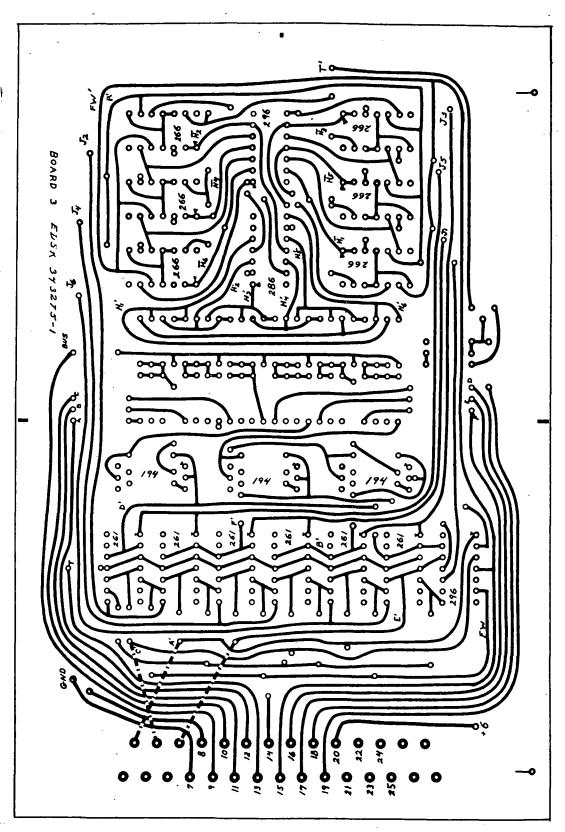


Figure 19. - Printed Wiring Layout For Printed Circuit Board No. 3

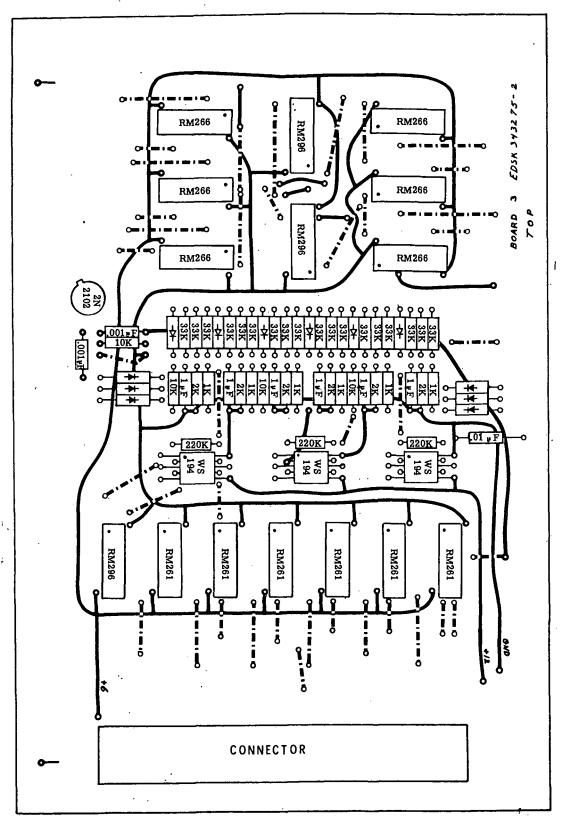


Figure 20. - Component Layout For Printed Circuit Board No. 3

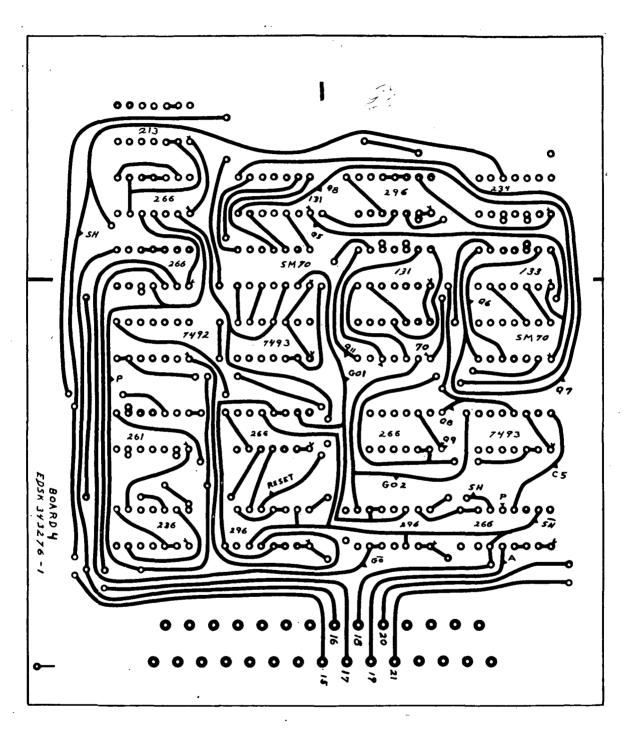


Figure 21. - Printed Wiring Layout For Printed Circuit Board No. 4

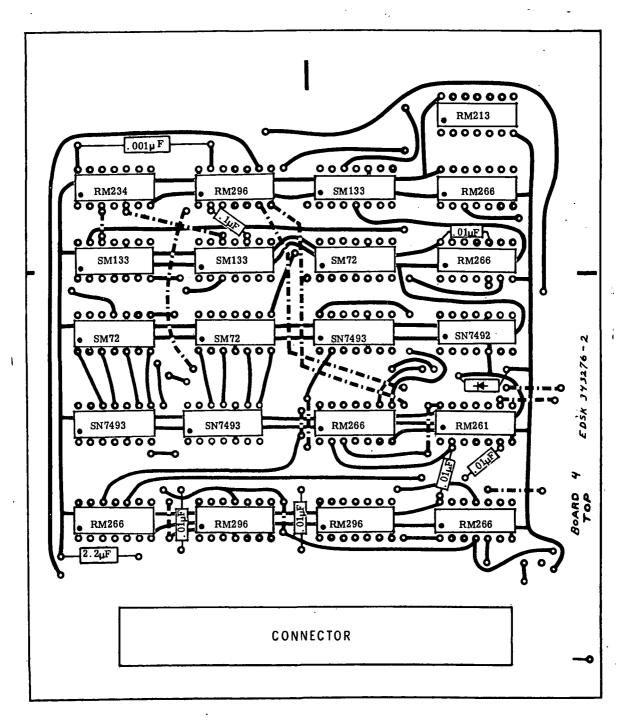


Figure 22. - Component Layout For Printed Circuit Board No. 4

equivalent. The integrated circuits are identified by the manufacturer's type number. Prefixes of the integrated circuit type numbers are listed below with the manufacturer's name.

RM Raytheon
SM Sylvania
SN Texas Instruments
WS Westinghouse

## SOLAR SENSOR AMPLIFIER ASSEMBLY

The small package shown in figure 23 is the solar sensor amplifier which is electrically a part of the control unit. A separate unit is required because it must be mechanically isolated from the non-rotating control unit. The circuit of the solar sensor amplifier is laid out on a printed circuit board shown in figure 24.

# EXTERNAL COMMAND UNIT

The function of the external command unit is to simulate remote control over the reorientation system. The circuit of the unit is shown in figure 25. Three switches are located on the unit. The switch on the right marked "STANDBY" is a single pole, single throw switch. Toggling the handle down opens the switch and produces the STANDBY signal which disables the reorientation system causing it to stop and remain inactive. When the handle is toggled up the STANDBY signal becomes zero and normal control resumes in the system.

The switch located in the center of the external command unit is a double-pole, triple-throw switch having two distinct functions. One pole is connected in series with the "STANDBY" switch and is connected so that it is normally closed except when it is thrown from one position to another, as shown by figure 25. As its position is changed, its circuit is momentarily opened producing the STANDBY signal which initializes the controls. The other pole acts as a selector switch. In the center or "TRACK" position, the system is in automatic control which allows reorientation of the solar array and normal tracking. Also in the center position the switch maintains the signal EXS in the zero state preventing interference with automatic control. In the "FORWARD" position the signal EXF is produced and the signal EXS is no longer inhibited. This removes



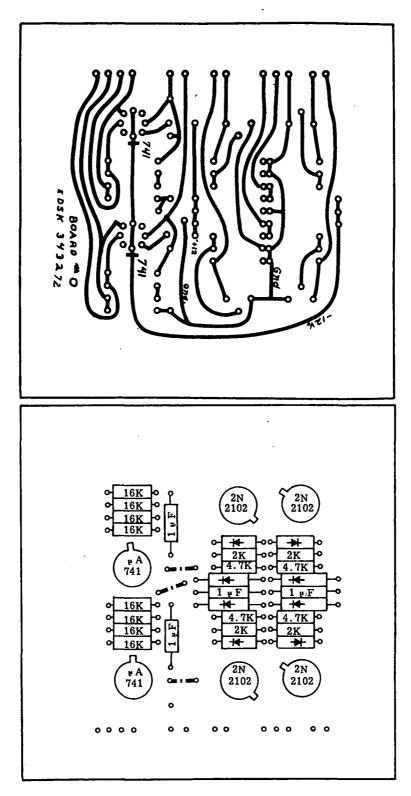


Figure 24. - Printed Circuit and Component Layout For Solar Sensor Amplifier

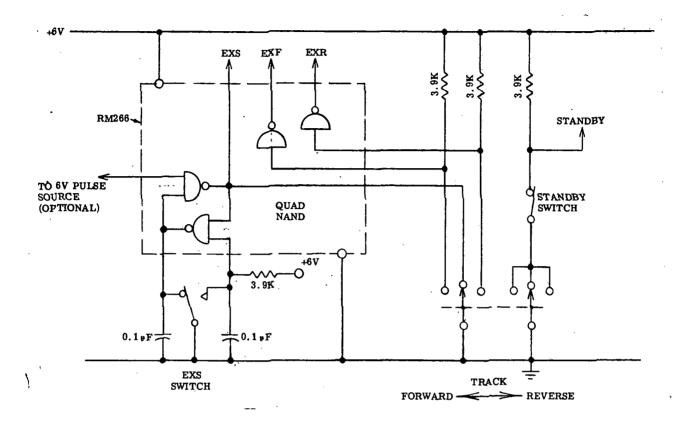


Figure 25. - Circuit of External Command Unit

all automatic control functions and the array turns in the forward direction at the command of pulse signal EXS (approximately one half degree per pulse). Similarly, with the switch in the "REVERSE" position the signal EXR is produced and allows the array to be driven in the reverse direction on command of the pulse signal EXS.

The third switch, marked EXS on the external command unit, is a single-pole, double-throw switch which has one momentary position. In the normal released position it sets a NAND gate flip-flop circuit which produces the signal EXS as a steady-state logical "l". Toggling the switch to its momentary position resets the flip-flop causing the signal EXS to go to zero. Thus by toggling the EXS switch the array may be driven either forward or reverse depending on the position of "FORWARD-TRACK-REVERSE" switch. If the optional pulse source is used the signal EXS will be transmitted so long as the EXS switch is held in MOMENTARY ON position. Six-volt pulses at a rate of one or two per second are recommended. The pulse voltage should be less than one volt in the "zero" state.

The external command unit is shown in figure 26, which also includes the control unit, the solar sensor amplifier, the rotary transformer and connecting cable.

# INTERCONNECTION OF CONTROL COMPONENTS

The control unit is interconnected with the external command unit, the rotary transformer, and the motor by means of a cable system wired to connectors which mate with connectors on the components. The cable may be seen in the photograph, figure 26.

Interconnections are defined in the table I which includes the interconnections of the printed circuit boards of the control unit. In the first column, the signal names and supply voltages are listed. The corresponding numbers in the next five columns refer to printed circuit board connector pin numbers. If the signals are brought out of the control unit a letter appears in the column headed "Control Unit" corresponding to the signal name. Connections to the signal transformers appear in the "Transformer" column. Similarly, connections to the external command unit and the motor are indicated in the last three columns.

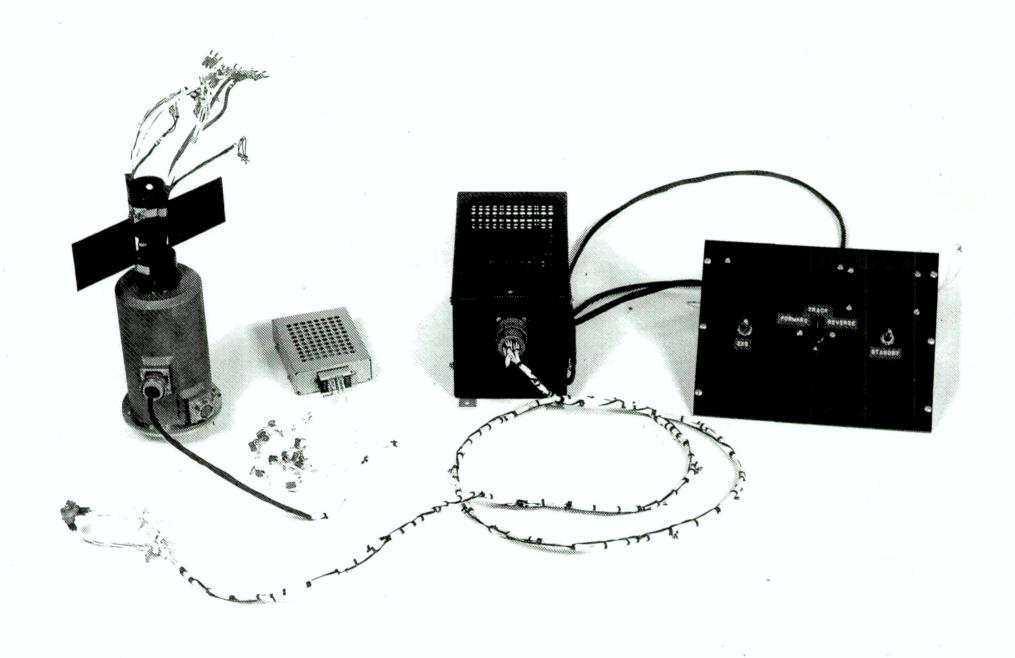


FIGURE 26

Table I. - Wiring Table

	BOARD OR CONNECTOR PIN NUMBER									
Signal Name	#1		nnecto Circu #3	r of uit Boa #4	rd #5	Control Unit	Trans- former	External Command Unit	Motor Connector 5 Pin	Motor Connector 7 Pin
ESC EX SH	1 2 3	20 18		16 18	!					
STB SH EL	4 5 6	10 23 6	·							
EX T FW'	7 8 9	19	13 15							,
FW +6V SL	10 11 12	1 3 13	14 20	15	23	A		6V		
N GND -12 V	13 14 15	15 29	7	20	10,14 18,20 9	f,h,j	G, R	GND	В	н
+12 V E <sub>CC</sub> T <sub>CC</sub> 1	16 17 18	5 28	8	9	11	R	С			
T <sub>CC2</sub> T <sub>CW1</sub> T <sub>CW2</sub>	19 20 21					S T U	D E F			
N BUS LAG	22 23 24	16 2	9							
E <sub>CW</sub> -6V PWM	25 26 27	27			8	L			E	
LT +28V REV	28 29	11 4			22	M c			A C	
FWD STANDBY EXF		9 12 14				b C V		STB EXF	D	
EXR A' C'		17 24 26	2 4			w		EXR		
E' MA MB		25	6 12 11			F G				A B
MC MD ME			10 18 17			H J Y				C D E
MF Z AC1		22	16	19	12	Z g e	A			F
AC <sub>2</sub> EXS PULSE				21 17,14	13	d B D	В	EXS		

#### INVERTER

One of the system components developed under this contract was the rotary transformer assembly (sec. IV). The rotary transformer power section requires 500 watts of 10 kHz square-wave power for excitation. The inverter described in this section was built to test this transformer.

A simple and efficient form of square-wave inverter is the type driven by a saturating transformer (sometimes called a Jensen type oscillator). Figure 27 is a schematic diagram of the inverter and rotary transformer.

Transformer T2 is a saturating transformer which alternately drives power switches Q1 and Q2 at the 10 kHz switching frequency. Base current is provided by windings N2 of T2 through resistors R1, R2, R3 and R4 and diodes CR2, CR3, and CR4. Capacitor C3 provides negative bias to aid in turning off Q1 and Q2. To minimize storage time in Q1 and Q2 at light loads, windings N3 of T2 and diodes CR5 and CR6 siphon off base current to maintain the transistors slightly out of saturation. Resistor R5 limits primary current when T2 saturates.

Transistors Ql and Q2 are matched pairs to minimize overlap in transistor switching times. Transistor overlap results in short circuiting the supply by switching both primaries of Tl to ground simultaneously. The input filter (Cl, C2, Ll and CR1) aids in limiting current during the small overlap period.

Figure 28 shows the rotating transformer and packaged breadboard inverter. Figure 29 shows an internal view of the inverter.

The inverter's function is to transform  $80 \pm 1$  volt d-c power between two platforms rotating relative to each other. The operating characteristics of the system were measured by adding the circuit designated as LOAD to the secondary of the rotary transformer. The voltage transfer ratio was lower than designed. The input voltage had to be increased to 84 volts to achieve 28 volts at 400-watt load. Figure 30 shows the effect of load on output voltage regulation and efficiency at 84 volts input.

The inverter provided does not have appreciable overload capability and will be damaged if short circuits are applied to its output.

Table II comprises the parts list for the inverter.

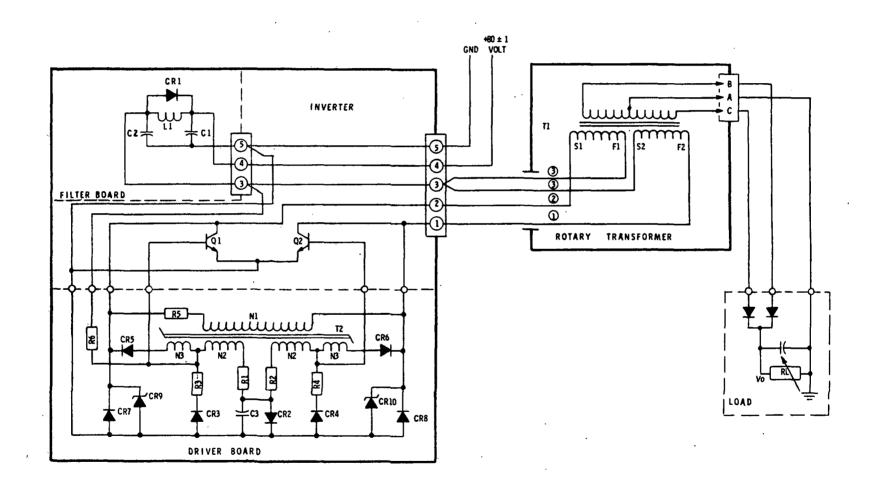
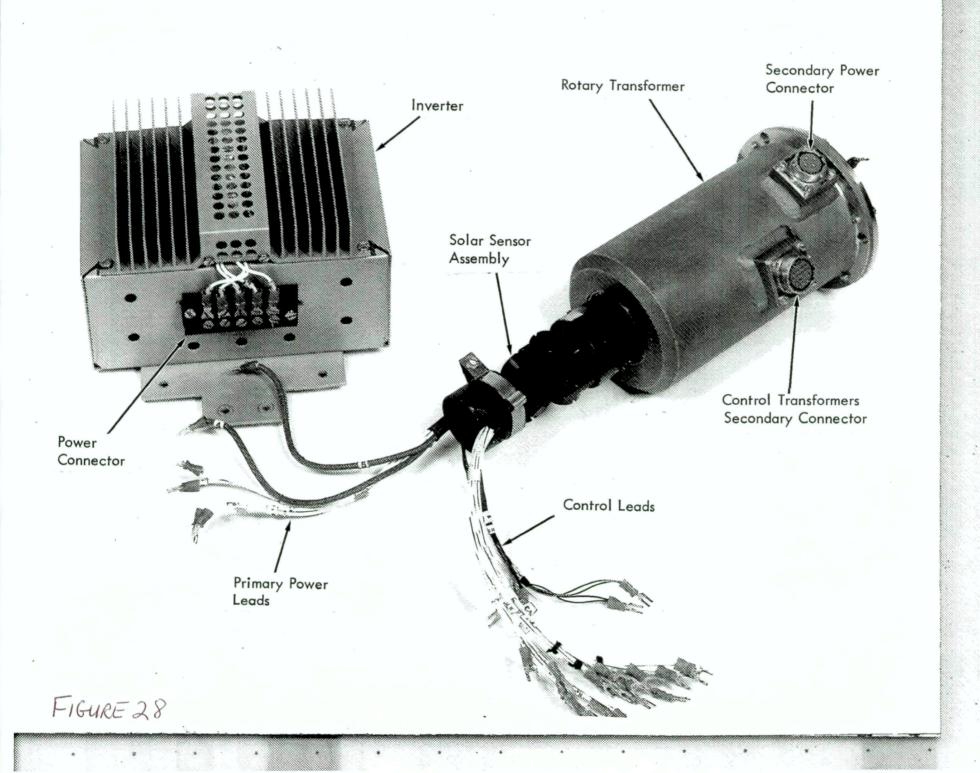


Figure 27. - Schematic Diagram 500-Watt, 10-kHz Inverter



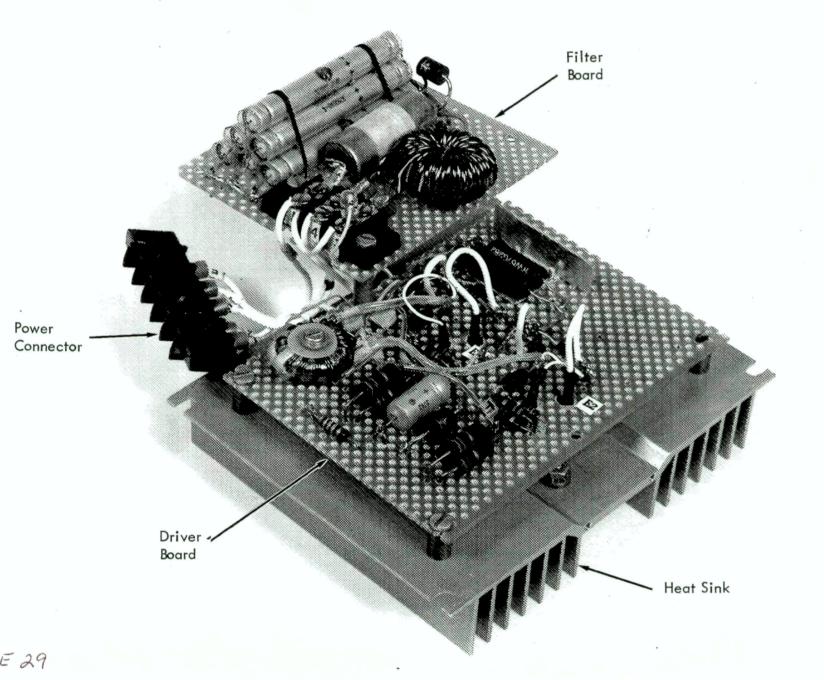


FIGURE 29

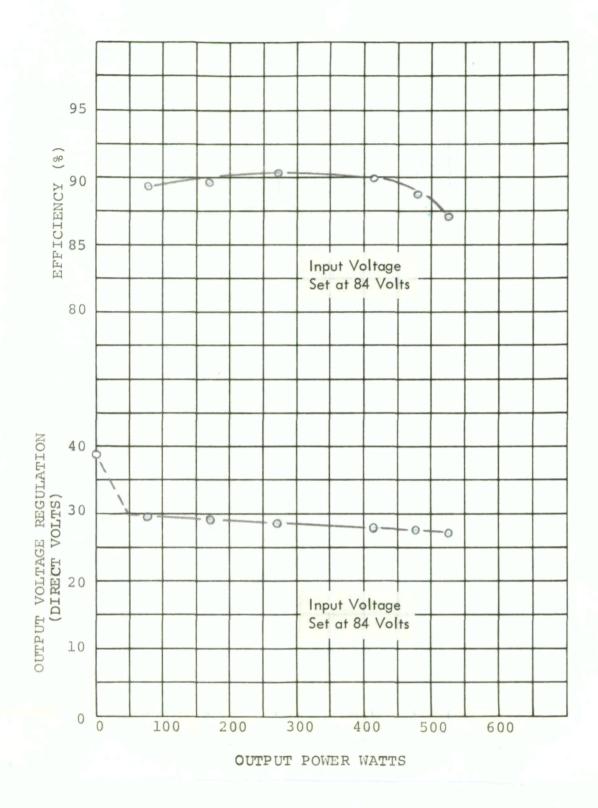


Figure 30. - Efficiency and Regulation Versus Output Power 500-Watt, 10-kHz Inverter

# Table II. - Inverter Parts List (See figure 27)

HEAT SINK COMP	ONENTS
Q1, Q2	Solitron 34SE104 V <sub>CeO</sub> = 300V (Selected Matched Pairs)
DRIVER BOARD C	OMPONENTS
CR7, CR8	Electrolytic 150 µf, 30V dc Solitron SNS 3000 Solitron SNS 2000 Westinghouse 388F Diode Westinghouse 388F Diode Unitrode UZ5220, 220 volt, zener Two 15-ohm & one 120-ohm 1 watt carbon composition parallel Two 15-ohm & one 120-ohm 0.5 watt carbon composition tion parallel Two RW676282 resistors parallel (2.8K ohm, 5 watt each) 33,000-ohm 0.5 watt carbon composition  Core: Magnetics Inc. Type 52000-10 Turns: Primary (N1) = 477 turns, AWG 35 wire Secondary (N2) = 15 turns, AWG 22 wire Secondary (N3) = 2 turns, AWG 22 wire
FILTER BOARD C	COMPONENTS
Cl	Six Westinghouse P/N 939D090-6 36 $\mu f$ each, 100-volt electrolytic
C2	One 4µf, 200-volt
Ll	Powdered Iron Cored Choke
CR1	Solitron SNS 3000
POWER TRANSFOR	RMER

See section IV.

Tl

### DESCRIPTION OF LABORATORY MODEL

## AND ASSEMBLY PROCEDURE

#### MECHANICAL ASSEMBLY

The completely assembled laboratory model - except for the controller, external control unit, and load - is shown in figure 31.

The model consists of the following four basic subassemblies:

- 1. A tripod structured base containing the drive mechanism to simulate spacecraft rotation and a light projector to simulate the sun.
- 2. The solar array brushless d-c drive motor and rotary transformer subassembly.
- 3. The simulated solar array with inverter and solar sensor amplifier.
- 4. An antifriction, adjustable counterweight suspension system.

The model is designed to simulate the conceptual configuration and operating conditions of a solar array reorientation control system for an actual spacecraft wherever practical and possible. In particular, the effect of weightlessness of space on drag torques sensed by the control system is simulated by attempting to minimize radial and thrust loads on all bearings and by avoiding twisting of electrical leads and the support cable.

Radial bearing loads are minimized by mounting all components in the vertical position. Thrust loads are minimized by supporting the weight of all components, which rotate with respect to the spacecraft, by the suspension and counterweight system.

The laboratory model test assembly is provided with slip rings to bring in 80-volt, dc power to the system in place of the solar array power. Lead wire wind-up is thus avoided during simulation of spacecraft rotation. The ends of the d-c leads to the slip ring brushes are visible in the lower left of figure 31.

The suspension system utilizes a ball bearing coupling to avoid support cable wind-up.

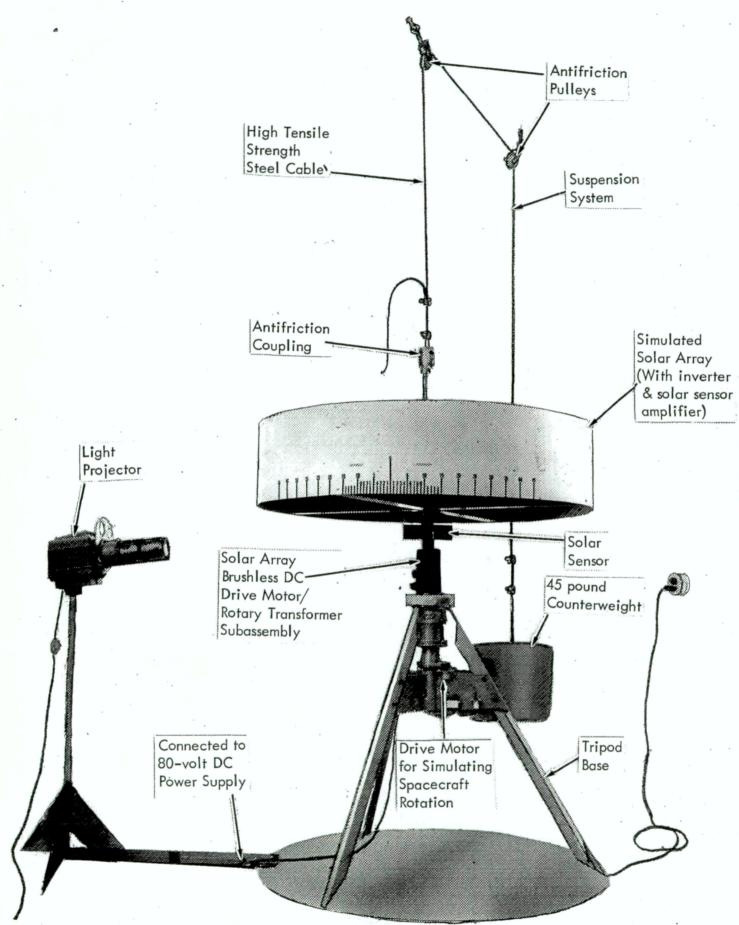


FIGURE 31

The following paragraphs contain more detailed discussion of the individual subassemblies in an order corresponding to the assembly sequence for the complete laboratory model. Comments on assembly procedures are included when appropriate.

Tripod Base and Light Projector Subassembly. - The tripod base with rotating drive assembly for simulating spacecraft rotation and the light projector are shown in figure 32.

The base and the light projector are the same used in Phase I except for a modified ring at the top of the tripod to accommodate the rotary transformer added in Phase II.

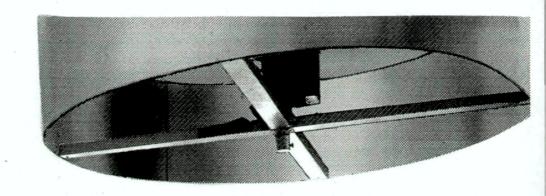
The rotating fixture for simulating spacecraft rotation is discussed in section II.

Brushless D-C Motor/Rotary Transformer Subassembly. - The brushless d-c motor/rotary transformer subassembly consists of the following components, and is assembled prior to mounting on the rotating mounting fixture:

- 1. Solar array brushless d-c drive motor part number 915F359.
- 2. Rotary transformer EDSK 349968.
- 3. Slip ring assembly.
- 4. Solar sensor assembly.

The brushless motor and rotary transformer shafts are coupled by a sleeve type coupling with a light press fit between the coupling and the two shafts and by two dowel pins, one through each shaft and the coupling. The motor and rotary transformer rotors probably would be mounted integrally on a common shaft straddled by single bearings in an actual spacecraft solar array drive. For purposes of the model, the individual motor and rotary transformer shafts rigidly joined by the sleeve coupling simulate the common shaft.

The motor and the rotary transformer each have two bearings. This constitutes a four bearing system. If the motor and rotary transformer housings were fastened rigidly together, misalignment caused by diametral and concentricity tolerance build-up might impose unacceptable loads on the bearings. Since it is desirable to maintain a rigid common shaft, a flexible coupling is provided between the motor and rotary transformer housings.



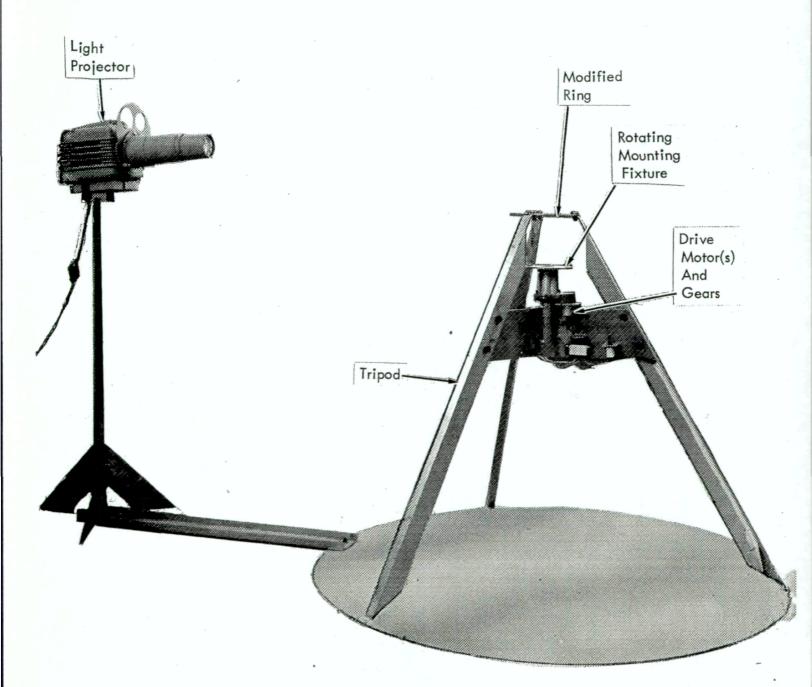


FIGURE 32

This coupling consists of three adjustable steel dowels rigidly attached to a special adapter plate mounted on the face of the electronic commutator portion of the motor. These dowels engage mating holes in the rotary transformer flange to transmit torque from the motor housing to the rotary transformer housing. The dowels may slide freely through the holes.

Three coil springs ride on the dowels between the motor and rotary transformer housing. The springs support the weight of the rotary transformer housing, locate it axially, and provide flexibility so that the rotary transformer housing may align itself with its own bearings. The compressive preload in the springs is adjusted by rotating the dowels so that when the weight of the motor and rotary transformer rotors are supported by the suspension system, the weight of the rotary transformer housing is balanced or supported by the springs.

The slip rings are mounted on a sleeve which is mounted between the motor and the rotary transformer on the shaft coupling with a light press fit. The slip ring sleeve captures and retains the shaft/coupling dowel pins. The two slip ring leads are brought through holes in the rotary transformer shaft and through matching slots in the shaft coupling and slip ring sleeve to terminals on the slip rings. These leads are run up the center of the rotary transformer shaft and out through the top of the solar sensor.

The solar sensor is the same device used in Phase I. It is attached to the top of the rotary transformer using the same sliding coupling and spring dowel pin used before (motor and rotary transformer shafts are same diameter).

The complete motor/rotary transformer assembly is shown mounted to the rotating mounting fixture on the tripod base in figure 33. The motor flange is secured to the rotating mounting flange using the four threaded cap screws provided. Figure 33 also shows the slip ring brush box assembly attached to the motor adapter ring. Figure 34 shows the complete motor/rotary transformer subassembly being lowered through the top tripod ring to the rotating mounting fixture.

After the motor/rotary transformer subassembly is installed, the brushes should be installed in the brush boxes and the slip ring cover lowered over the rotary transformer using the slot provided to clear the rotary transformer connectors, and fastened to the top tripod ring.

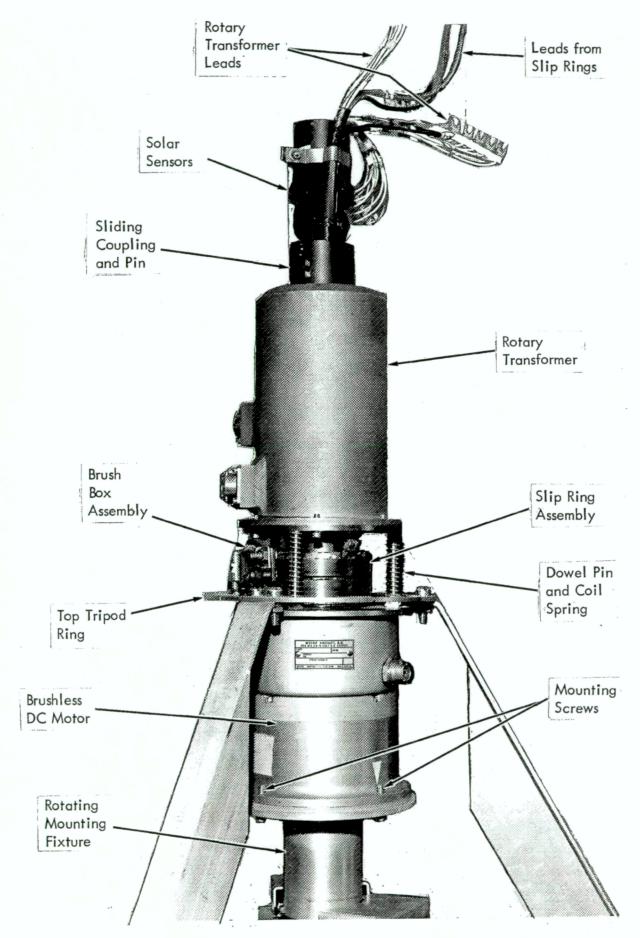


FIGURE 33

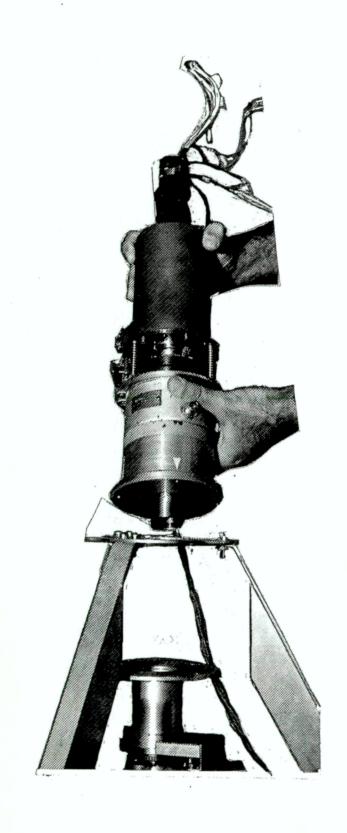


FIGURE 34

Simulated Solar Array Subassembly. - The simulated solar array is the same as used in Phase I (sec. II), except that the inverter and the solar sensor amplifier are mounted inside the array drum. Two terminal boards are also mounted on the drum cross braces.

The array should be suspended from the suspension system and aligned with the top of the solar sensor. See figure 35.

The solar sensor shadow fins are inserted into the solar sensors.

Figure 35 also shows the slip ring cover installed.

The simulated solar array subassembly is lowered and the array stub shaft is mated with the hollow stub shaft at the top of the solar sensor matching the index marks on the two parts. The parts are fastened with the locking bolt shown. The locking bolt is secured with locking wire.

The leads are connected to the inverter and/or terminal boards as shown in figures 36 and 37.

Suspension System. - The suspension system is shown in figure 38. It consists of:

- 1. Antifriction coupling
- 2. High tensile strength, flexible steel cable
- Antifriction pulleys
- 4. 45-pound counterweight.

The antifriction coupling utilizes a ball bearing to minimize drag torque and prevent reaction torque from suspension cable twist as the array rotates.

The high tension steel cable is used to provide sensitivity to vertical displacement during counter balancing procedures, and to avoid subsequent creep.

The antifriction pulleys utilize ball bearings to provide maximum sensitivity during counter balancing procedures.

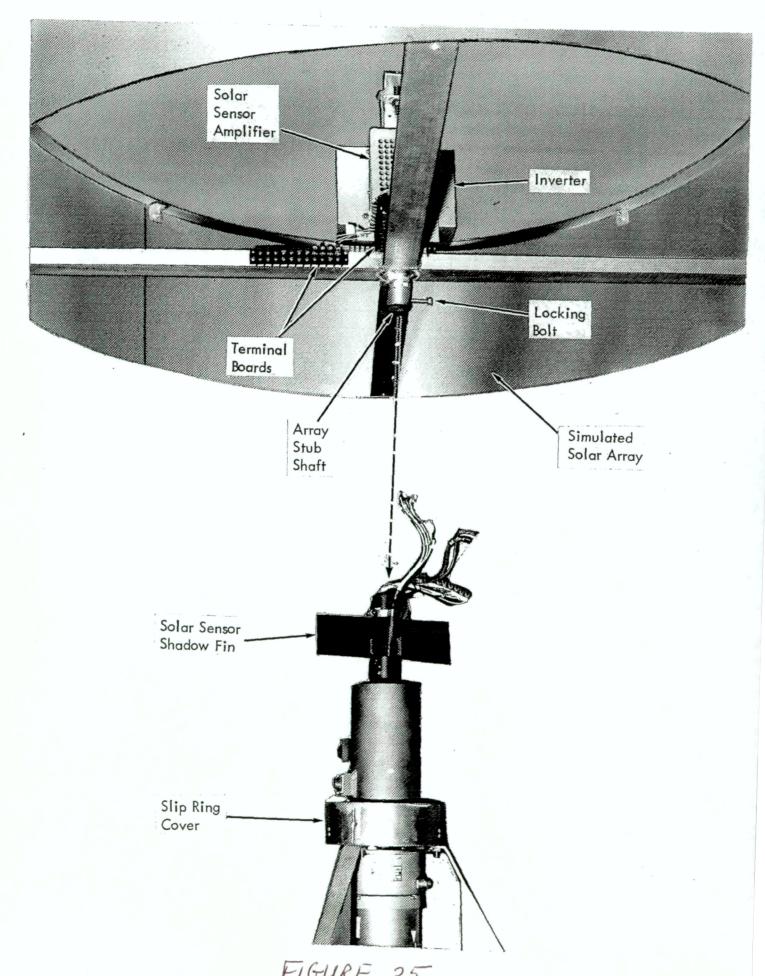


FIGURE 35

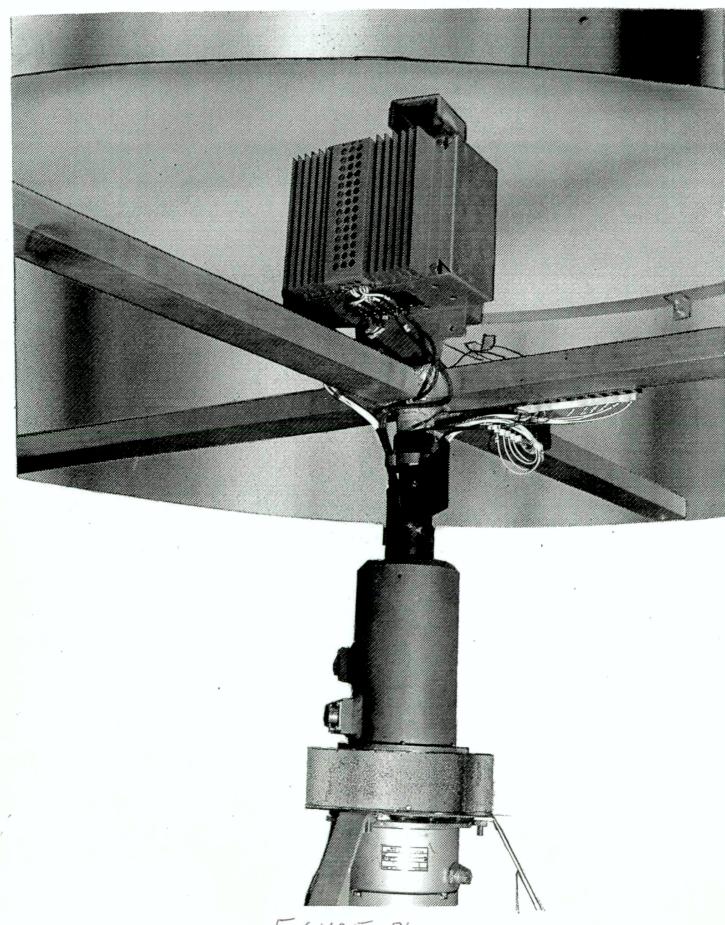


FIGURE 36

Fie To

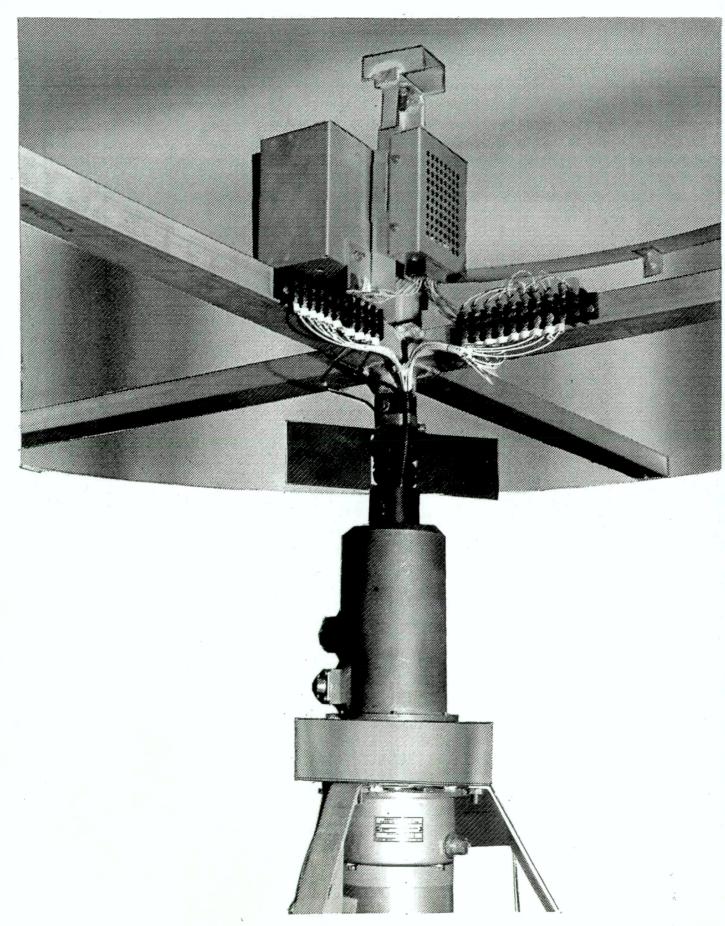


FIGURE 37

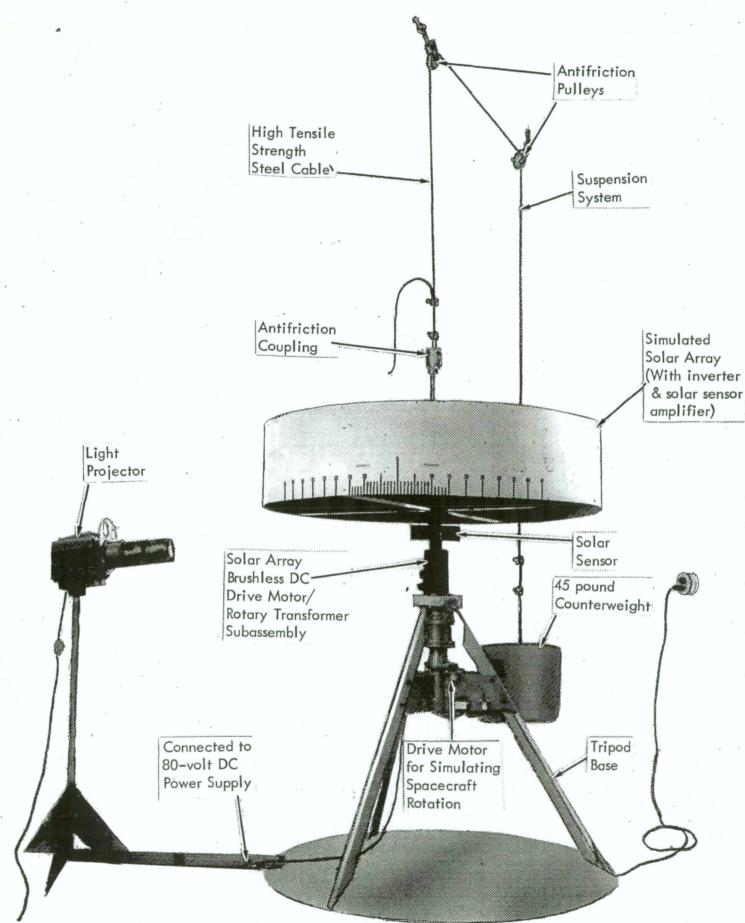


FIGURE 38

The 45-pound counterweight is enough to counterbalance the motor rotor, rotary transformer rotor, the solar sensor, the simulated array subassembly and appropriate parts of the suspension system so that minimum thrust load is exerted on the bearings.

#### ELECTRICAL CONNECTION

Assembly of the laboratory model is completed by making the necessary electrical connections. A schematic diagram of the model is shown in figure 39. In addition to the interconnecting cable connecting the control unit with its associated components, other interconnections are indicated. The solar sensors, the solar sensor amplifier and the sensing transformers are interconnected through a terminal board, TBl. The inverter and the rotary transformer power windings are interconnected through TB2. The 80-volt, d-c supply is brought in through slip rings to the "array" side of the system. These connections are specified in the following "Laboratory Model Wiring Chart," Table III. All identification symbols on the chart refer to the connector, terminal board or lead markings of the component identified in the heading of the column.

In addition to the 80-volt, d-c power supply to the inverter, a 28-volt, d-c supply is required for the control and the brushless motor, and 60-Hz, 117-volt service outlets for the projector and the orbital-rate drive motors. The projector which uses a 1000-watt light bulb should be powered from a variable transformer (variac). Full intensity for the system is provided with an 85% setting. This arrangement, aside from prolonging bulb life, provides for simulation of sunrise and sunset.

Simulation of orbital rotation is provided by a pair of timer motors geared to the brushless motor shaft. The timer motors are prewired through a reversing switch to allow rotation in either direction. It may be desirable to operate the laboratory model at a greater orbital speed. If so, the timer motors may be replaced by higher speed motors.

#### TESTS

System tests of the laboratory model were limited to performance testing. Except for operation of the inverter with the rotary transformer, the performance tests were a repeat of those conducted in Phase I. Tests were run with the inverter-transformer turned off. There was no difference detected due to operation of the inverter-transformer. Further, the results of performance

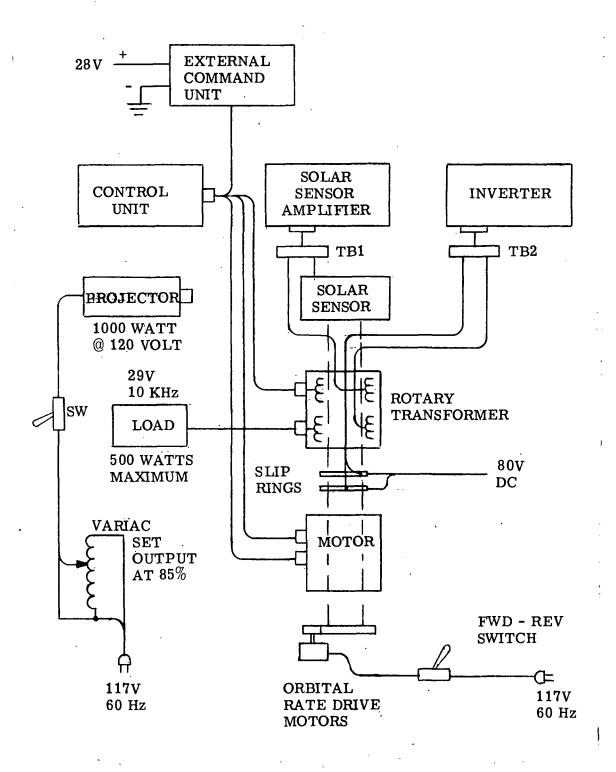


Figure 39. - Laboratory Model Connection Diagram

Table III. - Laboratory Model Wiring Chart

Solar Sensor	Solar Sensor Amplifier	TB1	Trans- former Leads	TB2	Inverter	Slip Rings
	3C 4A 4C	1 2 3	A B C			
	4D 3A 3B	4 5 6	D E F			
	2A 4B 1A	7 8 9	G U R	<i>.</i>		
		10	,			,
			K H J	1 2 3		
			N L M	4 5 6 7		
S1 RED S1 BLACK S3 RED S3 BLACK	1D 1C 2D 2C			8 9 10 11		
			F1 S2 F2,S1		1 2 3	
					4 5	4 5

tests were almost identical to the results obtained in Phase I tests. The reader is, therefore, referred to section II of this report pages 50 to 58. "Performance testing" for data and discussion of performance tests.

Tests were not run on the rotary transformer except as part of the inverter-transformer unit. Again tests were confined to performance tests. Voltage regulation and efficiency data are plotted in figure 30 of this section. The efficiency curve includes losses in both the inverter and the rotary transformer.

#### OPERATION LIMITATIONS

Two areas of caution should be observed in operation of the laboratory model.

- 1. Load on the transformer must be limited to 500 watts. The reason for this limitation is not the transformer, but the inverter which does not have overload protection.
- 2. Operation in the dark-period mode should be preceded by 90° orbital rotation to assure proper setup of the counting circuit of the dark period control. Failure to set up the counting circuit will cause the array to be driven too fast and pull out of proper orientation.

# Page Intentionally Left Blank

#### SECTION VI

#### CONCLUSIONS AND RECOMMENDATIONS

A laboratory model of a brushless, direct-drive solar array reorientation system has been designed and developed according to the specification of NAS 5-10459. From the results of performance tests, it has been concluded that the system meets the intent of the specification.

### Functional Operation

The control system is capable of reorienting a simulated solar array having an inertia of 5 to 10 slug feet square from any position, smoothly within a three-minute period. Acceleration from rest to a speed-controlled return to proper orientation occurs with a minimum of speed oscillation. Acceleration is limited by the design of the controller to minimize reaction between the array and the spacecraft. Upon approaching proper orientation, anticipatory circuits in the controller act to prevent undesirable reactions caused by overshoot or hunting and thus cause a smooth transfer from the reorientation mode to the normal tracking mode.

Operating in the sunlit normal tracking mode, the controller tracks the sun vector at almost a constant error of 0.7 degree. There is no perceptible oscillation and the variation in tracking errors is about 0.1 degree. Transition of the system into the dark period has little effect on the average tracking error (a maximum of 1/2 degree). Total variation of the tracking error during dark period tracking was observed to be 1.2 degree, while the maximum deviation from the sun vector was less than 2 degrees.

Simulation of solar power from the array required that power be brought from an external source to the simulated array through slip rings. Performance tests were made with slip rings. This condition gives a slight amount of damping which improves performance, particularly during the dark period of operation where the system is driven by pulses. An electrical damping method using phase lead compensation of signals derived from the offset tooth sensor is described in reference 4, and can be considered in a follow-on system design.

One area where improvement in operation could be made is in the manual forward and reverse control. Presently, pulses must be supplied and the array is moved 0.47 degree per pulse. A better method would result by changing the circuit so that

the manual "Forward" or "Reverse" commands would simulate the speed limited operation of the large error reorientation mode. (See section II, page 33, Speed-Controlled Reorientation.) In this case a steady-state control voltage would replace the pulse inputs and much smoother operation would result.

#### D-C TOROUE MOTOR

The problem areas outlined in appendix IV were analyzed, and development work was done to correct these problems. The inequality of signals from the magnetic sensor (reluctance switch) was corrected by modification of the output windings so that each pair of poles (for each of the six output signals) have approximately the same number of turns per pair. It is recommended that all sensor output coils be identical in future motors.

The major problem area involved the electronic commutator and speed control system. Variation in pulse width of the voltage applied to the motor windings as a function of rotor position aggravated torque variations and caused erratic low-speed operation. The primary cause of pulse-width variation was irregularities in the magnetic sensor wave form. After analysis and testing it was decided to eliminate the effect of the magnetic sensor wave form by rectifying the sensor outputs and to revise the circuit to operate from the resultant dc signals. The primary consequence of the circuit revision was the replacement of the six Schmidt trigger circuits with three differential voltage comparators and integrated circuit logic modules.

The changes made in the circuit corrected the problem areas cited in appendix IV. The pulse-width variation with rotor rotation is nil. Torque variation (or ripple torque) was reduced to a minimum. The remaining ripple torque is caused almost exclusively by variation in rotor permanent magnet flux distribution.

Circuit changes required the elimination of some parts and substitution of other parts. The original printed circuit boards could not be fully utilized in the revision, thus it was necessary to add a board to complete the circuit modification. It is, therefore, recommended that new circuit boards be designed when additional motors are built. This will eliminate the need for the additional board and simplify the wiring.

If it is desirable to have a brushless dc motor having less ripple torque it is recommended that further development work be undertaken to produce such a motor. Techniques such as pole shaping might be employed to obtain a flat-topped, rather than sinusoidal, torque curve relative to each motor winding. It is believed that further work with the electronic commutator-control circuit will bear minimal results relative to ripple torque.

#### ROTARY TRANSFORMER

A 500-watt, 10-kHz rotary transformer and five signal transformers were designed and built in a single package for use as part of the laboratory model. Emphasis of the design was on efficiency where 99% was the goal. Accurate efficiency measurements could not be made with available equipment, but calculations indicate 99% to be a reasonable value. At any rate, the transformer efficiency is much greater than that of any inverter which can be used in the power system.

No attempt was made in the transformer design to minimize weight since it is to be used only as part of the laboratory model. It is strongly recommended that in any flight hardware version the rotary transformer package be integrated with the d-c torque motor. In such an arrangement the assembly would have a common bearing system which would eliminate the problem of proper alignment. Minimization of weight can then be accomplished in such a design

# Page Intentionally Left Blank

#### SECTION VII

#### REFERENCES

- 1. Veillette, L. J., A Functionally-Integrated Controller-Commutator for Use in Brushless Direct-Drive Solar Array Reorientation Systems, X-716-66-473, dated September, 1966.
- 2. Yates, W. W. et al, Second Quarterly Report, Advanced Brushless D-C Torque Motor, NASA Contract NAS 5-10263, Report No. WAED 66.69E.
- 3. Final Report for the Design and Development of a Non-Dissipative Charge Controller using a Rotary transformer, Report No. M2139P800C. Matrix Research Corp., NSAS Contract NAS 5-9204.
- 4. Veillette, L. J., "<u>Highlights of a Brushless Direct-Drive Solar Array Control System Design</u>", IEEE Transactions on Aerospace and Electronic Systems, March 1971.

Page 160

Blank

APPENDICES

Page 162

Blank

Grid of Regular membered

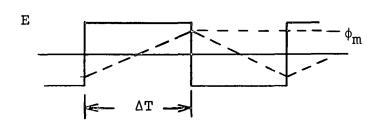
proper of Start with

Oppendix program I-1.

#### APPENDIX I

#### ROTARY TRANSFORMER MAGNETIC CALCULATIONS

Assume shape and dimensions of rotary transformer as shown in sectional view in figure I-1. The input voltage is assumed to be a square wave of magnitude E volts and frequency of f Hertz.



$$E = N(\Delta \phi / \Delta T)$$
 volts

$$\Delta \phi = \phi_m - (-\phi_m) = 2\phi_m$$
 webers

$$\Delta T = \int 1/2f$$
 seconds

$$\phi_{m} = \frac{E}{N_{p}} \cdot \frac{\Delta T}{2} = \frac{E}{4N_{p}f}$$
 webers

where  $\mathbf{N}_{\mathbf{p}}$  is the number of primary turns

# Magnetic circuit losses

Section 1 (inside cylindrical section)

$$A_1 = (D_2^2 - D_1^2)\pi/4 \text{ in}^2, \text{area}$$

$$V_1 = A_1 (A - 2B) in^3$$
, volume

$$B_1 = \phi_m/A_1$$
 webers/in<sup>2</sup>, flux density (max.)

= 
$$0.155 \times 10^8 \phi_{m}/A_{1}$$
 gauss

$$K_1 = (1.12 + f/56000)(B_1/1000)^{2.26}(10^{-6}) \text{ watts/cm}^3 \text{ Hz}$$

This equation has been developed from loss data supplied by Stackpole on Ceramag 24B.

$$P_1 = K_1 \left(\frac{\text{watts}}{\text{cm}^3 \text{Hz}}\right) V_1 \left(\frac{\text{in}^3}{\text{in}^3}\right) \text{ f (Hz)} \quad 16.4 \left(\frac{\text{cm}^3}{\text{in}^3}\right)$$

= 16.4K<sub>1</sub> V<sub>1</sub> f watts, loss in Section 1

Section 2 (Outside Cylindrical Section)

$$A_2 = (D_4^2 - D_3^2) \pi/4 \text{ in}^2$$

$$V_2 = A_2 (A + 2B) in^3$$

$$B_2 = 0.155 \times 10^8 \phi_m/A_2$$
 gauss

$$K_2 = (1.12 + f/56000) (B_2/1000)^{2.26} (10^{-6}) \text{ watts/cm}^3 \text{ Hz}$$

$$P_2 = 16.4 K_2 V_2 f$$
 watts, loss in Section 2

Section 3 (Cylindrical Section, one end)

$$A_3 = \pi D_5 (B + C) in^2$$

$$V_3 = A_3(D_3 - D_2)/_2 in^3$$

$$B_3 = 0.155 \times 10^8 \phi_m / A_3$$
 gauss

$$K_3 = (1.12 + f/56000) (B_3/1000)^{2.26} (10^{-6}) \text{ watts/cm}^3 \text{ Hz}$$

$$P_3 = 16.4 K_3 V_3$$
 f watts, loss in Section 3

$$P_M = P_1 + P_2 + 2P_3$$
 watts, total magnetic loss.

Winding Loss - These calculations are based on the winding volume available and the utilization of the volume.

Assume two-section (center-tapped) round copper wire coils. Each section may consist of several wires connected in parallel.

 $R_W$  = wire resistivety of primary coil in ohms/1000 ft.

 $A_T$  = wire area in circular mils/turn.

 $R_W A_T = 10500$  cir. mil ohm/1000 ft. turn at 25° C.

N = total number of turns on primary.

 $N_P$  = primary turns per section.

 $W_P$  = turns in parallel per active turn.

 $N = N_P \text{ (turns/sec) } W_P \text{ (2 sec).}$ 

= 2 Np Wp turns.

 $A_P = A[(D_5 - D_2)/2](10^6)$  square mils, winding area (cross section)

Kp = Ratio of copper area (total turns) in circular
 mils to winding area in square mils.

 $A_T = A_P K_P / N cir mils/turn.$ 

 $R_W = 10500/A_T$ 

$$= \frac{10500 \text{ N}}{[A(D_5 - D_2)/2] \text{ K}_p 10^6}$$

$$= \frac{0.042 \text{ N}_{p}\text{W}_{p}}{\text{K}_{p}\text{A}(D_{5} - D_{2})} \text{ohms/1000 ft.}$$

 $Lp = (D_2 + D_5)\pi/2$  inch/turn, mean length of turn.

$$R_{pt} = \frac{L_p R_W}{12000}$$
 ohms/turn

Primary coil resistance is then

 $R_P = N_p R_{pt} / W_p$  ohms/section

Exciting Ampere-turns

Air gap N-I

 $NI = \phi/P$ 

 $P = \mu A_3/2g$  webers/amp turn, permeance.

 $\mu$  = 3.192 x 10<sup>-8</sup> webers/amp turn inch

(NI)g =  $2g\phi_m/\mu A_3$  amp turns

Split shell air gap (assume 0.002 inch gap)

 $(NI)j = 0.002 \phi_m/\mu A_2$ 

Iron section ampere turns

H = B (gauss)/MU (gauss/oersted)

MU = 4280 gauss/oersted, for Ceramag 24B

 $(NI)_1 = 2.02(A + B)B_1/MU$  amp turns, Section 1

 $(NI)_2 = 2.02(A + B)B_2/MU$  amp turns, Section 2

 $(NI)_3 = 2.02(D_3 - D_2)B_3/MU$  amp turns, Section 3

 $NI_x = (NI)_g + (NI)_j + (NI)_1 + (NI)_2 + (NI)_3$ total exciting amp turns

 $I_X = NI_X/N_D$  amperes, peak exciting current

Exciting current is reactive, lagging 90°, and triangular

$$i_X = (2t/\Delta T - 1)I_X$$
 for 1/2 period,  $\Delta T$ 

Power loss in primary winding is

$$P_{p} = \frac{R_{p}}{\Delta T} \int_{0}^{\Delta T} |(I_{L} - i_{x})|^{2} dt \quad watts$$

With a resistive load,  $I_{\rm L}$  will be a square wave of period 2  $\Delta T.$   $I_{\rm L}$  is the primary current due to the secondary load.

$$P_{p} = \frac{R_{p}}{\Delta T} \int_{0}^{\Delta T} (I_{L} + 2I_{x}t/\Delta T - I_{x})^{2}dt$$

= 
$$R_p [(I_L - I_x)^2 + 2 I_x (I_L - I_x) + I_x^2 + I_x^2/3]$$
  
=  $R_p (I_L^2 - I_x^2/3)$  watts

Secondary coil power loss

$$L_S = (D_3 + D_5)\pi/2$$
 inches/turn, mean length

 $R_S = N_S R_{ST}$  ohms

$$R_{ST} = \frac{10500 L_{S}}{12000} \cdot \frac{N_{S}}{A_{S}K_{S}} \text{ ohms/turn}$$

$$A_S = [(D_3 - D_5)A/_2] 10^6$$
 square mil

$$P_S = I_S^2 R_S$$
 watts

$$I_S = I_L N_P/N_S$$
 amperes

$$P_S = \frac{0.0105 L_S N_P^2 I_L^2}{6000 A(D_3 - D_5) K_S}$$
 watts

Secondary power loss  $P_S$  is based on a single section secondary coil with resistive load. If secondary is a center-tapped winding with a rectified load, the winding loss will be  $2P_S$ .

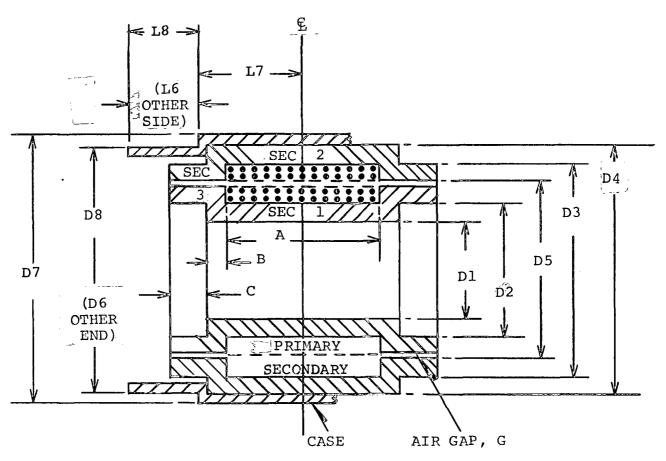
$$P_L = P_M + P_P + P_S$$
 watts, total loss  
 $\eta = (P_{in} - P_L)/P_{in}$  efficiency

The above calculations are for 25°C temperature. The effect of temperature rise on the efficiency may be taken into account by estimating the temperature rise and calculating the losses based on the assumption. Consider the change in winding resistance the only significant error in power loss. The power loss at the final temperature will be

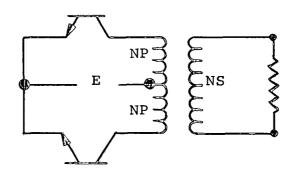
$$P_{L}' = P_{M} + (P_{P} + P_{S}) (1 + 0.0039T_{R})$$

where  $T_{\mathsf{R}}$  is the temperature rise.

The temperature rise may be verified by the method outlined in appendix II. If the calculated temperature rise is significantly different from the assumed value, a new value may be assumed and verified by recalculating the temperature.



ASSUMED SHAPE OF CORE AND WINDINGS



CIRCUIT DIAGRAM (SQUARE WAVE)

Figure I-1. - Rotary Transformer Core and Windings

#### APPENDIX II

# ROTARY TRANSFORMER; TEMPERATURE CALCULATION EQUATIONS AND METHOD OF USE

#### Assumptions

- a. Shape of core and windings is shown in figure II-1. b. All generated heat flows through surface  $A_7$ .
- Thermal properties are not temperature dependent. Temperature at any radius, r, is constant. c.

### List of Symbols

$in^2$	Transformer area at any diameter
	Length of core end
	Specific heat
	Emmisivity
$watts/(in^2 \circ C)$	Local connective heat transfer coefficient
	Average connective heat transfer coefficient
	Current density
watts in/(in $^2$ °C)	Coefficient of conductance
$(ohm in)^{-1}$	Property of material
in -	Length of coil
watts	Heat generated
watts/in <sup>2</sup>	Heat transfer per sq. in.
watts/in <sup>3</sup>	Heat generated per unit volume
°C	Temperature at any radius
°C	Temperature of ambient
°C	Temperature of primary coil interface
°C	Temperature of secondary coil interface
in <sup>3</sup>	Volume
	Grashot number
	Prandtl number
in <sup>2</sup> /sec	Thermal diffusivity
1/°K	Expansion coefficient
_	Average temperature difference; surface to ambient air
watts/in <sup>2</sup> °C <sup>4</sup>	Stefan-Boltzman constant
in	Boundary-layer thickness
lb/sec in	Dynamic viscosity
in <sup>2</sup> /sec	Kinematic viscosity
in	Vertical distance along surface
	watts/in <sup>2</sup> watts/in <sup>3</sup> °C °C °C °C °C in <sup>3</sup> in <sup>2</sup> /sec 1/°K °C watts/in <sup>2</sup> °C <sup>4</sup> in lb/sec in in <sup>2</sup> /sec

### Surface Temperature

### Convective Coefficient

$$\frac{d}{x} = 3.93P_r^{-1/2}(0.952 + P_r)^{1/4} (G_r)^{-1/4}$$

$$Gr = \frac{32.2 \beta \Theta_w(x/12)^3}{v^2}$$
(1)

$$P_r = \frac{\mu C_p}{K} = \frac{V}{\alpha}$$

$$h = \frac{2K_{air}}{d}$$
 local coefficient

$$\bar{h} = \frac{4}{3} h$$
 average coefficient

### Radiation Coefficient

$$h_{\rm r} = 100 \,\sigma \, \frac{(T_7/100)^4 - (T_A/100)^4}{(T_7 - T_A)} \tag{2}$$

### Combined Coefficient

$$U = \bar{h} + h_r \tag{3}$$

#### Surface Temperature

$$T_{\chi} = \frac{q}{UA} + T_{A} \tag{4}$$

#### Core and Wire Temperature

$$\frac{\text{Define}}{S_{e} = \frac{I^{2}}{K_{e}}} \tag{5}$$

#### From Heat Balance

$$\frac{d}{d_r} (rq_r) = (S_e)r$$

$$rq_r = (S_e)\frac{r}{2}^2 + C_1 \qquad Integration$$

$$q_r = S_e\frac{r}{2} + C \qquad Simplify$$
(6)

$$r = o$$
,  $q_r = o$ ,  $C = o$  Boundary Conditions

then

$$q_r = \frac{(S_e)r}{2}$$
 Substitution (7)

Fourier's Law

$$q_r = -K \frac{dT}{dr}$$
 (8)

Combine (7) and (8)

$$-K \frac{dT}{dr} = \frac{(S_e)r}{2}$$

$$-T = \frac{(S_e)r^2}{4K} + C_2 \qquad Integrating$$

$$r = R_7$$
,  $T = T_7$  Boundary Conditions

$$T - T_7 = \frac{(S_e)R^2_7}{4K} \left[ 1 - (\frac{r}{R_7})^2 \right]$$
 (9)

Temperature Across Rotor-Stator Gap

$$T_{P5} = 100 \left[ \left( \frac{T_{S5}}{100} \right)^4 + \left( \frac{q_{p}}{\sigma EA_5} \right) \right]^{1/4}$$
 (10)

In vacuum, convection = 0.

In the thermal calculation, the rotary transformer dimensions, heat generation and the ambient temperature are input. Then, using equations (1) through (4), surface temperature T7 is calculated.

Next, equation (9) is used to calculate interface temperature  $T_{S5}$ , by substituting  $R_5$  for p and  $T_{S5}$  for T. This value is substituted into equation (10) and  $T_{P5}$  is calculated.

This value of  $T_{P5}$  is substituted for  $T_7$  and  $R_5$  for  $R_7$  in equation (9), r is set equal to  $R_1$  and the maximum transformer temperature, T at radius  $R_1$ , is calculated.

ant of the

The equations preceding were incorporated into a digital computer program. Although temperatures  $T_7$ ,  $T_{S5}$ ,  $T_{P5}$ , and  $T_1$  are computed, the actual calculated values are not printed out as output data. Instead, average primary and secondary coil temperatures are computed for the electrical design portion of the program, and these are printed out.

Various heat generator cases were run. Typical average temperatures are as follows:

- 1. Operation in Air (25° C ambient temperature)
  - Average secondary temperature (° C): 36° to 82° Average primary temperature (° C): 36° to 84°
- Operation in Vacuum (-34° C ambient temperature)
  - Average secondary temperature (° C): -3° to 106° Average primary temperature (° C): 4° to 151°

SURFACE AREA
AT GAP = A5

R5

SURFACE
AREA, A7

L

PRIMARY
COIL

July 1885

Figure II-1. - Transformer Core and Windings

Appendix III

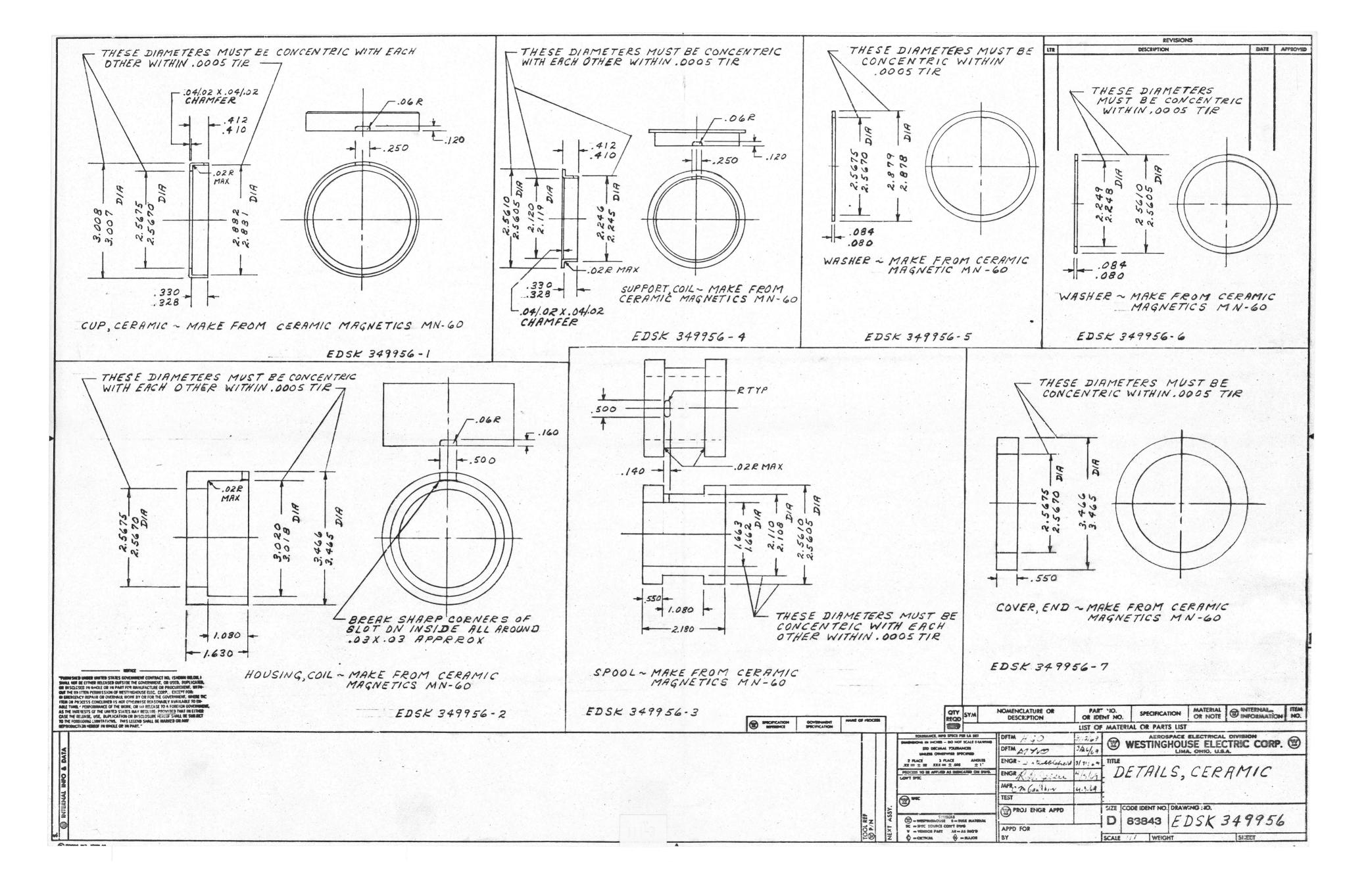
Il foldont pages.

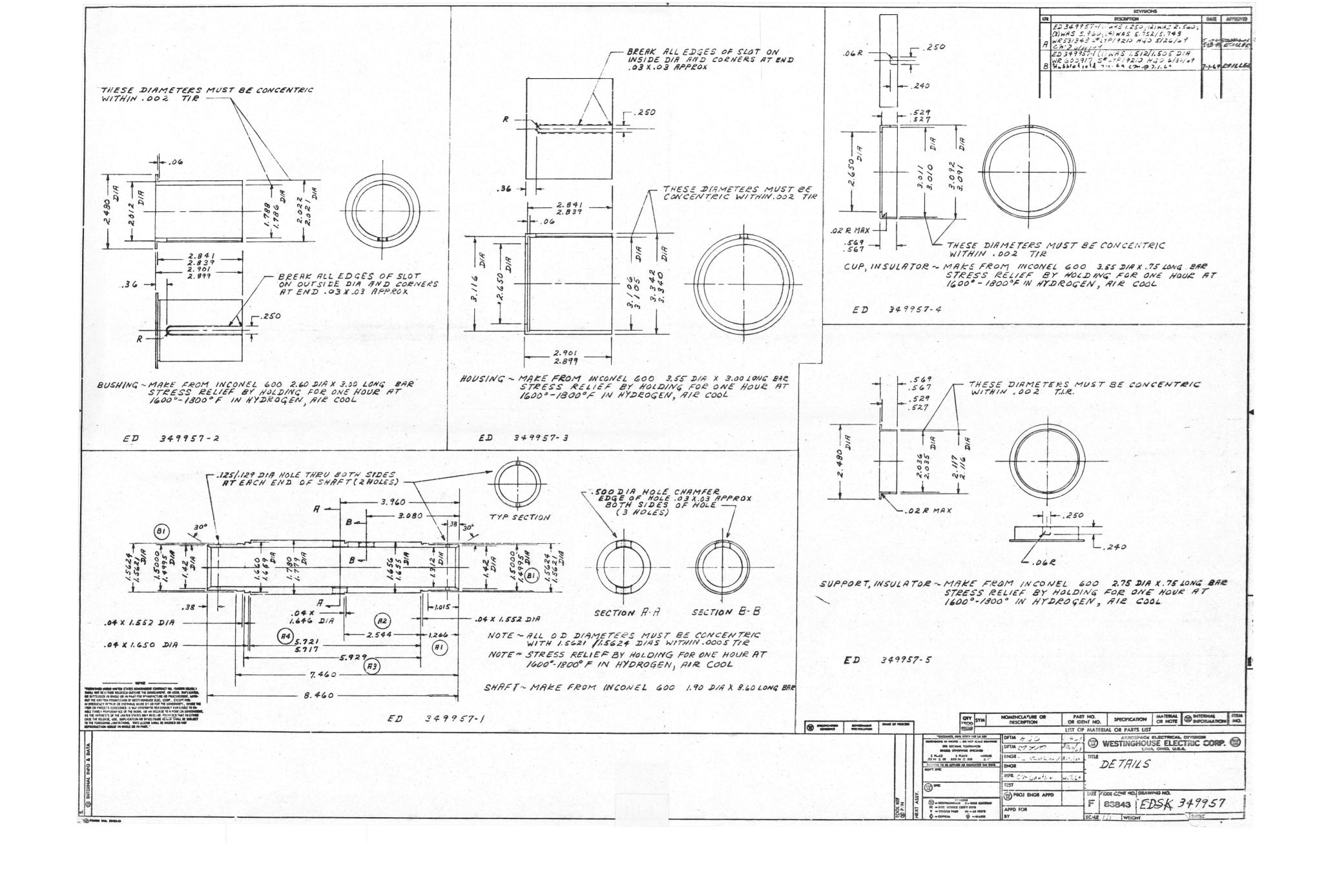
### APPENDIX III

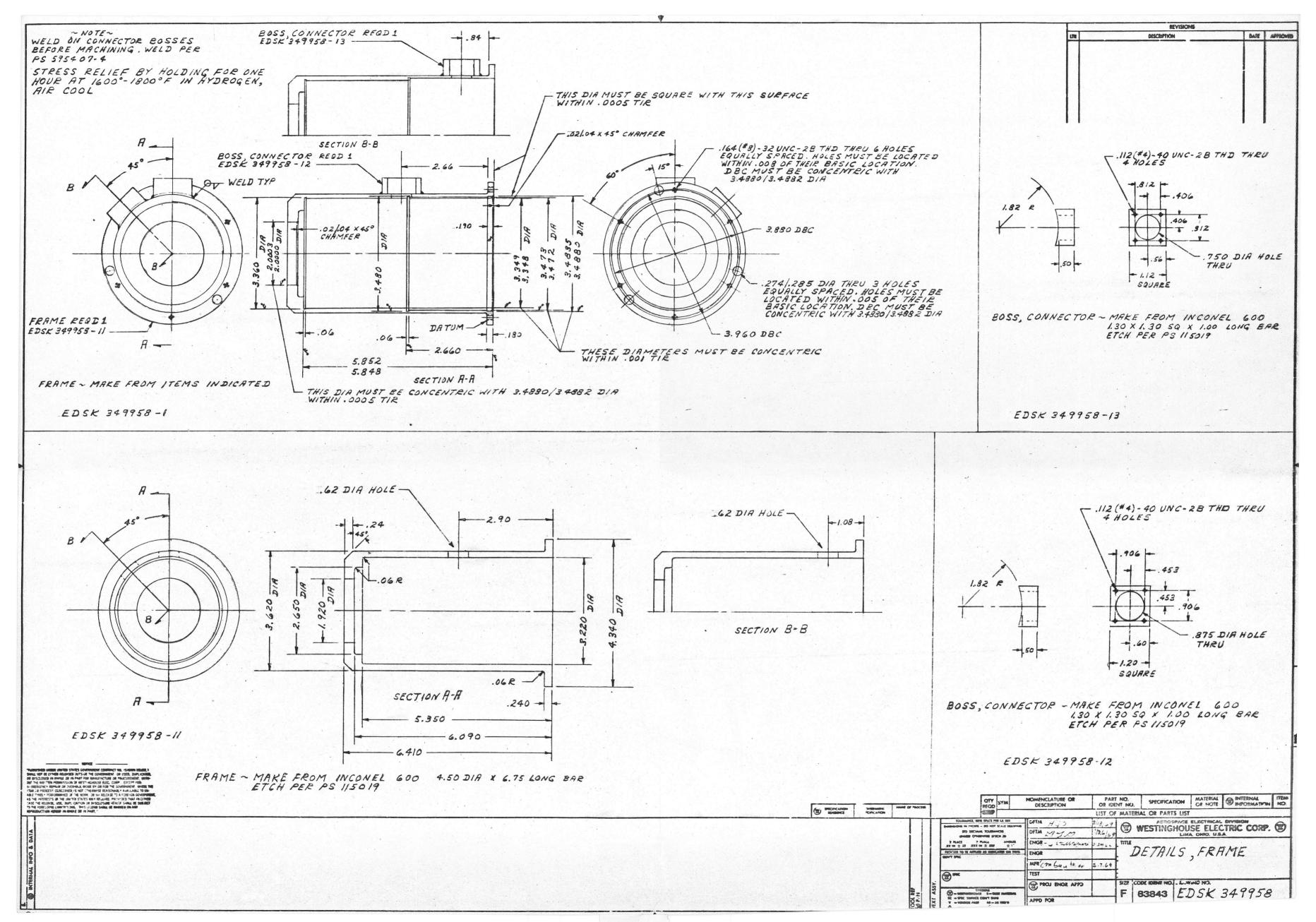
### DETAILED MANUFACTURING DRAWINGS

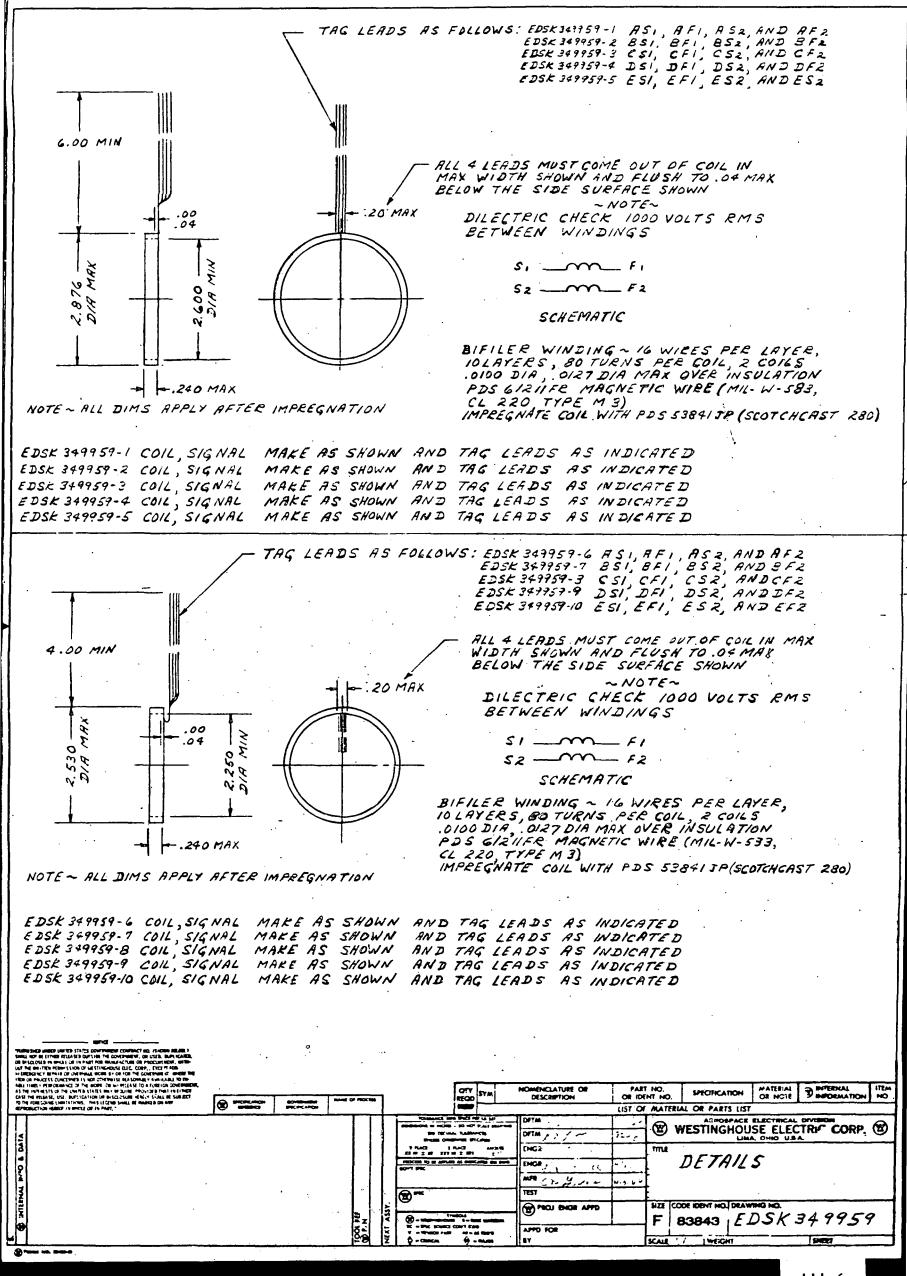
# ORDER OF DRAWING ARRANGEMENT

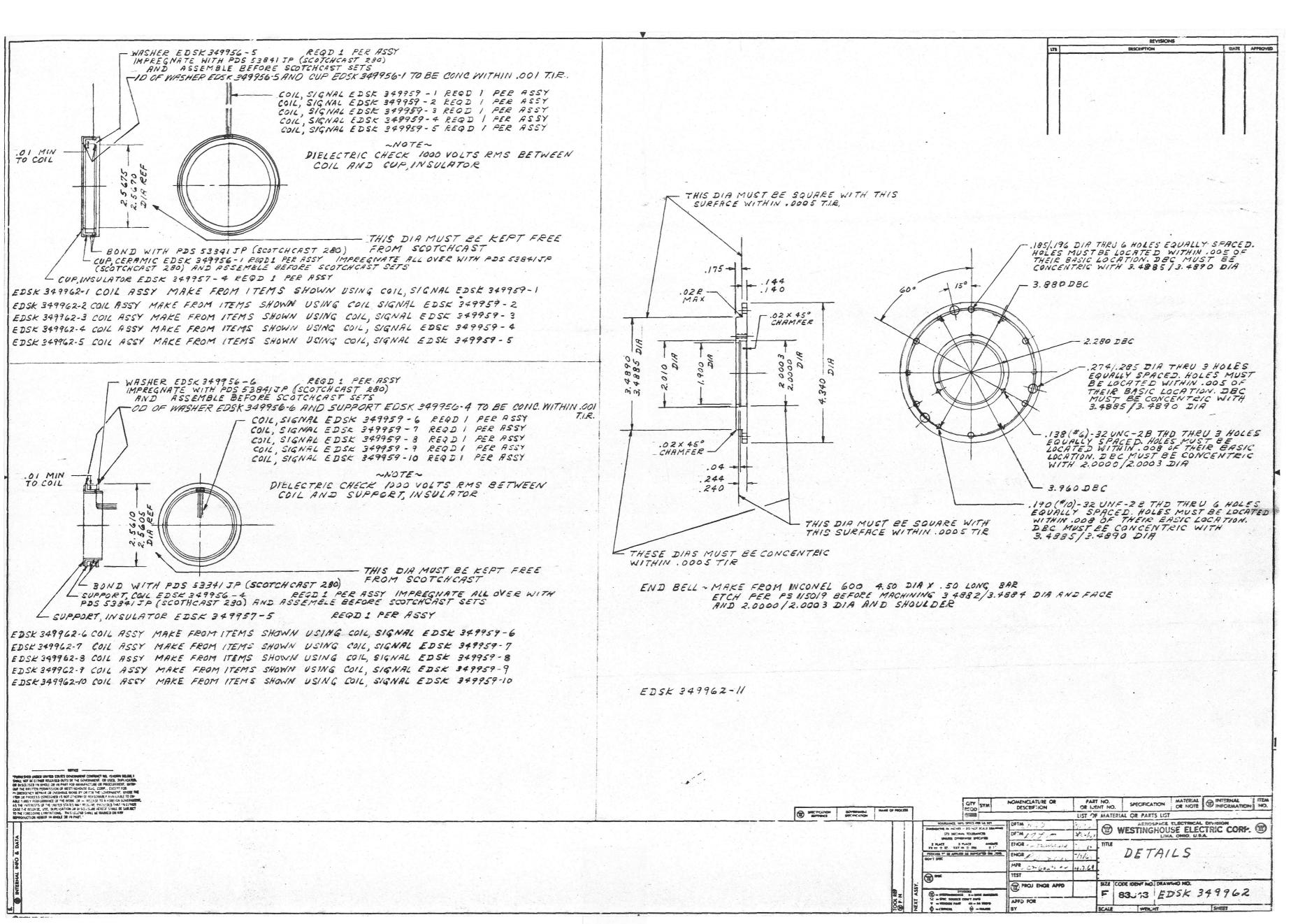
EDSK	349956	Detail, CeramicIII-3
EDSK	349957	DetailsIII-4
EDSK	349958	Details, FrameIII-5
EDSK	349959	DetailsIII-6
EDSK	349962	Details
EDSK	349963	DetailsIII-8
EDSK	349964	Signal Coil AssyIII-9
EDSK	349965	Signal Coil AssyIII-10
EDSK	349966	Rotor AssyIII-1]
EDSK	349967	Frame AssyIII-12
EDSK	349968	Rotary TransformerIII-13

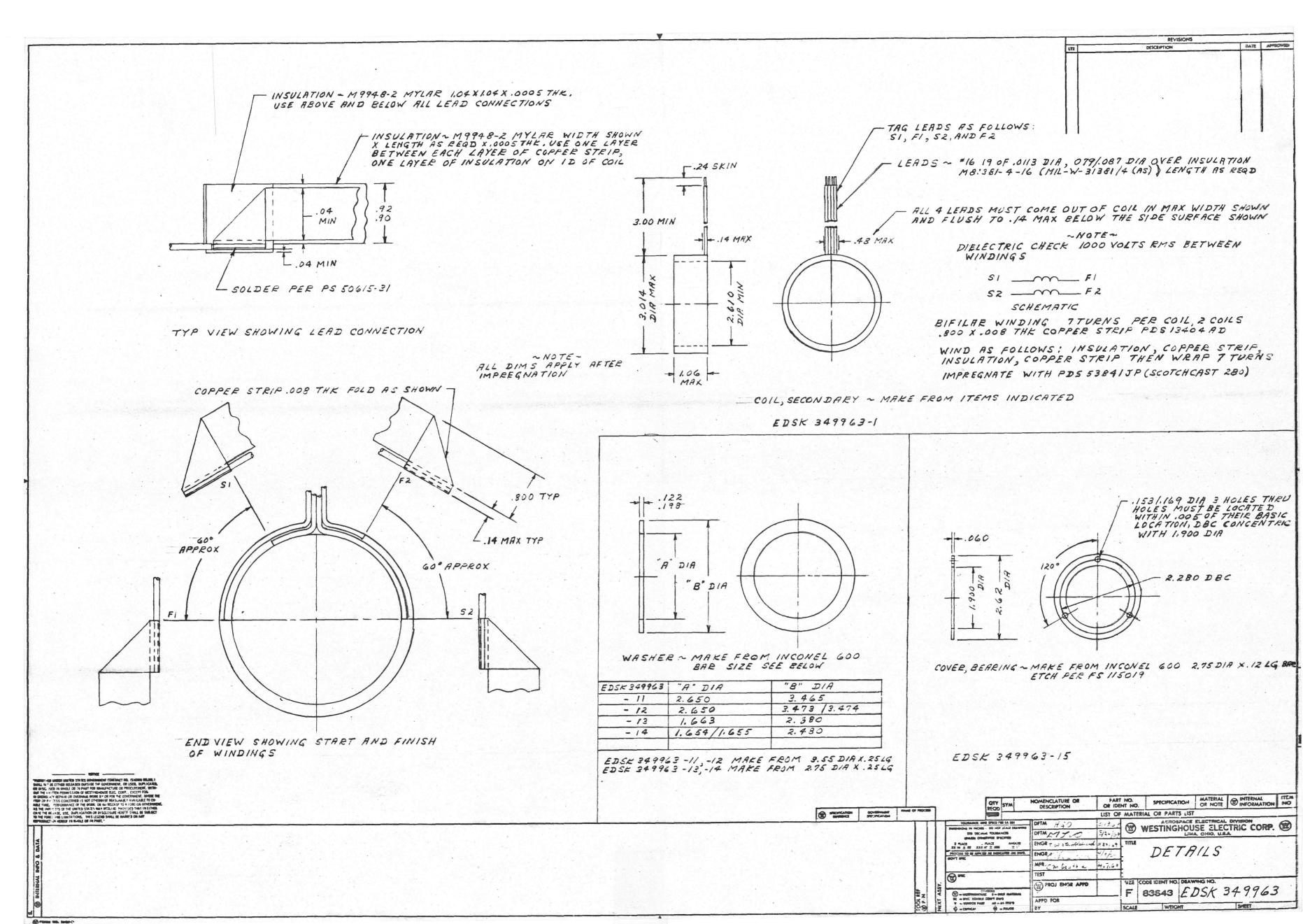


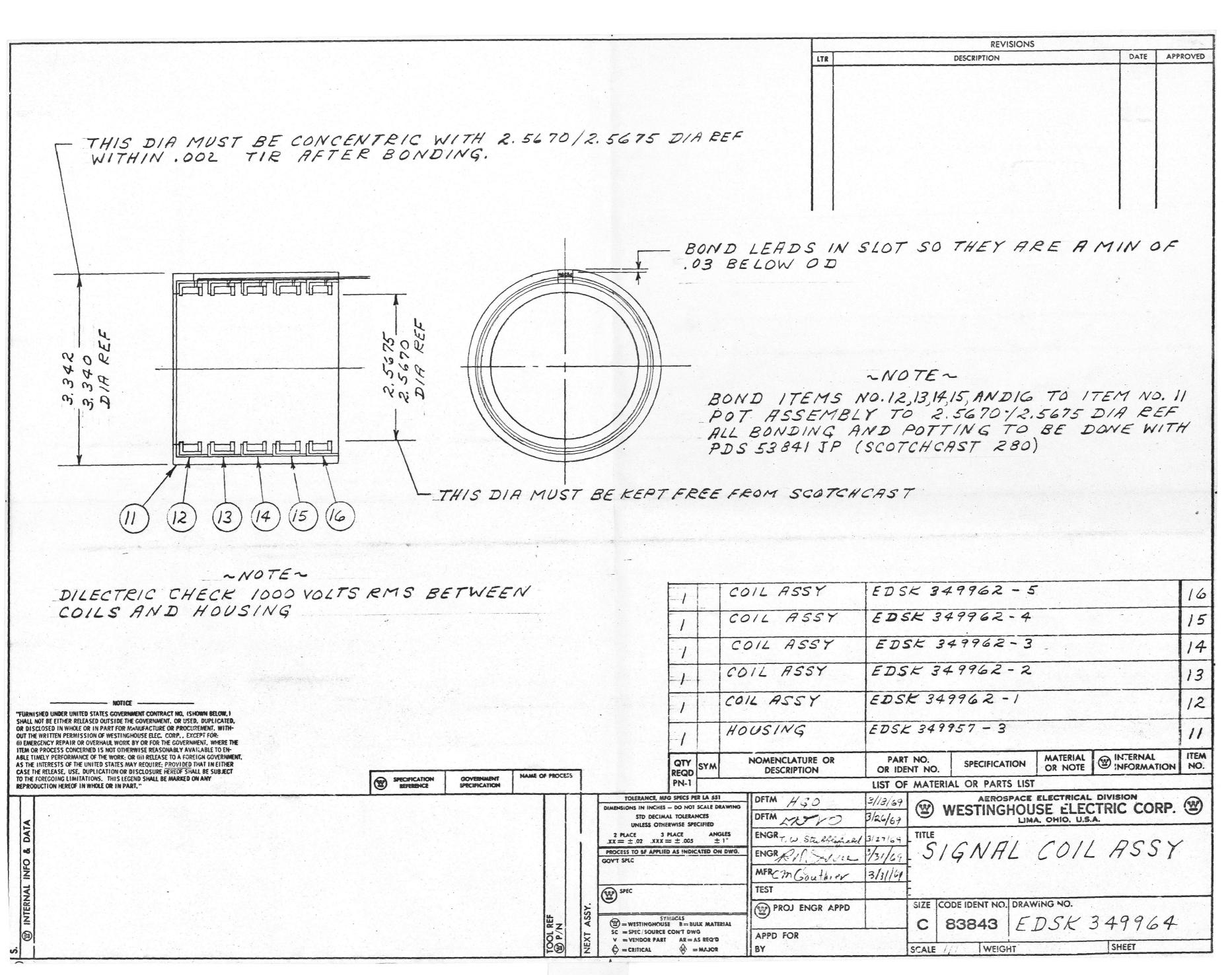


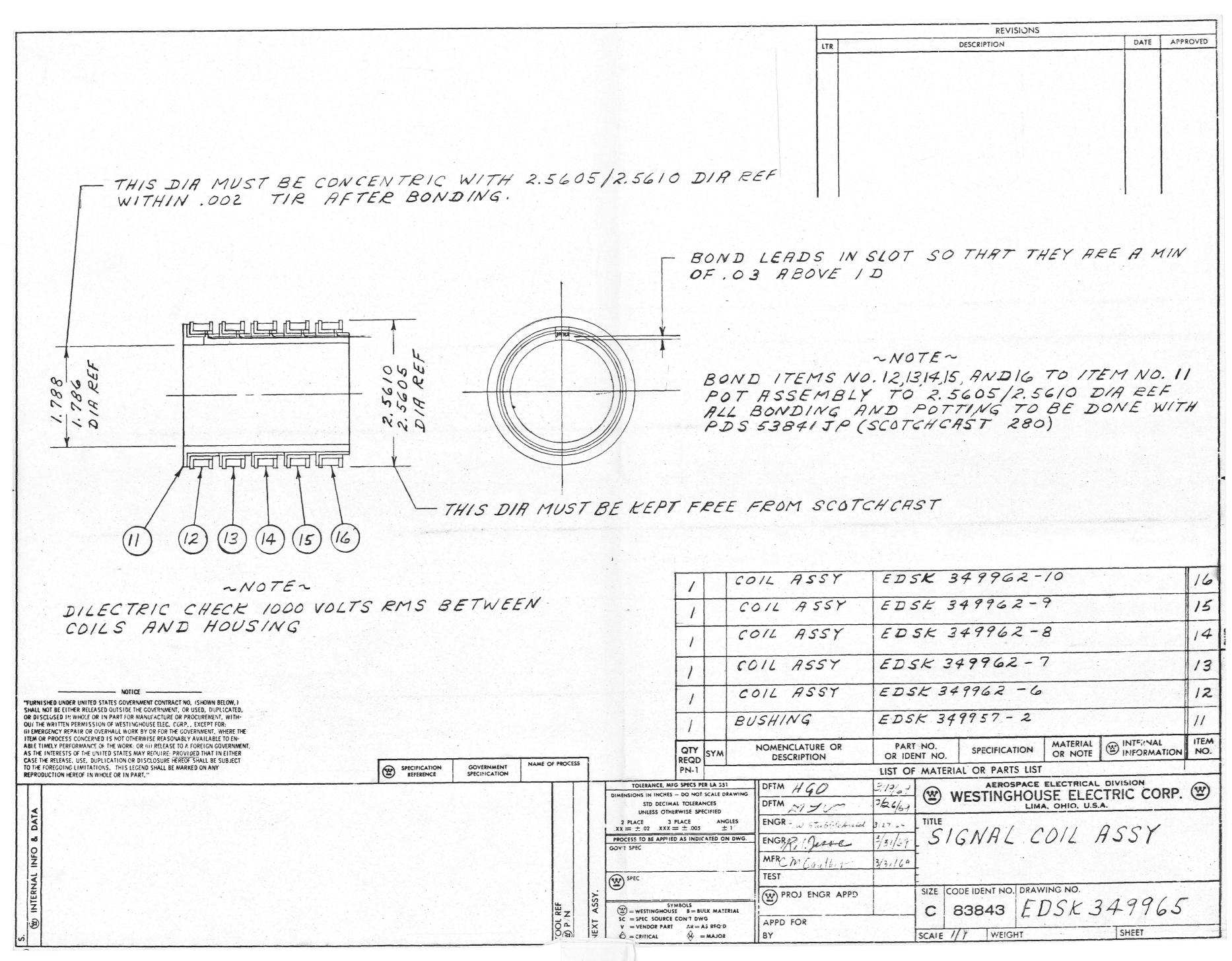


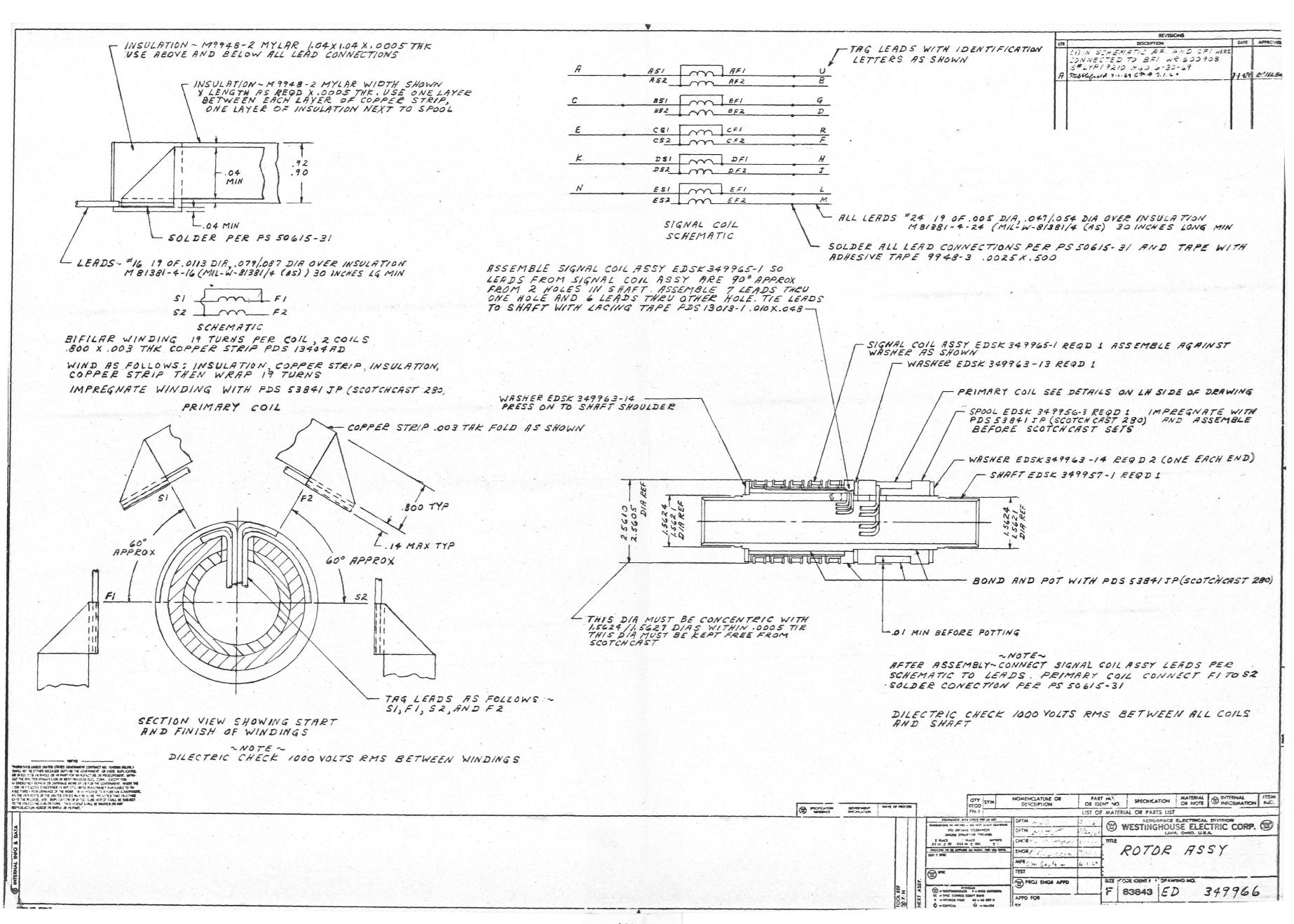


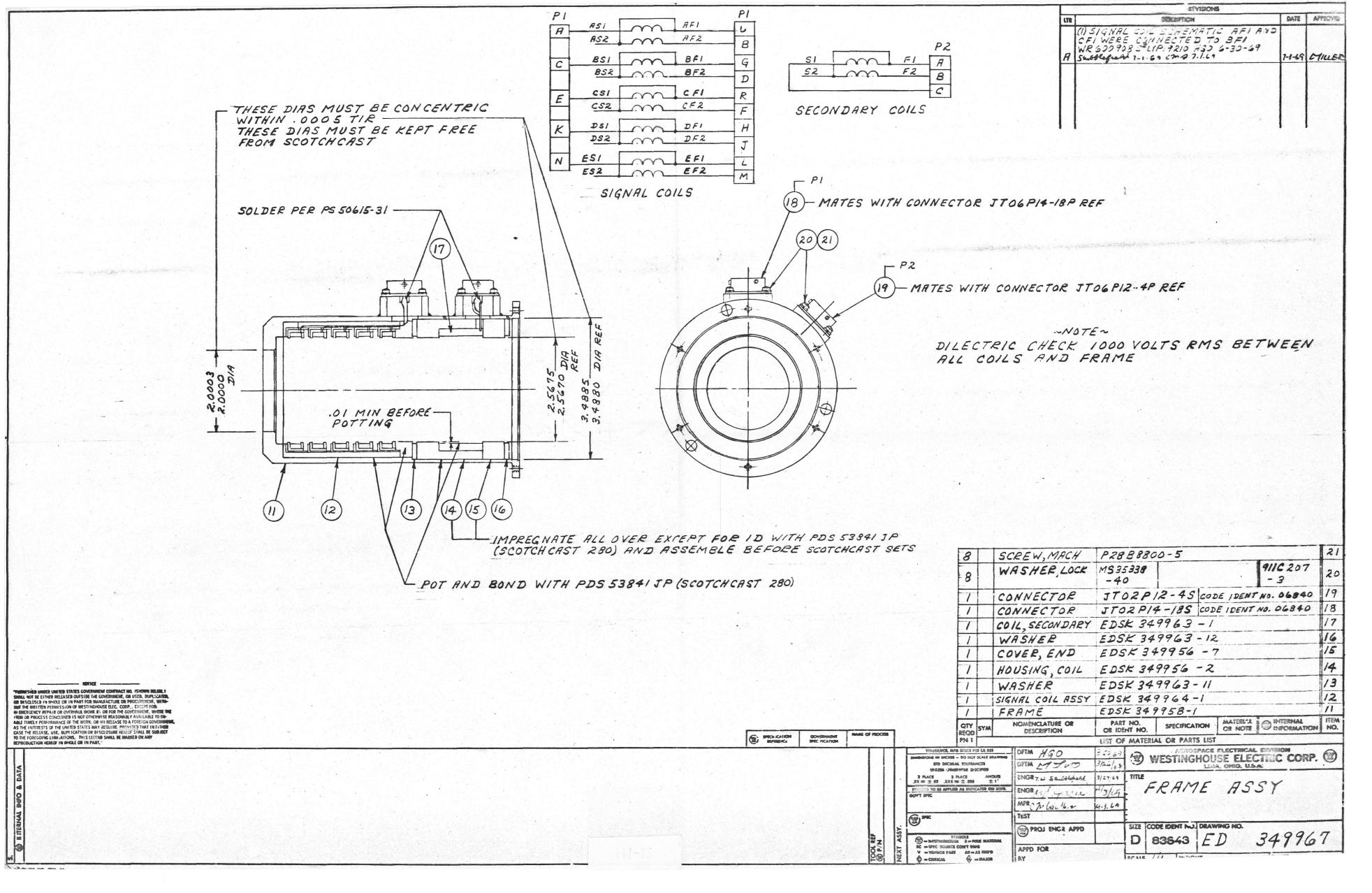


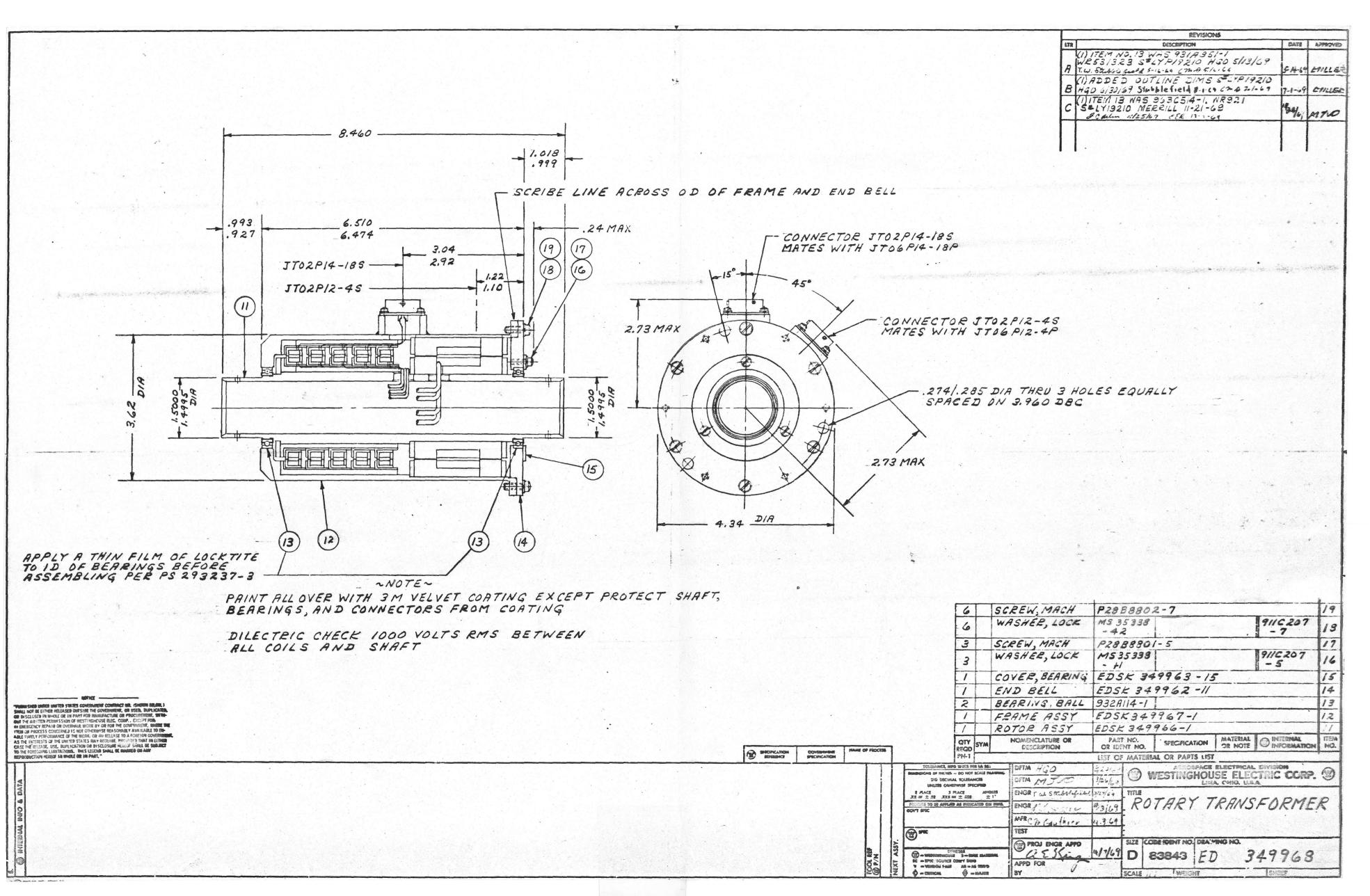












### APPENDIX IV

ADVANCED BRUSHLESS DC TORQUE MOTOR

Blank

#### FINAL REPORT

### ADVANCED BRUSHLESS DC TORQUE MOTOR

30 NOVEMBER 1968

CONTRACT NO. NAS5-10263

Prepared by

Westinghouse Electric Corporation Aerospace Electrical Division Lima, Ohio

Prepared by:

W. W. Yates

Motors and Support Equipment Section

W F Wier

Motors and Support

Equipment Section

F. 1/ Bertoldo

Marketing Manager

Utilization Systems Dept.

for

Goddard Space Flight Center Greenbelt, Maryland

#### **ABSTRACT**

This final report covers the work performed on NASA contract NASS-10263 commencing September 30, 1966 and ending November 30, 1968. This contract covers the development of an advanced version of a brushless dc torque motor using magnetic sensing of position. The motor combines the functions of speed control and commutation, and in addition provides position and rate information.

In fulfillment of the contract, the motor, magnetic sensor, and controller were designed. Two complete units were built according to the original terms of the contract. A third unit, being made as a back-up unit, was completed with a wye-connected motor winding. The tests conducted on the first unit indicate that the motor and controller operate generally as predicted. However, ripple torque was higher than predicted, especially at low speeds, due to some unexpected characteristics of the controller. Further development on the controller circuit and complete testing will be accomplished on NASA contract NASS-10459.

### CONTENTS

	•	Page
INTRODUCTION	•	IV-11
Purpose	• `	IV-11
Summary of Work Performed	•	IV-12
DISCUSSION	•	IV-13
Dimensions	• \	IV-13
Motor Electrical Design		IV-14
General Description	•	IV-14
Design Criteria and Assumptions		IV-18
Design		IV-20
Magnetic Sensor Design		IV-37
General Description	_	IV-37
General Description		IV-37
Pata Sanging	•	IV-41
Rate Sensing	• `	IV-43
Material		IV-43
Material	• •	IV-45
Summary of Core Design	•	IV-45
Winding Design	•	IV-51
Controller-Commutator Circuit Design		IV-51
General Description	•	IV-74
Efficiency	• /	
Reliability, Materials, and Components		IV-76
Mechanical Design	•	ĮV-77
General Discussion	• .	IV-77
Manufacturing Procedure	•	IV-77
Specific Comments		IV-79
Weight Estimate		IV-80
Materials and Finishes		IV-80
Materials and Finishes		IV-80
Motor	•	IV-80
Magnetic Sensor		IV-82
Controller		IV-82
Operating Characteristics of Motor-Controller	•	IV-83
Physical Configuration	•	IV-83
Forward, Reverse, and Standby	• /	IV-83
Chood Control	•	IV-83
Speed Control	•	IV-83
Rate and Position Information	• .	
Testing Procedure	•	IV-89
Design of Magnetic Sensor	• ,	IV-89
Engineering Tests	•	IV-89
Laboratory Tests	•	IV-90
Problem Areas	•	IV-90
Magnetic Sensor Output		∷IV-90
Dithering	• ,	IV-95
Pulse-Width Variation		IV-96

### CONTENTS - Continued

																									Page
Ot St	her 'Cont: Cont: Cont: Weigh atus Cond:	restrolling roll ht . of itic	er To er er Dev	ope Ope Que Pow velo	rater opme	Dr ent	on aw	· · · · · · · · · · · · · · · · · · ·	•	•	•	•	•	•	•	•	•	•	•	•	•	•	•	•	IV-100 IV-100 IV-101 IV-101 IV-101 IV-102 IV-102 IV-103
																									IV-105
																									IV-107
BIBL	IOGR	АРНУ			•	•	•	•	•		•	•		•		•	•	•	•	•	•	•	•	•	IV-109
	NDIX		· C7	ALCU	T.A'	ri c	NC	OF	, E	E	RM7	١NA	CNT	. 1	1A(	GNE	ΞT								IV-4,11
APPE	NDIX	в -	- DI	ESCE	ripi	ric	N	OF	י ו	/A	IOI	3 7	roc	)L]	ENC	J.			_			_	_		IV-115

### LIST OF ILLUSTRATIONS

Figure	Title	Page
·1	Motor Armature Punching	IV-22
2	Permanent Magnet Rotor	IV-23
3	Magnetizing Fixture	IV-26
4	Magnetizing Keeper	IV-27
. 5	Magnetizing Assembly	IV28
6	Preparation of Present Rotors	IV-31
7	Sleeve	IV-32
8	Spacer	IV-33
9	Rotor Assembly	IV-34
10	AC Equivalent Circuit - Permanent Magnet Motor	IV-35
11	Magnetic Sensor Rotor Core	IV-38
12	Magnetic Sensor Stator Core	IV-39
13	Magnetic Sensor Winding Diagram	IV-40
14	Amplitude of Sensor Output Signals Versus Angula Position for Magnetic Circuit Configuration of figures 11 and 12	r   IV-42
15	Equivalent Half-Circuit for Magnetic Sensor	. <b>Ιν∸4</b> 7
16	Fully Linked Output Pulse Versus Time	IV-52
17	Controller-Commutator Circuit Schematic	IV-53
18	Oscillator and DC Drives	IV-55
19	Connection Diagram Forward Rotation	_IV-56
20	Connection Diagram Reverse Rotation	IV-58
21	Armaturė Switching Sequence	IV-58
22	Current Flow Diagrams Delta Winding - Six Switching Positions	_ IV59

## LIST OF ILLUSTRATIONS - Continued

Figure	Title	Page
23	Vector Diagrams Showing the Resultant Fields for Two Positions in the Forward and Reverse Cycles	
24	Diode Logic Reversing Circuit	
25	Diode Logic Circuit Flip-Flop	IV-62
26	Transistor Reversing Bridge	IV-63
27	Transistor Reversing Bridge Flip-Flop	
28	Crossover Point Position	_IV-66
29	Equivalent Circuit of Armature Winding with Top and Bottom Switches Operating at 10 kc/s	
30	Equivalent Circuit of Armature Winding with Top Switch Driven Half Wave and Bottom Switch Drive Full Wave	en
31	Armature Switch Storage Time Without Bias	IV-71
32	Armature Switch Storage Time With Bias	_IV71
33	Ideal Speed Control Characteristics	IV-73
3'4	Switching Characteristics with Inductive Load - PNP Transistor 2N3201	
35	Mechanical Configuration	IV-78
36	Motor Controller Outline	IV-84
37	Pulse-Width Versus Signal Voltage	IV-8,5
38	Calculated Speed Torque Curves Versus Speed Control Signal Voltage	IV- IV-86
39	Detail of Amplitude Envelope Pulse	.IV=88
40	Magnetic Sensor Secondary Voltages Versus Position - Experimental Unit	. IV <del>-</del> 91
41	Magnetic Sensor Secondary Voltages Versus Position - No. 1 Unit	_IV=9.2

### LIST OF ILLUSTRATIONS - Continued

Figure	Title	Page
42	Uncoupled Secondary Voltage	IV-93
43	Uncoupled Secondary Voltage With 0.01 Mfd Capacitor Across Primary	IV-93
44	Sensor Output Voltage From Winding No. 1 Just Prior to Reaching Schmidt Firing Level	IV-94
45	Sensor Output Voltage From Winding No. 3 Just Prior to Reaching Schmidt Firing Level	\IV-94
46	Circuit Modification to Eliminate Dither	IV-95
47	<pre>Input Schmidt Trigger Voltage - Bottom Row - Firing Condition</pre>	JEV-97
48	Input Schmidt Trigger Voltage - Bottom Row - Locked-Out Condition	IV <del>-</del> 97
49	<pre>Input Schmidt Trigger Voltage - Top Row - Firing Condition</pre>	IV÷98
50	Input Schmidt Trigger Voltage - Top Row - Locked-Out Condition	IV-98
51	Pulse Width Variation Over Switching Cycle - Constant Speed Control Voltage	IV-99
52	Reconnection of Saturable Reactor Circuit	IV-101
53	Approximate Shape of Permanent Magnet Flux Path	IV-111
54	Punching Punches and Dies	IA⊷Ĵ16
55	End Punching Nest	IV-117
56	Armature Punching Nest	IV-118
57	Armature Punching Separator Die	IV-119
58	Armature Stack Dip and Bake Fixture	IV-120
59	Armature Shaping Plugs	IV-121
60	Diaphragm Chuck Inserts	IV-122

### LIST OF ILLUSTRATIONS - Concluded

Figure	Title	Page
61	Bore Tube Welding Fixture	IV-123
62	Secondary Winding Mold	IV-124
63	Rotor Grinding Dogs	IV-125
64	Transformer Sealing Fixture	IV-126
65	Shim Nest	IV-127

### LIST OF TABLES

Title Page	[able
	. I
gn Characteristics	II
Comparison IV-44	III
ensor Design Characteristics IV-48	IV
ensor Half-Circuit Constants IV-49	V
Controller Commutator IV-75	VI
e Component Derating Practice IV-76	VII
ist	VIII

#### INTRODUCTION |

#### **PURPOSE**

The purpose of the effort on this contract was to develop an advanced version of a brushless dc torque motor and controller. A previous version was built on NASA contract NAS5-3934. The new motor-controller uses a simple magnetic sensor which senses position for commutation and also provides position and rate information for control purposes. Other advanced features, in addition to the commutator function, include speed control with pulse-width-modulation using a variable input control voltage, reverseability using only one sensor in response to input signal voltages, stand-by operation with zero power draw in response to an input signal, lower ripple torque than the previous version, insensitivity to line voltage variation, and miniaturization of the control circuit. The motor is designed specifically for use in orientation systems for solar arrays on space vehicles.

Other specification requirements of the motor are listed below:

- (1) The circuit will be designed for maximum simplicity and reliability with a design goal of less than 100 components.
- (2) Maximum angular resolution consistent with other performance factors will be obtained.
- (3) The motor and control will be as small and as lightweight as possible.
- (4) The motor will provide a minimum of 90 ounce-inches of torque at stall, with 28 volts applied. Maximum average current under these conditions will be 0.4 amperes.
- (5) The motor will be provided with a 1.5 inch diameter hollow shaft and will have a maximum outside diameter of 4.00 inches. The total package weight will be approximately 4.5 pounds.
- (6) Peak-to-peak ripple torque will be a maximum of 15 percent of the average torque or 0.5 ounce-inches, whichever is larger.
- (7) The magnetic rotor position sensor will be designed to operate at 10 kc/s.
- (8) The motor will be capable of continuous operation at speeds up to 100 rpm.
- (9) The motor will be designed to operate in a vacuum of  $1 \times 10^{-9} \text{mm}$  hg for five years.

- (10) The motor will operate properly over an ambient temperature range of -10° to +70°C.
- (11) The motor will operate properly after 50 g, 2 msec shock and 5 minutes of random vibration from 20 to 2000 c/s at 15 g rms in each of three mutually perpendicular directions.

#### SUMMARY OF WORK PERFORMED

A breadboard comparison was made between a GSFC developed circuit and a Westinghouse developed circuit. Both circuits proved to be feasible and practical. It was decided to use the Westinghouse circuit with the GSFC rate-sensing concept in a fabrication design made adaptable to either of the two circuits. Other work derived the optimum configuration, material, and drive frequency of the magnetic sensor.

A detailed design of the motor-controller with complete manufacturing drawings was made. A breadboard of the controller-commutator circuit was made of the detail design using actual parts to be used in the final motor-controller. Operational tests were made to determine proper functioning of all parts of the circuit.

Two units were completely manufactured. A third back-up unit was completed with an equivalent wye-connected winding in the motor instead of the delta-connected winding used in the others.

Preliminary tests on the first completed unit revealed some problems both with the motor and controller. The motor was determined to have low torque due to insufficient magnetic flux from the rotor. The controller had several problems contributing to high ripple torque. The rotor magnet was redesigned using a fabricated rotor with high-energy magnetic material increasing the motor torque to above the specified level of 90 in.-oz. Some preliminary modifications were made to the first controller to improve the operation and the unit was shipped for use on NASA contract NAS5-10459.

The motor rotors of the remaining two units were rebuilt to obtain higher flux levels. The controllers were not modified. Further development of the controller circuit will be conducted on NASA contract NASS-10459.

### DISCUSSION

#### DIMENSIONS

Unless otherwise indicated, the dimensions used throughout this report are listed in table I.

Table I.- Dimensions

Length

Weight

Area

Volume

Torque

Magnetic Flux

Magnetic Density

Magnetic Field Intensity

Magnetomotive Force (mmf)

Permeance

Temperature

Voltage

Current

Power

Resistance

Capacitance

Inductance

inches

pounds

square inches

cubic inches

ounce-inches

lines or Maxwells

lines per square inch

ampere-turns per inch

ampere-turns

Maxwells per ampere-turn

degrees centigrade

volts

amperes

watts

ohms

microfarads

henries

#### MOTOR ELECTRICAL DESIGN

#### General Description

Motor Type and Number of Poles. The motor constructed on a previous NASA contract NAS5-3934 was capable of 100 ounce-inches with 40 watts input. This motor was basically a good design, using a high energy permanent magnet rotor of Alnico V with the stator magnetic circuit tailored to the magnet characteristics. Hiperco 27 steel was used and slots were filled to a practical maximum. Some improvement in torque capabilities could be obtained with a higher energy magnet and by forcing a shorter perimeter winding, but generally the motor is a good reference design. Using a ratio from this design for the present specification value of 0.4 amperes at 28 volts, the motor with a different winding would be capable of 53 ounce-inches torque at stall.

For motors of this type, the applicable formula for stall torque is the following:

Torque (oz-in.) = 
$$\frac{(22.6) (p) (\emptyset) (z) (I_a) 10^{-8}}{(pp)}$$

where

p = number of poles

 $\emptyset$  = flux per pole in Maxwells

Z = total effective series conductors

Ia = armature current

pp = number of parallel paths

Assuming that a magnet of a higher number of poles is capable of sustaining the same magnetic flux density, the flux,  $\emptyset$ , will go down as the number of poles increase because of the decrease in the area of the pole. In general, the torque would remain constant. In using a higher number of poles, the perimeter of the coils decrease, which allows a higher strength winding for a given voltage and current. This is especially true for short stack lengths. This tends to be offset by higher flux leakage in the permanent magnet rotor since the poles are spaced closer together.

Because the leakage increases, a thinner magnetic structure in the stator may be used giving consequent increased winding area. Also, since less mmf is required, the length of the magnet can be decreased allowing more winding area in the stator. However, in the stator design, at least one slot per phase per pole must be provided. For instance, a 16 pole, three-phase motor gives 48 slots. Mechanical minimums in tooth width and yoke width will be encountered if the poles continue to increase.

A sample electrical design for a 16 pole motor was made of the same size as the previous 8 pole motor. Tooth widths of 0.05 and a yoke width of 0.08 were used and were considered the practical mechanical minimums. The mechanical minimum was also encountered in attempting to lower the stator diameter, since a minimum slot opening is necessary. The results gave torques approximately equal to the previous design. However, any further increase in number of poles would see the performance fall off rapidly.

The other approach, using a variable reluctance motor, was considered. A comparison between the permanent magnet type and this type may be made by considering a few simple generalized energy relationships. The energy stored in a magnetic circuit is proportional to the product of the total flux and the mmf. If the energy change is found in moving from a position of zero torque to the next position of zero torque, this energy change divided by the angular movement is proportional to the average torque.

For a motor with a permanent magnet rotor, the relationship is between the position where the stator mmf exactly opposes the magnet mmf, and the position where the two mmf's aid. Therefore, the following can be written, if  $A_{\text{m}}$  is equal to  $A_{\text{a}}$  and the usable magnet curve is flat.

$$EC = K_1 (\emptyset m (A_m + A_a) - \emptyset m (A_m - A_a))$$
$$= 2K_1 \emptyset m A_a$$

where

EC = energy change per pole

 $K_1 = constant$ 

 $\emptyset m = flux per pole$ 

 $A_m$  = average mmf of magnet per pole

 $A_a = mmf of armature per pole$ 

Average Torque =  $2K_2 \phi_m A_a p^2$ 

where

K<sub>2</sub> = constant of proportionality
p = number of poles

The p is squared in the equation because the angular movement is one pole pitch, which makes the movement inversely proportional to the poles.

If it is assumed that  $A_m = A_a$ , which is desirable to keep the magnet from demagnetizing; then if  $A_a$  operates in a reluctance circuit without the magnet and disregarding saturation,  $A_a$  will produce  $\emptyset_m$  if the poles are aligned (assuming the same air gap). If a permeance variation of 2 to 1 is assumed which is optimistic, then

$$EC = K_1 \left( \emptyset_m A_a \frac{-\emptyset_m A_a}{2} \right)$$
$$= \frac{K_1 \emptyset_m A_a}{2}$$

Average Torque =  $K_2 p_m A_a p^2$ 

A multiplier of 2 occurs in this equation because the angular movement from minimum to maximum permeance is 1/2 pole pitch.

Although the above equations are kept simple by disregarding saturation and the sinusoidal nature of the armature mmf, the superiority of the permanent magnet motor in producing torque is evident. A sample design of a reluctance motor was made of the same size as the permanent magnet motor. Approximately 1/4 of the permanent magnet torque was obtained. The same general type of relationship may be used to analyze the effect of the number of poles on a variable reluctance type of motor.

Average Torque = 
$$K_2 g_m A_a p^2$$

If the poles are assumed to double, with the armature current and conductors held constant,  $\mathbf{A}_{\mathbf{a}}$ , which is the mmf per pole, will be one-half the previous value.  $\boldsymbol{\varnothing}_{\mathbf{m}}$  will be one-half because the mmf is one-half and will be one-half of this value because of the decreased pole area. Therefore the torque would be one-half. Since the mmf is half the previous value, the magnetic densities are one-half, and the winding area can be increased giving more mmf for the same current. If it could be assumed that the winding area varied inversely as the mmf, the new mmf would be the old over the square root of 2 and the resultant torque

would be equal. This is not usually true because mechanical minimums are encountered, insulation penalty increases as the number of slots increase, end extensions vary, etc. The exact optimum would have to be obtained by design but generally the torque tends to remain constant regardless of the number of poles.

Another type of motor, the "Vernier" motor, was considered for the contract. The "Vernier" motor is a variable reluctance motor with a certain number of teeth on the stator inside diameter and 1 less or 1 more tooth on the rotor outside diameter. As the stator field moves one pole pitch, the rotor steps one rotor tooth pitch. With this motor, the main poles can be held constant while the number of teeth can be varied. The same relationship used before can be used.

Average Torque =  $K_2 \phi_m A_a pT$ 

where

T = number of rotor teeth per pole pitch.

As can be seen from the above equation, as T increases with p held constant,  $A_a$  and  $\emptyset_m$  will remain constant, so that torque increases with T as long as mechanical and magnetic minimums are not the limiting factor. It appears that this principle could be used to increase torque and resolution. However, since the rotor moves one rotor tooth pitch as the stator field moves one pole pitch, for a 60° switching angle the rotor moves 1/3 of a rotor tooth pitch. A full 180° torque angle is only 1/2 of a stator tooth pitch giving a switching angle in terms of torque angle of approximately 2/3 of 180 or 120°. (Stator tooth pitch assumed equal to rotor tooth pitch.) Actual values of switching angle in terms of torque angle are 135° for one rotor tooth less and 108° for one rotor tooth more. From past experience, it is known that the wave form of torque versus position of a variable reluctance motor is more peaked than a sine wave. Therefore, with these switching angles, the ripple torque would be excessive. If a 30° switching angle was used, the above torque angles would be reduced to one-half, but the effect of the varying mmf would be greater than on a permanent magnet motor because of the effect on flux as well as mmf, so that the ripple torque would still be excessive.

The same difficulty is encountered on a reluctance motor having a number of rotor poles equal to motor poles. The torque angle is 1/2 of the pole pitch, so that a  $60^{\circ}$  electrical switching angle becomes  $120^{\circ}$  of the torque angle.

One approach to lowering the switching angle would be to use less than one tooth difference per pole pitch between stator and rotor. However, conditions would not repeat every pole pitch,

and it would be necessary to have part of the magnetic circuit idle.

Stepper motor techniques must be used with sufficient separate circuits to insure low ripple and repeated conditions every stator field rotation. This approach does not appear feasible because of the large part of the magnetic circuit that must be idle.

The only approach remaining is to decrease the switching angle by increasing the number of phases or circuits in the motor armature. However, to reduce the switching angle by one-half would require 7 circuits or 14 power switches which would be a tremendous complication of the control.

It is evident that the permanent magnet motor is best from a torque and ripple standpoint. It is also evident from design calculations that designs having more than 16 poles would have much less torque output per pound. The preliminary 16-pole design used mechanical minimums on stator tooth width, depthbelow-slot, and stator slot openings.

However, the design was based on the previous specification of 3.5 inches outside diameter. The increase in outside diameter from 3.5 to 4.0 inches will increase the magnet outside diameter and allow the optimum design dimensions to increase over the mechanical minimums. Practically the full benefit of going to 16 poles will be obtained without the design being marginal mechanically or any other way.

With the 60° switching angle, the 16 pole motor has an angular resolution of 7.5 mechanical degrees. This is the best that can be obtained without considerable sacrifice in motor performance or weight. Previous work indicates that the ripple torque of the motor will be below 15 percent. Cogging torque can be reduced to the specification level by placing a thin magnetic sheet in contact with the stator bore.

It is concluded that a 16-pole motor having a rotating permanent magnet and a stationary three-circuit, delta connected armature is the optimum configuration for this application.

Design Criteria and Assumptions

# Fixed Inputs.

- (1) Armature punching outside diameter = 3.812 obtained from the limiting motor outside diameter and frame thickness.
- (2) Magnet inside diameter = 1.563 obtained from the shaft outside diameter and bearing bore.

- (3) Torque Output = 90 ounce-inches minimum at 0.4 amperes average maximum with 28 volts applied. The average voltage that the motor sees with halfwave modulation is 14 volts minus the forward transistor drop. The current thus drawn is 0.8 amperes at 14 volts.
  - (4) Ripple Torque = 15 percent maximum.
  - (5) Forward transistor voltage drop = 1.2 volts.

Initial Design Decisions. - The following characteristic values have been determined from past experience as being satisfactory, close-to-optimum, or practical.

- (1) Pole enclosure 0.667
- (2) Stator punching slot opening 0.05
- (3) Stator punching tooth tip thickness 0.025
- (4) Thickness allowed for slot insulation 0.008
- (5) Stator punching stacking factor 0.95
- (6) Bore can thickness it has been found necessary to use a thin magnetic tube in the stator bore to decrease cogging. This can will be made of an 0.006-inch thick, 50 percent nickel steel (Westinghouse Hipernik).

## Materials.

- (1) Permanent Magnet (Initial concept) Alnico V. The magnet rotor, in the initial concept, is a one-piece casting. Higher energy magnets are available, but they cannot be magnetized in a one-piece casting since they can only be magnetized in a straight line. To use them requires a fabricated rotor with a more costly and complicated construction. However, the revised rotor on the last two units was fabricated using Alnico 5-7 magnets when it was discovered that the cast magnet did not give the expected magnetic strength.
- (2) Armature Insulation The insulation system is composed mostly of products related to the polyimide type of insulation. DuPont ML enamelled wire and Pyre ML (glass and ML resin) slot liners and Westinghouse Doryl varnish are used. Silicone glass wedges and some teflon lacing cord are also used. Leads have teflon insulation. This system has high temperature capabilities and low vacuum outgassing characteristics.
- (3) Westinghouse Electrical Steel Hiperco 50. This steel is among the best in having the highest flux density capability

and the highest permeability at high densities. A lamination thickness of 0.010 inch is used. Punchings are insulated with a coating of aluminum orthophosphate to minimize high frequency core loss.

Heat Factor .- Since the mounting of the motor in the application is unknown, it is not possible to determine the actual operating temperature of the motor in a vacuum. The previous motor had a temperature rise in room ambient temperature and pressure of 65°C with 36.6 watts loss with no conductive cooling. this motor has approximately 10.3 watts loss and is larger, a temperature rise of approximately 15°C is expected under the This will tend to be higher in a vacuum, but same conditions. the addition of conductive cooling will decrease it. ambient temperature is quite variable. In view of the unpredictability of actual operating conditions, the specification limits were assumed to apply at a winding temperature of 40°C which is the expected temperature under room conditions. Higher temperatures will decrease the torque and lower current; lower temperature will do the opposite.

#### Design

Number of Stator Punching Slots and Ripple Torque.— The first step in the design is the determination of the number of stator slots. Since at least one slot per armature circuit per pole is needed, there must be at least 48 slots. However, to reduce cogging, it is necessary to minimize the permeance variation between the rotor magnet and the stator at the air gap as the magnet rotates. This can be done by making the number of stator slots not evenly divisible by the number of poles. It is also desired to keep the number of slots to a minimum to keep the stator teeth from becoming too thin mechanically. The lowest number of slots which accomplishes the above and still allows a balanced three-circuit winding is 51. Therefore, 51 slots were selected. The theoretically zero variance in permeance plus the magnetic can in the bore should make cogging torque a minimum.

The next consideration is that of ripple torque. If slot openings are disregarded and a sinusoidal space distribution of air gap magnetic flux density is assumed with one slot per armature circuit per pole, the ripple torque can be calculated as exceeding 14 percent. If a quasi-square wave of density is assumed and slot openings are disregarded, the theoretical ripple torque is zero. However, slot openings cannot be disregarded and therefore a layout of slots is necessary to obtain a value for ripple torque. Such a layout was made of the 51 slot stator with the 16 pole rotor assuming a quasi-square flux density wave. Zero skew was used with a coil throw of 3 slots. The rotor was moved under the slots to the theoretical extremes and middle of

the switching angle. Conductors in the field were counted and together with the current in the conductors, this figure was used to calculate the ripple torque. The actual figure obtained was 1.09 percent ripple. The ripple will exceed this because of irregularities in the manufacture, the deviation of the flux density wave from the quasi-square ideal, and departure from the ideal switching points. Skewing could be utilized to lower cogging torque slightly, but this would entail some sacrifice in ripple torque and average torque.

Stator and Rotor Magnetic Design. The object of the design is to use the magnetic materials to the fullest with some margin for conservatism to be reliable. That is, the operating point on the magnet should be such as to obtain the maximum flux with sufficient mmf reserve to avoid demagnetization, and the magnetic steel in the stator should be worked at its highest capabilities. When the above is done, the highest torque per pound of weight with the required input power limitation should be obtained.

The same design methods described in the final report on NASA contract NAS5-3934, "Final Report for a Brushless DC Torque Motor", Report No. CR-374, dated February, 1966, were used. Considerable iteration is necessary to determine the final It was necessary to increase the thickness of the section between the stator outside diameter and the slots slightly above the magnetic optimum for mechanical reasons. Also it was found in the final design that the mmf capability of the magnet was used very conservatively, primarily due to the necessity for making the slot area fit an integral wire That is, the magnet outside diameter could have been lowered from an mmf standpoint, but not enough to increase the slot area sufficiently to allow use of the next wire size. Therefore, the design would suffer since there would effectively be no increase in wire size and flux would be lowered. sequently, the excess mmf capability was used to increase the air gap length from 0.008 to 0.010 which helps to lower cogging torque.

The final design of the stator punching is shown in figure 1. The final design of the cast rotor magnet is shown in figure 2. Complete calculated design characteristics for the motor with the cast magnet rotor are given in table II.

Magnetic Development and Revised Rotor Design. The initial concept of the cast permanent-magnet on the rotor was the same as that used on the 8-pole rotor built on the previous contract. That is, the magnet was to be oriented with alternate poles so that the yoke, or the portion of the magnet between the poles, was oriented in the flux carrying direction. The flux obtained from the previous magnet met the expected value after stabilization. However, the magnet supplier stated that because of the large number of poles and the sharp angles, the magnet could only

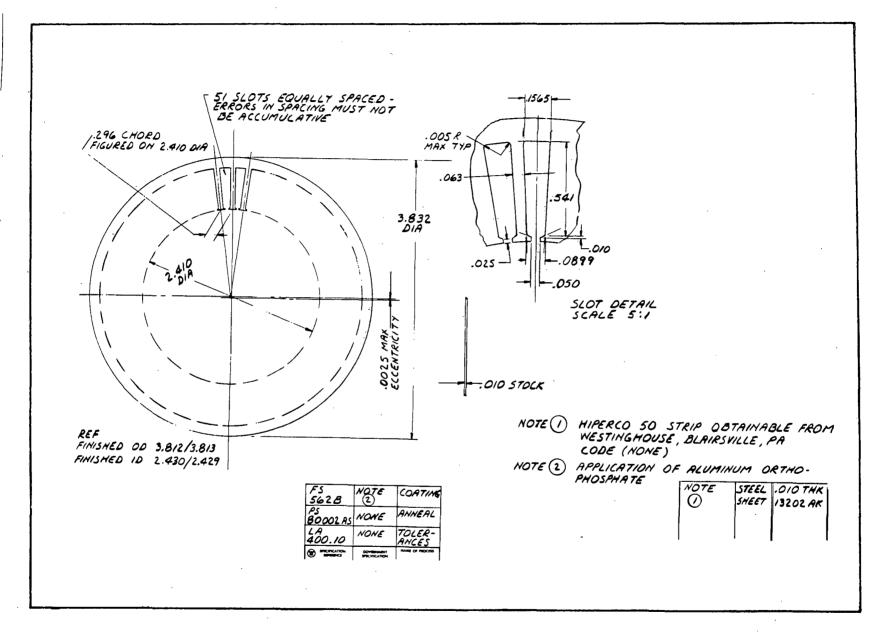


Figure 1.- Motor Armature Punching

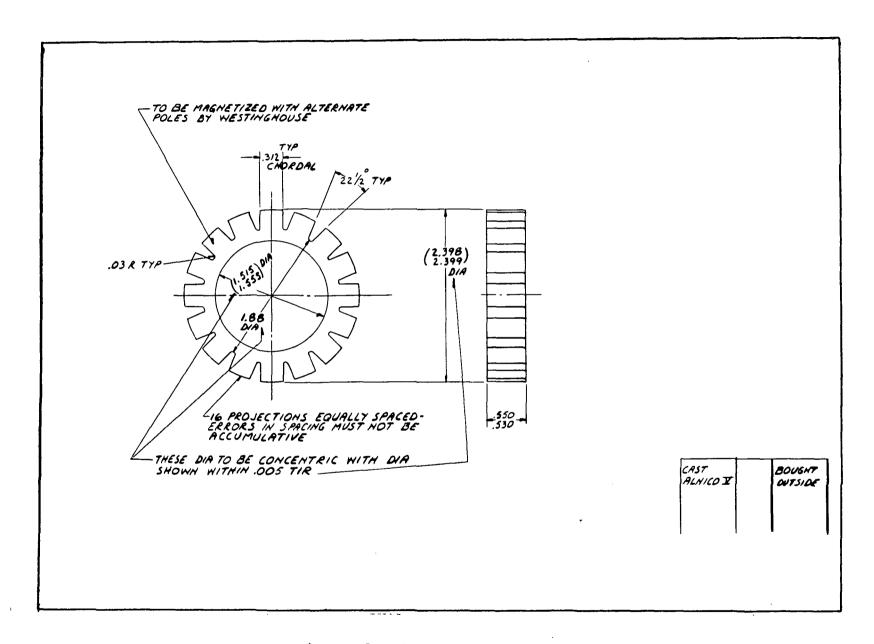


Figure 2.- Permanent Magnet Rotor

Table II.- Motor Design Characteristics (See table I for units.)

Motor Core Length Magnet Operating Flux Density (calculated)	0.53 70,000
Magnet Operating MMF	480
Magnet Leakage Permeance per Pole	15.3
Air Gap Flux Density	49,500
Stator Tooth Flux Density	132,000
Stator Depth Below Slot Flux Density	70,700
Leakage Factor	1.286
Saturation Factor	1.09
Effective Air Gap Permeance per Pole	53.4
Air Gap Flux per Pole	9030
Stator Tooth Flux per Pole	8710
Slot Area Minus Insulation Slot Fullness - Percent Coil Throw	0.053 67.0 3 slots
Coil Perimeter	2.84
Turns per Coil Total Number of Coils per Phase Wire Size Total Series Conductors per Phase Cold Resistance per Phase	81 17 #28 2750 22.8
Assumed Winding Temperature	40°C
Total Circuit Hot Resistance Total Effective Series Conductors Locked Torque - Full Voltage No Load Speed - Full Voltage	16.05 3770 95 150 RPM

be oriented radially so that the yoke would carry flux in a direction perpendicular to the orientation. The supplier recommended that a magnetic steel shell be placed under the magnet with an area sufficient to carry the pole-to-pole flux. It was expected that the required flux would be obtained with this procedure.

A magnetizing fixture was made to magnetize the magnet on the rotor. A keeper was constructed which would be slipped over the magnet and removed as the rotor was slipped into the stator. The fixture, keeper, and assembly are shown in figures 3, 4, and 5.

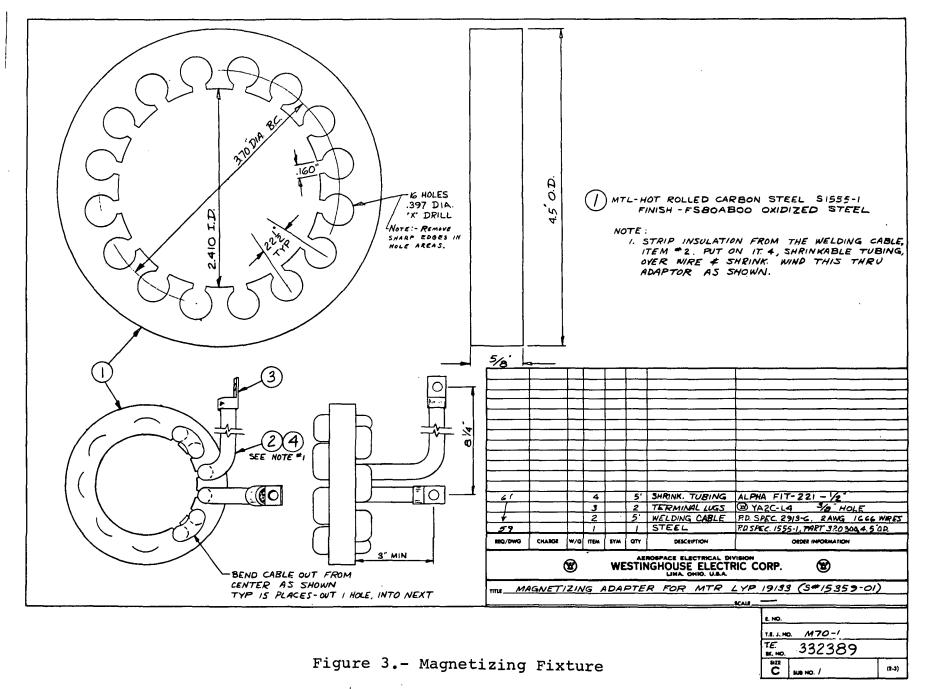
The fixture, which is made of solid steel, has deep narrow slots to provide some winding area. Originally, it was wound with one-half turn per pole with a relatively large wire for use on an impulse magnetizer. A lower flux than was anticipated was obtained when magnetization was attempted. Although some improvement was obtained by moving the wire closer to the magnet, this was not sufficient.

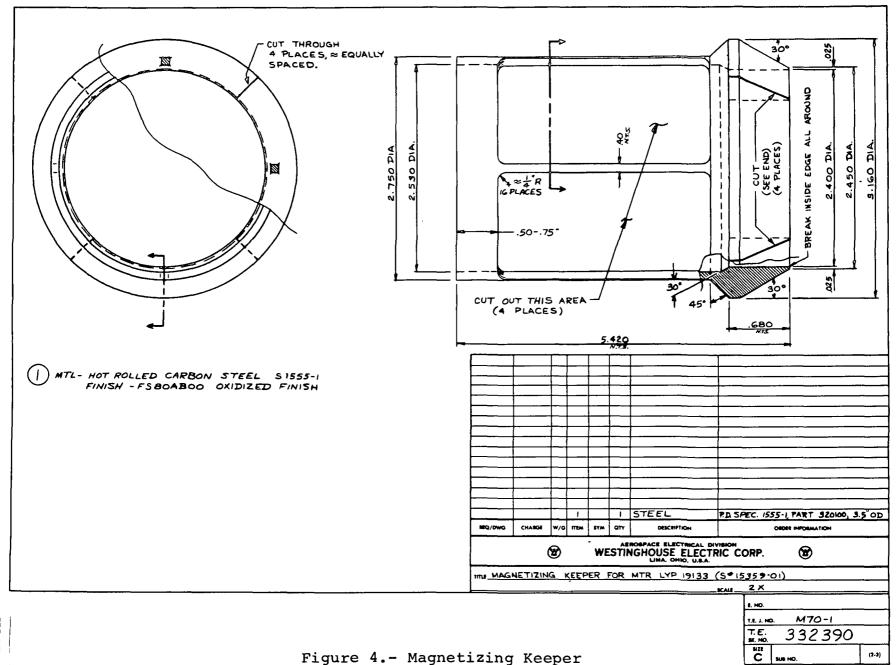
The measured flux obtained was approximately 22 to 25 percent lower than anticipated. The torque measured on the assembled motor was also approximately 22 to 25 percent low.

It was conjectured that possible reasons for the foregoing results were:

- (1) the solid iron structure of the fixture was having eddy currents induced which resisted flux build-up and caused higher leakage;
- (2) the flux path in the fixture is long;
- (3) the inability to place the wire immediately around the magnet;
- (4) the leakage flux in the long narrow slots was causing saturation of the fixture;
- (5) there was the possibility of saturation of the steel ring under the magnet.

Subsequently, the fixture was rewound, packing it as full of wire as possible. Magnetization was attempted by connecting the winding across a 300 amp DC generator. The winding overheated in approximately five seconds. Calculations of the magnetizing force obtained indicated that it would be sufficient to magnetize a simple bar magnet of the same equivalent length.





·IV-27

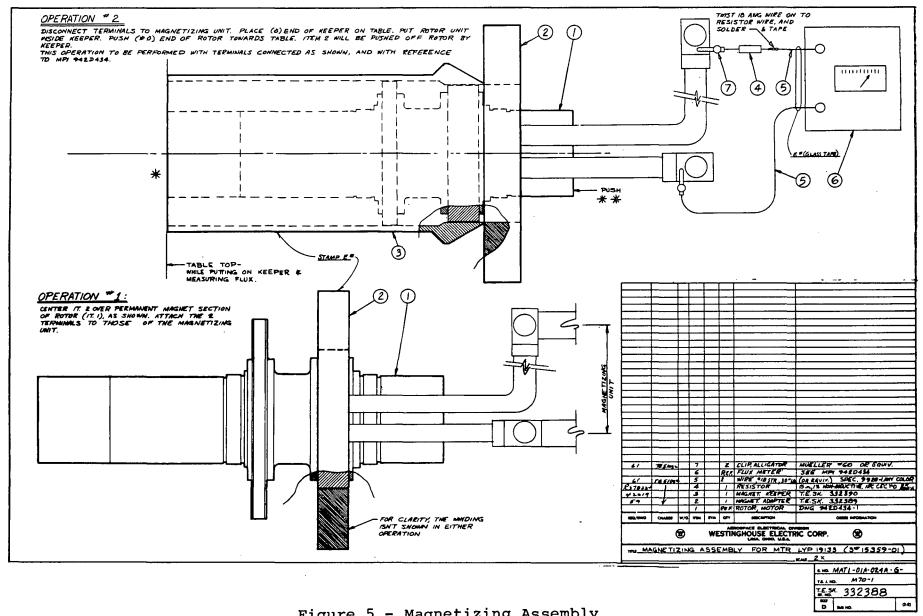


Figure 5.- Magnetizing Assembly

However, it is possible that saturation of the fixture may have occurred again because of the high leakage flux in the long narrow slots. Also, the unique magnet configuration is expected to require more magnetizing force. No improvement was obtained in the flux level by this second method.

The rotor was then sent to the magnet supplier for analysis. The supplier concluded that the magnet was not sufficiently magnetized. They were able to increase the rotor flux by remagnetizing with a small wire wrapped around the magnet; however, the full value expected was not obtained. Higher values were obtained on the supplier's master magnet on which it was possible to use a larger wire. (The spacers on the sides of the magnet on the rotor restrict the size of the wire which may be wrapped around the poles.)

The supplier was able to obtain a closed circuit flux level on their master magnet within five percent of the expected value in the motor magnetic circuit. However, since the value changed with each attempt to magnetize the unit, it was concluded that the magnet was still not fully magnetized. The supplier felt they could not pursue the problem further without a magnetization fixture and consequently, the rotor was returned to WAED. No effect was noticed after removing a steel slug in the inside diameter of the master magnet. This fact would seem to eliminate saturation of the steel ring as a deterring factor.

At WAED, the shoulders on the spacers surrounding the magnet were removed to allow wrapping the magnet with a relatively large wire. Magnetization was attempted on an impulse magnetizer with the rotor in place inside the stator of the motor. The measured flux was again approximately 20 percent low. It was subsequently determined that the necessary magnetizing flux would saturate the stator steel.

Magnetization was then attempted with the wrapped magnet in the previous magnetizing fixture resulting in a flux level which was again approximately 20 percent low. A laminated fixture was then constructed consisting of a stack of silicon steel punchings just fitting over the magnet. The magnet was again wrapped and magnetization was attempted. Again the resulting flux was approximately 20 percent low.

Because of the consistency of the flux levels obtained with repeated and varied attempts at magnetization, it was concluded that the magnet construction was inherently bad and could not be magnetized to give the levels expected. It was decided to rebuild the rotors using Alnico 5 - 7 material which is a higher energy material than the Alnico 5.

Since the Alnico 5 - 7 can be magnetized only in straight-line segments because of its highly oriented nature, it was necessary to fabricate the rotor. Two rotors were reworked as shown in figures 6.7.8, and 9. Sixteen small rectangular magnets,  $0.294 \times 0.312 \times 0.530$ , oriented parallel to the 0.294 dimensions were bonded in place as shown.

One rotor was then magnetized on an impulse magnetizer by wrapping the magnets with one-half turn per pole and slipping the laminated fixture over the magnet. Flux measurements on the magnet were much higher than the previous cast magnet. A motor was temporarily assembled. The rotor was transferred to the stator using the keeper. Rated dc current was passed through the armature winding. A peak torque of 100.8 ounce-inch was measured versus the previous peak torque reading with the old magnet of 73 ounce-inch. It was concluded that the new rotors would exceed the specification torque requirements. The flux from the Alnico 5 - 7 magnets was approximately at the expected level.

Time Constant. - One of the features of the new motor is the method of speed control by pulse-width-modulation. The voltage to the motor at full speed is turned on and off at the drive frequency of the magnetic sensor. Reduction in speed is obtained by reducing the ratio of "on" to "off" time at the constant frequency. It is necessary to evaluate the effects of this mode of operation on motor losses and torque variation.

If the voltage to the motor is pulsed at sufficiently high frequency, the time constant of the motor will be much more than the pulsing period. Therefore, the current in the motor windings will not vary significantly as the voltage is turned "on" and "off". The current will remain essentially constant and, during the off period, will transfer to the commutation paths provided in the circuit. Therefore, at a specific frequency, the time constant of the motor will determine the variation of the current. The variation of current in the motor windings will determine flux variations and hence core loss, and will also determine torque variations.

Since the new motor is similar in size and rating to the motor built on the previous contract, one of these previous motors was tested to determine the time constant. Tests were made in three ways: (1) with an applied step function of voltage to the winding, (2) with a 10 kc/s and 5 kc/s pulsed wave, and (3) with an applied sinusoidal voltage at 10 kc/s and 5 kc/s.

With methods (1) and (2), the effective time constant was approximately 2.0 msec. Since the dc resistance was 32.1, the inductance was approximately 0.06 henries. With method (3), by measuring current, voltage, and angle of lag between the two, it was found that the motor had an effective inductance

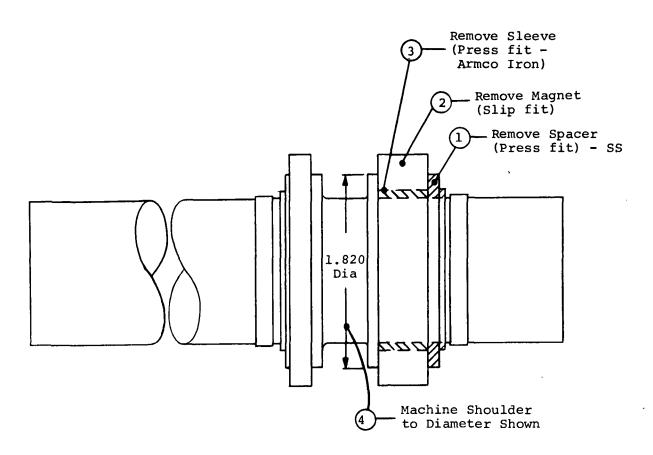
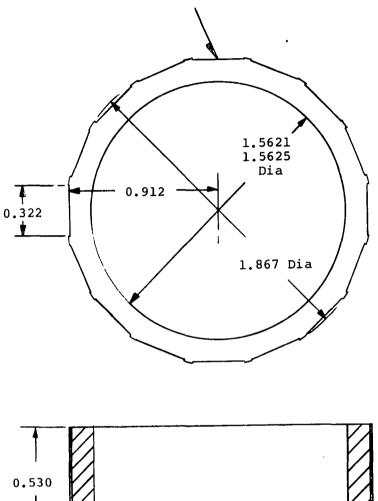
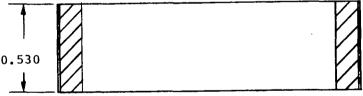


Figure 6.- Preparation of Present Rotors

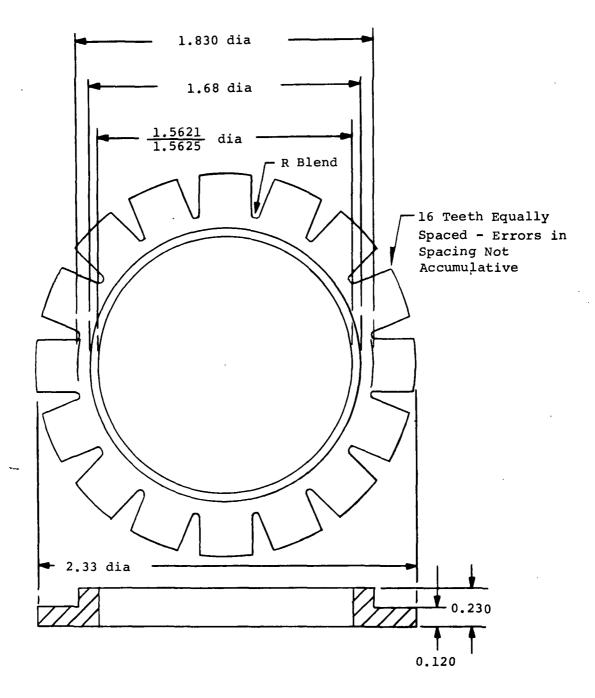
16 Flats Equally Spaced Errors In Spacing Not Accumulative



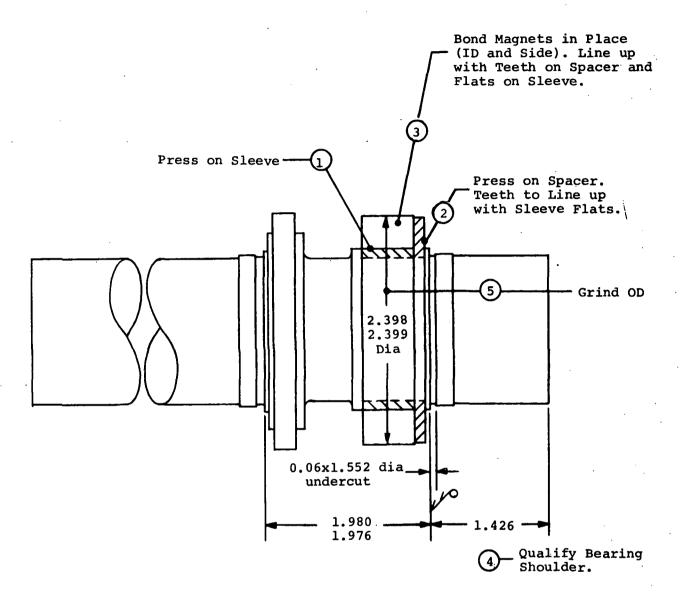


MATERIAL - Armco Iron (annealed)

Figure 7.- Sleeve



MATERIAL - AISI Type 303 Stainless Steel Figure 8.- Spacer



BONDING - Westinghouse PS 293915-1

Armstrong A701 Anhydride Cured Epoxy Adhesive (350°F cure)

Figure 9.- Rotor Assembly

of 0.0458 henries and an effective resistance of 936 ohms at 10 kc/s. At 5 kc/s, these values were 0.0491 henries and 244 ohms respectively. These values did not agree with the assumption of a simple series resistance-inductance circuit.

The actual ac equivalent circuit is shown in figure 10. The resistance  $R_p$ , is the dc resistance of the winding. The inductance  $L_p$ , represents the flux that links the winding, but does not go into the permanent magnet rotor. The inductance  $L_m$ , represents the flux caused by the winding mmf that enters the rotor. The resistance  $R_r$ , represents the core loss caused by flux variation in the permanent magnet rotor. The Alnico magnet has a relatively low electrical resistivity and the small flux variations generate eddy currents. The resistance  $R_m$ , represents the core loss in the stator steel.

The values for all the parameters of the equivalent circuit were roughly calculated for 10 kc/s. The leakage inductance was calculated using formulas long in use in ac induction motor design for slot, end turn and zig-zag leakage. In this calculation, the magnetic can in the stator bore was assumed to be so highly saturated that it constituted an air path to the leakage flux. The resistance  $R_{\rm p}$ , is the dc resistance of the primary winding. The stator core loss resistor  $R_{\rm m}$ , was obtained from an estimate of stator core loss. The resistance was so large as to be negligible in the circuit. The rotor core loss resistance was estimated by an approximate procedure described in Appendix A, page IV-111.

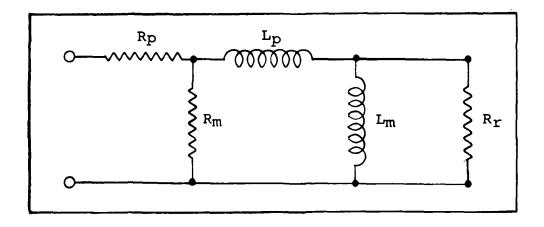


Figure 10.- AC Equivalent Circuit - Permanent Magnet Motor

The air gap and magnet inductance  $L_m$ , is quite difficult to estimate accurately as it is composed of the air gap and the flux path in the magnet. The magnet adjusts its load point as the stator mmf varies so as to present a high reluctance to flux variations. From a magnetization curve of the magnet material, the permeability to ac flux is approximately 5 times that of air. The calculation by standard formulas of  $L_m$  gave a value of 0.031. The tests indicated that a value of 0.038 should be used.

The final values for the circuit of the old motor are as follows:

 $R_{m} = 298,000$   $R_{p} = 32.1$   $L_{p} = 0.0429$   $L_{m} = 0.038$   $R_{r} = 1100$ 

The solution for the circuit is

$$i = \frac{V}{32.5} (1 - 0.993e^{-400t} - 0.00653e^{-54800t})$$

The fast term in the above solution is practically negligible in its effect on the effective time constant. Over one-half period at 10 kc/s, the above yields an effective time constant of 2.3 m/sec. This time constant is practically a function of the primary resistance and the sum of the inductances. The total losses, tested with the 10 kc/s sinusoid applied, were 0.001275 watts.

Operation in this mode would cause a slight torque pulsation at 10 kc/s which would be too fast to sense because of mechanical inertia. This pulsation would be greater as the pulse width is lowered.

Operation at lower frequencies would increase the losses and would lower the frequency of torque pulsation. Therefore the 10 kc/s frequency provides negligible losses and is fast enough so that the torque pulsations would not be harmful. Since higher frequencies would increase the core loss burden of the magnetic sensor and would tend to make the switching speed of the solid state components more critical, the 10 kc/s frequency is in the most desirable frequency range.

The same calculating procedures were used to determine the time constant of the new motor. The results gave a calculated value of 0.0018 seconds. This was shown to be acceptable in the tests on the old motor; that is, there was no appreciable variation in motor current and losses were negligible when a half-wave pulsed 10 kc/s voltage was applied.

#### MAGNETIC SENSOR DESIGN

## General Description

The magnetic sensor is depicted in figures 11, 12, and 13. The basic purpose of the sensor is to provide rotor position (and rate) information suitable for brushless commutation and position and rate control of the torque motor shaft. The primary windings are excited by a 10 kc/s oscillator. The 10 kc/s flux generates voltages in the windings on the secondary teeth that are aligned with the rotor poles. The rotor of the sensor is mechanically attached to the motor shaft. Since the rotor position is sensed, position information is also available for control purposes. With an offset-tooth design, a linear rising or falling pulse amplitude with position can be obtained for every position of the rotor on at least one of the six secondary windings. This information can be used for rate sensing at very low velocities. The offset-tooth sensing feature was originally conceived at NASA GSFC. Preliminary tests and extensive analytical results on the rate sensing are recorded in NASA GSFC Report No. X716-66-473 and Invention Disclosure No. D-1033.

## Functional Description

The magnetic sensor for a 16 pole motor with three armature circuits must have six sensing windings contained in 45 mechanical degrees. With the offset tooth design proposed by NASA GSFC, only three actual teeth would be contained in the 45-degree angle with the other three teeth occurring diametrically opposite, but offset by one-half tooth pitch. The teeth and winding space are increased by incorporating more groups of teeth which would be positionally equal. These groups would be connected in series with the other groups. Although it is possible to provide three parallel groups, two groups will give practically the same performance, and will permit a simpler design.

The design of the sensor core is shown in figures 11 and 12. The offset-tooth design is utilized in two parallel groups of teeth. The offset tooth design provides tighter coupling between the primary and secondary so that changes in secondary load are less effective in producing secondary voltage changes.

Since, for a 16-pole motor, the complete switching sequence must be traversed 8 times in one revolution, 8 rotor poles are necessary. The span of the rotor pole is determined by the necessity for having two secondaries coupled at all times, and by the linearity criteria of the rate sensing signal. Rate sensing also determines the ratio between the stator tooth span and slot opening at the air gap. Other design parameters

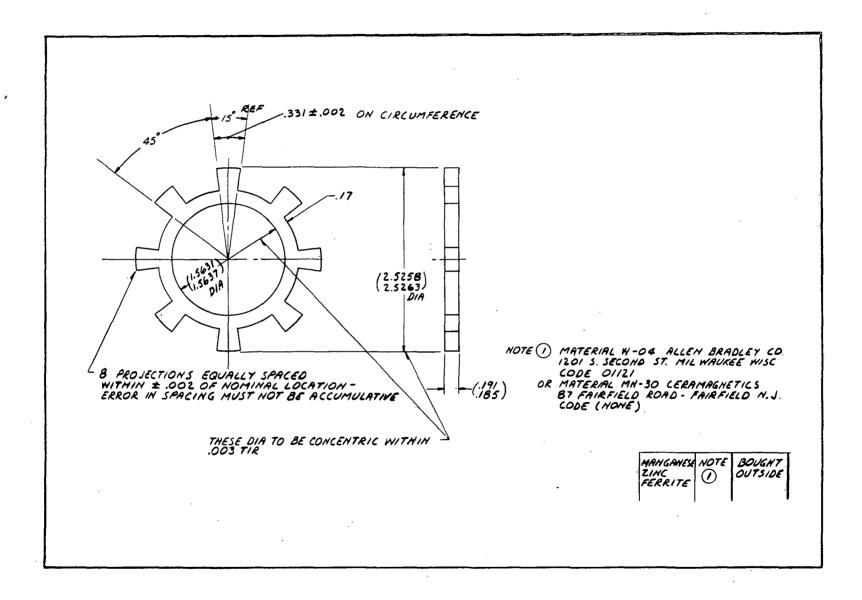


Figure 11.- Magnetic Sensor Rotor Core

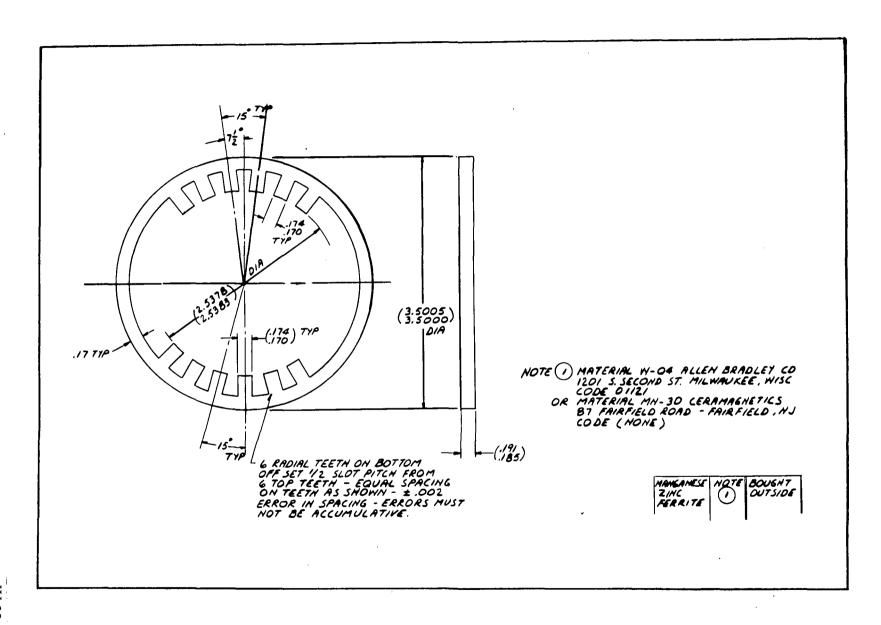


Figure 12.- Magnetic Sensor Stator Core

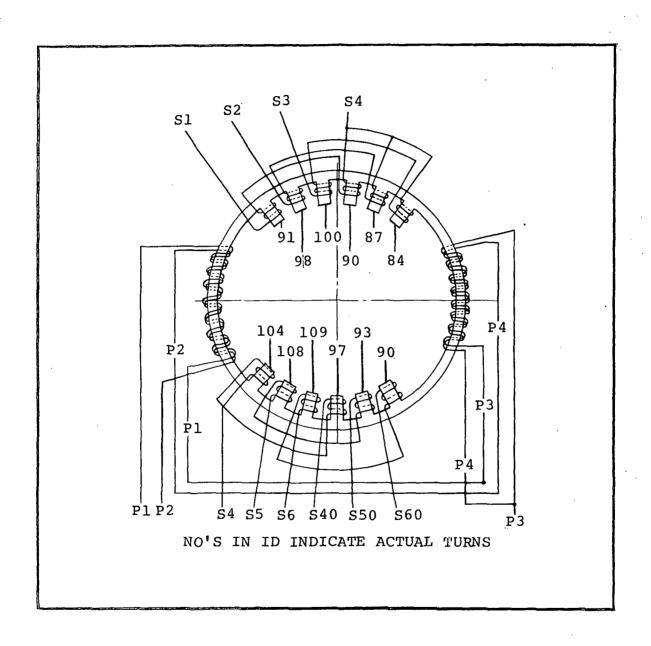


Figure 13.- Magnetic Sensor Winding Diagram

are structural soundness, flux carrying capability, mechanical size, and minimizing leakage paths and electrical losses.

## Rate Sensing

Preliminary tests and extensive analytical results recorded in NASA GSFC Report No. X716-66-473 and Invention Disclosure No. D-1033 have indicated the feasibility of obtaining continuous rate-sensing information at very low velocities by utilizing the amplitude variation of the sensor output signals with position. Figure 14, which is adapted from the above Invention Disclosure on this method, depicts the variation in amplitude of the output signals of the six secondaries with position for the sensor shown in figures 11 and 12. For simplicity, only one of the parallel groups of teeth are shown in the upper part of the figure. It was proposed in the above report that the rising or falling slopes of the signal amplitude envelope can be used for continuous rate information.

To be satisfactory for rate information, the slopes must be linear with position and must be continuously available for 360 degrees. NASA GSFC has shown that the latter condition is satisfied if the stator teeth widths are equal or wider than the slot opening at the air gap and that, ignoring leakage, linearity is obtained if the rotor pole width is equal to one stator slot pitch. In figure 12, the stator tooth width is slightly larger than the slot opening. It can be seen that there is a linearly rising signal for every angular position of the rotor. The fact that making the rotor pole width equal to one stator slot pitch provides linearity, is seen to be a result of a linear interchange of the constant flux between two adjacent teeth as the rotor rotates. The use of a different rotor pole width would result in a non-linear interchange because of a variation in permeances and consequent variation in leakage flux. The stator tooth is made slightly wider than the slot opening to allow for tolerance and to insure overlap of the linear portion of the rate sensing information.

The use of wide stator teeth results in lessening of available secondary winding area. However, since the teeth are wider, the magnetic flux per tooth can be increased, which results in fewer turns required and partially offsets the decrease in area. Another deleterious effect would be the necessity for increasing the stator core width (or depth-below-slot) to handle the increased flux. The wire size must decrease even though the resistance does not increase materially and there is a practical limit to the size of wire.

It is possible to obtain other configurations giving linearity by staggering parallel groups of teeth without affecting the winding space. However, these configurations would

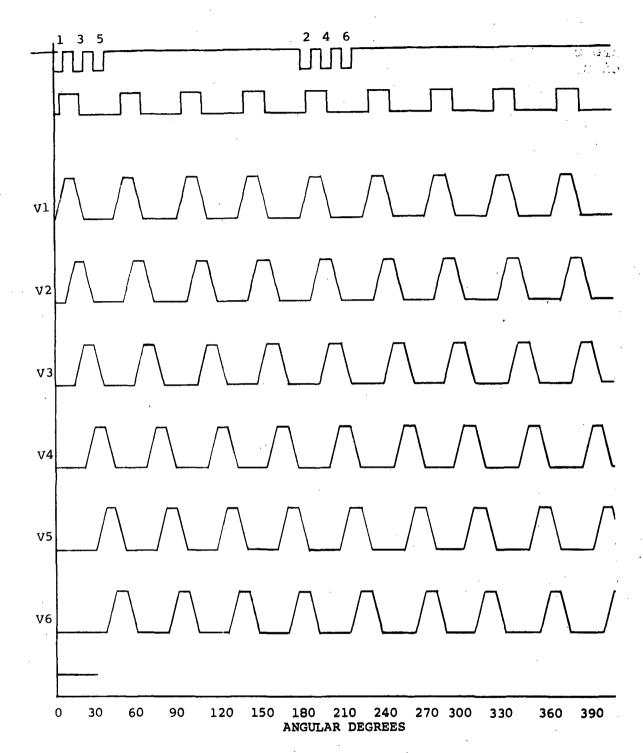


Figure 14.- Amplitude of Sensor Output Signals Versus
Angular Position for Magnetic Circuit
Configuration of figures 11 and 12

complicate the structure of the reluctance switch. The wide teeth give adequate winding space so that a practical size of wire can be used. The secondary resistance has a negligible effect. It is therefore concluded that the wide tooth approach is best.

There are some secondary effects on linearity which must be considered in the design. Tests on a previous magnetic sensor indicated some variation in the flux leakage paths with rotor position which would affect the linearity.

Although a nominal number of turns per tooth was calculated, the actual number on each individual tooth was determined by test on a bench setup. The number of turns on each tooth was adjusted to give equal peak amplitudes from each secondary winding.

Another effect to consider is the effect of load current on secondary voltage. To minimize this, flux leakage paths were kept to a minimum. This also keeps the uncoupled voltages low to provide increased rate sensitivity. Also, the load current was reduced as much as possible so that it would have a negligible effect.

# Nulling Capability

It was desired to obtain a signal indicating one unique position in the full 360 degrees of angle to provide nulling capability. Since the reluctance switch is functionally a symmetrical device which repeats all possible conditions every 45 degrees for a 16 pole design, it is necessary to provide some unique non-symmetry in the rotor to obtain such a signal.

Various means were considered to accomplish this, such as providing one rotor tooth with a larger air gap, making one rotor tooth wider axially and providing an extra rotor pole. However, to obtain a signal of sufficient strength, all of these methods affect the level of the reluctance switch output voltage either directly or through variations in the leakage flux. Although the commutation function would not necessarily be affected by the variations in secondary voltage, the accuracy of the rate information could be seriously affected. It is therefore concluded that the nulling capability should be provided by a separate structure.

#### Material

Since the sensor operates at a frequency of 10 kc/s, the magnetic core must be a low core loss material. One such material is ferrite. However, ferrite is a hard, brittle

material and fractures easily in the thin cross-sections visualized for the reluctance switch core. An attempt was made to find a magnetic steel which would have equivalent loss since such a material would have fewer structural problems.

In the sensor for the previous contract, "Monimax" steel was used. This steel, made by Allegheny Ludlum, is especially made for high frequency applications and is among the lowest in core loss of the magnetic steels. However, it has approximately twice the core loss of ferrite at a density of 2 kilogauss. For one preliminary design of the sensor for this motor, the difference in core loss would amount to approximately 0.25 watts.

Another steel that looked promising at this frequency was 6.5 percent silicon steel made by Westinghouse. This steel has extremely high resistivity and low hysteresis. However, no high frequency data existed. Therefore, some tests were made on a ring sample made of 0.004 inch thick laminations. The results showed that this steel had approximately twice the core loss of the "Monimax" steel. It was therefore concluded that the sensor core should be made of ferrite. Core loss data for the "Monimax" steel, silicon steel, and ferrite are shown in table III.

Table III.- Core Loss Comparison

·	Core Loss Watts/lb	
Flux Density (Kg)	<u>1</u>	<u>2</u> .
*Monimax (0.004 thk)	2.7	10.0
6.5% Silicon Steel (0.004 thk)	9.44	34.07
Manganese Zinc Ferrite	2.07	7.89

\*The values for Monimax have to be multiplied by a factor (approximately 1.5) to account for punching stresses. The silicon steel should be free of this effect. The figures for Monimax and ferrite were taken from commercially published data.

## Summary of Core Design

A summary of the design criteria for the core is given below.

- (1) 16-Pole Design Requires 6 secondary sensing windings in 45 degrees of rotation and 8 rotor poles.
- (2) Offset Tooth In this type of design, only 3 secondary teeth are contained in 45 degrees. The remaining 3 teeth occur 180 degrees away, offset by one-half stator tooth pitch.
- (3) Parallel Groups Teeth displaced by 45 degrees are positionally equal. One parallel group of teeth is added to the basic six with the tooth windings connected in series to obtain more secondary winding space.
- (4) Stator Tooth Width Originally set equal to the slot opening. This theoretically gives a linear rising amplitude with position of at least one secondary output signal for every position of the rotor. The width of the teeth was slightly increased in the final design to allow for tolerance and to assure overlap.
- (5) Rotor Pole Span Set equal to one stator tooth pitch to give linearity to the rate sensing signal. This condition maintains a constant air gap permeance with rotation, giving zero cogging torque and minimizing the effect of leakage flux variations on linearity.
- (6) Other Parameters Other dimensions of the sensor core were determined from the criteria of structural soundness, flux carrying capability, mechanical size, and minimizing flux leakage paths and electrical losses.
- (7) Material Manganese Zinc Ferrite is used to obtain low core loss at the 10 kc/s cycling rate.
- (8) Air Gap An air gap of 0.006 was considered to be the minimum practical gap.

## Winding Design

General Description. The object of the design of the winding is to obtain a sufficiently strong device so that the output voltage amplitude is negligibly affected by the load current to be drawn by the circuit. Changes in load current will thus not affect the accuracy of the rate sensing information. It is

desirable to accomplish this with the minimum size, weight, and electrical losses. Since the size and weight were practically determined by the core design, it is the function of the winding design to obtain minimum electrical losses. There is no set criteria for arriving at this minimum. The design procedure was to calculate the performance with windings of successively less strength until it was felt that any appreciable further reduction would compromise the rate-sensing function. To be conservative, the performance was calculated with a secondary load of 0.010 amperes. The actual peak predicted load in the circuit was approximately 0.003 amperes. It is intended in the design to obtain a 12.5 volt peak amplitude on the secondary with a 28 volt input to the primary.

Design. - The first step in the design is to estimate the leakage and mutual permeances. This was done by a rough procedure using the methods of Roters'. Because of the complex leakage paths in the inner core and on the ends, the estimation of leakage is necessarily approximate. However, because a trial and error design will later be made, it is felt that the procedure is adequate.

The total estimated leakage permeance for one-half of the total path on one side of the core is 14.10 of which 5.95 is intercore and 8.15 is end effect. The estimated mutual permeance (one tooth) is 21.7 of which 2.13 is end effect. The secondary slot leakage permeance (for one tooth) is 1.17 of which 0.59 is end effect. These permeances were for one particular position of the rotor. It is assumed that:

- (1) The leakage and mutual permeances do not change with rotor position.
- (2) The division between mutual and leakage flux is the same on the top as on the bottom of the sensor.
- (3) Partial linking of an inactive winding in the mutual path is regarded as mutual flux rather than leakage.
- (4) The circuit will be analyzed on a half-circuit basis. The two half-circuits are assumed to be equal.

The analysis using only a half-circuit can be visualized as though the core was cut in two down the vertical centerline. Since there are primary windings on both sides of the core connected in series, only one-half the primary voltage is applied to the half-circuit. The effective primary turns are those on one side only (1/2 the total). The total secondary turns are visualized as the sum of the turns on the top and bottom tooth. Although these are not connected, they are connected in series with a tooth in the other half-circuit, so the net

result is the same when analyzing two fully linked secondary windings because the two half-circuits are identical. Thus the currents, resistance, voltage, and inductance are the same as though the two windings were connected in series.

The equivalent circuit for two fully linked secondary windings in the secondary on a half-circuit basis is shown in figure 15. The symbols in the circuit are defined below.

V = 1/2 applied line voltage (square wave peak)

 $R_D = 1/2$  of the total calculated primary resistance

 $R_{m}^{p}$  = this value is derived from an estimate of the core loss and the fact that the half circuit must contain 1/2 the core loss or  $R_{m} = \frac{2V^{2}}{Core\ Loss}$ 

Lp = Primary leakage inductance. The permeance used to calculate this is the permeance for one side of a half-circuit (value previously given) divided by 2 to obtain the permeance for both sides. Inductance is obtained by multiplying by (total primary turns/2) 2(10-8).

 $L_{m}$  = Mutual inductance. Obtained same as above.

L<sub>S</sub> = Secondary leakage inductance. This is the slot leakage only for two slots in parallel, one in the top and one in the bottom.

 $L_S = (2) \text{ (primary turns/2)}^2 \text{ (one slot leakage permeance)}$  (10<sup>-8</sup>).

T = Turns ratio. This is defined as (primary turns/2)/ (secondary turns) where secondary turns are for 2 teeth windings in series.

 $R_s$  = Actual calculated secondary resistance for two teeth windings in series times  $T^2$  to refer to primary.

 $R_1$  = Actual calculated load resistance time  $T^2$  to refer to primary.

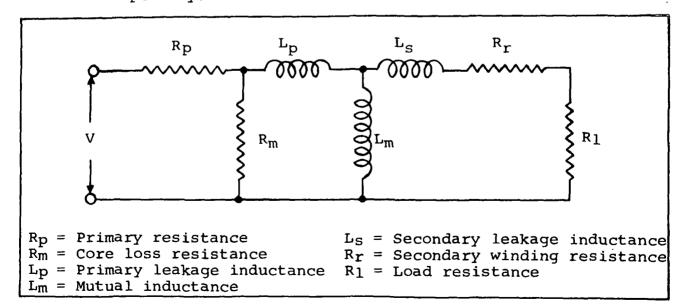


Figure 15.- Equivalent Half-Circuit for Magnetic Sensor

When the circuit is solved, the input current will be the actual primary current since the two half-circuits are connected in series on the primary side. Calculated losses will be one-half the total. The secondary current will be the actual multiplied by T. The secondary voltage will be the actual divided by T. The analysis of the circuit on an incremental basis will determine the peak value of the fully coupled secondary voltage and the shape of the output pulse.

Although several iterations were made in the design, only the final design is given. The characteristics of the final design are given below in table IV. The half-circuit constants are given in table V. The nominal calculated number of turns per secondary tooth is given in table IV. See figure 13 for the adjusted values found by bench test.

Table IV. - Magnetic Sensor Design Characteristics

=			
=	1.036		
(See figure 13 for test values per tooth.)			
=	7.05		
=	10.85		
=	2.34		
= e	0.444 ohms and to center tap		
=	2.00 ohms (2 windings in series)		
=	5680 lines per inch squared		
=	9350		
=	2840		
=	9350		
=	292 lines		
=	0.284 watts		
	= tooth. = = = = = = = = = = = = = = = = = = =		

Table V.- Magnetic Sensor Half-Circuit Constants

$$R_{p} = 0.222$$

$$R_{m} = 1380$$

$$L_{p} = 0.001014$$

$$L_{m} = 0.001560$$

$$L_{s} = 0.000337$$

$$R_{s} = 0.91$$

$$R_{1} = 570$$

$$T = 0.675$$

The primary and secondary winding resistances are so low and  $R_{\rm m}$  so high that they may be neglected for an approximate solution. The approximate solution for secondary current when this is done is:

$$i_z = \frac{b}{a} (1-e^{-at}) + i_0 e^{-at}$$

where

 $i_z$  = secondary current

 $i_{O}$  = initial value secondary current

t = time

$$b = \frac{L_m V}{L_p L_m + L_s L_m + L_s L_p}$$

$$a = \frac{R_1 (L_p + L_m)}{L_p L_m + L_s L_m + L_s L_p}$$

Solving this at t = 1/2 cycle of 10 kc/s = 0.5 x 10<sup>-4</sup> sec

(1) 
$$i_{z1} = 0.0149 (1-e^{-29.9}), i_{o} = 0$$
  
 $i_{z1} = 0.0149$ 

(2) 
$$i_{22} = -0.0149 (1-e^{-29.9}) + 0.0149e^{-29.9} = 0.0149$$

The analysis over the second interval shows this to be the steady state value with resistances neglected.

Actual secondary current = (0.0149)(T) = 0.01006Output voltage =  $(0.0149)(R_1/T) = 12.58$ 

The formula shows that the final current =  $b/a = \frac{L_mV}{(L_p + L_m)R_1}$ 

which indicates that the reactances act like a voltage divider same as they would at no load so that there is no difference between unloaded secondary voltage and loaded secondary voltage with resistances neglected.

The drop in  $R_p$  due to the load current = (0.222)(0.0149) = 0.0033. Referred to the secondary, this is 0.0049 which is negligible.  $R_m$  takes 14/1380 = 0.01015 amperes which provides negligible drop in  $R_p$ . The effect of secondary resistance on voltage is obviously negligible because of its relative value with  $R_1$ .

It is concluded therefore, that there would be negligible secondary voltage drop with 0.010 amperes load on the secondary. The effect of the secondary load on voltage levels therefore, is negligible even at the half-linked point where circuit switching takes place.

The primary current can be determined by the following at the same time interval.

$$i_{m} = \frac{Vt}{2(L_{D} + L_{m})} = \frac{(14)(0.5)(10^{-4})}{(0.02574)(2)} = 0.136$$

Total primary peak current = 0.136 + 0.0149 + 0.010 = 0.161 amperes with 0.010 amperes actual secondary current.

The primary voltage = 14 volts which is 14/0.675 = 20.7 volts referred to the secondary with 12.58 volts out. This means that 8.12 volts worth of flux is shunted into the leakage paths. By ratioing the permeance in the leakage path associated with flux that would link one uncoupled tooth to the total leakage times this voltage, the uncoupled voltage is obtained. This was equal to:

$$\left(\frac{3.829}{14.10}\right) \quad (8.12) = 2.21$$

The difference between coupled voltage and the uncoupled voltage = 10.37 volts. An approximate value for the angle sensitivity can be obtained by dividing this value by the mechanical angle of the tooth face, taking approximately 90 percent of the value to allow for non-linearities at the beginning and end of the linear range.

Angle sensitivity = 
$$\frac{(0.9)(10.37)}{7.5}$$
 = 1.24 volts/degree.

To obtain the shape of the fully linked output pulse, the circuit was solved incrementally on a digital computer. The plot of output voltage versus time is shown in figure 16.

#### CONTROLLER-COMMUTATOR CIRCUIT DESIGN

## General Description

The circuit provides the functions of commutation, speed control, reverseability and standby operation. A complete circuit diagram is shown in figure 17.

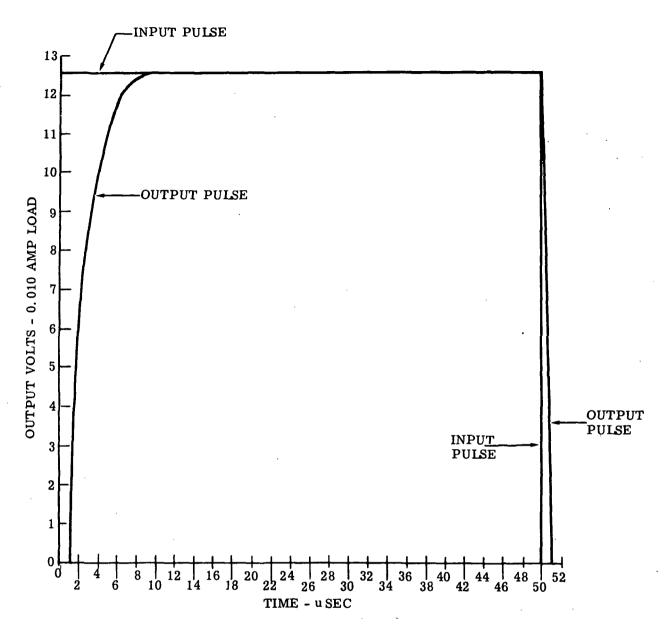
The commutator circuit, exclusive of the magnetic sensor which is considered part of the motor, consists of six subcircuits. These are:

Oscillator
Reversing Bridge
Regenerative Triggers
Commutator Bridge
Lockout Circuit
Pulse-Width-Modulator

Oscillator. - The magnetic sensor drive oscillator with auxiliary drive windings is shown in figure 18. The added windings, plus the diodes, provide isolated dc drives for the Schmidt Triggers and armature switches.

Transistor Q16 is normally off until a gating signal is applied to the base circuit. When Q16 is off, the oscillator is disabled (in standby condition).

Since all drive voltages are supplied by the oscillator, no power will be drawn from the 28 volt supply during the standby condition.



# DATA FOR OUTPUT PULSE

TIME	VOLTS
1	0
1. 25	2.49
1.75	4. 99
2.6	7. 51
4.0	10.0
9.5	<b>12.</b> 58
50.0	12. 58
51.0	0

Figure 16.- Fully Linked Output Pulse Versus Time

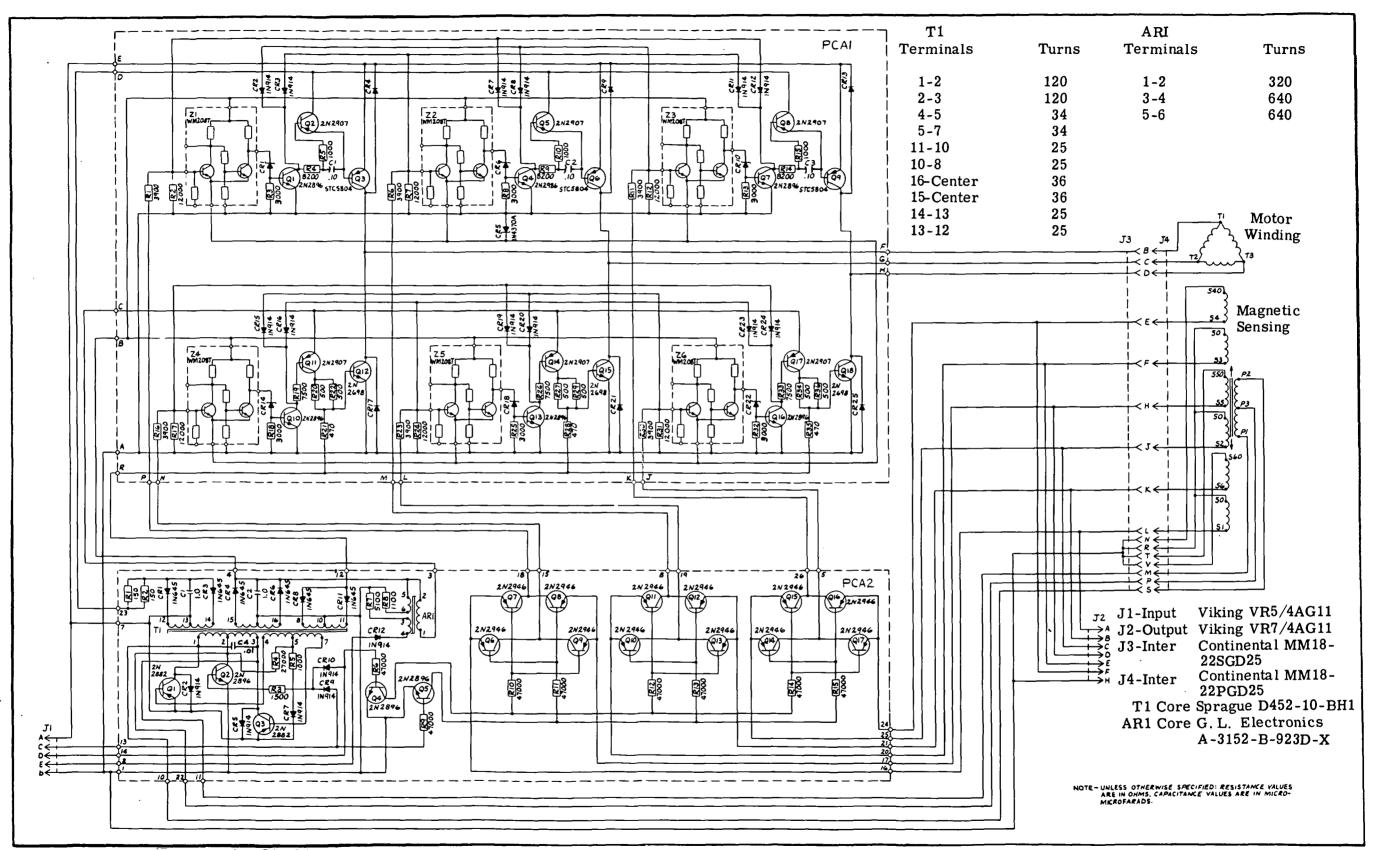


Figure 17. Controller-Commutator Circuit Schematic

Pg <u>TV-53</u> Fig 17.

Photomat

Pg IV-54 Black

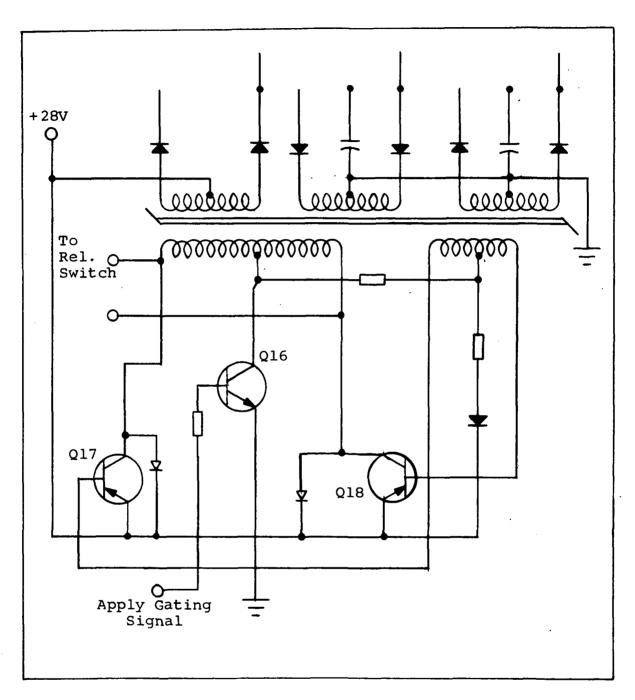


Figure 18.- Oscillator and DC Drives

The basic oscillator is a core-timed multi-vibrator designed so that the saturating element of the oscillator does not have to carry the magnetic sensor primary current. The 10 kc/s output of the oscillator is fed directly to the sensor with no attempt to modulate the pulse width at this point. Pulse width modulation at this point is unsatisfactory, since it interferes with the rate sensing information that is taken from the sensor output windings.

Reversing Bridge. In the earlier effort on NASA contract NAS5-3934, two magnetic rotor - position sensors were used to obtain forward and reverse rotation. The present circuit eliminates one of the position sensors and retains a bi-directional drive capability.

The direction of rotation is dependent upon the relative position of the position sensor rotor with that of the motor rotor. Changing their relative positions by 180 electrical degrees will reverse the torque. A solution to this problem would be mechanically shift the position of the position sensor rotor with respect to the motor rotor. Functionally, this is not a practical solution. Therefore, it must be accomplished statically in the electronic circuit. The connection diagrams for forward and reverse rotation are shown in figures 19 and 20.

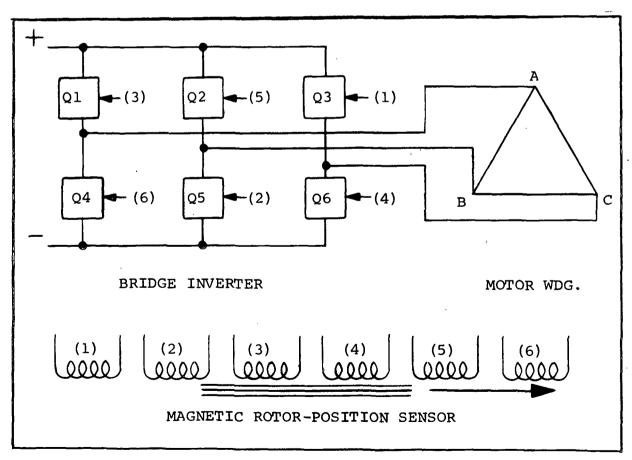


Figure 19.- Connection Diagram Forward Rotation

Observing these two figures, it is seen that reverse rotation is accomplished by reversing the input signals to the transistor switches in each leg of the three phase commutator bridge. This is further substantiated by constructing the armature switching sequences, figure 21, the current flow diagrams, figure 22, and finally looking at the vector diagrams in figure 23. vector diagrams show the resultant armature fields for two positions in the forward and reverse cycles. It should be noted that in position 1, for both the forward and reverse switching sequence, sensor windings 3 and 4 are excited. Comparing position 1 (forward) with position 1 (reverse) in figure 23, it is shown that a 180 electrical degree shift in the armature field is obtained by reversing the input signals to the transistor switches in each leg of the three phase bridge. It is also shown in figure 23 that the advancement from position 1 (forward) to position 2 (forward) generates a field which rotates counterclockwise. The reverse cycle generates a field which rotates in a clockwise direction.

In this program, several methods of switching the input signals to the bridge transistors were considered. Among these were (1) using saturating transformers, (2) using diode logic as shown in figure 24, and (3) using the transistor bridge shown in figure 25. In each case, only one magnetic rotor-position sensor and one set of sensor windings are required. The saturating transformer method had some basic operational problems, besides being complex, and was given very little consideration. The basic theory was to change control by reversing the bias on a saturating transformer.

Figure 24, which shows the second method for obtaining bidirectional drive, uses diode logic to obtain reversal of the drive signals. Reversal is obtained by grounding either input "A" or input "B".

A flip-flop such as that shown in figure 25 can be used to ground either input. It is desirable to use a flip-flop to perform this function because it provides a lock, that is, either input "A" or "B" will always be tied to ground, preventing an ungrounded condition. If both inputs are ungrounded, both transistors in the leg of the bridge will turn on, causing a short circuit. Figure 24 shows the bi-directional drive circuit for only two of the sensor windings. The circuit must be repeated for the other two sets of sensor windings; however, only one flip-flop is required for each system.

Figure 26 shows a third method of obtaining reversibility. This method utilizes a "transistor bridge" to give the correct logic. Reversal is obtained by grounding either input "A" or input "B". Grounding input "A" activates one pair of diagonal transistors, thus giving one direction of rotation. Grounding

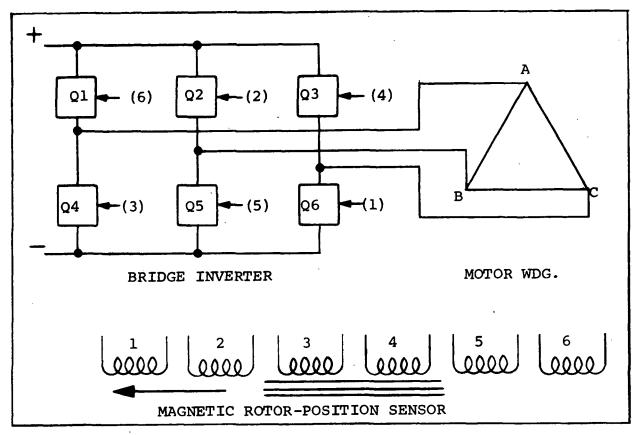


Figure 20.- Connection Diagram Reverse Rotation

<del></del>				
FORWARD ROTATION - REFER TO FIGURE 19				
POSITION	SENSOR WINDINGS EXCITED	TRANSISTORS "ON"		
1 2 3 4 5 6	3 - 4 4 - 5 5 - 6 6 - 1 1 - 2 2 - 3	Q1 - Q6 Q6 - Q2 Q2 - Q4 Q4 - Q3 Q3 - Q5 Q5 - Q1		
REVERSE ROTATION - REFER TO FIGURE 20				
POSITION	SENSOR WINDINGS EXCITED	TRANSISTORS "ON"		
1 2 3 4 5	4 - 3 3 - 2 2 - 1 1 - 6 6 - 5	Q3 - Q4 Q4 - Q2 Q2 - Q6 Q6 - Q1 Q1 - Q5		
6	5 - 4	Q5 - Q3		

Figure 21.- Armature Switching Sequence

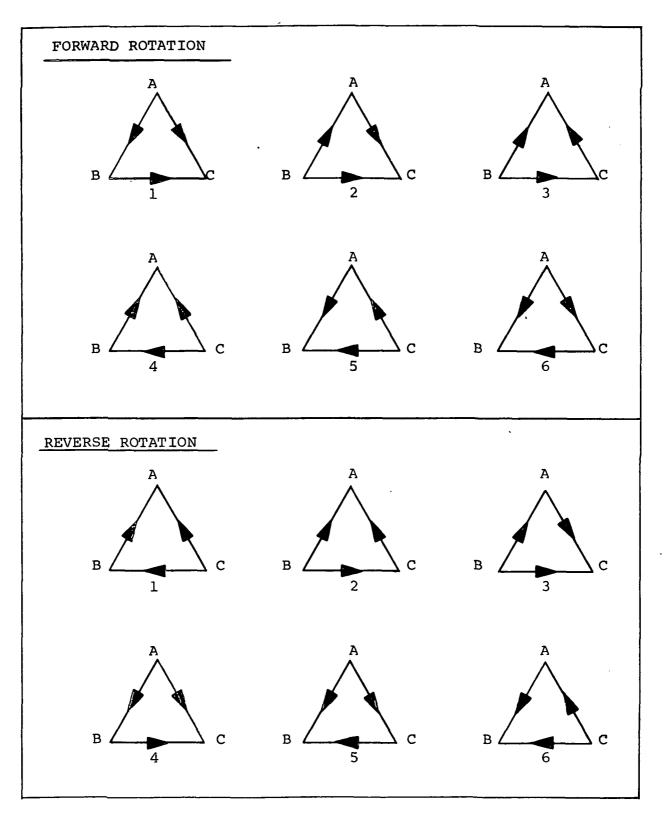


Figure 22.- Current Flow Diagrams Delta Winding - Six Switching Positions

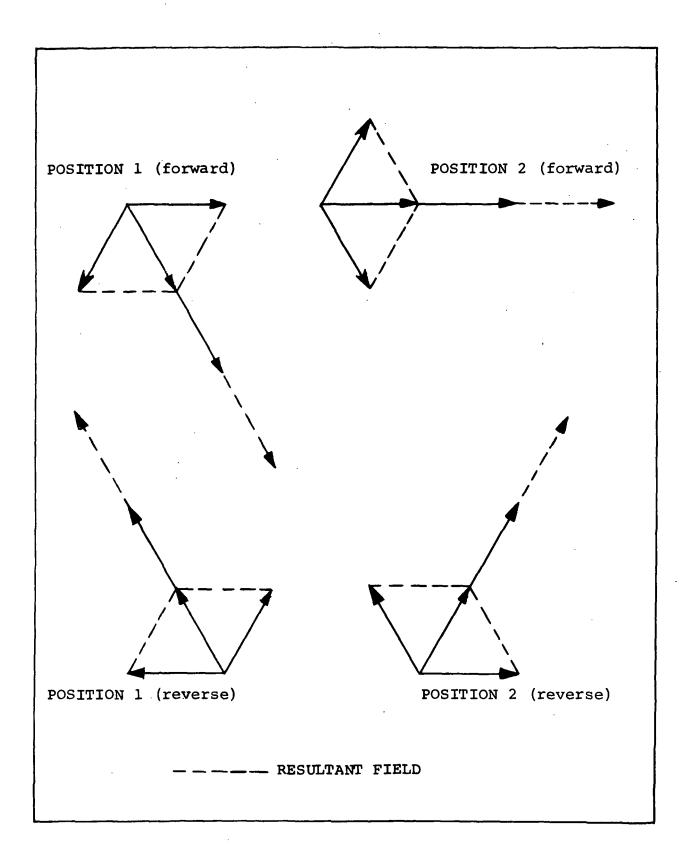


Figure 23.- Vector Diagrams Showing the Resultant Fields for Two Positions in the Forward and Reverse Cycles

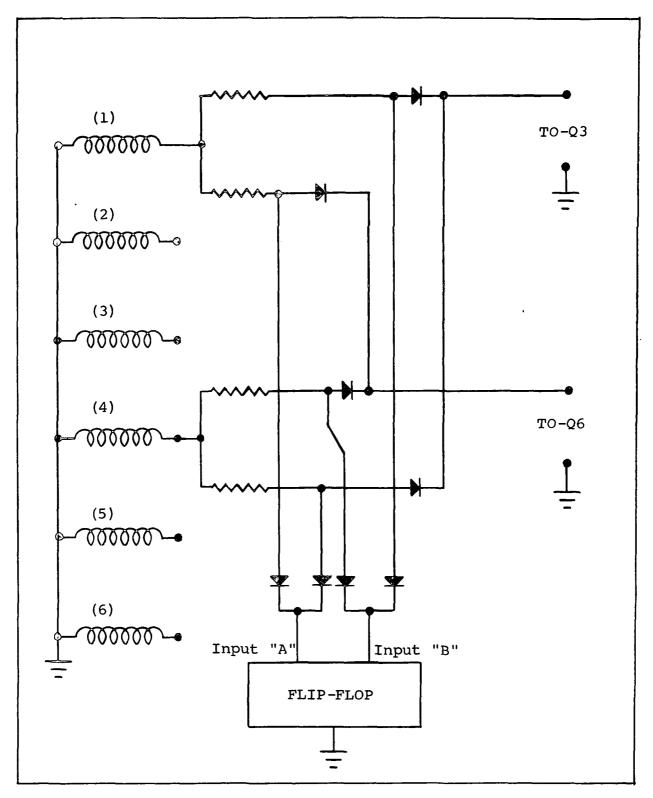


Figure 24.- Diode Logic Reversing Circuit

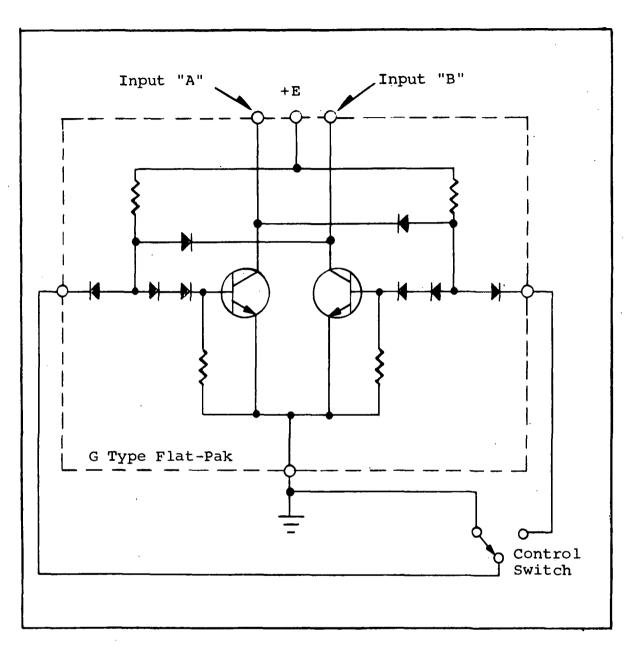


Figure 25.- Diode Logic Circuit Flip-Flop

input "B" activates the other pair of diagonal transistors, thus giving the reverse direction of rotation. Reverse rotation is obtained by switching the signals from the two sensor windings to the upper and lower bridge switches in each leg of the armature control bridge.

The transistor bridge reversing scheme was selected for the final circuit because of its simplicity and improved reliability. A total of 18 components, plus one flip-flop is required for this reversing scheme.

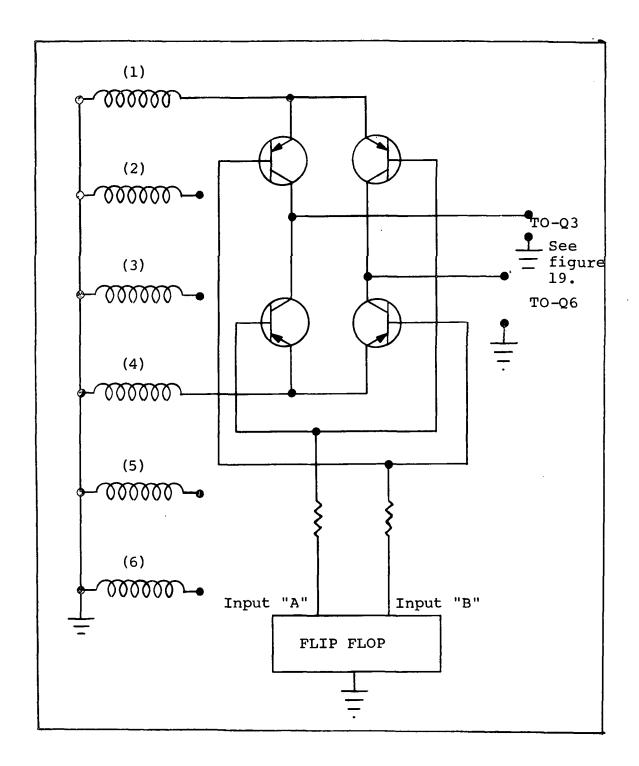


Figure 26.- Transistor Reversing Bridge

Should input "A" and input "B" both become ungrounded, no harmful effects will result. In this case, no signal from the magnetic sensor will be conducted to the armature switches, and motor operation will cease.

The flip-flop shown in figure 27 can be used with the transistor bridge reversing scheme since one of "A" and "B" need not be tied to ground at all times.

Addition of the two diodes provides a signal to activate the oscillator when either a forward or reverse gate signal is applied to the flip-flop. With neither a forward nor reverse gate signal applied, the entire circuit is in the standby condition.

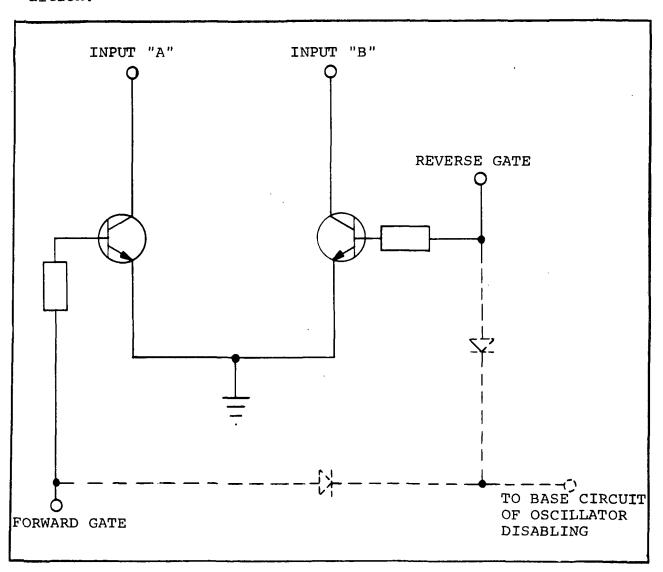


Figure 27.- Transistor Reversing Bridge Flip-Flop

Regenerative Trigger. It has been established that the controller-commutator circuit must drive the armature switches regeneratively to permit operation at the stall condition for any angular position of the rotor without damage to the circuit.

The trigger used in the circuit is a basic level detecting regenerative Schmidt Trigger. The triggering level of the Schmidt Trigger is established by the value of the resistance in the emitter circuit. Increasing the value of this resistance also increases the trigger's hysteresis. An integrated circuit Schmidt Trigger is used to save space and to increase reliability, speed, and efficiency. The Westinghouse type T package (similar to a TO-5 transistor can) was selected because of its rigidity and mounting simplicity.

The basic Schmidt Trigger inherently has a certain amount of hysteresis which can be changed as mentioned above. It should be noted at this point that the lockout scheme, to be discussed later, makes the controller commutator operation independent of the Schmidt Trigger's hysteresis.

Commutator Bridge.- In order to maintain conservative design margins, it is necessary to drive the armature switches with enough current to completely saturate them at locked rotor collector currents. This requires that the base drive current for the armature switches be relatively high with actual value depending on the gain of the transistor used. To keep drive losses down, it is necessary to supply the drive current with as small a voltage as practical. The most efficient method to obtain the drive current is with an isolated power supply of 4 to 6 volts which can be obtained from the oscillator with the addition of a winding and two rectifiers. Refer to figure 17 for the following discussion.

The base-emitter circuits of the bottom row switches have both a drive voltage and a reverse bias voltage supplied by the oscillator. The reverse bias voltage is supplied continually through R21, R28 and R32. The base drive current is supplied at a 10 kc/s rate to the appropriate armature switch by the isolated drive winding through either Q11, Q14 or Q17, depending on which Schmidt Trigger is activated. The same isolated drive winding supplies voltage for the Schmidt Triggers.

The top row switches have a base drive voltage applied from the third supply of the oscillator. The base drive current is directed to the appropriate armature switch through Q2, Q5 or Q8, depending on which Schmidt Trigger is active. The base drive current for the top row switches is not switched on and off at a 10 kc/s rate like the bottom row switches (the reason will be discussed later). During the time that the driver transistor is saturated, the armature switch drive current is conducted through the saturated driver.

The capacitor Cl, C2 or C3, associated with that driver, discharges through the driver's base-emitter circuit. During the half cycle that the Schmidt Trigger is not active, the driver transistor is kept on by the capacitor's charging current, supplying base drive to keep the armature switch saturated until the next half cycle.

The upper armature switches are driven at a 100 percent duty cycle.

Lockout Circuit. - To minimize ripple torque and eliminate dead spots, two conditions must be met (1) at any one time, two and only two armature switches must be on and (2) transfers from one armature switch to the next switch must take place without appreciably changing the torque level at that shaft position. These conditions must be met within the supply voltage range of 22 to 34 volts, and in either direction of motor rotation.

Refer to figure 28. The crossover point is defined as the shaft position at which the output voltage at one sensor secondary winding equals the output voltage of the next secondary winding. The crossover position is independent of applied voltage and the direction of rotation. The circuit has been designed to take advantage of this unique situation by transferring from one switch to the next switch at the crossover point in both the top and bottom row switches.

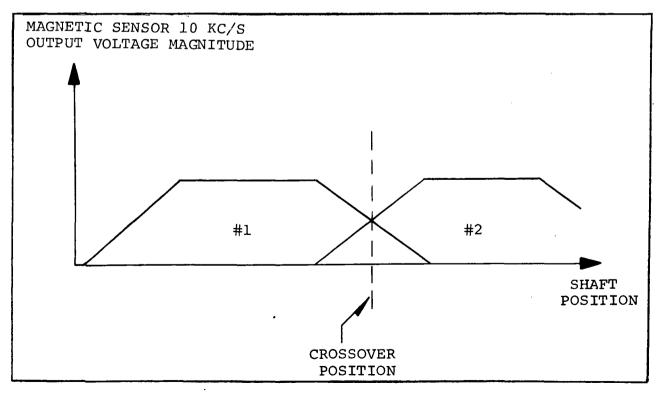


Figure 28. - Crossover Point Position

Diodes CR2, CR3, CR7, CR8, CR11, CR12, CR15, CR16, CR19, CR20, CR23, and CR24 provide the proper logic for the lockout scheme. Refer to the top three Schmidt Triggers of figure 17. When the first Schmidt Trigger is activated, the input signals to the other two Schmidt Triggers are grounded through transistor Q1 and diodes CR2 and CR3. Initially the Schmidt Trigger that has the highest magnitude input signal from the sensor is the trigger that will be activated first, thus locking "off" the remaining two triggers. This logic takes place at the beginning of each positive 10 kc/s pulse received from the sensor output. As a result, the Schmidt Triggers are functioning as level comparator switches rather than level detecting switches. Since the interlock logic takes place on a 10 kc/s basis, transfer occurs exactly at the crossover point.

The same situation applies to the bottom row switches.

Pulse-Width Modulator. The permanent magnet rotor generates a back emf in the stator winding as the rotor turns. The speed at which the motor runs is then determined by the applied voltage and shaft load. The speed tends to increase in order to balance the generated back emf and the applied voltage.

Since the armature switches are turning on and off at a 10 kc/s rate, and since the time constant of the armature winding is very long compared to this rate, speed control can be obtained by varying the on to off time ratio of the armature switches (pulse-width modulation).

The inductance of the armature winding is such that the reactance at 10 kc/s is very large compared to the resistance. As a result the 10 kc/s current, being limited by the winding reactance, will be small but the dc current, being limited by the winding resistance, will be large.

The maximum duty cycle of the 10 kc/s armature switches is: on for 50  $\mu\text{-sec}$  and off for 50  $\mu\text{-sec}$ , which is a 50 percent duty cycle. The resulting dc current flow will be one half of the applied 28 volts, divided by the winding resistance. Neglecting losses, the no-load speed of the motor will be just great enough to generate a back emf of 14 volts. Reducing the duty cycle below the maximum 50 percent value reduces the effective level of the applied motor voltage proportionally, and the motor speed reduces accordingly. The duty cycle can be reduced to zero, giving no torque or motor rotation.

It has been established that switching both the top and bottom armature switches at a 10 kc/s rate will not give rise to significant net dc armature currents.

Figure 29 depicts an equivalent circuit of the case where a 50 percent duty cycle is used in both top and bottom armature switches.

During the period of time that the top and bottom transistors are saturated, a current begins to flow and builds up flux in the armature core. Both transistors cut off after 50  $\mu$ -sec and the armature windings commutate through the commutating diodes and the 28-volt supply. Current begins to decay as the diodes clamp the armature commutating voltage to -28 volts. This results in a 10 kc/s ac voltage being applied to the armature winding with negligible value of dc voltage. The current, being limited by the high reactance is very small and does not contribute significantly to torque.

To overcome this problem, either the top row or the bottom row of armature switches must have a 100 percent duty cycle, while the remaining row of armature switches has the pulse width modulated 50 percent duty cycle.

Figure 30 will verify the point. When the top transistor is saturated, the current starts to build up. When cutoff is reached, the winding commutates through one diode and the bottom transistor which is still conducting because of the 100 percent duty cycle. The commutating voltage is now clamped to zero volts rather than ~28 volts. As a result, the armature winding voltage never goes negative and has an effective value of dc voltage applied. This gives rise to a dc current with only a very small 10 kc/s ripple component. The dc current level, limited by the winding resistance, results in a net motor shaft torque. Hence, the effective applied armature voltage and the resulting current flow is directly proportional to the duty cycle of the top armature switches.

To be conservative, the armature switches must be driven with enough current to insure saturation at locked rotor collector This relatively high drive current causes the armature switch storage time to increase a significant amount. The storage time of a hard driven transistor is shown in figure 31. It can be noted that the transistor continues to conduct, even though its base drive has been removed. As a result, the effective applied armature voltage will not vary directly with the base drive duty cycle. Also the storage time of the transistor is subject to change with temperature. The resulting open loop speed control of the motor would be unreliable. Hence, the storage time of the transistor must be effectively eliminated to obtain linear open-loop speed control. The method used to eliminate the transistor storage time is to back bias the base-emitter junction of each of the armature switches during the period when forward base drive is zero. The result of the reverse bias addition is shown in figure 32. The storage time is small enough to be neglected.

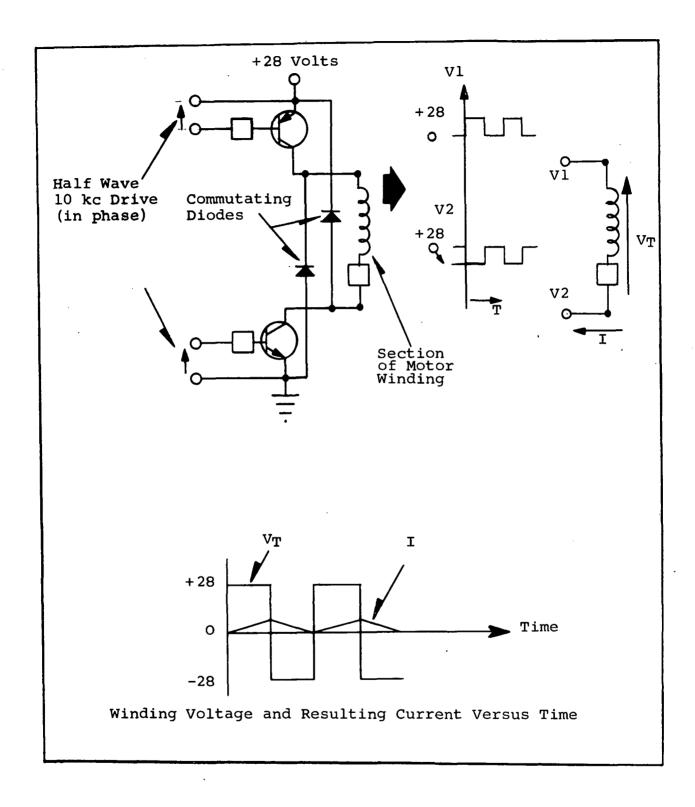


Figure 29.- Equivalent Circuit of Armature Winding with Top and Bottom Switches Operating at 10 kc/s

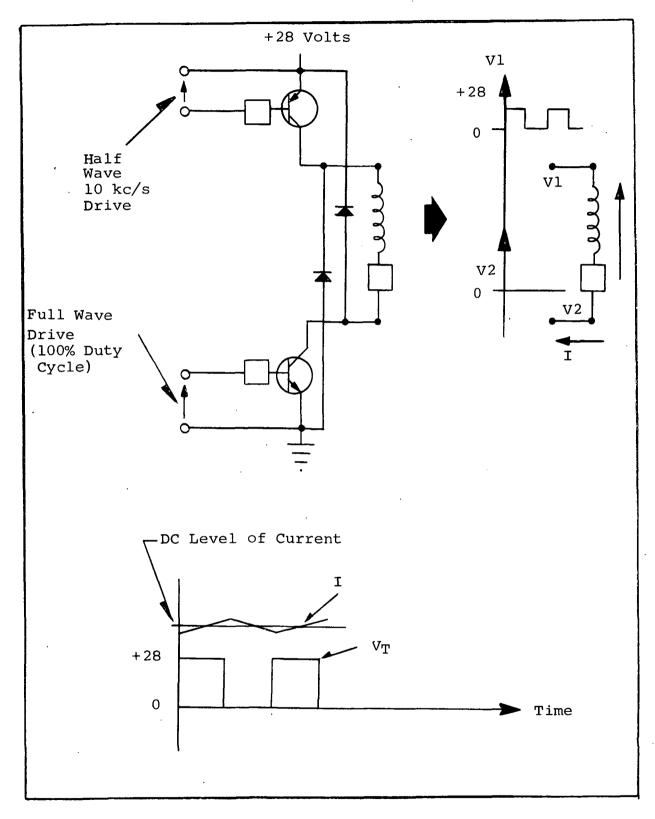
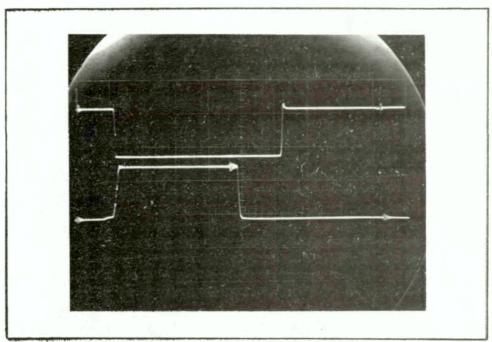
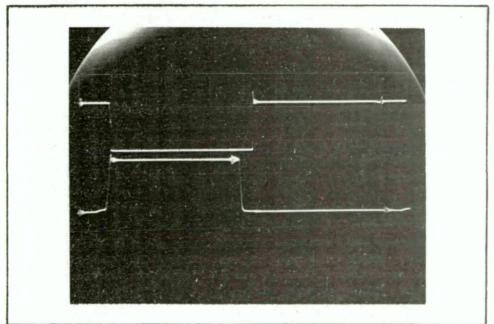


Figure 30.- Equivalent Circuit of Armature Winding with Top Switch Driven Half Wave and Bottom Switch Driven Full Wave



TOP: Collector to emitter voltage of armature switch and BOTTOM: Base drive to armature switch without back bias vs. time = 10 u-sec per cm

Figure 31.- Armature Switch Storage Time Without Bias



TOP: Collector to emitter voltage of armature switch and BOTTOM: Base drive to armature switch with back bias vs. time = 10 u-sec per cm

Figure 32.- Armature Switch Storage Time With Bias

The armature switches are pulse-width-modulated by a saturable reactor placed in the base drive circuit of only the bottom row switches. Refer to figure 17 for the following discussion.

Since only one of the three switches is on at any one time, only one saturable reactor is required in the common return path. A permanent reset bias is applied to the saturable reactor through resistor R8, and the bias winding. The control winding has a variable 0 to 15 volt external supply for speed control.

The entire base-emitter drive circuit for the bottom row pulse-width-modulated armature switches, consists of the driver switches, Q11, Q14, and Q17, the saturable reactor, the current limiting resistors R20, R22, R27, R29, R34, and R36, and the isolated drive from the oscillator.

With the external 0 to 15 volt supply set at zero volts, the saturable reactor has full reset applied by the bias winding. This allows the reactor to drop the entire drive voltage across the gate winding for the half cycle that the driver switch is saturated. During the remaining half cycle, the driver switch is cut off and the core is reset by the permanent bias winding, resulting in no motor rotation.

Increasing the external control to 15 volts saturates the reactor completely. None of the drive voltage is supported across the reactor's gate winding. This results in full current drive to the armature switches during the half cycle that the driver switch is saturated, giving 50 percent duty cycle and full motor speed.

The amount of external control applied between zero and 15 volts determines the amount of reset applied to the reactor and hence the length of time the gate winding will drop the base drive voltage. Since the saturable reactor operates on a voltsecond basis, the time required before the drive voltage saturates the core is directly related to the amount of reset which is in turn inversely related to the external control. Hence, the drive current pulse width or the duty cycle is directly proportional to the applied external control and the motor speed is directly proportional to the external bias voltage in the zero to 15 volt range. Figure 33 illustrates the theoretical speed versus control (external bias) voltage characteristic curve of the circuit. Some minimum voltage is required for the motor to overcome its own static friction so that the zero speed point will not exactly occur at zero bias and will tend to vary because of variation in friction and cogging torque. Also it is difficult to obtain full speed at exactly 15 volts. However, the operation is stable at the two end points.

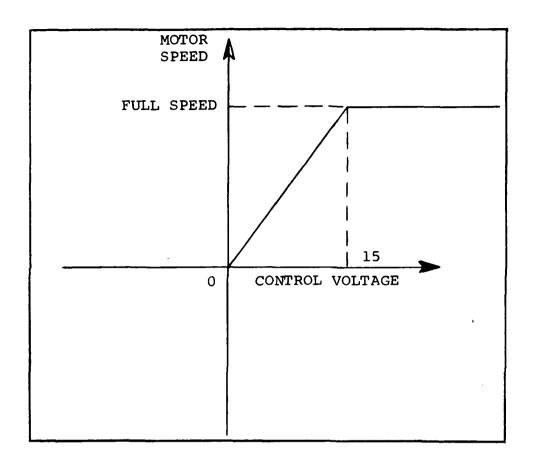
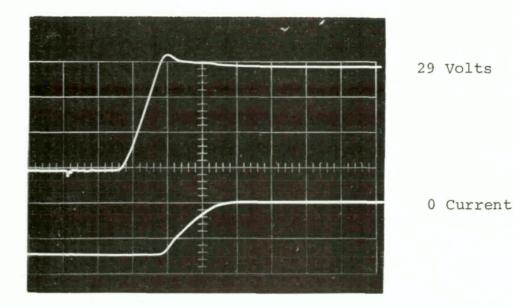


Figure 33.- Ideal Speed Control Characteristics

Increasing the control voltage above 15 volts only drives the reactor further into saturation, but since it saturates at 15 volts, the speed cannot increase further because the duty cycle is limited to 50 percent by the driver transistors. A negative external control tends to reset the core faster. As a result, the drive current remains zero because the reactor still drops the drive voltage and the motor does not run.

At the original conception of the circuit, it was intended to use the top row switches for pulse-width-modulation which results in a simpler circuit configuration. However, because of the circuit configuration the top row switches are necessarily PNP transistors. A canvas of suppliers determined that high-speed PNP transistors could not be obtained.

Tests were taken on one of the best available PNP transistors to determine switching losses at the 10 kc/s rate. Superimposed traces of current and voltage drop in the transistor with a simulated inductive load revealed the phenomena that the full current is maintained through the transistor almost to complete shutoff. A picture of these oscillograph traces is shown in figure 34.



Time progresses left to right Top trace - Voltage drop across transistor Bottom trace - Current through transistor Time scale = 1  $\mu sec/cm$  Line voltage = 28 volts

Figure 34.- Switching Characteristics with Inductive Load - PNP Transistor 2N3201

The explanation of the action lies in the fact that the current cannot transfer to the commutating path until a reverse voltage across the commutating path is attained. This does not happen until the voltage drop across the transistor rises to above line voltage. The tests demonstrated that excessive switching losses would occur if the pulse width modulation was attempted with the slow PNP transistors.

It was therefore necessary to pulse-width modulate the bottom row transistor and to keep the top row switches on continuously.

# Efficiency

For a given motor speed torque setting, the losses within the controller commutator are fixed except for the power dissipated in the armature transistors. That is, as the motor load increases, the resulting increase in motor current causes an increase in commutating losses only at the armature switches. That power is the collector to emitter satuation voltage, times

the motor current, for the top switches and also, times the fraction of duty cycle, for the bottom switches. This loss varies from zero to approximately 0.9 watts maximum.

Table VI gives a breakdown of the estimated watts lost in the controller commutator. These values are based on a full speed motor setting (a 50 percent duty cycle on the upper armature switches).

Table VI. - Losses in Controller Commutator

	Watts
Oscillator Drive and Losses	0.10
Magnetic Sensor Losses (estimated max.)	0.40
Reversing Bridge Drive and Voltage Divider	0.02
Schmidt Trigger Drive	0.06
Top Row Armature Switch Drive	0.50
Top Row Armature Switch Driver Drive	0.01
Bottom Row Armature Switch Drive (a)	0.25
Bottom Row Armature Switch Driver Drive (a)	0.02
Bottom Row Armature Switch Reverse Bias (a)	0.05
Pulse Width Modulator Permanent Bias	0.01
Other	0.40
TOTAL	1.82

(a) Will decrease as duty cycle is decreased below 50 percent.

### Reliability, Materials, and Components

The entire controller commutator circuit has a total of 133 components counting the integrated Schmidt Triggers as one component. Possibly other components of the circuit could be combined in the form of integrated circuitry but a canvass of suppliers revealed no standard items that were applicable.

The derating practices given in table VII were followed as a minimum in the design.

Component values were selected and their operation verified in the final breadboard of the circuit. The final values selected plus the part numbers of the solid state devices and connectors are shown on the schematic of figure 17. The main power transistors are heat sinked for vacuum operation.

All the solid state devices used are silicon. Resistors are carbon composition and wire wound. Capacitors are solid electrolyte (tantalum). Transformer cores are either Hi-Mu 80 or Orthonik with phenolic core boxes wound with DuPont ML enamelled wire which has high temperature capability (in excess of 200°C). The transformers are potted in silicone potting compound. The printed circuit boards are epoxy glass with silver plated terminals. Teflon insulated lead wire is used for interconnections. Corrosion resistant hardware, either stainless steel or beryllium copper is used throughout. The aluminum container is chemically filmed per MIL-E-5541.

Connectors compatible with a space environment were selected. The five pin input connector contains terminals for the forward and reverse signals, the speed control voltage, and the line voltage. The seven pin output connector contains terminals for the rate and position information from the magnetic sensor. All connections to the connectors are shown in the schematic.

Table VII. - Solid State Component Derating Practice

Resistors	20% on power
Capacitors	50% on voltage
Transistors	50% on voltage 30% on current
Diodes	40% on PIV 50% on current
Zener Diodes	20% on power
Schmidt Triggers	70% on voltage

#### MECHANICAL DESIGN

### General Discussion

The unit is designed so that the control circuit package and the motor-sensor package are combined with the control package mounted on the end. However, the control can be separated and the two components operated separately if a jumper cable is used. The magnetic sensor stator is permanently mounted in the end bell. Adjustment is accomplished by rotating the end bell. Adjusting slots are provided in the end bell for the mounting screws.

### Manufacturing Procedure

A cross-sectional view of the motor controller is given in figure 35. The various major parts are identified on the drawing.

Motor Stator. The armature punchings are annealed and treated with aluminum orthophosphate for insulation. The punchings are then bonded together with epoxy cement. The core is wound, dipped and baked and machined. The bore can is inserted (shrink fit) into the bore which is then re-machined. The frame is heated to allow insertion of the wound core which has an interference fit.

Motor End Bells. - The end bells are rough machined from bar stock. Knurled stainless steel inserts are pressed into the bearing housings. The end bells are then finish machined, treated with chemical film, and a gold flash is given to the inserts.

Magnetic Sensor Stator and Rotor.— The completely machined cores are bought outside (Ceramagnetics, 87 Fairfield Road, Fairfield, New Jersey). End punchings of 0.031 inch thick Doryl-glass laminate are glued in place with a silicone adhesive. The stator is wound and dipped and baked. The stator is then mounted permanently in the right end bell.

Rotor Assembly (original concept). The shaft is machined from bar stock. The sensor rotor and permanent magnet are then mounted on the shaft against the inner shoulders. The sensor rotor sides are coated with Doryl varnish. Spacers are pressed on against the two components. The permanent magnet is pinned in place through the interpolar gaps to the spacer and inner shaft shoulder. The pins are shimmed to provide a solid hold on the magnet and the shims coated with varnish to hold them in place. The varnish is cured and then the bearing journals qualified. The revised rotor construction is shown in figures 6, 7, 8, and 9.

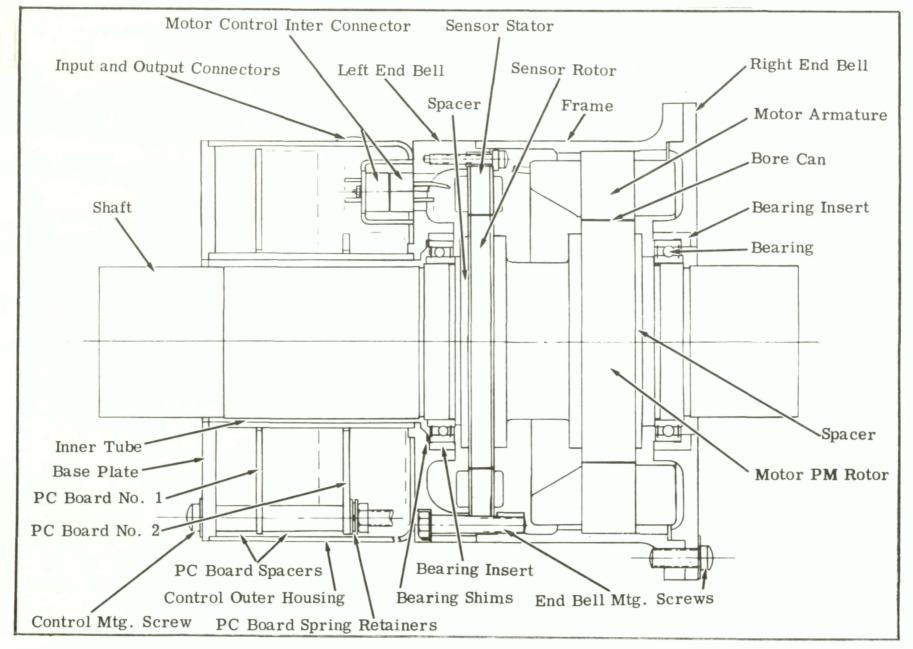


Figure 35.- Mechanical Configuration

Motor Assembly. The rotor is temporarily inserted into the stator with the end bells mounted. The bearings have slip fits on both the shaft and housing. The proper number of shims in the right end bell housing is determined so that total rotor axial movement is limited to 0.004 to 0.006 inch with a two pound load applied axially in both directions. The unit is then disassembled. The rotor permanent magnet is magnetized with a keeper placed on the magnet. The unit is then reassembled with the keeper being removed during insertion of the rotor. Connections are made and the connector mounted to the motor.

Control Package. The circuit boards are connected and mounted to the base plate with the spacers and three mounting screws. The boards are held in the base-spacer assembly with a spring retainer against the mounting screws. The outer housing is placed over the assembly and connections made to the connectors. After the inner tube is inserted, the control is ready for assembly to the motor. This is accomplished by turning the mounting screws into threaded holes in the end bell. A pilot is provided on the end bell for locating.

# Specific Comments

Bearing System. The bearings are Barden bearings, catalogue number A543SSTB. This bearing is a thin bearing with a large bore having a T-type retainer composed of glass fiber reinforced teflon with  ${\rm M_{O}S_2}$ . This solid lubricant is a proprietary Barden material with the trade name of "Bar-Temp". Consultation with Barden Engineering determined that this bearing has been used previously in space application and that it did not exhibit any severe "sticking" characteristic. Other characteristics also appear to be satisfactory for this application. The bearing is double shielded to prevent particle contamination.

According to Barden Engineering, this bearing is capable of continuously sustaining a radial load of approximately 10 pounds. Barden Engineering recommended that if preloading was used, it should be limited to one or two pounds. Because of the large diameter of the bearing and the unusually light force required, it would be quite difficult to obtain a spring to accomplish the preload. Also, because of the low speed, preloading was not considered necessary. Consequently, no preload is used on the bearings. The axial clearance in the housing is taken up with shims until a movement slightly above the expected axial free play in the bearing is obtained. The bearing free play is greatly in excess of the differential thermal expansion of the frame and shaft over the temperature range. The bearings have a slip fit on the shaft and in the housing. The bearing inserts are gold-plated to prevent cold-welding of the bearing to the housing in a vacuum.

Structural Integrity of Sensor Cores. The structural integrity of the ferrite cores is enhanced by cementing 0.031 inch thick punchings of Doryl-glass laminate on the core sides. These punchings have the same shape as the cores. The Doryl-glass laminate, produced by Westinghouse, is a high temperature, low outgassing material with high structural strength. The flexural strength, which is the characteristics of most interest in this purpose, of the laminate is in excess of 70,000 psi. This compares with a flexural strength of most epoxy coatings of approximately 12,000 psi. The cement used is a silicone varnish which in the past has given the most satisfactory results in cementing end punchings to stator cores. The varnish, a thin fluid when uncured, gives its adhering properties with a very thin film.

## Weight Estimate

The total estimated weight of the motor-controller is 4.7 pounds. This is broken down as follows:

Motor electrical weight	-	1.45
Magnetic Sensor weight	_	0.28
Shaft and Spacers	_	0.86
Frame and End Bells	_	0.98
Circuit Package	-	0.80
Miscellaneous	_	0.33

Total - 4.70 pounds

## Materials and Finishes

A complete list of materials used in the motor-controller excluding the printed circuit boards, circuit components, and connectors, is given in table VIII. All aluminum parts used are given a chemical film per MIL-C-5541. All other parts used are inherently corrosion resistant and are given no surface treatment for retarding corrosion. No paint is applied to the unit.

### CHANGES DURING MANUFACTURE AND CHECKOUT

#### Motor

Only one significant change was made in the motor design during manufacture. It was found that lack of concentricity of the stator bore and stator outside diameter plus irregularities in the magnetic can in the bore caused the can to become too thin in spots after final grinding. The thickness was

# Table VIII. - Material List

Item	Material	Govt. Spec.	Supplier and Identification
Leads 19/0.003	Teflon Insulated	MIL-W-16878, Type E	
Brg Inserts, Spacers, Shaft	303 SST Bar	QQ-S-763, Class 303, COND A CD	
Stator Slot Wedges	Silicone-glass Laminate	MIL-P-997, Type GSG	
Stator Pchg. Bond	Epoxy Cement		EIP-REZ 510 Jones Dabney
Slot Insulation	ML Resin Treated Glass Cloth		Pyre ML, DuPont
Insulating Tape	ML Resin Tape		EE 6379, Permacel Tape Corp.
Magnet Wire	ML Resin Enamel	MIL-W-583, CL220, Type M3	
Lead Connection	Brazing Alloy	QQ-S-561, Class 3	
Sensor End Pchgs.	Glass-Doryl Resin Bonded Laminate		Doryl Laminate, Westinghouse
Stator Bore Can	50% Nickel Steel		Hipernik, Westinghouse
Stator Punching	Cobalt Steel		Hiperco 50, Westinghouse
Stator Pchg. Insulation	Aluminum Orthophosphate		
Permanent Magnet	Cast Alnico V		
Sensor Core	Manganese-Zinc Ferrite		MN-30, Ceramagnetics
Sensor End Pchg. Bond	Silicone Varnish	MIL-I-24092, Type M, Class 200	
End Bells, Frame	Aluminum Bar	QQ-A-225/6 T4	
Shim Brg. Housing	Beryllium Copper	QQ-C-533, COND 1/2H	
Shim - PM Shaft Pins	Copper	QQ-C-576, CR Soft Temper	
Sensor - Lock Plate - Control Housing	Aluminum	QQ-H-250/8 H34	
Connector Spacer	Stainless Steel	QQ-S-763, CL 416, COND A, CD	
PC Board Spacer	Glass-Plastic Tube	MIL-P-79 Form TR, Type GMG	
Control Housing Tube	Aluminum	QQ-A-225/5 T4	
Control Housing Cover	Aluminum	QQ-A-318B Condition Half Hard	
Lacing Tape	Teflon-Glass		Warren Wire Co.
Insulating Varnish	Doryl Resin		Doryl B109-3, Westinghouse
Hardware, Lockwire	Stainless Steel		
Solder - Connector	Pure Tin Solder	MIL-S-6872	
Flux	Flux	MIL-F-4995, Type I	

changed to 0.0075 instead of the 0.006 thickness originally planned. The change in thickness should have a negligible effect on performance.

During the checkout of the first unit, it was found that the magnet flux was low resulting in low torque. This resulted in reconstruction of the last two rotors as shown in figures 6, 7, 8, and 9.

### Magnetic Sensor

Some trouble was experienced with primary winding shorts when constructing an experimental model of the magnetic sensor for preliminary tests. It was found necessary to insulate with approximately 0.006 inch thick tape between the winding and the ferrite core to prevent the winding shorts.

During manufacture, it was found necessary to change the wire size on the primary winding from a No. 22 to a No. 25 AWG because of excessive buildup of the wire. This amounts to doubling the primary resistance which, however, is still negligible in its effect on the performance. The secondary winding wire size was increased from a No. 33 to a No. 32 to partially compensate, since room was available.

Also after dipping one sensor stator in Doryl varnish and baking, a crack was discovered in the ferrite, although the whole assembly was held rigidly together by the end punchings. For the subsequent units the varnish was changed to silicone varnish which does not cure as hard as the Doryl and a controlled heating and cooling cycle was used during bake. No further cracking was observed.

#### Controller

Two changes were made in all of the controller circuits. Resistors R3, R8, R13, R18, R25, and R32 in figure 17 were changed from 1000 to 3000 ohms. This change was made to secure more definite turn on of the transistors being driven by the Schmidt Triggers. Capacitor C4 was added across the primary of the oscillator toroid to aid in suppressing spikes. These changes are shown in figure 17.

### OPERATING CHARACTERISTICS OF MOTOR-CONTROLLER

## Physical Configuration

The physical configuration, connector inputs, and connector part numbers are given in figure 36. The total weight of the unit was measured at 4.28 pounds.

## Forward, Reverse, and Standby

The forward and reverse voltage connection to the input connector is shown on figure 36. The operation is such that if a 15 volt dc signal is applied to the forward terminal and none to the reverse terminal, the motor will rotate in one direction. If this voltage is removed and applied to the reverse terminal, the motor will rotate in the opposite direction. If the voltage is removed from both terminals, the motor will be in a standby condition. No current will be drawn and the circuit will be completely idle. The motor will provide no torque in this condition. The impedance offered in the circuit to the voltage is 1500 ohms. Voltage should never be applied simultaneously to the forward and reverse terminals. Circuit damage would result if this is done since tandem transistors in the bridge would be driven on, resulting in a direct line short through the transistors. The circuit will operate satisfactorily with an input voltage from 12 to 18 volts.

### Speed Control

The input terminal for the speed control voltage is also shown on figure 36. A variable voltage from 0 to 15 volts applied at this point will control the speed of the motor. With zero or negative voltage applied, there will be no voltage applied to the motor and the motor will be idle. However, current will still be drawn in the logic portion of the circuit. With 15 volts or higher applied, the motor will be driven at half line-voltage since the maximum pulse width gives a 50 percent duty cycle. This is the maximum speed attainable.

The ideal curve of pulse width versus input signal voltage is shown in figure 37. Superimposed on this curve is an actual curve taken on a test circuit using the same methods of control. This curve should be regarded as typical. The actual curve may deviate from this somewhat due to different component values. The linearity of the curve breaks down at the ends because of the inability to obtain a completely square loop material for the saturable reactor through which the control is accomplished and the inability to obtain the end points exactly.

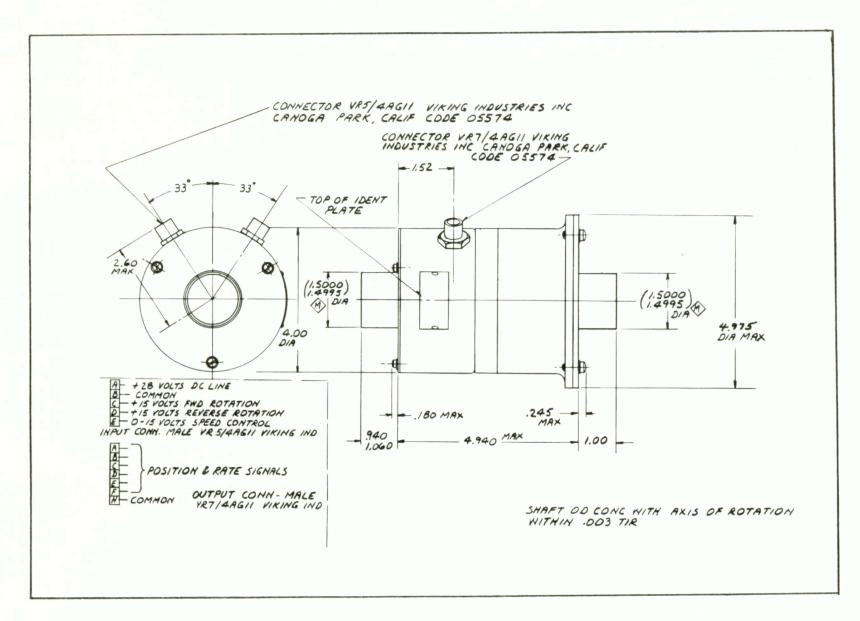


Figure 36.- Motor Controller Outline

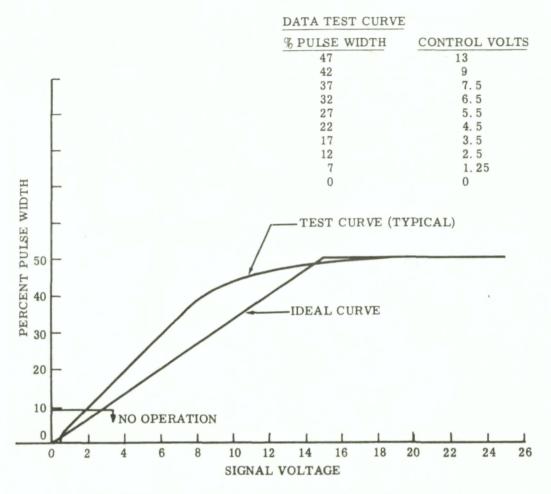


Figure 37.- Pulse-Width Versus Signal Voltage

The calculated full-voltage speed torque curve for the motor is shown on figure 38. Also shown on this figure are a family of curves at different speed control voltages. These are obtained by ratioing directly with the effective applied voltage as determined by the pulse width obtained from the test curve of figure 37. Since the motor requires a little voltage to overcome its own circuit drops and residual friction, no operation can be expected below a pulse width of approximately nine percent or a signal voltage of two volts.

These curves are shown for a 28 volt line voltage. If line voltage varies, the speed can be expected to follow the variation, but not directly except at full speed. Some compensation is obtained because a constant bias is provided the saturable reactor from the line and the variation in bias with line voltage will tend to compensate for the variation in voltage to the motor by varying the percentage pulse width. The compensation is not complete because part of the bias is

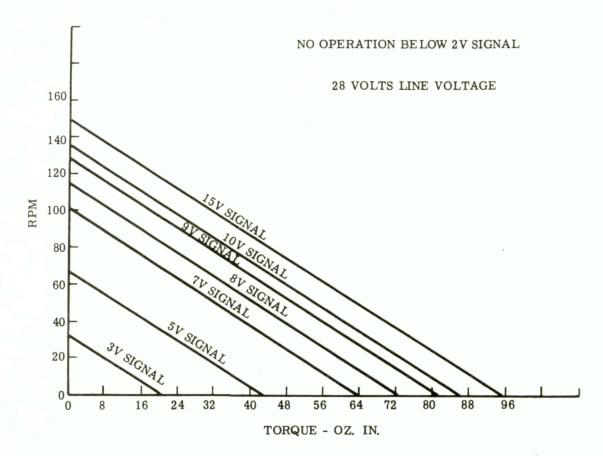


Figure 38.- Calculated Speed Torque Curves Versus Speed Control Signal Voltage

supplied by the speed control signal which presumably remains constant. The amount of compensation is also variable depending on the original operating point.

The motor at full voltage will draw an average line current of 0.4 amperes at locked rotor. This will drop to approximately 0.075 amperes at no load. Average line current at a constant torque can be expected to vary directly with the pulse width except that a nearly constant current of approximately 0.065 amperes will be drawn by the logic circuit.

Another source of variation in the speed-torque curves is the temperature of the winding. Variation in winding temperature will cause variations in the slope of the speed-torque curve. The locked torque will vary inversely with the resistance of the winding while the no-load speed will remain practically constant. The calculations were performed at a constant winding temperature of 40°C, which is the expected temperature at locked rotor and full voltage under room conditions with no conductive or forced cooling. The operating ambient temperature range is given as -10 to 70°C. The heat factor (multiplier on resistance at 25°C) at 40°C is 1.058. The heat factor at -10°C with a 15°C rise is 0.924. The heat factor at 70°C with a 15°C rise is 1.24. Therefore, the locked torque will vary from approximately 1.15 times the 40°C value in a -10°C ambient temperature to approximately 0.85 times the 40°C value in a 70°C ambient. These figures are based on having a 15°C winding temperature rise. The actual rise during operation in space would depend on the method of mounting used and the heat conducting area. It would also vary with the motor loading and pulse width. The temperature effects on the magnet are negligible compared to the effect on the winding.

The impedance offered by the circuit to the speed control voltage is 5100 ohms.

#### Rate and Position Information

The six secondary windings of the magnetic position sensor plus a common lead are connected to the output connector as shown on figure 36. These six connections contain continuous position information. The type of information present on each secondary is shown in figure 39 for a small angular rotation. This figure pictures the expected configuration of one amplitude envelope pulse. The rise in amplitude with position is linear for approximately 7.5 degrees. A plot of the positive half of the amplitude envelope pulses versus position for all six lines is shown on figure 14. It is noted that the linear rise or fall portions of the amplitude envelope pulses overlap in the six lines so that for any position there is at least one line with a linear increasing amplitude. The linear regions could be utilized to continuously sense velocity at extremely low rates.

If line voltage varies, the amplitude of the pulses will vary almost directly with the line voltage. The frequency will also vary directly with the line voltage since a magnetic oscillator is used. The pulse width varies inversely with line voltage. Therefore, in the linear region of the pulse amplitude envelope the volt-second integral of the pulses will be almost constant at a given position regardless of the line voltage variation.

The sensor has an output capability of at least 0.010 amperes without affecting the pulse amplitude significantly. The motor commutating circuit uses approximately 0.003 amperes of this capability.

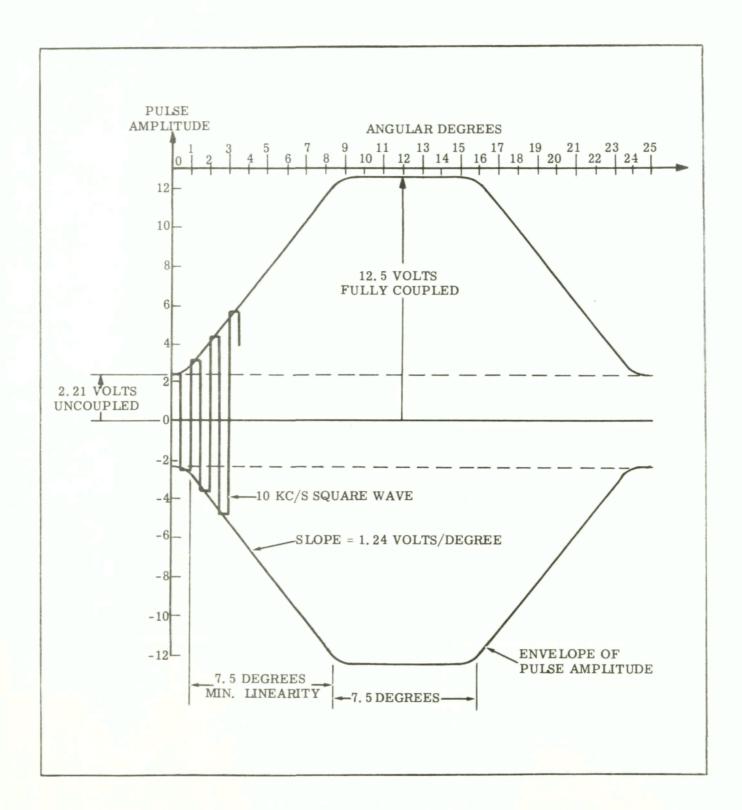


Figure 39.- Detail of Amplitude Envelope Pulse

#### TESTING PROCEDURE

The following test procedures were followed in testing the first unit only. Subsequent units were not tested.

### Design of Magnetic Sensor

Obtain a magnetic sensor stator and rotor core when available. Glue on the end punchings if available. Wind stator core per drawing except do not dip and bake, tape coils or attach leads. Mount the stator and rotor core in the bearing and shaft system fabricated in the Research room.

Design. - Move the rotor until a rotor pole is exactly centered under a stator tooth. Drive the sensor with the breadboard oscillator excited at 28 volts. Using an oscilloscope, determine the amplitude of the output pulse on the winding associated with that particular tooth. Repeat this for all six stator teeth positions. Adjust turns on the teeth until all secondary pulse amplitudes are equal at 12.5 volts.

Rate Sensing. - After the above design adjustment, attach the rotor to the hour hand drive of an electric clock with a second hand. Take readings of secondary pulse amplitude of all six secondary windings with the clock not energized. Energize the clock and allow the second hand to make two revolutions (two minutes on the time scale), this corresponds to 1.0 degree of movement. Stop the clock by removing power and again record pulse amplitudes. Repeat for a total revolution of 45 degrees (45 readings).

### Engineering Tests

The following tests were performed by engineering on the first complete motor-controller.

- (1) Oscillator. Check the output waveform, frequency, and losses. Check the voltages of all secondaries.
- (2) Magnetic Sensor. Check the output waveform and voltage level on all secondary windings.
  - (3) Reversing Bridge. Check operation.
- (4) Schmidt Triggers. Check the firing level of the Schmidt Triggers. Check the output voltage.
  - (5) Lockout. Check operation.

- (6) Main Bridge Circuit. Check the operation, drive voltages, and the capacitor delay operation.
  - (7) Speed Control. Check operation.
- (8) Control Losses. Record current input without motor operation.
- (9) Rough Adjustment of Sensor. Operate the motor at no load. Adjust the sensor stator position until maximum speed is obtained.
- (10) Operational Check. Check functioning of all circuits with motor operating. Determine the minimum and maximum range of input voltage. Do not exceed 34 volts peak input.

### Laboratory Tests

No laboratory tests were made on the units because of schedule and because of incomplete resolution of the problems encountered. Some torque measurements were taken by engineering to identify problems and solutions.

#### PROBLEM AREAS

# Magnetic Sensor Output

The envelope of the tested output voltage amplitudes for all six secondary windings are shown in figure 40. This data was taken using a bench setup on an experimental model wound in the engineering laboratory with secondary windings adjusted to give equal peak amplitudes. As can be seen, there is still some variation in peak amplitudes which is thought to be due to minor air gap variations in the test setup after the coils were adjusted.

For comparison, the output voltages from the sensor in the first complete unit were monitored. These results are shown in figure 41. As can be seen, there is considerable variation in the peak amplitudes. The peak amplitudes of those windings on one side of sensor were considerably different from those on the other side. This is believed to be due to a non-concentric air gap. Tests taken on the bench setups indicated considerable sensitivity to air gap variation. Some variation in air gap is unavoidable on manufactured units because of tolerance buildup.

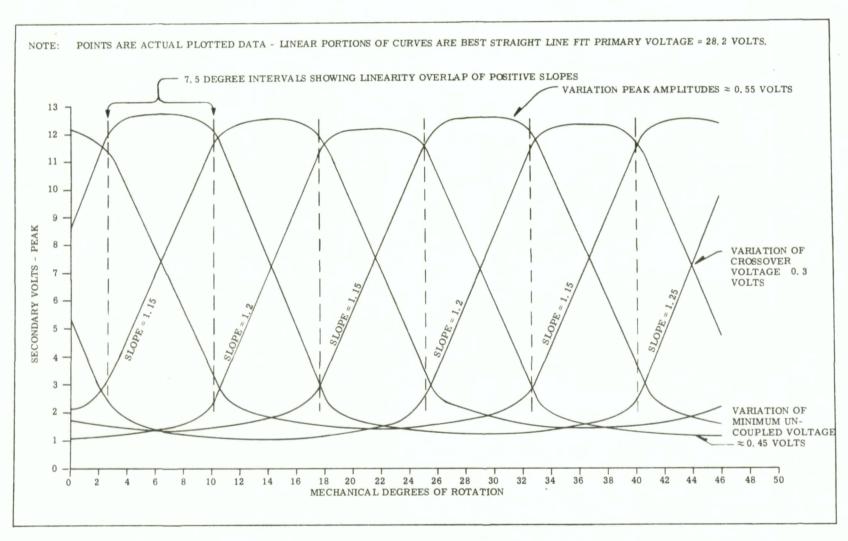


Figure 40.- Magnetic Sensor Secondary Voltages Versus Position - Experimental Unit

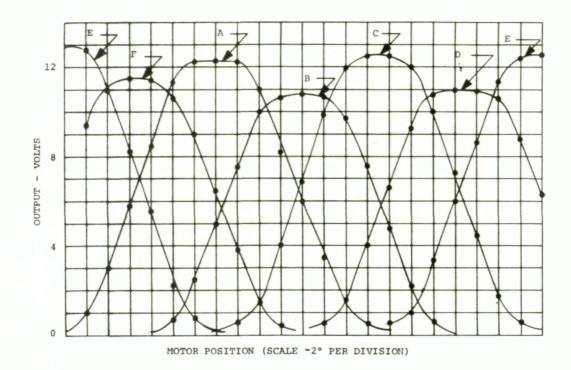


Figure 41.- Magnetic Sensor Secondary Voltages Versus Position-No. 1 Unit

Another characteristic of the sensor noted was a considerable ringing in the voltage output. This was reduced considerably with the addition of a 0.01 mfd capacitor across the sensor primary winding. The difference is illustrated in figures 42 and 43. Loading of the secondaries also reduced the ringing but no way was found to eliminate it entirely.

Another related problem encountered with the sensor outputs is illustrated in figures 44 and 45. Shown in figure 44 is the output voltage of sensor winding No. 1 just prior to reaching the Schmidt Trigger firing voltage. Figure 45 is the same condition for winding No. 3. Examination of the leading edge of the pulses reveals that winding No. 1 has an irregularity at approximately 60 percent of the peak value while winding No. 3 has the same irregularity but occurring at a higher level and being less in magnitude.

The lockout circuit makes the Schmidt Triggers act as comparators between two pulses. That is, during the initial part of the pulse, the Schmidt seeing the highest magnitude will fire, removing the signal from the other Schmidt. This comparison is made on the leading edge of the pulses. It can be seen that, given the two pulses illustrated, the more pronounced irregularity in winding No. 1 pulse would cause preference to be given to

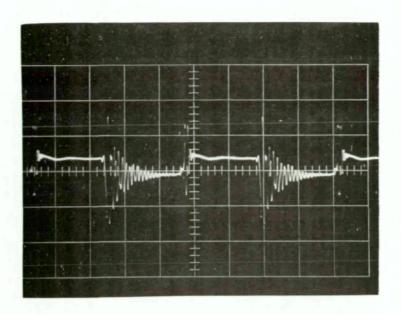


Figure 42.- Uncoupled Secondary Voltage

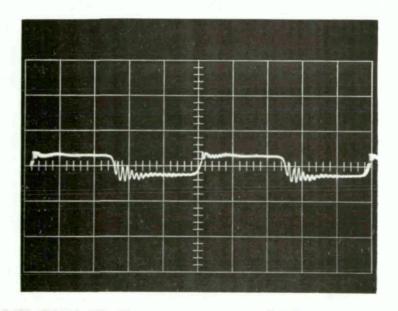


Figure 43.- Uncoupled Secondary Voltage With 0.01 Mfd Capacitor Across Primary

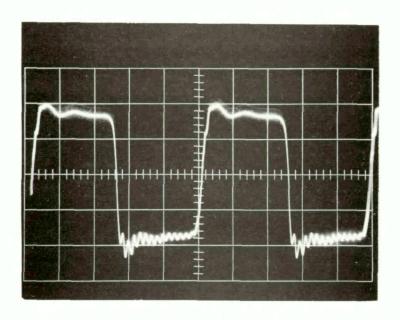


Figure 44.- Sensor Output Voltage From Winding No. 1
Just Prior to Reaching Schmidt Firing Level

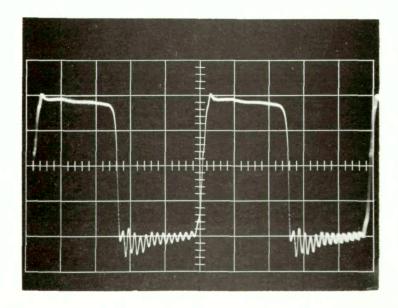


Figure 45.- Sensor Output Voltage From Winding No. 3

Just Prior to Reaching Schmidt Firing Level

IV-0

IV-94

winding No. 3. The Schmidt associated with winding No. 1 would not take over until the overall pulse level was considerably higher. Thus the switch over point to winding No. 1 would occur late causing a low point in the motor torque.

This irregularity, which is apparently due to the ringing previously noted, is present in varying magnitude on all six secondaries, but is much more pronounced on one or two of the windings.

### Dithering

The bottom row switches had a tendency to trade control back and forth at the switching points. This resulted in a vibratory oscillation of the shaft which will be termed dithering. The basic reason for this dithering is apparently electrical rather than electro-mechanical since it was present when a resistive load was connected in place of the motor. There was also a slight tendency for the top-row switches to do this.

Although the basic cause is electrical, the actual vibration of the shaft apparently is electro-mechanical since the trade-off rate would be too fast for the shaft and rotor inertia to respond. It is believed that the constant trade-off results in low effective motor winding currents, giving low torque, and that the shaft vibration is caused by moving into and out of the trade-off point.

One solution to the problem would be to build in a preference for the switch that has been on to come back on with the next pulse. This was accomplished on the bottom row switches as illustrated in figure 46.

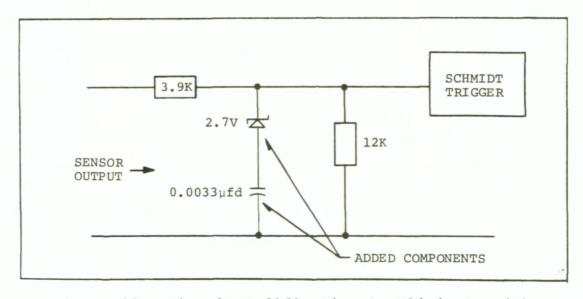


Figure 46.- Circuit Modification to Eliminate Dither

A 0.0033 mfd capacitor and a 2.7 volt zener diode were added in series across the 12k resistor input to the Schmidt Triggers. The capacitor charges to a voltage equal to the difference between the Schmidt firing voltage and the 2.7 volt zener voltage when the Schmidt Trigger is firing. Discharge does not begin until the trailing edge of the pulse drops to this voltage. When the Schmidt is not firing, the capacitor completely discharges because the input voltage is shorted by the lockout circuit to a value below the 2.7 volts. In this manner the capacitor does not significantly disturb the shape of the useful part of the pulse which would affect the pulse-width-modulation. On the top-row switches the zener was not used because the shape of the pulse does not matter.

The capacitor charge remaining after an off period of a Schmidt that has been firing gives it some preference on the next comparison. The addition of these components removed the tendency to dither. Figure 47 and 48 show the input voltage to the Schmidts in the bottom row for the firing condition and the locked-out condition. Figures 49 and 50 show the same conditions for the top switches.

#### Pulse-Width Variation

It was discovered during checkout that for a given speed control voltage, the pulse width applied to the motor varied significantly from the mid-point of a switching cycle to the switching points. At the switching points, the on-time was lower than at the mid-point resulting in low voltage and hence low torque at the switching points. This variation was not significant at full pulse widths, but became more and more severe at lower pulse widths. That is, the variation appeared to be constant regardless of pulse width.

Part of the problem was that the power switch driver transistor for the bottom row switches did not appear to be going off cleanly. The addition of a 3k resistor connected from the emitter to the base of these transistors alleviated this problem and lessened the variation considerably. However, the remaining variation was still significant. The extent of the remaining variation is shown in figure 5l for a low pulse width. The variation amounts to over a 33 percent decrease for this particular pulse width which should be reflected directly in ripple torque.

The explanation for the variation appears to lie in the shape of the sensor pulse. The sensor pulse is not as wide at the top as it is at the bottom. At the mid-point of the switching cycle, the Schmidts are firing on peak value pulses and are therefore on over the width of the pulse at approximately the

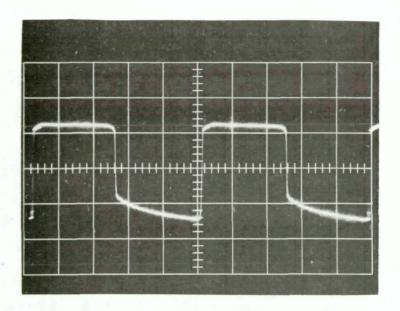


Figure 47.- Input Schmidt Trigger Voltage - Bottom Row - Firing Condition

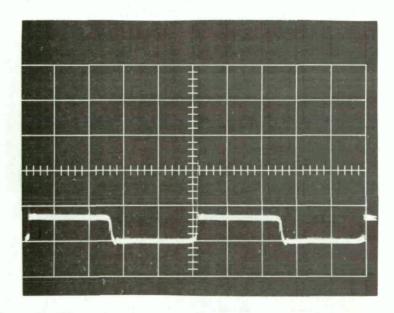


Figure 48.- Input Schmidt Trigger Voltage Bottom Row - Locked-Out Condition

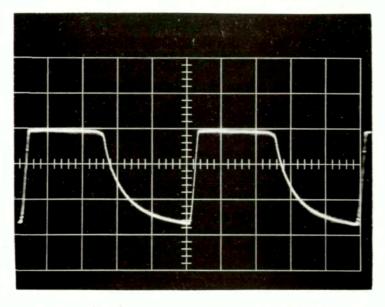


Figure 49.- Input Schmidt Trigger Voltage - Top Row - Firing Condition

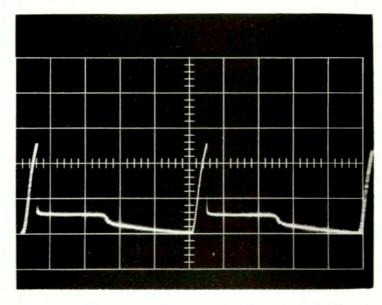
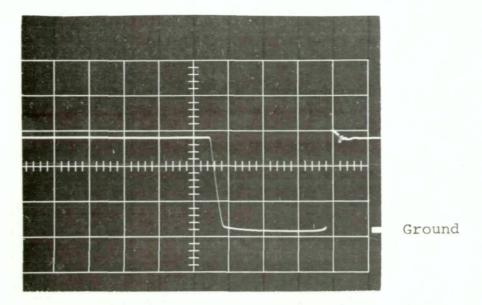
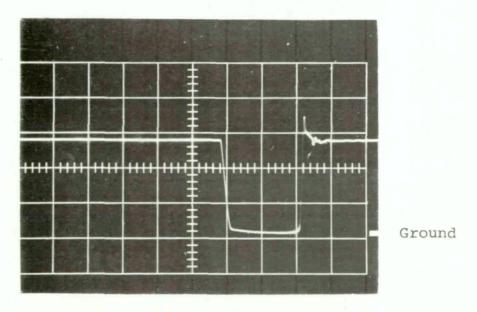


Figure 50.- Input Schmidt Trigger Voltage -Top Row - Locked-Out Condition

14.98



Line to Ground Voltage - 7.5 µsec Pulse Width Mid-point of Switching Cycle



Line to Ground Voltage - 5  $\mu sec$  Pulse Width At Switching Point

Figure 51.- Pulse Width Variation Over Switching Cycle - Constant Speed Control Voltage

4.5 volt level of a 12.5 volt pulse. However, at the switching points, the Schmidts are on over the width of the pulse at approximately the 4.5 volt level of a 6.25 volt pulse. The latter on-time is less than the former because of the taper of the pulse.

However, the taper of the sensor pulse is slight and is not sufficient to account for the pulse width variation experienced. The explanation lies in the amplification of the variation by the saturable reactor used to vary the pulse width. The reset time of the saturable reactor corresponds to the off-time of the Schmidt Triggers. If the on-time of the Schmidt Triggers is less at the switching points, the off-time must be longer. The saturable reactor thus obtains more reset and will support voltage longer during the on time of the Schmidt Triggers. The pulse width supplied to the motors is the total on time less the time the saturable reactor supports voltage. In this manner, the variation due to sensor pulse taper is amplified.

In an attempt to lessen the sensitivity of the saturable reactor to reset time caused by the Schmidt Trigger, the circuit associated with the bias windings was reconnected and resistor values changed as shown in figure 52. The reconnected circuit essentially applies half-wave reset to the reset winding in time to the oscillator 10 kc/s square wave. The reconnected circuit appeared to improve the variation slightly but not by a significant amount. The first unit was left connected in this fashion. The other units are connected as shown in the original circuit.

## Low Motor Torque

This problem was previously discussed under "Motor Electrical Design" in the "Magnetic Development and Revised Rotor Design" paragraph. The problem has been resolved with the revised rotor. The rotor of the first unit was not modified.

#### OTHER TEST RESULTS

# Controller Operation

Other than the problems previously discussed, the controller operated as designed. Voltages, frequencies, and currents were all within limits. The oscillator, reversing bridge, lockout, and main bridge circuits functioned normally over a voltage range of 19 to 34 volts. The speed control in the original circuit did not obtain the full speed range from 0 to 15 volts. The revised connection of the saturable reactor did obtain full control.

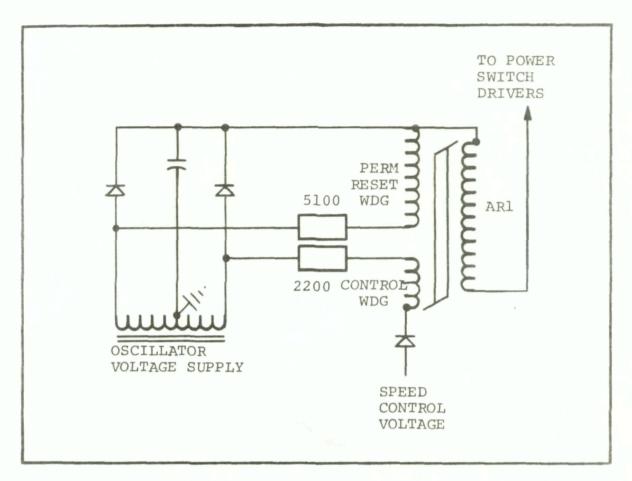


Figure 52.- Reconnection of Saturable Reactor Circuit

### Cogging Torque

Cogging torque was not measured on the full flux unit, but appears to be quite low. It was barely discernable on the low flux unit.

#### Controller Power Draw

The entire controller, including the magnetic sensor required 2.1 watts of power. This is compared to an estimated value of 1.82. Approximately 0.2 watts of power were added when the capacitor was connected across the primary of the sensor.

#### Weight

The measured weight of the entire unit was 4.28 pounds versus a calculated weight of 4.7 pounds. The weight is divided into 0.76 pounds for the controller and 3.52 pounds for the motor.

#### STATUS OF DEVELOPMENT

#### Condition of Units

Unit No. 1.- This unit Serial No. 1 was the first built, and was shipped for use on NASA Contract NAS5-10459.

- (1) Low-flux rotor.
- (2) Reconnected saturable reactor per figure 52.
- (3) Dithering suppression capacitors and zeners added per figure 46.
- (4) Added 3k resistor from collector to base of bottom row power switch driver transistors.
- (5) Position of Magnetic Sensor only set roughly.

Unit No. 2.- The second unit was assigned Serial No. 2.

- (1) High-flux rotor.
- (2) Original controller circuit per figure 17.
- (3) Controller circuit not checked out.
- (4) Magnetic sensor position not set.

Unit No. 3.- This unit was originally intended as a back-up unit. Some parts used were not full quality as described below.

- (1) High-flux rotor.
- (2) Equivalent wye-connected motor winding instead of delta. This was done to allow comparison with a wye-winding in any further development.
- (3) Shaft has flat applied accidentally during tool withdrawal but is entirely functional.
- (4) Magnetic sensor. The magnetic sensor core is cracked, but is held rigidly in place by the end punchings. It was necessary to hand grind the ID to avoid rubs after assembly, resulting in a large air gap length-up to 0.012. This will probably result in slightly low voltage outputs.
- (5) End Bell. One end bell was not gold-plated in the bearing bore.

- (6) Original controller circuit per figure 17.
- (7) Magnetic Sensor position not set.

# Remaining Development Problems

- (1) Unequal peak values of output voltages from the sensor. See "Magnetic Sensor Output" paragraph under "Problem Areas", page 90.
- (2) Irregularities on the leading edge of the sensor output pulse. See "Magnetic Sensor Output" paragraph under "Problem Areas", page 90.
- (3) Pulse-Width Variation. See "Pulse-Width Variation" paragraph under "Problem Areas", page 96.

IV-104



# NEW TECHNOLOGY

A patent disclosure has been written on the controller-commutator circuit developed on this contract. The disclosure will be submitted in the normal manner. No other disclosures are contemplated on the motor-controller.

IV-106

Blank

## CONCLUSIONS AND RECOMMENDATIONS

- (1) Three complete units have been manufactured as described previously in the DISCUSSION SECTION under "Status of Development", in the "Condition of Units" paragraph, but testing was not completed pending further development on remaining problem areas to be performed on contract NASS-10459.
- (2) Static tests on the motor with a rebuilt permanent-magnet rotor show that, with the new rotor, the torque output of the motor is approximately 100 ounce-inch with 0.4 amperes current versus a specification requirement of 90 ounce-inch.
- (3) Cogging torque was not measured on the motor with a rebuilt rotor but appears to be quite low.
- (4) Ripple torque was not measured pending resolution of the problem areas affecting it.
  - (5) Weight of the complete unit was 4.28 pounds.
- (6) The control power drawn by the controller, including the magnetic sensor, was 2.1 watts.
- (7) Total number of components in the circuit was 133 components versus a design objective of 100. Resolution of the problem areas may require additional components or may eliminate some.
- (8) All functions of the motor-controller required by the specification were provided with the exception of nulling capability. It was felt that this could only be provided by a dissymmetry in the magnetic sensor design which would affect the rate information.
- (9) A problem with dithering or vibration of the shaft at the commutating points was solved on the first unit with the addition of nine components. The other two units were not modified.
- (10) Remaining problem areas. All of the remaining problem areas are associated directly or indirectly with the magnetic sensor output pulse. The variation in peak amplitude, ringing, and the taper of the pulse are all associated with the problems.

Variation in peak amplitudes: This disturbs the accuracy of the rate information. Because of the sensitivity of the peak amplitude to air gap variations and because of practical

manufacturing tolerances, it is doubtful that this can be completely eliminated. This can be compensated for by trimming the output signals with potentiometers. Another possibility would be a redesign of the sensor to obtain each output signal from several windings connected in series on positionally equal teeth distributed around the periphery of the air gap.

Ringing: The ringing causes irregularities in the leading edge of the pulse. These irregularities cause problems ultimately associated with low torque points or high ripple torque as described in the DISCUSSION SECTION under "Problem Areas", in the "Magnetic Sensor Output" paragraph. The ringing is a natural characteristic of the ferrite core because of its low inherent damping characteristics. It is recommended that in the future sensor cores made of low-core-loss laminated steel be investigated. The eddy currents in the steel would naturally suppress the ringing. Although more core loss would be obtained, this would be partially offset by elimination of the losses associated with damping the ringing in the ferrite core. It would also be more economical and more reliable. For the present, the solution to the problem appears to lie in applying adequate damping techniques to the sensor input and output.

Pulse shape: The taper of the pulse together with its interaction with the speed control saturable reactor cause the pulse width applied to the motor to vary significantly over a switching cycle as described in the DISCUSSION SECTION under "Problem Areas", in the "Pulse-Width Variation" paragraph. This causes high ripple torque at low pulse widths. A reconnection of the saturable reactor circuit was made on the first unit in an attempt to lessen the interaction. This did not obtain a significant improvement. Further investigation is required to find a solution.

# BIBLIOGRAPHY

- 1. Yates, W. W.; Skamfer, R. E.: Final Report for a Brushless DC Torque Motor, NASA Contractor Report, NASA CR-374, February, 1966.
- Veillette, L. J.: Offset-Tooth Magnetic Rotor-Position and Velocity Sensor, NASA Invention Disclosure D#1033 (unpublished)
- 3. Roters, Herbert C.: <u>Electromagnetic Devices</u>, John Wiley and Sons, Inc. 1941
- 4. Manual 7, Design and Application of Permanent Magnets, Published by Indiana General Corporation, Magnet Division Valparaiso, Indiana.
- 5. Veillette, L. J.: NASA GSFC Report No. X716-66-473.

IV-110

Blank

#### APPENDIX A

#### CALCULATION OF PERMANENT MAGNET CORE LOSS RESISTANCE

The following assumptions were made in the derivation.

- 1) The flux flowing through one pole of the magnet is a pulsating sinusoid of flux density having a quasisquare wave space distribution. Although the mmf of the primary is such as to generate approximately a sinusoidal space distribution, the opposition of the eddy currents in the magnet and the high air gap reluctance in the interpolar space would tend to force the flux into a quasi-square wave distribution.
- 2) The shape of the flux path in the magnet was assumed to be a simple rectangular solid with a square cross section. This shape approximates the actual flux path in the magnet. See Figure 53.

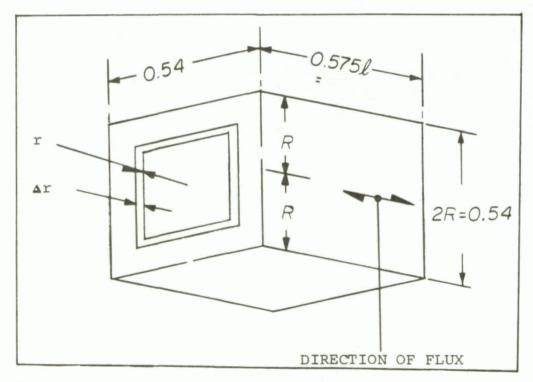


Figure 53.- Approximate Shape of Permanent Magnet Flux Path

$$B_{m} = 1.1B$$

 $B_{m}$  = peak fundamental component of flux density in air gap.

B = peak of quasi-square wave of flux density
 in air gap.

$$\emptyset_m = B A_m$$

 $\phi_{m}$  = peak flux entering rotor.

 $A_m$  = Area of magnet.

$$\emptyset_{\text{m}} = \frac{B_{\text{m}} A_{\text{m}}}{1.1}$$

$$e = \frac{N \, d\emptyset \times 10^{-8}}{dt}$$

Where e = voltage induced in incremental loop of material in magnet having turns, N = 1

 $\phi_{m}$  sin 2  $\pi$  ft = total flux

Peak 
$$\frac{d\emptyset}{dt} = \emptyset_m \ 2\pi \ f = \frac{2\pi}{1.1} \ B_m A_m f = 5.7 \ B_m A_m f$$

Proportion of flux linking incremental ring =  $\frac{r^2}{R^2}$ 

$$E = 5.7r^2 B_m f \times 10^{-8}$$

$$R^2 = A_m$$

E = peak voltage in incremental loops.

Resistance of ring = 
$$\frac{\rho \, \ell}{A} = \frac{\rho \, 8r}{\ell \Delta r}$$

 $\rho$  = resistivity in ohm-inches.

See Figure 53 for others.

i peak = 
$$\frac{E}{Rest.}$$
 =  $\frac{.713 \text{ r Bmf} \ell \Delta r \times 10^{-8}}{\rho}$ 

Loss = 
$$\left(\frac{\text{ip}}{\sqrt{2}}\right)^2$$
 x resistance  
=  $\frac{2.03 \text{ r}^3 \text{B}_{\text{m}}^2 \text{f}^2 \ell \Delta \text{r} \times 10^{-16}}{\rho}$   
Total loss =  $\frac{2.03 \text{ B}_{\text{m}}^2 \text{f}^2 \ell 10^{-16} \text{ P}}{\rho} \int_0^{\text{R}_3} dr$   
=  $\frac{\text{R}^4 \text{B}_{\text{m}}^2 \text{f}^2 \ell \times 10^{-16}}{1.97 \rho} \times \text{P}$ 

Where P = number of poles

$$Erms = \frac{Ckw \, \emptyset_{ff} \, x \, 10^{-6}}{45}$$

Erms = phase voltage induced in stator from fundamental flux  $\emptyset_f$ .

Ckw = effective series conductors per phase in stator

$$Ø_f = 2/\pi B_m A_m \times \frac{3}{2}$$

 $\phi_f$  = peak fundamental flux in air gap

 $A_m \times 3/2 = area$  of one pole pitch.

Since the equivalent circuit is on a line-to-line voltage basis, with the connection used,  $\rm E_{1-1} = 1.5~E_{ph}$ 

$$E_{1-1} = \frac{\overline{1.5}^2 \times Ckw \times 2/\pi \quad B_m A_m f \times 10^{-6}}{45}$$

This is the voltage at the air gap.

$$\frac{(E_{1-1})^2}{R_r} = loss$$

Therefore: 
$$(1.5)^4 (\text{Ckw})^2 4 \text{ Bm}^2 \text{ Am}^2 \text{ f}^2 \times 10^{-12}$$
  
 $\pi^2 (45)^2 \text{ Rr}$ 

$$= \frac{P \times R^4 B_m^2 f^2 \ell \times 10^{-16}}{1.97 \rho}$$

$$R_{r} = \frac{200 \rho (Ckw)^{2}}{P \ell}$$

This resistance only accounts for the eddy current loss in the magnet. There is another hysteresis component of loss the value of which is impractical to calculate. The test results indicate a factor of approximately 1.25 times the eddy current loss as calculated. Therefore the formula for Rr becomes the following:

$$R_{r} = \frac{89 \rho (Ckw)^{2}}{p \ell}$$

#### APPENDIX B

#### DESCRIPTION OF MAJOR TOOLING

The following is a description of the design of the items of tooling necessary to construct the motor controller.

Figure 54 shows the index punching and die for both the protective organic laminate end punchings (which are cemented to the magnetic sensor core) and the armature punchings. Several other pieces (not shown) are necessary to utilize the punches and dies.

Figure 55 and 56 show nests for the previously mentioned punchings. The round hole dies were available. Figure 57 shows the separator die for the armature punching.

The armature stack is made by cementing the punchings together with epoxy. This is accomplished by a vacuum impregnation of a loose stack of punchings with the epoxy, tightening the stack, and curing. The fixture to be used for all these functions (including removal of the stack from the fixture) is shown on figure 58. Item 9 on the sketch is used to press the stack off the arbor.

To maintain the end extensions of the armature winding within the proper dimensions, it is necessary to use shaping plugs during the dip and bake operation. A 30 angle away from the inside diameter is necessary on one end to make room for the rotor magnet keeper during insertion. These shaping plugs are shown on figure 59. Figure 60 describes some diaphragm chuck inserts necessary for the armature machining.

It is necessary to make the thin magnetic can in the armature bore from sheet stock which has been welded into a tube. This can is for the purpose of lowering ripple torque. The fixture to be used to accomplish the welding of the can is shown in figure 61.

Other miscellaneous tools shown are a winding mold for the secondary windings of the magnetic sensor, figure 62, some grinding dogs for the rotor shaft, figure 63, a sealing fixture for encapsulating a toroidal transformer, figure 64, and a nest for the shims used to adjust rotor axial movement, figure 65.

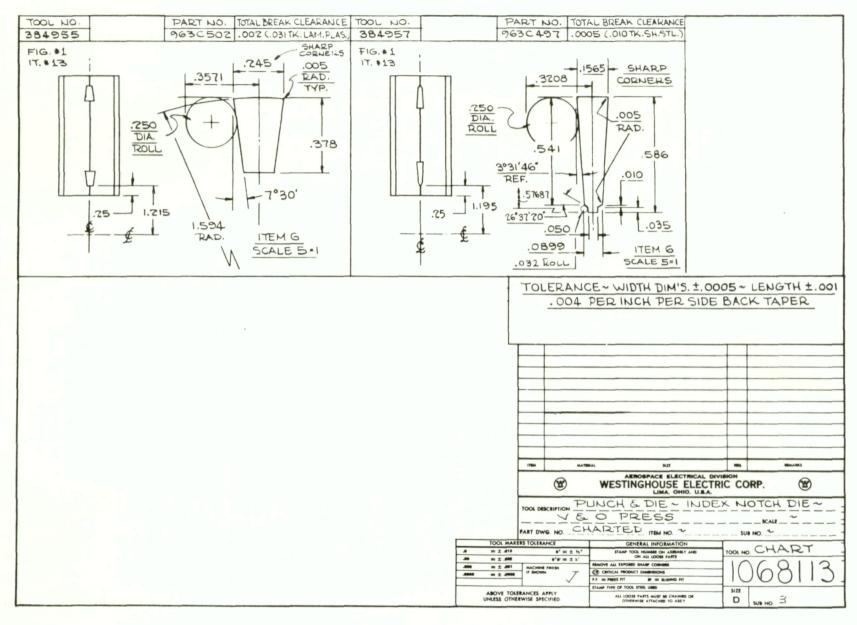


Figure 54.- Punching Punches and Dies

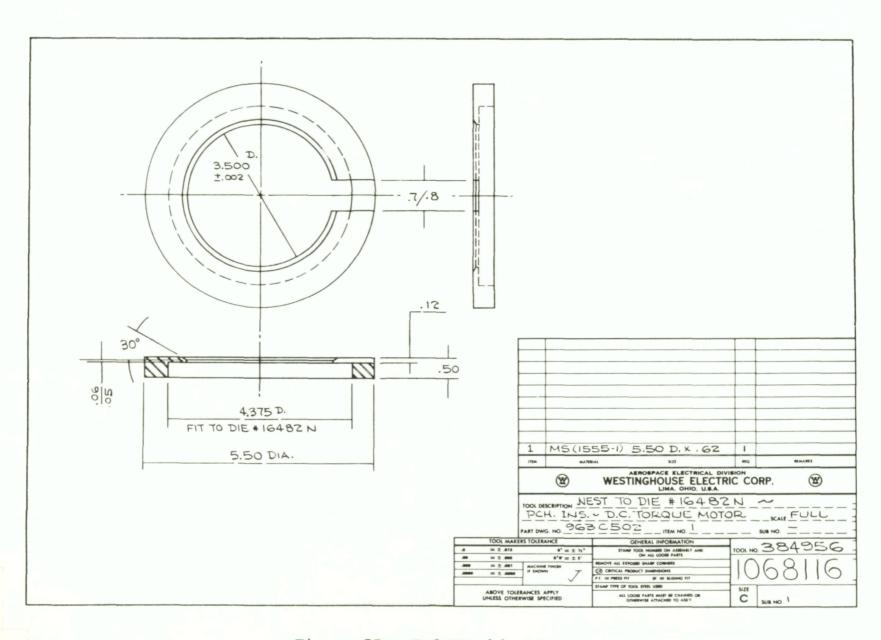


Figure 55.- End Punching Nest

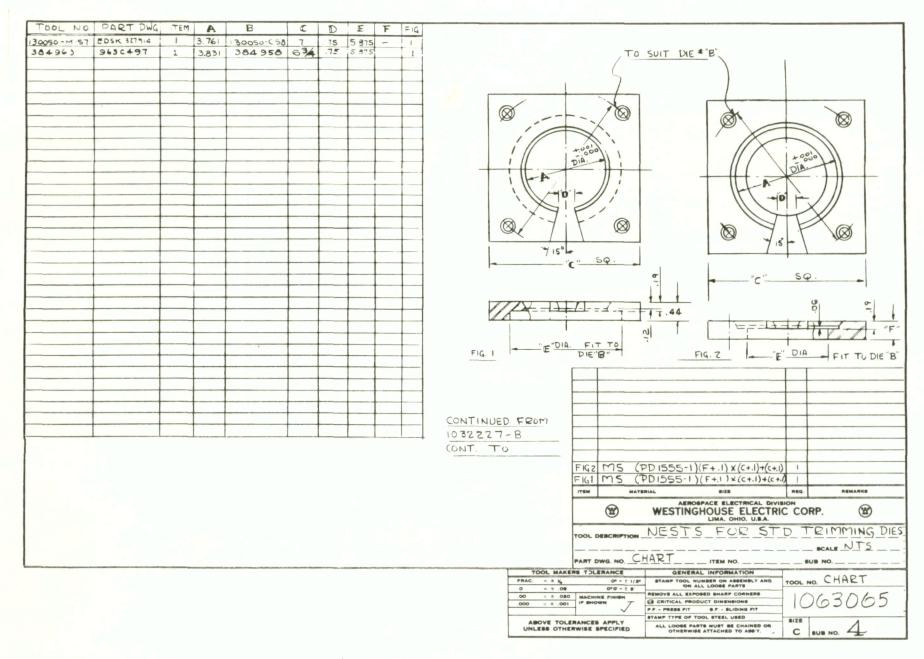


Figure 56.- Armature Punching Nest

Figure 57.- Armature Punching Separator Die

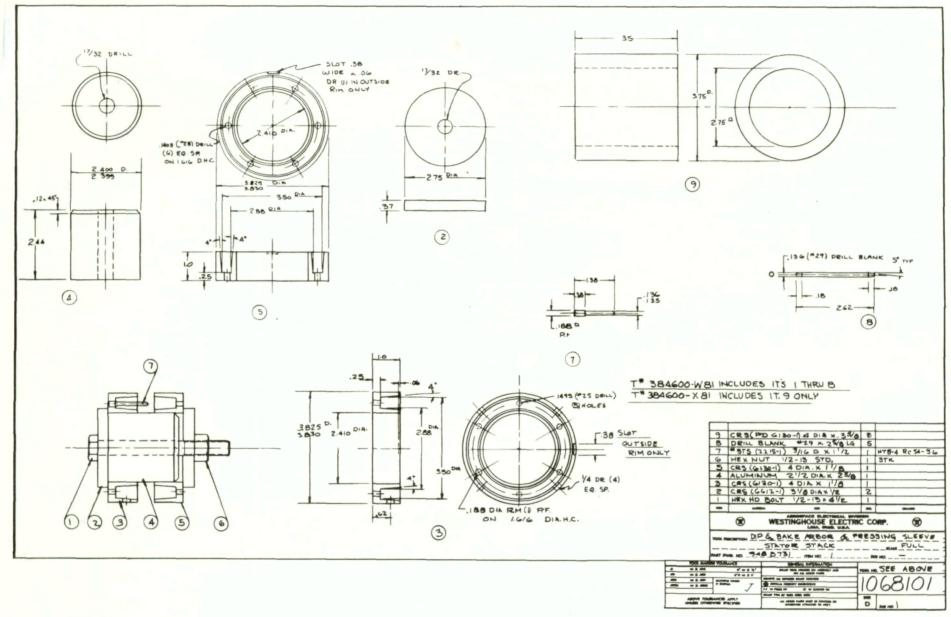


Figure 58.- Armature Stack Dip and Bake Fixture

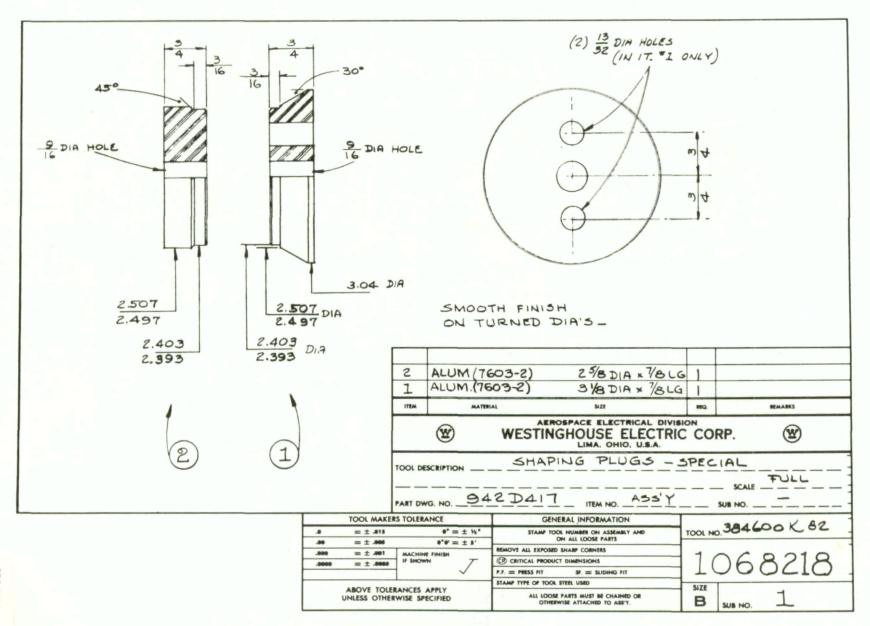


Figure 59.- Armature Shaping Plugs

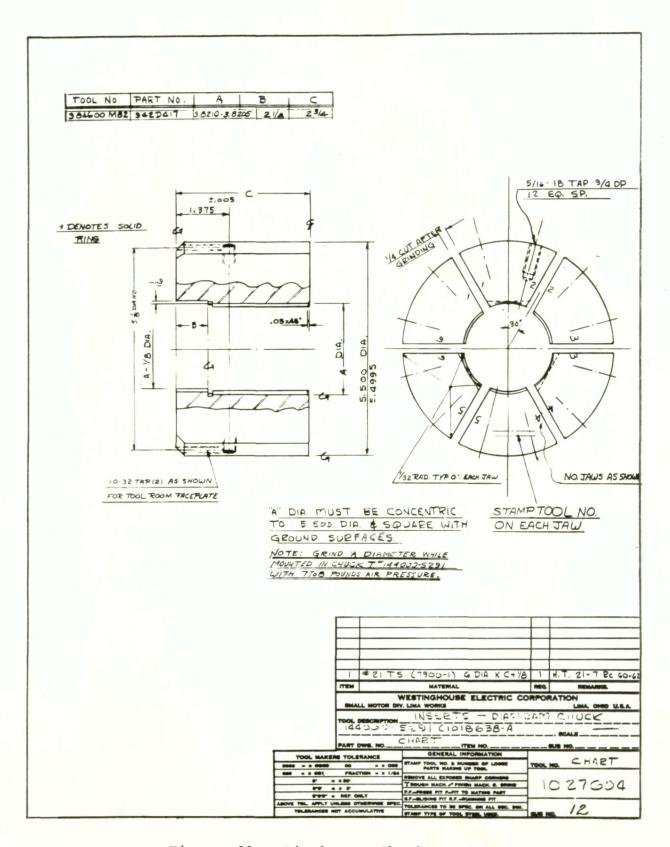
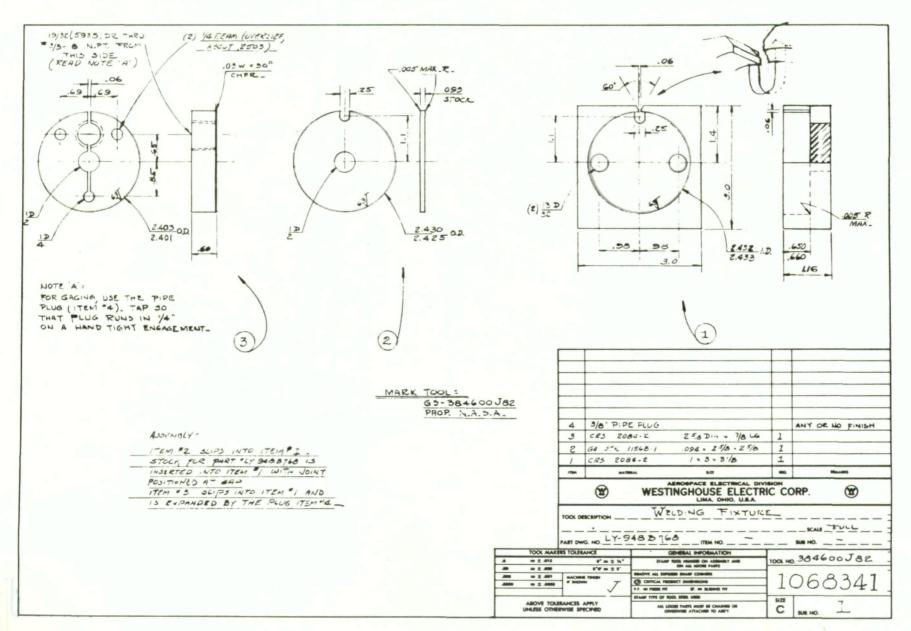


Figure 60.- Diaphragm Chuck Inserts



---

Figure 61.- Bore Tube Welding Fixture

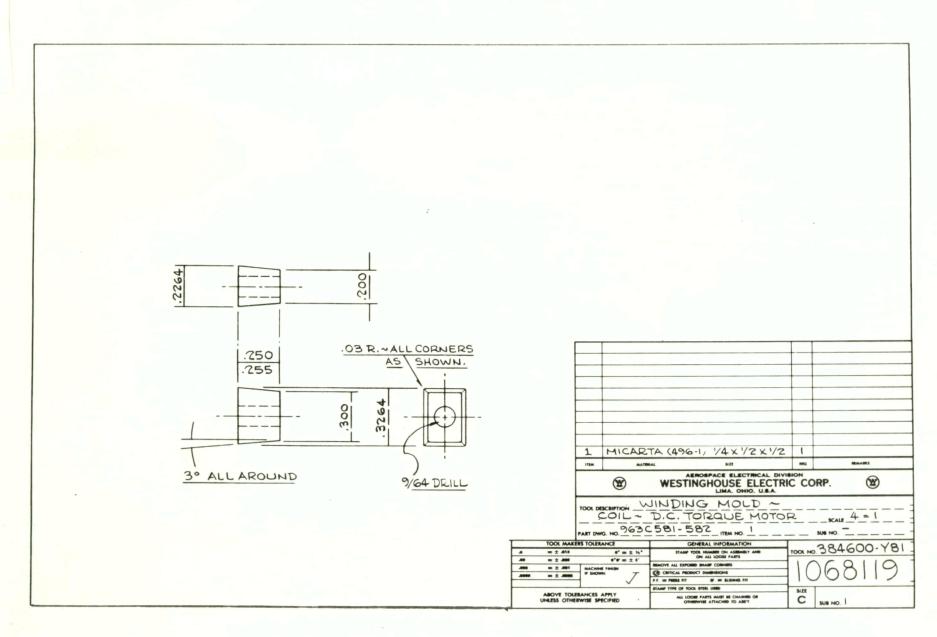


Figure 62.- Secondary Winding Mold

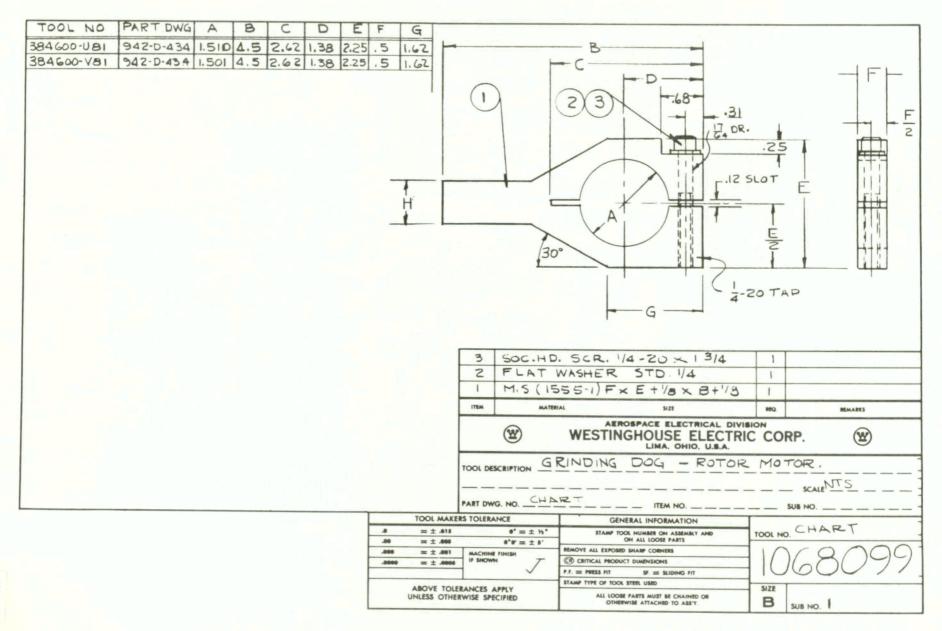


Figure 63.- Rotor Grinding Dogs

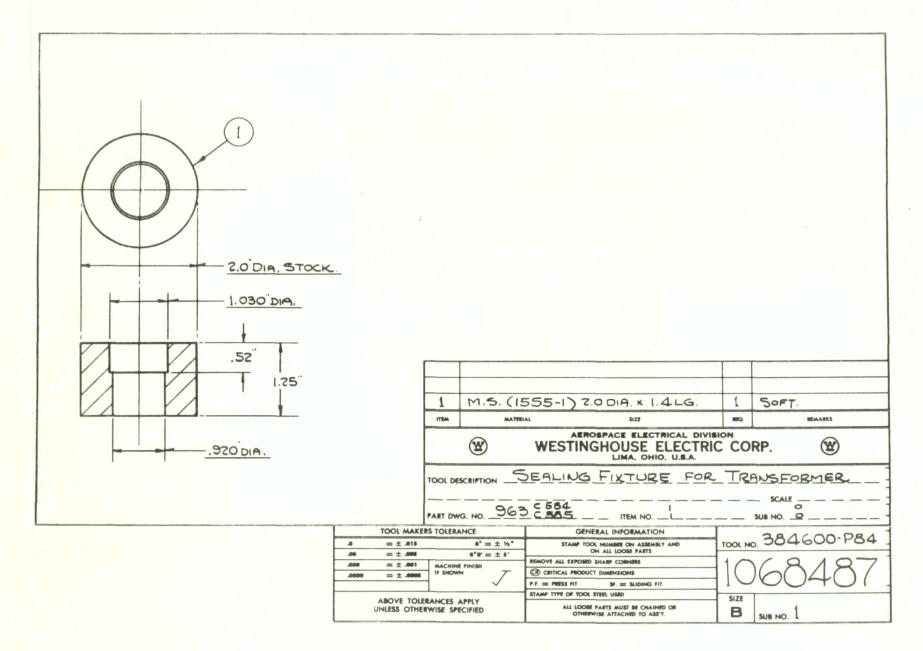


Figure 64.- Transformer Sealing Fixture

•

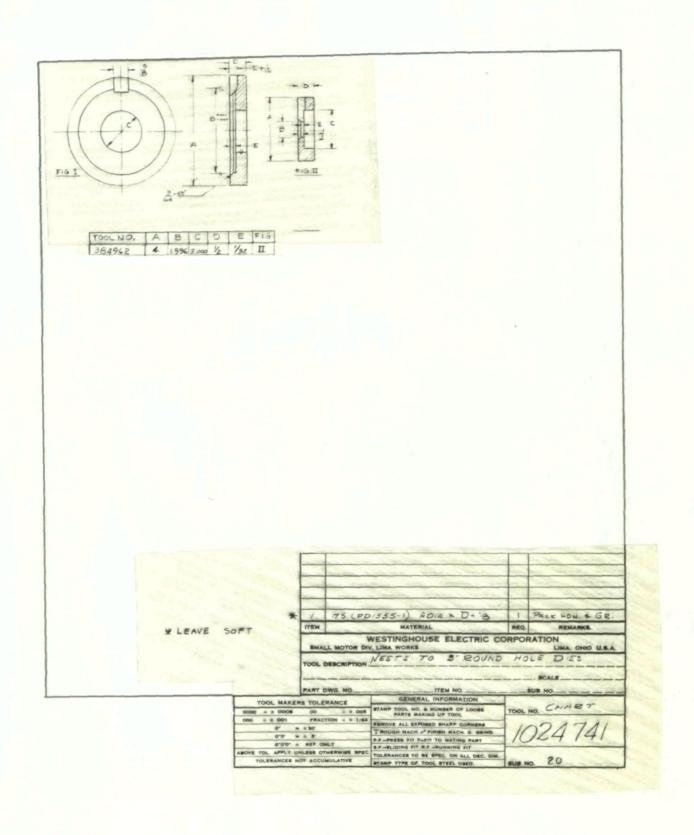


Figure 65.- Shim Nest